The University of Nottingham

UNITED KINGDOM · CHINA · MALAYSIA

Alterations in cytoskeletal proteins and microtubule stability following 26S proteasome dysfunction in mouse brain cortical neurons

Hala Alhadi Ali Mohamed

M.B.Ch.B, M.Sc

Thesis submitted to the University of Nottingham for the degree of Doctor of Philosophy

June 2017

List of Abbreviation

2D-DIGE	2-dimensional difference gel electrophoresis
Actin	B-actin
AD	Alzheimer`s diseases
ALP	Autophagy-lysosome pathway
ALS	Amyotrophic lateral sclerosis
AMPS	Ammonium per-sulphate
APES	Amino-propyl-tri-ethoxy-silane
ApoE	Apolipoprotein E
AU	Auditory cortex
BAX	Bcl-2-associated x protein
Bcl-2	B-cell lymphoma 2
BID	Bh3 interacting-domain death agonist,
BIM	Bcl-2-like protein 11
BSA	Bovine serum albumin
CaMKIIα	Calcium calmodulin-dependent protein kinase IIα
Caspases	Cysteine-aspartic proteases, cysteine aspartases or cysteine-dependent aspartate-directed proteases
CNBr	Cyanogen bromide activated-sepharose-4b
COX	Cytochrome c oxidase, mitochondrial
CP	Core particles
Cre	Causes recombination
DNA	Deoxyribonucleic acid
DUBs	Deubiquitinating enzymes
FOXO3	Forkhead box o3
GAPDH	Glyceraldehyde 3-phosphate dehydrogenase
GDP	Guanosine diphosphate
GTP	Guanosine -5`- triphosphate
HD	Huntington`s diseases
HSP7C	Heat shock cognate 71 kda protein
IL-1β	Interleukins-1β
LB	Lewy bodies
LC3	Microtubule-associated protein 1a/1b-light chain 3
MAP2	Microtubule-associated protein-2
MDA	Malondialdehyde
MFs	Microfilaments
mFUMH	Mitochondrial fumarate hydratase
MPP1	1-methyl-4-phenylpiridinium
MPTP	1-methyl-4-phenyl-1, 2, 3, 6-tetrahydropyridine
MT	Microtubule

MTs	Microtubules
NFH	Neurofilaments high- molecular weight
NFL	Neurofilaments low- molecular weight
NFM	Neurofilaments middle- molecular weight
NFs	Neurofilaments
NFT	Neurofibriallary triangle
NF-βB	Nuclear factor kappa-b
Noxa	Phorbol-12-myristate-13-acetate-induced protein 1
P53	Protein 53 or tumor protein 53
PAC	Proteasome assembly chaperone
PB	Pale body
Pba	Proteasome biogenesis associated protein
PD	Parkinson`s diseases
PFs	Protofilaments
PLA2	Phospholipase A2
POMP	Proteasome maturation protein
PRDX-6	Peroxiredoxin-6
PSMA	Proteasome subunit mouse-a
PSMB	Proteasome subunit mouse-b
PSMC	Proteasome subunit mouse-c
PSMD	Proteasome subunit mouse-d
PTM	Post-translational modification
PUMA	P53 upregulated modulator of apoptosis
ROS	Reactive oxygen species
RP	Regulatory particles
SCAs	Spinocerebellar ataxia
SDS	Sodium dodecyl sulphate
SEM	Standard error of the mean
SEM	Standard error of the mean
SEPT-7	Septin-7
SNAB	Beta-soluble nsf attachment protein
STMN1	Stathmin 1
TBHP	Tert-butyl hydrogen peroxide
TBS	Tris-buffered saline
TBS-T	Tris-buffered saline-triton
TCA	Trichloroacetic acid
TCB	Thrombin cleavage buffer
TEMED	N, n, n, n- tetramethylene diamine
TMOP	1, 1, 3, 3-tetramethoxypropane

Ub	Ubiquitin
Uba52	Ubiquitin a-52 residue ribosomal gene
Ubc	Ubiquitin conjugating enzyme
UBD	Ubiquitin binding domains
UBP	Ubiquitin binding proteins
UCH	Ubiquitin carboxy-terminal hydrolases
UCHL1	Ubiquitin carboxyl-terminal esterase l1
UPS	Ubiquitin proteasome system
VIME	Vimentin

Abstract

The mechanisms involved in the cause and progression of chronic neurodegenerative diseases are still unclear. The ubiquitin proteasome system (UPS) plays an essential role in the maintenance of intracellular protein homeostasis by degrading unwanted proteins. The accumulation of ubiquitinated proteins is a hallmark of major neurodegenerative diseases, including Alzheimer's and Parkinson's diseases. In most cases, these diseases are also associated with changes in cytoskeletal proteins and microtubule stability. We previously reported decreased levels of microtubule destabilizing protein stathmin (STMN) following 26S proteasome dysfunction in mouse cortical neurons; associated with neurodegeneration and the formation of intraneuronal protein inclusions in surviving neurons. This suggested a role for the 26S proteasome in maintaining the neuronal cytoskeleton.

This thesis investigates the levels and localisation of cytoskeletal proteins in mouse cortical neurons following 26S proteasome dysfunction (*Psmc1*$^{fl/fl}$*;CaMKIIα-Cre*). This study provides new insights into the role of the UPS in maintain cytoskeletal proteins that may be important in neurodegenerative disease. We found an early increase in neurofilaments following 26S proteasome dysfunction; before obvious changes in microtubule stability. An increased free/polymerised tubulin ratio was evident at later stages indicative of microtubule instability in *Psmc1*$^{fl/fl}$*;CaMKIIα-Cre* mice. In addition, we found decreased levels of microtubule proteins, microtubule-associated proteins and detyrosinated-tubulin; with increased tyrosinated-tubulin following 26S proteasome dysfunction. These changes are contrary to decreased STMN expression observed in *Psmc1*$^{fl/fl}$*;CaMKIIα-Cre* mice. We suggest that decreasing STMN may be part of a negative feedback loop to stabilize MT following 26S proteasome dysfunction. STMN is known to be a downstream target of p53, p27 and the PI3K/Akt pathway. We found expression of p53 was increased in the cortex following

26S proteasome dysfunction, correlating with decreased phosphorylated-Akt expression at an early stage and may effect STMN expression. However, we did not observe any significant differences in pro- and anti-apoptotic proteins of the Bcl-2 family between control and *Psmc1*$^{fl/fl}$*;CaMKIIα-Cre* mice, which may also by effected by p53 and phosphorylated-Akt.

Immunohistochemical studies revealed changes in cortical neuron morphology accompanied 26S proteasome dysfunction. Cortical thickness was significantly decreased; associated with less neurons in the layers III and V. However, nuclear size of cortical neurons was increased, as well as the length and arborisation of their apical dendrites. Taken together, our novel data contributes to our understanding of molecular and cellular events underlying neurodegeneration and suggest that control of microtubule changes may help to slow or restore pathology of neurons.

Acknowledgments

The completion of my PhD study could not have been possible without the help and support of so many people whose names may not all be mentioned. Their contributions are sincerely appreciated and gratefully acknowledged.

I would like to express my deep appreciation and indebtedness particularly to my supervisor Dr Lynn Bedford; for all her help and support along the way. She has been a great supervisor, constantly supporting, guiding and encouraging me during my PhD.

I must also express my appreciation to my second supervisors Dr Claire Friel and Dr Laura Conforti for their helpful suggestions, encouragement and kindness, providing me with some materials for my research.

I would like to acknowledge and thank many people that I have met during my study, in particular Karen Lawler for her kind help and support, and all the AMU staff for their valuable help.

My family who have always been by my side during these years. I offer very special thanks to my husband Mr Alsanose Kalefa who has been by my side. I struggle to find words to describe all that he has done to support me in this process and to thank my children and my parents who prayed for me.

Table of contents

Chapter 1 1

Introduction 1

1.1 Introduction 2

1.2 The ubiquitin proteasome system 3

1.2.1 Ubiquitin and ubiquitination 4

1.2.2 26S proteasome structure and assembly 5

1.2.2.1 The 20S core particle 7

1.2.2.2 20S core particle assembly 8

1.2.2.3 The 19S regulatory particle 9

1.2.2.4 19S regulatory particle assembly 10

1.3 Cytoskeleton changes in neurodegenerative disease 11

1.3.1 Microfilaments 12

1.3.2 Microtubules 13

1.3.2.1 Tubulin isotypes 16

1.3.2.2 Dynamic instability 17

1.3.2.3 Microtubules in neurodegenerative disease 18

1.3.2.4 Post-translational modifications of tubulin 18

1.3.3 Microtubule-associated proteins 23

1.3.3.1 MAP2 24

1.3.3.2 Tau 26

1.3.3.3 Stathmin 29

1.3.4 Stathmin regulator proteins 32

1.3.4.1 p53 32

1.3.4.2 PI3K-Akt pathway 35

1.3.4.3 p27 38

1.3.5 Neurofilaments 41

1.3.5.1 Structure and assembly of neurofilaments 42
1.3.5.2 Transport of neurofilaments 44
1.3.5.3 Degradation of neurofilaments..... 45
1.3.5.4 Neurofilaments in neurodegenerative diseases..... 46
1.4 Histological structure of cerebral cortex in mouse brain ... 47
1.4.1 The neocortex 48
1.4.2 Neuronal cells in the neocortex..... 51
1.4.2.1 Pyramidal neurons 51
1.4.2.2 Spiny stellate neurons 53
1.4.2.3 Inhibitory interneurons 54
1.5 26S proteasome depletion mouse model; *Psmc1*$^{fl/fl}$*;CaMKIIa-Cre* 55
Aims 58
Chapter 2 59
Materials and Methods 59
2.1 Experimental animals..... 60
2.1.1 Conditional deletion of the 26S proteasome mice..... 60
2.1.2 Extraction of genomic DNA from mouse tissue..... 60
2.1.2.1 Reagents 60
2.1.2.2 Method 62
2.1.3 Polymerase chain reaction 62
2.1.3.1 Reagents 62
2.1.3.2 Method 62
2.1.4 Agarose gel electrophoresis 63
2.1.4.1 Reagents 63
2.1.4.2 Method 63
2.2 Protein analysis 63
2.2.1 Tissue homogenisation 63

2.2.1.1 Reagents 63
2.2.1.2 Method 64
2.2.2 Bradford assay 64
2.2.2.1 Reagents 64
2.2.2.2 Method 64
2.2.3 Sodium dodecyl sulphate polyacrylamide gel electrophoresis (SDS-PAGE) 64
2.2.3.1 Reagents 64
2.2.3.2 Method 66
2.2.4 Western blotting analysis 67
2.2.4.1 Reagents 67
2.2.4.2 Method 67
2.2.5 Membrane blotting 68
2.2.5.1 Reagents 68
2.2.5.2 Method 68
2.2.6 Stripping nitrocellulose membrane 69
2.2.6.1 Reagents 69
2.2.6.2 Method 69
2.3 Purification of free and polymerized tubulin 71
2.3.1 Reagents 71
2.3.2 Method 71
2.4 Gene expression analysis 73
2.4.1 RNA extraction 73
2.4.1.1 Reagents 73
2.4.1.2 Method 73
2.4.2 cDNA synthesis 73
2.4.2.1 Reagents 73
2.4.2.2 Method 73

2.4.3 Quantitative polymerase chain reaction 74
2.4.3.1 Reagents 74
2.4.3.2 Method 74
2.4.4 Gene expression quantification 75
2.5 Histology 76
2.5.1 Tissue processing 76
2.5.1.1 Reagents 76
2.5.1.2 Method 76
2.5.2 APES (amino-propyl-tri-ethoxy-silane) coating of slides 76
2.5.2.1 Reagents 76
2.5.2.2 Method 77
2.5.3 Immunohistochemistry of paraffin-embedded tissue sections 77
2.5.3.1 Reagents 77
2.5.3.2 Method 78
2.6 Statistical analysis 82
Chapter 3 83
Microtubule instability following disruption of the 26S proteasome in mouse cortical neurons 83
3.1 Introduction 84
3.2 Results 91
3.2.1 Normalization of Western blots 91
3.2.2 Decreased cortical expression of microtubule proteins following disruption of the 26S proteasome in mouse cortical neurons 95
3.2.3 Post-translational modifications of α-tubulin following disruption of the 26S proteasome in mouse cortical neurons 99

3.2.4 Increased free/polymerised tubulin ratio following disruption of the 26S proteasome in mouse cortical neurons 103

3.2.5 Microtubule-associated protein expression following disruption of the 26S proteasome in mouse cortical neurons 110

3.3 Discussion 118

3.3.1 Decreased α-tubulin and βIII-tubulin levels following disruption of the 26S proteasome in mouse cortical neurons 119

3.3.2 Increased tyrosinated-tubulin and decreased detyrosinated-tubulin suggest decreased MT stability following 26S proteasome dysfunction in mouse cortical neurons. 122

3.3.3 Decreased MT polymerization following disruption of the 26S proteasome in mouse cortical neurons 124

3.3.4 Decreased tau and MAP2 associated with polymerized-tubulin following disruption of the 26S proteasome in mouse cortical neurons 125

Chapter 4 128

Stathmin and its regulators following disruption of the 26S proteasome in mouse cortical neurons 128

4.1 Introduction 129

4.1.1 Stathmin and p53 131

4.1.2 Stathmin and PI3K/Akt pathway 133

4.1.3 Stathmin and p27 134

4.2 Results 138

4.2.1 Decreased stathmin expression following 26S proteasome dysfunction in mouse cortical neurons.....138

4.2.1.1 Stathmin protein expression is decreased at 6 weeks-of-age 138

4.2.1.2 Stathmin gene expression is decreased following disruption of the 26S proteasome in mouse cortical neurons... 143

4.2.2 Stathmin regulatory proteins 145

4.2.2.1 Increased p53, but no change in the Bcl2 family, following 26S proteasome disruption in mouse cortical neurons 145

4.2.2.2 Changes in the PI3K/Akt pathway following 26S proteasome disruption in mouse cortical neurons 149

4.2.2.3 p27 expression does not change following 26S proteasome disruption in mouse cortical neurons 152

4.3 Discussion 154

4.3.1 Stathmin expression decreases following disruption of the 26S proteasome in mouse cortical neurons 154

4.3.2 Increased p53, but no change in the Bcl2 family, following 26S proteasome disruption in mouse cortical neurons 156

4.3.3 Changes in the PI3K/Akt pathway following 26S proteasome disruption in mouse cortical neurons 158

4.3.4 p27 expression does not change following 26S proteasome disruption in mouse cortical neurons 163

Chapter 5 165

Morphological and neurofilament changes following disruption of the 26S proteasome in mouse cortical neurons 165

5.1 Introduction 166

5.1.1 Morphological insights into neurodegenerative diseases 166

5.1.2 Neurofilament proteins in neurodegenerative disease 167

5.2 Image processing and data analysis.....173

5.2.1 Cortical thickness.....175

5.2.2 Neuronal number and nuclear size 177

5.2.3 Apical dendrite length.....179

5.3 Results 182

5.3.1 Decreased cortical thickness following disruption of the 26S proteasome in mouse cortical neurons 182

5.3.2 The number of neurons is decreased following disruption of the 26S proteasome in mouse cortical neurons 186

5.3.3 Nuclear size is increased following disruption of the 26S proteasome in mouse cortical neurons.....191

5.3.4 Increased neurofilament expression following disruption of the 26S proteasome in mouse cortical neurons 195

5.3.5 Decreased neurofilament gene expression following disruption of the 26S proteasome in mouse cortical neurons 198

5.3.6 NF immunoreactivity following disruption of the 26S proteasome in mouse cortical neurons.....200

5.3.7 Increased apical dendrite length following disruption of the 26S proteasome in mouse cortical neurons.....209

5.4 Discussion 212

5.4.1 Cortical thickness decreases following disruption of the 26S proteasome in mouse cortical neurons 212

5.4.2 Hypertrophy of neurons with 26S proteasome dysfunction in mouse cortical neurons 213

5.4.3 Neurofilament changes caused by 26S proteasome dysfunction in mouse cortical neurons 215

5.4.4 Increased neurofilament proteins following disruption of the 26S proteasome in mouse cortical neurons.....215

5.4.5 Decreased neurofilament mRNA following disruption of the 26S proteasome in mouse cortical neurons.....217

5.4.6 NF immunoreactivity and increase apical dendrite length following 26S proteasome dysfunction in mouse cortical neurons 218

Chapter 6 223

General discussion and conclusion.....223

6.1 General discussion 224

6.2 Conclusion 228

6.3 Future work 229

Bibliography 232

Appendix.....283

Figures

Figure 1.1 Different modes of ubiquitination lead to different substrate fates……..6

Figure 1.2 The ubiquitin proteasome system……..7

Figure 1.3 Structure of the 26S proteasome……8

Figure 1.4 The cytoskeleton……12

Figure 1.5 Microtubules - Structure and dynamics……15

Figure 1.6 Molecular localization of tubulin posttranslational modifications……20

Figure 1.7 Structure of MAP2 isoforms……25

Figure 1.8 Structure of Tau isoforms……27

Figure 1.9 Microtubule-associated protein Stathmin……30

Figure 1.10 Stathmin and p53 pathway……33

Figure 1.11 Stathmin and PI3k/Akt pathway……36

Figure 1.12 Stathmin and p27 pathway……41

Figure 1.13 A schematic of the structure and the assembly of neurofilament subunits into neurofilaments……43

Figure 1.14 Cytoarchitecture of the neocortex in Golgi and Nissl staining-methods……49

Figure 1.15 Major neuronal cell types of the adult cerebral cortex. ……52

Figure 1.16 The main neuropathological and molecular change in *Psmc1*$^{fl/fl}$*;CaMKIIa-Cre* mouse cortex……57

Figure 2.1 Strategy for the generation of deletion of the 26S proteasome mice……61

Figure 2.2 Sandwiched assemble with grey side down cathode (-) ……68

Figure 2.3 Schematic for free and polymerized tubulin protocol preparations as described in the Experimental section……72

Figure 2.4 Schematic for immunohistochemistry method as described in the experimental section……81

Figure 3.1 Relative levels of copper staining in 6 week-old control and *Psmc1*$^{fl/fl}$*;CaMKIIa-Cre* mouse cortical samples……93

Figure 3.2 Relative levels of GAPDH in 6 week-old control and *Psmc1*$^{fl/fl}$*;CaMKIIa-Cre* mouse cortical samples……94

Figure 3.3 α-tubulin is significantly decreased in 6 week-old *Psmc1*$^{fl/fl}$*;CaMKIIα-Cre* compared to control mouse cortices……..96

Figure 3.4 βIII-tubulin is significantly decreased in 6 week-old *Psmc1*$^{fl/fl}$*;CaMKIIα-Cre* compared to control mouse cortices……..97

Figure 3.5 Expression of β-actin is not significantly different between control and *Psmc1*$^{fl/fl}$*;CaMKIIα-Cre* mouse cortices……..98

Figure 3.6 Detyrosinated-tubulin is significantly decreased in 6 week-old *Psmc1*$^{fl/fl}$*;CaMKIIα-Cre* compared to control mouse cortices……..100

Figure 3.7 Tyrosinated-tubulin is significantly increased in 6 week-old *Psmc1*$^{fl/fl}$*;CaMKIIα-Cre* compared to control mouse cortices……..101

Figure 3.8 Expression of acetylated-tubulin is not significantly different in *Psmc1*$^{fl/fl}$*;CaMKIIα-Cre* mouse cortices compared to controls……..102

Figure 3.9 Free/polymerized tubulin ratio and % tubulin polymerization in 4 week-old *Psmc1*$^{fl/fl}$*;CaMKIIα-Cre* mouse cortices……106

Figure 3.10 Increased free/polymerized tubulin ratio and decreased % tubulin polymerization in 6 week-old *Psmc1*$^{fl/fl}$*;CaMKIIα-Cre* mouse cortices……108

Figure 3.11 MAP2 expression is not significantly different in control and *Psmc1*$^{fl/fl}$*;CaMKIIα-Cre* mouse cortices……113

Figure 3.12 Total tau protein is significantly decreased in 6 week-old *Psmc1*$^{fl/fl}$*;CaMKIIα-Cre* compared to control mouse cortices……..114

Figure 3.13 % MAP2 in the polymerized fraction is significantly decreased in 6 week-old *Psmc1*$^{fl/fl}$*;CaMKIIα-Cre* compared to control mouse cortices……115

Figure 3.14 % Tau 46 in the polymerized tubulin fraction is not significantly different in control and *Psmc1*$^{fl/fl}$*;CaMKIIα-Cre* mouse cortices……116

Figure 3.15 Expression of phosphorylated tau in 6 week-old control and *Psmc1*$^{fl/fl}$*;CaMKIIα-Cre* mouse cortices……117

Figure 3.16 Schematic representation of microtubule dynamics in *Psmc1*$^{fl/fl}$*;CaMKIIα-Cre* mouse cortical neurons ……119

Figure 4.1 STMN1 is significantly decreased in 6 week-old *Psmc1*$^{fl/fl}$*;CaMKIIα-Cre* mouse cortices……..140

Figure 4.2 STMN1 immunostaining in 4 week-old cortical neurons ……..141

Figure 4.3 STMN1 immunostaining in 6 week-old cortical neurons. ……142

Figure 4.4 STMN1 mRNA expression is decreased in *Psmc1*$^{fl/fl}$*;CaMKIIa-Cre* mouse cortices……144

Figure 4.5 Increased p53 protein expression in *Psmc1*$^{fl/fl}$*;CaMKIIa-Cre* mouse cortices……147

Figure 4.6 Expression of Bcl2 family proteins does not change in *Psmc1*$^{fl/fl}$*;CaMKIIa-Cre* mouse cortices……148

Figure 4.7 Changes in the PI3K pathway in *Psmc1*$^{fl/fl}$*;CaMKIIa-Cre* mouse cortices at 4 and 6 weeks-old……150

Figure 4.8 No change in p27 expression in *Psmc1*$^{fl/fl}$*;CaMKIIa-Cre* mouse cortex……153

Figure 5.1 Image processing……173

Figure 5.2 NFH immunostaining……174

Figure 5.3 Cortical thickness……176

Figure 5.4 Neuronal number and nuclear size in the AU cortex……178

Figure 5.5 Apical dendrite length……181

Figure 5.6 Decreased cortical thickness in *Psmc1*$^{fl/fl}$*;CaMKIIa-Cre* compared to control mouse cortices at 4 and 6 weeks-old……184

Figure 5.7 Thickness of individual cortical layers in *Psmc1*$^{fl/fl}$*;CaMKIIa-Cre* compared to control mouse cortices……185

Figure 5.8 Ubiquitin immunostaining of the AU cortex of control and *Psmc1*$^{fl/fl}$*;CaMKIIa-Cre* mice at 4 and 6 weeks-old……188

Figure 5.9 Ubiquitin immunostaining of AU cortical neurons from control and *Psmc1*$^{fl/fl}$*;CaMKIIa-Cre* mice at 4 and 6 weeks-old……189

Figure 5.10 The total number of neurons is decreased, but the number of Ub-positive neurons increased in *Psmc1*$^{fl/fl}$*;CaMKIIa-Cre* mouse AU cortex compared to controls……190

Figure 5.11 Increased nuclear size of layer III and layer V AU cortical neurons in *Psmc1*$^{fl/fl}$*;CaMKIIa-Cre* mice……193

Figure 5.12: Increased NF protein expression in *Psmc1*$^{fl/fl}$*;CaMKIIa-Cre* compared to control mouse cortices……196

Figure 5.13 Decreased NF mRNA expression in 6 week-old *Psmc1*$^{fl/fl}$*;CaMKIIa-Cre* compared to control mouse cortices……199

Figure 5.14 NFH immunoreactivity in 4 week-old *Psmc1*$^{fl/fl}$*;CaMKIIa-Cre* mouse cortical neurons……202

Figure 5.15 NFH immunoreactivity in 6 week-old *Psmc1*$^{fl/fl}$*;CaMKIIa-Cre* mouse cortical neurons……203

Figure 5.16 NFL immunoreactivity in 4 week-old *Psmc1*$^{fl/fl}$*;CaMKIIa-Cre* mouse cortical neurons……204

Figure 5.17 NFL immunoreactivity in 6 week-old *Psmc1*$^{fl/fl}$*;CaMKIIa-Cre* mouse cortical neurons……205

Figure 5.18 Types of pyramidal neurons……206

Figure 5.19 NFM immunostaining in 4 week-old mouse cortical pyramidal neurons……207

Figure 5.20 NFM immunostaining in 6 week-old mouse cortical pyramidal neurons……208

Figure 5.21 Increase apical dendrites length in the *Psmc1*$^{fl/fl}$*;CaMKIIa-Cre* mice pyramidal neurons……211

Figure 6.1 Schematic representation summery to main change in cytoskeletal protein and microtubule stability in in *Psmc1*$^{fl/fl}$*;CaMKIIa-Cre* cortical neurons……229

Figure 6.1 Oval-shaped axonal swelling in *Psmc1*$^{fl/fl}$*;CaMKIIa-Cre* cortical neurons……230

Tables

Table 2.1 Sequence of primers used for mice genotyping 62
Table 2.2 Components of 10%, 12% and 15% SDS-PAGE gels . 66
Table 2.3 Components of stacking gel solution 66
Table 2.4 Antibodies used throughout all protein analysis 70
Table 2.5 RT-PCR assay IDs from Thermo Fischer Scientific 75
Table 2.6 Protocol for tissue processing. 76
Table 2.7 Antibodies used in the immunohistochemistry 79
Table 4.1 STMN1 gene expression.....143
Table 5.1 Total thickness of the AU cortex 176
Table 5.2 Total cortical thickness and thickness of the individual cortical layers. 183
Table 5.3 Number of haematoxylin-positive and Ub-positive neurons.....190
Table 5.4 Nuclear size of Ub-positive neurons.....192
Table 5.5 NF gene expression.....198
Table 5.6 Median apical dendrite length of cortical neurons.....210

Chapter 1

Introduction

1.1 Introduction

Proteins are essential complex macromolecules that participate in every process within cells (Benarroch, 2009). The balance between protein synthesis and degradation is important for cellular homeostasis. Proteostasis or protein homeostasis is controlled by protein synthesis, subcellular location, folding and degradation (Benarroch, 2009, Ciechanover, 2013, Ciechanover and Kwon, 2015). There are two major protein degradation systems in cells; the ubiquitin proteasome system (UPS) and autophagy-lysosome pathway (ALP) (Chen and Yin, 2011, Knecht et al., 2009). Suppression of protein degradation pathways leads to aggregation and accumulation of damaged, misfolded or unwanted proteins, which, if unresolved, leads to proteotoxicity and numerous physiological and pathological conditions, resulting in cellular dysfunction or death (Cuanalo-Contreras et al., 2013). The UPS is the major intracellular pathway for degradation of unwanted small soluble proteins (Carvalho et al., 2013, Sadowski et al., 2012).

The connection between the UPS and neurodegenerative diseases began with the identification of ubiquitinated proteins in their hallmark protein inclusions (Bedford et al., 2008, Bedford et al., 2009). Neurodegenerative diseases are identified as protein misfolding diseases or protein conformational disorders, and are characterized by progressive degeneration of specific neurons together with the formation of abnormal protein inclusions (Hamilton and Zito, 2013, Tutar et al., 2013). Neurofibrillary tangles and amyloid plaques are found in Alzheimer's disease (AD), Lewy bodies (LBs) in Parkinson's disease (PD), Bunina bodies in amyotrophic lateral sclerosis (ALS), and nuclear and cytoplasmic inclusions in polyglutamine expansion disorders such as Huntington’s disease (HD) and spinocerebellar ataxia (Layfield et al., 2005, Paine et al., 2011, Paine et al., 2013). The underlying mechanisms of protein aggregation and neurodegeneration remain unclear. Since these disorders share protein aggregation, it is possible that they also share molecular and cellular mechanisms of

pathogenesis leading to neurodegeneration (Ciechanover and Brundin, 2003, Ciechanover and Kwon, 2015). It is possible that dysfunction of the UPS or structural changes that prevent the recognition and degradation of protein substrates contributes to neurodegenerative disease (Huang and Figueiredo-Pereira, 2010, Hegde and Upadhya, 2011). Ubiquitinated proteins were first detected in neurofibrillary tangles (NFT) in the brain of patients with AD (Mori et al., 1987). Further support for a role of the UPS in disease pathogenesis was provided by the identification of mutations in Parkin, an E3 ubiquitin protein ligase, in autosomal recessive juvenile PD (Kitada et al., 1998, Bedford et al., 2008). McNaught and colleagues (2002) reported that systemic administration of pharmacological 20S proteasomal inhibitors lead to Parkinson-like neuropathological and behavioural changes in rodents (McNaught et al., 2002). A further significant study in 2008, involving genetic disruption of the 26S proteasome in forebrain and substantia nigra neurons of mice, showed 26S proteasome dysfunction caused neurodegeneration and the formation of Lewy-like inclusions resembling dementia with Lewy bodies (DLB) and PD respectively (Bedford et al., 2008a). In addition, extensive studies have shown the importance of the UPS in neuronal development and morphogenesis (Hamilton and Zito, 2013).

1.2 The ubiquitin proteasome system

The UPS is a complex and tightly regulated system for controlling ubiquitination and degradation of abnormal (misfolded or damaged) as well as normal unwanted proteins (Glickman and Ciechanover, 2002). This is the major intracellular pathway for the degradation of 80-90% of unwanted soluble short-lived proteins (Sorokin et al., 2009). The UPS proceeds in two steps: covalent attachment of multiple ubiquitin molecules to the unwanted protein substrate (ubiquitination) and then degradation of the ubiquitinated protein by the 26S proteasome complex with the

release of free recyclable ubiquitin (Glickman and Ciechanover, 2002).

1.2.1 Ubiquitin and ubiquitination

Ubiquitin (Ub) is 76 amino acid residues and carries out its functions via covalent attachment to other cellular proteins, changing their stability, localization and activity in a process termed 'ubiquitination' (Pickart and Eddins, 2004, Ciechanover and Brundin, 2003). Ubiquitination is a post-translational modification forming an isopeptide bond between the C-terminal glycine of Ub and the ε-amino group of a lysine in the protein substrate (Chau et al., 1989). Proteins can be ubiquitinated on a single or several lysine residues (Figure 1.1), resulting in mono- or multi-ubiquitination respectively (Petroski and Deshaies, 2005, Pickart and Eddins, 2004). In addition, Ub can form polyubiquitin chains using its seven lysine residues (Figure 1.1): K6, K11, K27, K29, K33, K48 and K63 (Peng et al., 2003). Different modes of ubiquitination lead to different substrate fates (Figure 1.1). For example, K48-linked polyubiquitination is associated with 26S proteasomal degradation. K63-linked polyubiquitination is involved in signal transduction, DNA repair and processing through the endosome-lysosome pathway (Chan and Hill, 2001, Abbott et al., 2007, Kravtsova-Ivantsiv and Ciechanover, 2012). Mono-ubiquitination has been shown in vitro to be sufficient for receptor endocytosis (Reggiori and Pelham, 2001, Sigismund et al., 2005).

Three enzymes are involved in the process of protein ubiquitination: Ub-activating (E1), Ub-conjugating (E2) and Ub-ligating (E3) (Figure 1.2) (Scheffner et al., 1995). First the Ub protein is activated via the E1 Ub-activating enzyme, forming a thioester bond between the C-terminus of Ub and the catalytic cysteine of E1 in an adenosine triphosphate (ATP)-dependent step. Activated Ub is then transferred from the E1 to the catalytic cysteine of an E2 Ub-conjugating enzyme. The E2-Ub conjugate then cooperates with an E3 Ub ligase to transfer Ub to the unwanted protein substrate. The E3 catalyses covalent attachment of Ub to the substrate protein, forming an isopeptide bond between

a lysine residue of the substrate and the C-terminal glycine of Ub (Sadowski et al., 2012, Ciechanover, 2013). Polyubiquitinated substrates are recognized by the 26S proteasome (Bedford et al., 2010). Deubiquitinating enzymes (DUBs) are involved in the removal of ubiquitin from protein substrates and break down of polyubiquitin chains (Figure 1.2) (Peng et al., 2003). Ub molecules are recycled for further signalling (Liu and Jacobson, 2013).

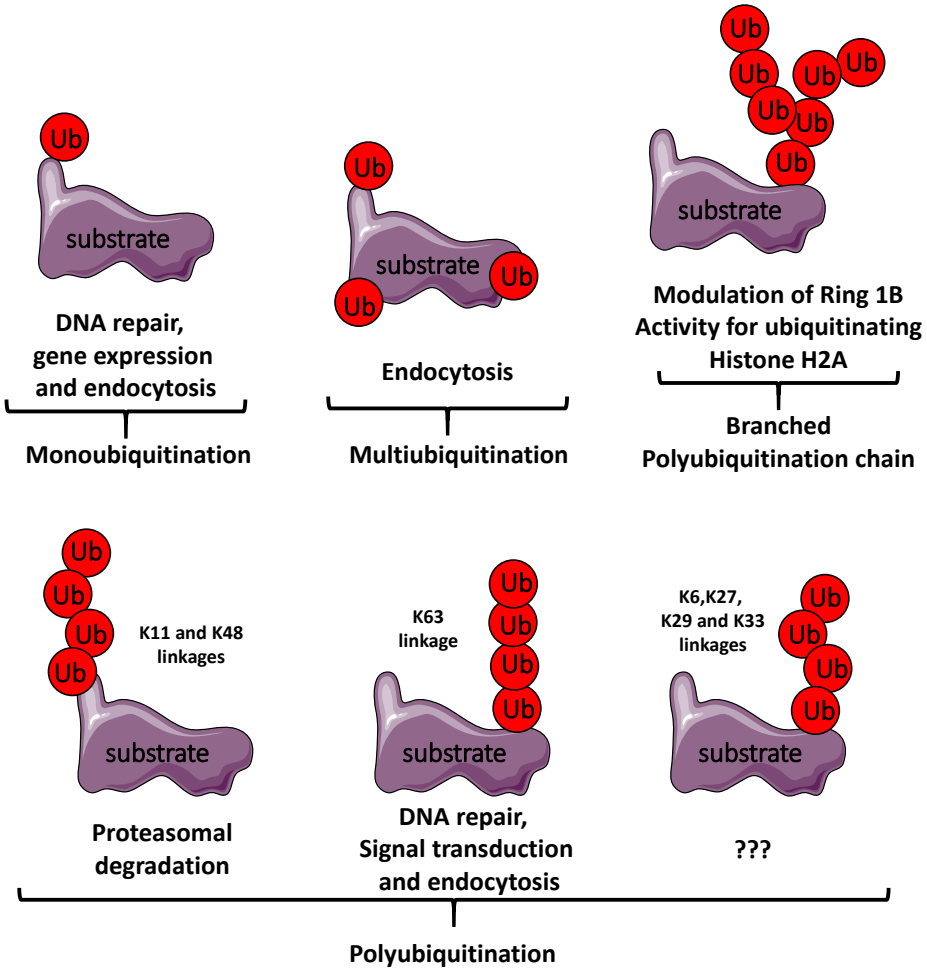


Figure 1.1 Different modes of ubiquitination lead to different substrate fates.

The versatility of Ub in regulating different processes is derived from its ability to be linked to proteins as a monomer on one (monoubiquitination) or more (multiubiquitination) lysine residues of a substrate or as a polymer (polyubiquitination) by the sequential addition of Ub to each other (Sadowski et al., 2012).

1.2.2 26S proteasome structure and assembly

The 26S proteasome is a large protein degradation machine that consists of two multi-subunit complexes (Figure 1.3); the catalytic

20S core particle (CP) of approximately 700 kDa and the 19S regulatory particle (RP) of approximately 900 kDa (Saeki and Tanaka, 2012, Hamazaki et al., 2007). The 26S proteasome is an essential intracellular proteolytic system found in both the cytoplasm and nucleus of all eukaryotes (Sorokin et al., 2009). Understanding the molecular mechanisms involved in the assembly of the 26S proteasome is important for protein degradation as well as regulation of proteasome activity (Murata et al., 2009).

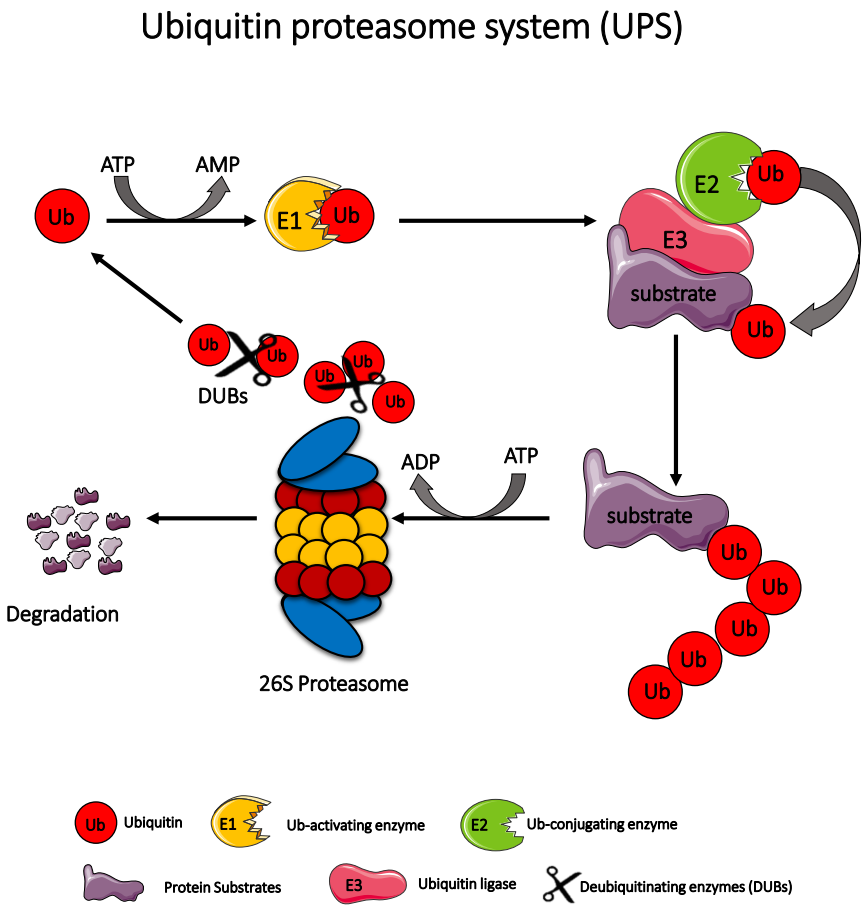


Figure 1.2 The ubiquitin proteasome system.

Free Ub is generated from the processing of Ub precursors or polyubiquitin chains by DUBs. An enzymatic cascade, involving E1, E2, and E3 enzymes, forms covalently conjugated K48-linked polyubiquitin chains on target proteins. The ubiquitinated protein substrate is recognized by the 26S proteasome, which unfolds and removes the Ub prior to hydrolysis of the protein in the 20S core particle.

1.2.2.1 The 20S core particle

The 20S proteasome (Figure 1.3) is the proteolytic core particle of the 26S proteasome (Sorokin et al., 2009). This complex is a barrel-like or cylindrically-shaped structure containing 28 subunits ranging in size between 20 and 35 kDa, and has a molecular weight of 700-750 kDa (Voges et al., 1999, Ciechanover and Schwartz, 1998, Dahlmann, 2005). The cylindrical core particle consists of four stacked heptameric rings; two outer alpha-type (α) surrounding two inner

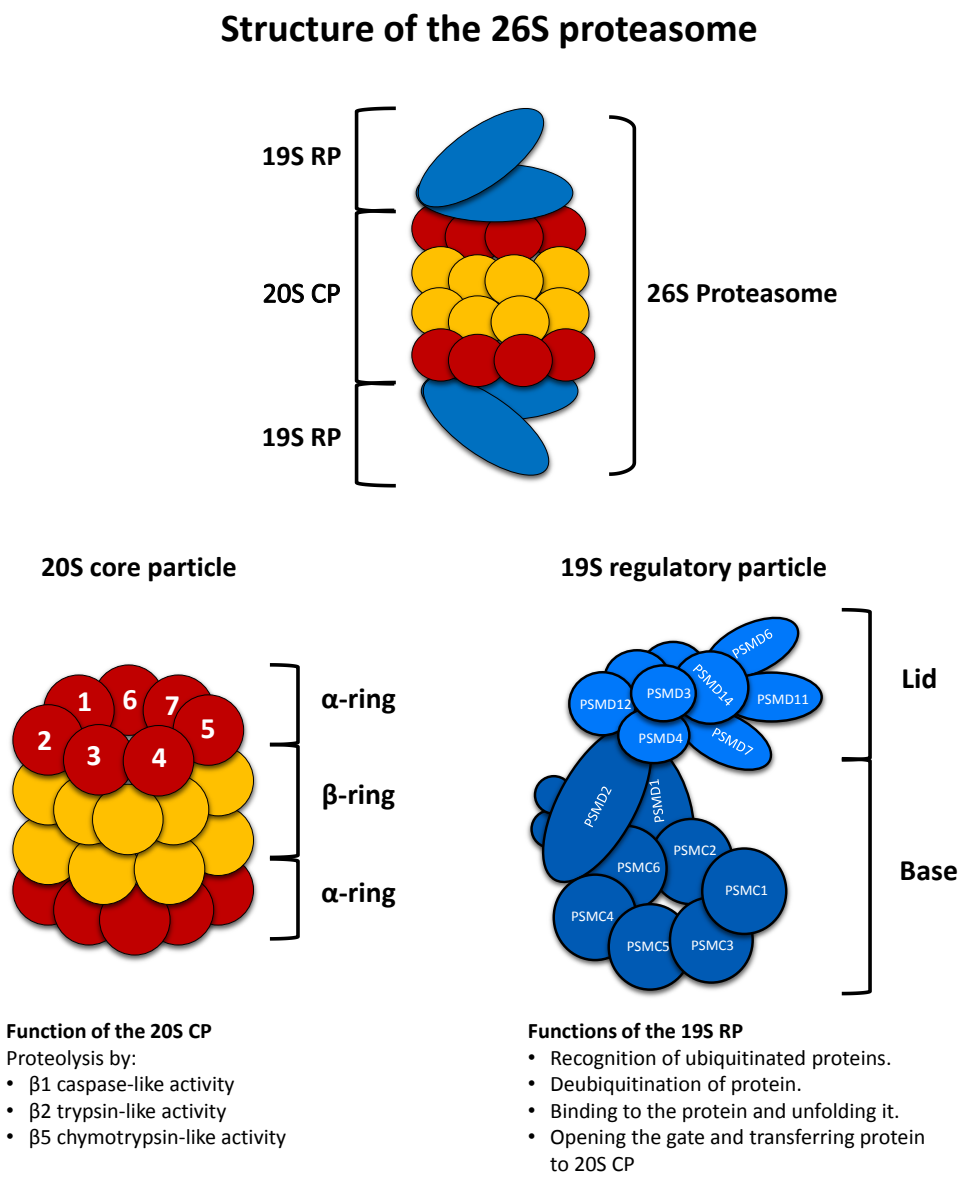


Figure 1.3 Structure of the 26S proteasome.

The 26S proteasome comprises two sub-complexes; the 20S catalytic core particle (CP) and the 19S regulatory particle (RP).

beta-type (β) rings, each of which is made of seven α and β subunits in an α1-α7, β1-β7 arrangement (Figure 1.3) (Sorokin et al., 2009, Voges et al., 1999). The β-rings contain the catalytic activity of the 20S proteasome; namely the β1, β2 and β5 subunits. The β1 subunit has caspase-like activity; hydrolysing peptide bonds after negatively charged amino acid residues. Subunit β2 has trypsin-like activity, hydrolysing peptide bonds after positively charged amino acid residues. The β5 subunit has chymotrypsin-like activity that hydrolyses peptide bonds after large hydrophobic amino acid residues. Two pairs of the three active sites face the interior of the 20S CP (Saeki and Tanaka, 2012, Glickman, 2000, Bar-Nun and Glickman, 2012). The α-rings act as a gate for entry into the narrow inner 20S proteolytic chamber. The gate is formed from the N-terminal residues of the α-subunits; namely α2, α3 and α4 subunits, and opening of the gate is controlled by docking of the 19S RP (Hegde and Upadhya, 2011, Sorokin et al., 2009).

1.2.2.2 20S core particle assembly

The assembly of the 20S CP starts with the formation of a ring of α-subunits by four chaperones; PAC (proteasome assembly chaperone) 1–4 in mammalian cells and Pba (proteasome biogenesis associated protein) 1–4 in yeast (Le Tallec et al., 2007). These chaperones form a pair of heterodimers; PAC1–PAC2 and PAC3–PAC4, which cooperate with each other to play a key role in the assembly of the α ring and half-proteasomes. Studies suggest that the PAC3–PAC4 heterodimer has important functions at the early stage of α ring assembly, which starts with the formation of a PAC3–PAC4–α5 tertiary complex, and assists in the recruitment and ordering of neighbouring α subunits (Le Tallec et al., 2007, Bedford et al., 2010). Furthermore, this tertiary complex binds to the surface of the α ring where the β subunits are assembled, and cannot bind to α rings that contain β4 because of steric hindrance between β4 and PAC3 (Bedford et al., 2010). The PAC1–PAC2 heterodimer can bind the α5 and α7 subunits to promote α ring formation and prevents aberrant dimerization of the α rings. After completion of CP assembly, the PAC1–PAC2 complex is degraded

by the newly formed CP (Hirano et al., 2005). Following α ring assembly, the β subunits are incorporated onto the α ring at their specific positions in a defined order. β ring assembly begins with the incorporation of the β2 subunit to the α ring, followed by β3, β4, β5, β6, β1 and finally β7 (Saeki and Tanaka, 2012). The fifth CP-chaperone (Ump1/POMP) is encoded by the Ump1 gene and also called proteasome maturation protein (POMP). Ump1/POMP has a dual role in β ring formation and dimerization of half-CPs, but has no role in α ring formation. The Ump1/POMP protein prevents stable dimerization of two half-CPs until all seven β subunits are assembled on the α ring, creating the half-CP. The dimerization of two half-CPs depends on the incorporation of β7 into the half-mer, which consists of all β subunits except β7, and intercalation of the C-terminal tail of β7 in a surface groove between β1 and β2 subunits of the trans β ring. The correct dimerization of two half-20S proteasomes is followed by degradation of Ump1/POMP and PAC1-PAC2. In general, all five chaperones aid in the formation of the 20S CP (Saeki and Tanaka, 2012, Bedford et al., 2010).

1.2.2.3 The 19S regulatory particle

The 19S regulatory particle (RP) is essential for recognition of ubiquitinated substrates, removal of the polyubiquitin chain, and unfolding and translocation of the protein substrate into the 20S CP for degradation (Figure 1.3) (Sorokin et al., 2009, Nandi et al., 2006). One or two 19S RPs attach to either end of the 20S CP forming RP1 CP- and RP2 CP-isoforms of the 26S proteasome (Murata et al., 2009, Sorokin et al., 2009). The 19S RP consists of at least 19 different subunits with molecular masses ranging from 10 to 110 kDa, and can be divided into two sub-complexes; the lid and the base (Figure 1.3) (Bar-Nun and Glickman, 2012). The base consists of a ring of six AAA-ATPase subunits known as PSMC1-PSMC6 in mammals or Rpt1-6 in yeast, together with four non-ATPase subunits; PSMD1, PSMD2, PSMD4 and ADRM1 in mammals or Rpn1, Rpn2, Rpn10 and Rpn13 in yeast (Saeki and Tanaka, 2012, Hegde and Upadhya, 2011, Husnjak et al., 2008). The base AAA-ATPase subunits facilitate protein unfolding and interact

directly with the 20S α-ring, opening the narrow 20S pore via their C-terminus (Sorokin et al., 2009, Husnjak et al., 2008). Rpn1 and Rpn2 are the largest proteasomal subunits that are stacked in the non-ATPase subunit ring and involved in gate opening. The Rpn10 and Rpn13 subunits are located on the periphery of the 19S complex and connect the lid and base sub-complexes. These subunits maintain structural integrity of the 26S proteasome as well as recognition and processing of the ubiquitinated substrate (Husnjak et al., 2008). The lid is composed of nine non-ATPase subunits; PSMD3, PSMC3, PSMD12, PSMD6, PSMD7, PSMD13, PSMD14, PSMD8 and DSS1 in mammals or Rpn3, Rpn5, Rpn6, Rpn7, Rpn8, Rpn9, Rpn11, Rpn12, and Rpn15 in yeast (Figure 1.3) (Lander et al., 2012). The lid is connected to the base complex by interactions between Rpn12 and Rpn2, and between Rpn11 and Rpn1. Rpn10 may be involved in stabilizing these interactions (Henke et al., 1999).

1.2.2.4 19S regulatory particle assembly

In yeast the lid and base sub-complexes of the 19S RP appear to assemble independently; how these complexes are assembled in mammals from their individual subunits is not well understood (Murata et al., 2009). The base complex is made up of six AAA-ATPase subunits and four non-ATPase subunits. The six ATPase subunits are thought to form a ring structure that binds to the α rings of the CP (Figure 1.3). The assembly of this structure is a highly ordered process involving four chaperone proteins; Nas2/p27, Nas6/gankyrin/p28, Rpn14/PAAF1 and Hsm3/S5b (yeast/mammals; miscellaneous nomenclature). The C-terminal domains of these chaperone proteins are involved in protein–protein interactions with subunits of the AAA-ATPase ring; Nas2 binds the C-terminal tail of Rpt5, Nas6 binds that of Rpt3, Rpn14 of Rpt6 and Hsm3 binds that of Rpt1 (Saeki and Tanaka, 2012). Because the C-termini of Rpt subunits are used for docking with the 20S CP, these chaperones prevent premature binding of the Rpt subunits to the α rings of the CP.

The mechanisms of assembly of the lid of the 19S RP are still poorly understood. The lid is composed of nine non-ATPase subunits as described in section 1.2.2.3. The assembly of the lid complex is thought to be a multistep process that begins with assembly of Rpn5, 6, 8, 9 and 11 to form a core module; joined by a second module containing Rpn3, 7 and 15. Genetic studies have suggested that the Hsp90 chaperone plays an important role in lid complex assembly (Bedford et al., 2010, Murata et al., 2009, Saeki and Tanaka, 2012).

26S proteasomal dysfunction in neurons has been implicated in neurodegenerative diseases such as Parkinson's disease (Bedford et al., 2008), but a causal relationship has not been confirmed. Cytoskeletal changes are also thought to play a key role in dopaminergic neuron degeneration in PD (Cartelli et al., 2013). The relationship between cytoskeletal disturbances and neurodegeneration remains unclear and is a subject of interest to understand processes involved in neurodegenerative disease.

1.3 Cytoskeleton changes in neurodegenerative disease

The cytoskeleton is a complex network of protein fibres that controls the shape of neurons in nervous tissue. It is essential for structural support, movement of organelles and separating chromosomes during the cell division (Monteiro et al., 2011). The neuronal cytoskeleton is composed of three classes of protein polymers called microfilaments (MFs), neurofilaments (NFs), and microtubules (MTs) (Figure 1.4); each formed by the self-association of protein subunits.

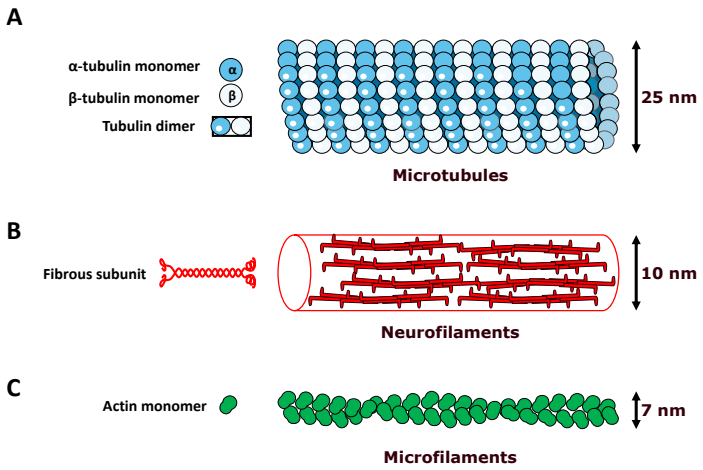


Figure 1.4 The cytoskeleton.

The cytoskeleton consists of microtubules (A), intermediate filaments (B) and microfilaments (C).

1.3.1 Microfilaments

Actin plays an essential role in morphological development of neurons as well as structural changes in the mature neuron (Kirkpatrick et al., 1999). Actin is a globular protein and its monomeric form is known as globular actin (G-actin). Actin is polymerized in long chains intertwined in a helix, generating filaments known as filamentous actin (F-actin). The distribution of both G-actin and F-actin are controlled and regulated by a large number of actin-interacting proteins that modulate the assembly and disassembly of actin filaments in the cell (dos Remedios et al., 2003). Development of axons and dendrites is led by a specialized end known as the growth cone, which is composed from finger-like filopodia and veil-like lamellipodia. In the neuron, actin filaments are concentrated as a meshwork with a large number of actin-binding proteins near to the plasma membrane; this forms the basis of the filopodia and lamellipodia that are essential for cell migration and the growth cone (Kirkpatrick et al., 1999). Actin is also involved in specialized microdomains of pre- and post-synaptic neurons on the cell surface (Kollins and Davenport, 2000, Schevzov et al., 2012).

Accumulation of actin and actin-binding proteins is associated with several neurodegenerative diseases, including Alzheimer's disease (Bamburg and Bernstein, 2016), amylotrophic lateral sclerosis (Griffin et al., 2014) and parkinsonism-dementia complex (Sousa et al., 2009). Hirano bodies have also been associated with general aging (Hirano, 1994). Rod-like structures containing cofilin, actin-binding proteins and actin have been reported in cell (Minamide et al., 2000) and animal (Yao et al., 2010, Zhang et al., 2012) models of AD. Increased cofilin levels associated with decreased miRNA-103/107 led to cofilin rod formation in an AD mouse model (Yao et al., 2010). Also, neurodegeneration in Drosophila and tauopathy mouse models was associated with formation of actin-rich rod-like structures, and this neurodegeneration could be attenuated by reducing actin accumulation (Fulga et al., 2007).

1.3.2 Microtubules

Microtubules (MTs) are a component of the cytoskeleton and play a crucial role in organelle transport, axonal elongation and cellular architecture in neurons (Guzik and Goldstein, 2004). Neuronal MTs have a similar structure to other eukaryotic cell MTs (Kapitein and Hoogenraad, 2015). MTs are dynamic polymers of α/β-tubulin heterodimers. The α/β-tubulin dimers arrange end to end to form protofilaments (PFs); 13 of these PFs join laterally to form a hollow 25 nm diameter tube (Figure 1.5). Heterodimers are oriented in the same direction in MT; therefore, MTs have asymmetrical ends (Akhmanova and Steinmetz, 2008). The β-tubulin subunit is at the 'plus (+)' end; where tubulin dimers join, and the α-tubulin subunit at the 'minus (-)' end, which grows more slowly (Mitchison and Kirschner, 1984b). Both MT ends can grow and depolymerize; however, the dynamics of the ends are very different (van der Vaart et al., 2009). The plus end (Figure 1.5) is a crucial site for regulating MT dynamics, growing faster and undergoing catastrophe more frequently (Akhmanova and Steinmetz, 2008). In contrast, microtubule minus ends are usually clustered and

anchored at a central microtubule-organizing center (MTOC), which hinder their dynamics (Goodwin and Vale, 2010).

MTs are characterized by switching between catastrophe (depolymerization or shrinkage phase) and rescue (polymerization or growing phase) in a process named dynamic instability (Duncan et al., 2013, Howard and Hyman, 2003). MT dynamics is regulated by the intrinsic properties of tubulin dimers as described in Figure 1.5. Free tubulin binds guanosine-5`-triphosphate (GTP), which (for β-tubulin) is hydrolysed to GDP shortly after incorporation into the MT network (Rice et al., 2008, Wang and Nogales, 2005). Because GDP tubulin tends to destabilize the MTs, stable growth is dependent on the presence of a cap of GTP-tubulin at the MT plus end, and loss of this cap will result in rapid disassembly (Rice et al., 2008). Unlike β-tubulin, α-tubulin usually contains a non-hydrolysable GTP (Figure 1.5), which is buried at the intradimer interface where it plays a structural role (Quiniou et al., 2013).

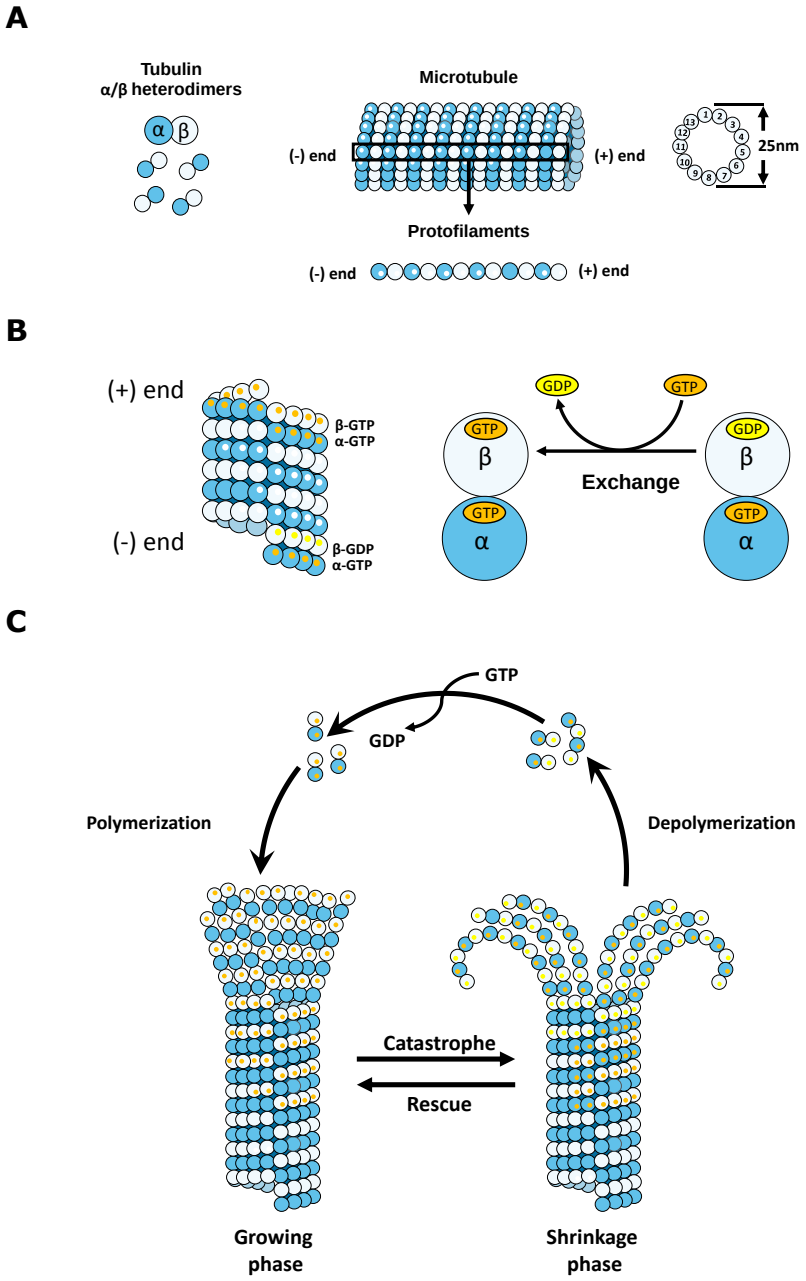


Figure 1.5 Microtubules - structure and dynamics.

(A) Microtubules are assembled from α/β-tubulin dimers, which associate head-to-tail to form linear protofilaments (boxed area). 13 protofilaments associate laterally to form the walls of the microtubule cylinder; diameter of ~25 nm. (B) Conformational change of α- and β-tubulin accompanying GTP hydrolysis. In the GTP state (β-tubulin; orange), α- and β-tubulin monomer interfaces result in a 'straight' tubulin dimer. In the GDP state (β-tubulin; yellow) the dimer interface is curved, leading to a 'bent' tubulin dimer. (C) The binding, hydrolysis and exchange of GDP/GTP on the β-tubulin monomer is the driving force for transitions between growth and shrinkage phases.

1.3.2.1 Tubulin isotypes

Both α- and β-tubulin exist as numerous isotypes, differing in their amino acid sequences and encoded by a family of six to seven functional genes (Sullivan and Cleveland, 1986). These distinct polypeptide isotypes differ primarily in their carboxy-terminal variable domain (Ludueña, 1993). The C-terminal sequence is used to assign the β-tubulin gene products into seven distinct classes: βI, βII, βIII, βIVa, βIVb, βV, and βVI (Joshi and Cleveland, 1989). The β isotypes differ in their amino acid sequences and patterns of expression in cells and tissues (Sullivan and Cleveland, 1986). Specific tubulin isotypes are present in nerve cells, suggesting that these tubulin isotypes play important roles during neuronal differentiation (Boucher et al., 1994, Gozes and Sweadner, 1981). Distribution of β-tubulin isotypes in mouse primary cultured cortical neurons found that neurons expressed the βI, βII and βIII isotypes in both embryonic and adult mouse brains, but not express βIV or βV (Guo et al., 2011). βIII-tubulin is considered to be the major brain β-tubulin isotype, expressed in neurons in mammalian brain (Lee et al., 1990). A study using differentiating neuroblastoma cells found that βI-tubulin played a major role in cell viability, βII was required for neurite outgrowth, while βIII-tubulin protected neurons against free radicals and reactive oxygen species (Guo et al., 2010). The expression of neuron-specific βIII-tubulin has been previously linked to hypoxia, where HIF-1α was able to increase βIII-tubulin expression in Glioblastoma Multiforme (Katsetos et al., 2009) and A2780 cells (Raspaglio et al., 2014). In addition, the anti-oxidative activity of curcumin against hypoxia decreased βIII-tubulin in rat prefrontal cortex (PFC) neurons (Shen and Yu, 2008). β-tubulin mutations have been show to induce neurological neuropathy symptoms by inhibiting the binding of axonal transport protein kinesin to microtubules, disrupting the localization of kinesin in hippocampal neurons (Niwa et al., 2013).

Six functional genes encode α-tubulin isotypes in mammals (Ludueña, 1993). αIII-tubulin is highly expressed during

development then deceases at postnatal and adult stages (Gloster et al., 1994, Miller et al., 1987). A previous study indicated that the α1-tubulin gene encodes a prominent neuronal and glial α-tubulin and that its expression has different functions in these cell types (Przyborski and Cambray-Deakin, 1996). Mutations in single tubulin isotypes have been linked to neurodevelopmental disorders due to imbalance in the levels of tubulins as a result of a lack of incorporation of mutant isoforms into the MT architecture or dynamics of the MT (Tischfield and Engle, 2010). Mutations in α-tubulin can affect the migration of neurons, leading to abnormal lamination of brain structures and behavioural deficits in mice (Keays et al., 2007).

1.3.2.2 Dynamic instability

Microtubules are in a balance between assembly and disassembly. Switching between growing and shrinking phases is known as 'dynamic instability' (Mitchison and Kirschner, 1984a). The dynamic state is highly sensitive to the concentration of free tubulin dimers at the MT plus end (Desai and Mitchison, 1997, Howard and Hyman, 2003). Low tubulin concentration promotes MT disassembly and shrinkage; whilst high tubulin concentration promotes MT assembly and rescue, or inhibits catastrophe (Howard and Hyman, 2009). MTs can continue to grow as long as the free tubulin concentration is above a critical level. The critical concentration of free tubulin at the minus end is higher than at the plus end; therefore, the minus ends tend to stop growing first (Al-Bassam and Chang, 2011). The ends of MTs grow randomly and MTs change between periods of tubulin subunit addition or growth and subunit loss or shrinkage, and pausing (Kerssemakers et al., 2006).

Many factors are known to affect dynamic instability. These include (1) the nature of tubulin isotypes and availability of tubulin heterodimers, (2) interactions with microtubule-associated proteins (MAPs), (3) post-translational modification (PTM) of tubulins, and (4) PTM of MAPs (Kurepa et al., 2012).

Loss of the balance between MT stabilization and destabilization is linked to pathologic conditions. Decreased microtubule stability has been observed in several neurodegenerative diseases, including AD and PD (Zhang et al., 2012, Cartelli et al., 2013). Hyperstable MTs are seen in hereditary spastic paraplegia (HSP) (Salinas et al., 2005).

1.3.2.3 Microtubules in neurodegenerative disease

Cytoskeletal dysfunction has been proposed as an important mechanism involved in the aetiology of several neurodegenerative diseases (D'Andrea et al., 2001). In vitro studies suggest that disassembly of MTs is an early event in PD pathology, followed by axonal transport impairment and mitochondrial damage in neurotoxin 1-methyl-4-phenylpiridinium (MPP+)-exposed PC12 cells (Cartelli et al., 2010). Treatment of PS19 tauopathy transgenic mice with the MT-stabilizer Epothilone D restored MT dynamics to baseline levels, reducing axonal dystrophy and cognitive deficits observed in these mice (Brunden et al., 2010). Since dopaminergic nigral neurons have very long axons projecting to the striatum, a high degree of cooperation between MTs and MT-dependent motor proteins is required to ensure transport of dopamine vesicles. Depolymerisation of MTs may lead to impaired dopamine transport and abnormal accumulation of dopamine vesicles in the soma of nigral neurons causing oxidative stress and eventually cell death (Parisiadou and Cai, 2010). Lewy bodies; the pathophysiological hallmark of PD, contain numerous proteins, including cytoskeletal proteins such as tubulin, MAPs and neurofilaments, as well as α-synuclein and ubiquitin (Liu et al., 2011, D'Andrea et al., 2001). We showed that decreased stathmin (STMN) accompanied neurodegeneration caused by 26S proteasome dysfunction in a mouse model resembling dementia with Lewy bodies (Elkharaz et al., 2013).

1.3.2.4 Post-translational modifications of tubulin

Post-translational modifications (PTMs) are reversible and change the properties of a protein by addition or removal of a chemical

group or another protein (Perdiz et al., 2011, Fukushima et al., 2009). These modifications affect the carboxy-terminal domain of α/β-tubulins, which is located on the outside of the microtubule and forms a readable code for microtubule-associated and motor proteins (Figure 1.6) (De Forges et al., 2012). Tubulin PTMs, including acetylation, tyrosination, detyrosination, Δ2 modification, polyglutamylation, polyglycylation, palmitoylation and phosphorylation have gained new interest for their role in neuronal differentiation and neurodegenerative disorders (Fukushima et al., 2009, Janke and Bulinski, 2011). PTMs of tubulin reflect the stability of MTs (Perdiz et al., 2011, Baas et al., 1993). In particular, α-tubulin acetylation takes place at the ends of MT and is mostly associated with stable MTs. Detyrosinated α-tubulin is often used as an indication of how long a MT has been assembled, while tyrosination is associated with young neurons and the most dynamic MT (Poulain and Sobel, 2010, Baas et al., 1993).

1.3.2.4.1 Tubulin acetylation

Acetylation of the α-tubulin subunit was found on lysine 40 (K40; Figure 1.6) of flagellar α-tubulin in Chlamydomonas reinhardtii (L'Hernault and Rosenbaum, 1985). K40 acetylation is on the MT lumenal surface (Soppina et al., 2012) and has no effect on the architecture of microtubules (Howes et al., 2014). Cryo-electron microscopy failed to find structural differences between acetylated and deacetylated MTs (Howes et al., 2014). Acetylation preferentially occurs on tubulin in MTs, and tubulin dimers are rapidly deacetylated when released from MTs (Perdiz et al., 2011). An acetylation site on β-tubulin at the tubulin dimer interface at lysine 252 (K252; Figure 1.6) has also been identified and shown to affect the polymerization kinetics of tubulin (Chu et al., 2011). As a result of its localization, K40 tubulin acetylation affects the binding of MT inner proteins, such as ribbons and calcium-binding (Rib) proteins (Linck et al., 2014). MT acetylation can also effect other protein interactions with MTs. Binding of heat shock protein 90 (Hsp90) to MTs was enhanced by acetylation, and recruiting

Hsp90 activated Akt and p53 (Giustiniani et al., 2009). In addition, MT acetylation can regulate intracellular transport by regulating the traffic of kinesin motors (Reed et al., 2006, Dompierre et al., 2007). In vitro, the binding affinity of kinesin-1 to MTs increases with increasing K40-acetylated α-tubulin (Reed et al., 2006). Stabilization of MTs in neurons by paclitaxel increased the levels of α-tubulin acetylation and detyrosination, and promoted accumulation of kinesin-1 in neurites (Hammond et al., 2010, Witte et al., 2008).

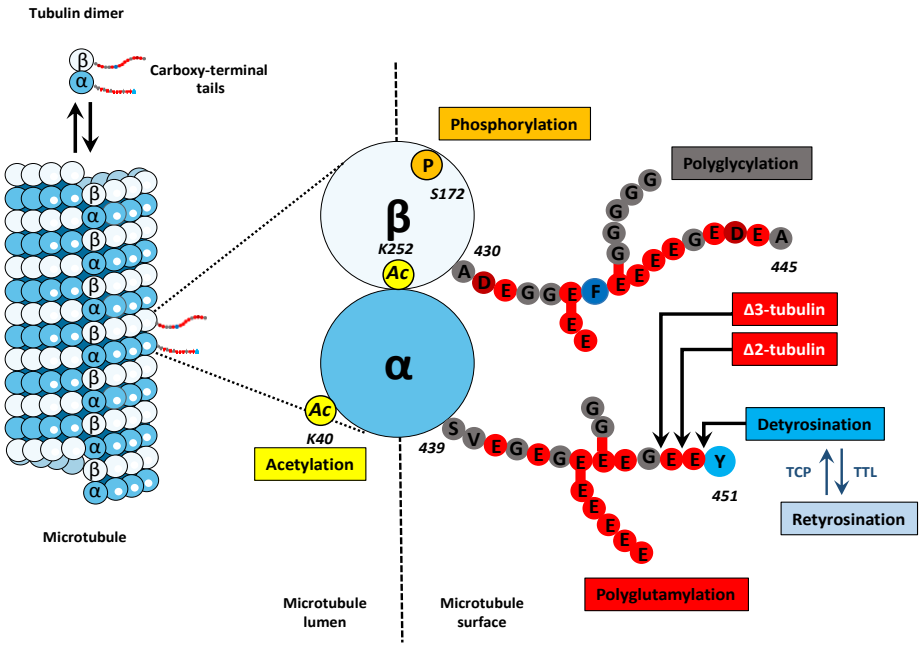


Figure 1.6 Molecular localization of tubulin posttranslational modifications.

Microtubules are assembled from α/β-tubulin dimers. The globular parts of the tubulins form the microtubule walls and luminal surface, while the carboxy-terminal tails decorate the outer surface of microtubules, where many MAPs and motors bind. PTMs are found on various regions of the tubulin dimer: the α-tubulin K40 acetylation site is found on the lumenal surface of MTs, while the K252 acetylation site of β-tubulin is at the boundary between α- and β-tubulin dimers. Phosphorylation at S172 in the globular, folded part of β-tubulin may influence assembly rates and stability of MTs. Detyrosination/tyrosination, Δ2- and Δ3-tubulin modulate the carboxy-terminal tails of α-tubulin. Tubulin detyrosination is driven by tubulin carboxypeptidase (TCP), while retyrosination requires the action of tubulin tyrosine ligase (TTL). The polyglutamylation and polyglycylation are found within the carboxy-terminal tails of both α- and β-tubulin. All modifications of the carboxy-terminal tails are likely to regulate interactions between microtubules and associated proteins.

Histone deacetylase family member 6 (HDAC6) and sirtuin 2 (Sirt2) enzymes are responsible for the removal of the K40 acetyl group (Hubbert et al., 2002, North et al., 2003). HDAC inhibitors were shown to be neuroprotective in Huntington's disease; inhibiting HDAC6 increased K40 acetylation of α-tubulin, leading to increased vesicular transport of brain-derived neurotrophic factor (BDNF) in effected neurons (Dompierre et al., 2007). αTAT1 is the major α-tubulin K40 acetyltransferase (Akella et al., 2010). Knockout mice lacking αTAT1 were less fertile as result of altered sperm morphology and motility (Kalebic et al., 2013). However, in αTAT1 knockout mice MTs were more resistant to nocodazole, suggesting increased MT stability (Kalebic et al., 2013).

1.3.2.4.2 Tubulin detyrosination/tyrosination

Most α-tubulin has a C-terminal tyrosine residue (Ludueña, 1993). The detyrosination–tyrosination cycle is initiated by removal of the C-terminal tyrosine (detyrosination; Figure 1.6) and retyrosination returns tubulin to its nascent state (Janke and Bulinski, 2011). Detyrosinated α-tubulin is mostly found on stable and long-lived microtubules in the neurons, suggesting this modification promotes microtubule stability (Robson and Burgoyne, 1989, Baas et al., 1993, Brown et al., 1992). The proximal segments of axon shafts are enriched in detyrosinated tubulin (Brown et al., 1993). In addition, tubulin detyrosination functions as a signal for the recruitment of intermediate filaments (Kreitzer et al., 1999). Tubulin detyrosination has an important role in regulating motor proteins; kinesin-1 binds more strongly to MTs enriched in detyrosinated α-tubulin (Konishi and Setou, 2009). Tyrosinated tubulin is enriched at growth cones and takes part in the relative arrangement of actin and MT cytoskeletons (Marcos et al., 2009).

Tubulin carboxypeptidase (TCP) is involved in detyrosination of α-tubulin and tubulin tyrosine ligase (TTL) in tyrosination (Figure 1.6) (Argarana et al., 1978, Hallak et al., 1977, Raybin and Flavin, 1975). Detyrosinated tubulin can be converted into Δ2-tubulin by

the irreversible removal of the penultimate glutamate residue of α-tubulin (Figure 1.6) (Janke and Kneussel, 2010). Depletion of TTL in hippocampal neurons using RNAi increased the levels of detyrosination in dendrites, leading to increased entry of kinesin-1 (Konishi and Setou, 2009). Another study showed that TTL can interact with both α- and β-tubulin (Prota et al., 2013). TTL binding to the tubulin dimer prevented its polymerization by capping the tubulin longitudinal interface, and TTL overexpression in vivo inhibited MT polymerization (Szyk et al., 2011). Stathmin (STMN1) is a MT regulatory protein that destabilizes MT by binding tubulin dimers, but can also regulate TTL function (Steinmetz, 2007). TTL and stathmin have partially overlapping binding sites and compete for binding on tubulin dimers (Szyk et al., 2013). TTL knockout mice show major developmental defects in the nervous system with accumulation of detyrosinated and Δ2-tubulin (Erck et al., 2005, Marcos et al., 2009). TTL is tubulin-specific; all observed defects in TTL knockout mice were directly related to deregulation of the microtubule cytoskeleton (Prota et al., 2013).

1.3.2.4.3 Other tubulin PTMs

Several other PTMs have been found on tubulin. Polyglutamylation and polyglycylation are PTMs in which glutamate or glycine side chains of variable lengths are formed at specific sites (Janke, 2014, Magiera and Janke, 2014). A glutamate residue located within the carboxy-terminal tail of α-tubulin has been shown to be modified by the attachment of polyglutamate side chains (Edde et al., 1990). Polyglycylation generates side chains of glycine residues within the C-terminal tails of α- and β-tubulin; the modification sites of glycylation are considered to be principally the same as for glutamylation (Figure 1.6) (Rogowski et al., 2009). Polyglutamylation is abundant in neurons, as well as cilia and centrioles (Audebert et al., 1994, Abal et al., 2005). In contrast to polyglutamylation, polyglycylation is restricted to ciliary tubulins (Sloboda, 2009).

Tubulin polyglutamylase enzymes are members of the TTL domain protein family, which add amino acids to tubulins through an RNA-independent enzymatic reaction (Janke et al., 2005). Different TTLs add glutamate or glycine to side chains initiated on one or more of the glutamates in the C-terminal domains of both α and β-tubulins (Janke et al., 2008, Mukai et al., 2009). Although high levels of polyglutamylation are evident in neuronal MTs, knockout of TTL1, the major polyglutamylase in brain, did not show lead to obvious neuronal defects in mice (Audebert et al., 1994, Janke et al., 2005, Ikegami et al., 2007, Ikegami and Setou, 2010). This suggests tolerance of neuronal MTs to variations in polyglutamylation. Increased polyglutamylation levels was shown affect kinesin-1–mediated transport in cultured neurons (Konishi and Setou, 2009).

Tubulin phosphorylation is another PTM that takes place at serine S172 of β-tubulin (Figure 1.6) (Gard and Kirschner, 1985, Caudron et al., 2010). Phosphorylation catalyzed by Cdk1 can inhibit tubulin polymerization and induce MT disassembly during cell division (Fourest-Lieuvin et al., 2006).

1.3.3 Microtubule-associated proteins

The polymerization, stabilization and dynamic properties of MTs are influenced by interactions with microtubule-associated proteins (MAPs) (Steinmetz, 2007). These proteins tend to have repeating tubulin binding domains, which allow each MAP to associate with more than one tubulin dimer (Maccioni and Cambiazo, 1995). The binding of these structural MAPs is controlled by kinases and phosphatases (Cassimeris and Spittle, 2001). During mitosis MAPs are phosphorylated and detach from tubulin; whose assembly and disassembly is controlled by proteins that operate more at the ends of MTs (Drewes et al., 1995). The best known MAPs with stabilizing activity are the heat-stable proteins MAP2 and tau; they are localized mainly in the dendritic and axonal compartments respectively, and share homologous repeats in the carboxy-terminal region that contribute to MT binding (Al-Bassam et al.,

2002, Zhang and Dong, 2012). MAP2 and tau oppose the action of stathmin (STMN), a common MT destabilizing protein in brain.

The MAP2/tau family consists of the neuronal proteins MAP2 and tau, and the non-neuronal protein MAP3/MAP4. Both MAP2 and tau appear to stabilize MTs in cells and facilitate the polymerization of tubulin in vitro (Hirokawa et al., 1996).

1.3.3.1 MAP2

MAP2 is found primarily in the dendritic extensions of post-mitotic, terminally differentiated neurons. MAP2 plays a critical role in neurite outgrowth and dendrite development (Sanchez et al., 2000) and MAP2 expression is considered a hallmark of neuronal differentiation (Megiorni et al., 2005). In human neurons there are four isoforms of MAP2 (MAP2a, MAP2b, MAP2c and MAP2d) resulting from alternative mRNA splicing of a single MAP2 gene (Shafit-Zagardo and Kalcheva, 1998). High molecular weight (280-270 kDa) MAP2 isoforms MAP2a and MAP2b are specifically expressed in neurons. Low-molecular weight (70-75 kDa) MAP2c and MAP2d are found mostly in glial cells (Dehmelt and Halpain, 2005). In the C-terminal region, both groups of isoforms have three or four repeated sequences of 18 amino acids, spaced by 13–14 amino acids that constitute the tubulin-binding domain (TBD), and a proline-rich region (PRD) that regulates its function (Figure 1.7) (Ferralli et al., 1994, Ludin et al., 1996).

MAP2 interacts with MTs through its tubulin-binding domain (TBD) and has important roles in neurite outgrowth, microtubule dynamics and organelle transport in axons and dendrites (Sanchez et al., 2000). MTs become stabilized as a consequence of MAP2 binding giving rise to longer polymers (Kowalski and Williams, 1993). MAP2 can also bind to actin through its tubulin-binding domain and promote microfilament stability as observed in dendritic spines (Fifkova and Morales, 1992). A previous study showed a role for MAP2 in regulating MFs and MTs, observing a transition from MFs to MTs during axonal growth of cultured rat hippocampal neurons (Kwei et al., 1998). MAP2 can also bind and

reassemble neurofilaments using domain sites different from the tubulin-binding domain (Heimann et al., 1985).

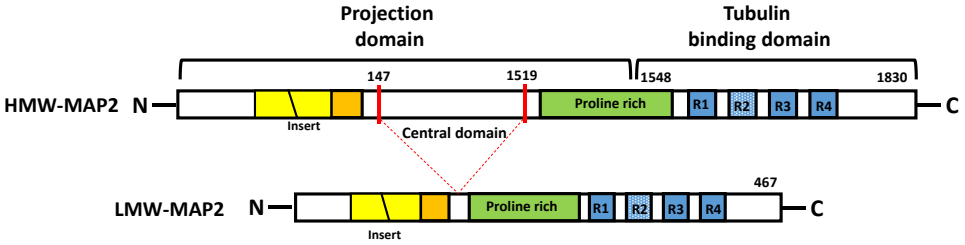


Figure 1.7 Structure of MAP2 isoforms.

Structure of MAP2 isoforms, which can be divided into two groups: high-molecular weight MAP2 (HMW-MAP2), including MAP2a and MAP2b, and low-molecular weight MAP2 (LMW-MAP2), including MAP2c and MAP2d. LMW-MAP2 contains the N- and C-terminal regions of HMW-MAP2 linked together, but lacks the central domain (CD). Both groups of isoforms have either three or four repeated sequences that constitute the tubulin-binding domain. Additionally, all isoforms have a proline-rich region (PRD) preceding the tubulin-binding domain. Finally, a sequence of 31 amino acids in the N-terminal region of MAP2 constitutes the binding region for regulatory protein and kinase.

MAP2 has a large number of serine and threonine phosphorylation sites located in the PRD and TBD (Hernandez et al., 1987, Silliman and Sturgill, 1989). The phosphorylation state of MAP2 has an important role in regulating its binding to microtubules (Yamamoto et al., 1988). Several kinases, including glycogen-synthase kinase 3 (GSK3), cyclin-dependent kinases (CDKs) and microtubule-affinity-regulating kinases (MARKs), have been identified that phosphorylate MAP2 at specific sites in the PRD and TBD (Malmendal et al., 2003, Sanchez et al., 2000). High levels of phosphorylation decrease the association of MAP2 with tubulin (Quinlan and Halpain, 1996). MAP2 isoforms are the substrates for the activated calpain, which can alter MAP2-tubulin association and inhibit microtubule assembly through MAP2 degradation (Fifre et al., 2006, Springer et al., 1997). MAP2 is also linked to the UPS and contributes to cytotoxicity following proteasome inhibition by increasing MT stabilization (Poruchynsky et al., 2008)

MAP2 plays an important role in maintaining dendritic structure through its interaction with MTs, stabilizing and spacing mature MT

bundles in the dendrite (Teng et al., 2001). Loss of MAP2 immunoreactivity across several cortical regions has been closely linked to dendritic spine pathology in schizophrenia brain tissue (Shelton et al., 2015). In addition, a reduction in dendritic length was observed in MAP2 deficient mice (Harada et al., 2002), and MAP2 depletion in primary cultured neurons prevented dendritic differentiation (Farah and Leclerc, 2008). A recent study in AD brain tissue showed that tau and MAP2 have different fates in inclusion formation, raising the possibility of a pathoetiological role of MAP2 in the generation of AD and tauopathies (Xie et al., 2014). Amyloid beta toxicity in AD brain tissue mainly localizes to the somatodendritic area where MAP2 is located (Xie et al., 2015, Xie and Miyasaka, 2016).

1.3.3.2 Tau

Tau is a MT stabilizing protein, promoting tubulin assembly into MTs (Drechsel et al., 1992). Tau is found primarily in neurons, where its phosphorylated isoforms bind to tubulin to promote polymerization and stabilization of axonal MTs (Billingsley and Kincaid, 1997). Abnormal phosphorylation of tau is associated with Alzheimer's disease and other neurodegenerative disorders (Goedert et al., 1992). In the adult human brain there are six isoforms of tau: 0N3R, 0N4R, 1N3R, 1N4R, 2N3R and 2N4R, produced by alternative mRNA splicing of the microtubule-associated protein tau gene (Figure 1.8). The microtubule-binding domains (3R and 4R) are located at the carboxyl terminal of tau and consist of three or four 31 amino acid repeats (Mandelkow and Mandelkow, 2012) (Figure 1.8).

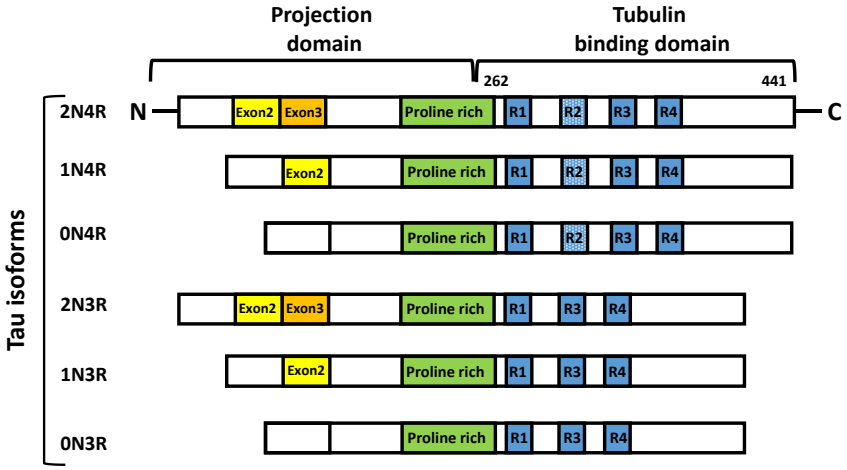


Figure 1.8 Structure of tau isoforms.

Six tau isoforms are shown. Tau isoforms differ by the presence or absence of one or two 31 amino acid inserts encoded by exon 2 (yellow) and 3 (orange) in the N-terminal region, in combination with either three (R1, R3 and R4) or four (R1-R4) repeat regions in the C-terminal region. The R2 repeat is encoded by exon 10. The tubulin-binding domain is indicated in blue; depending on inclusion of exon 10 there are tau isoforms with 4 (4R) or 3 (3R) tubulin-binding regions. All isoforms have a proline-rich region (PRD) preceding the tubulin-binding domain.

Human tau has more than 80 serine/threonine phosphorylation sites and 5 potential tyrosine phosphorylation sites (Stoothoff and Johnson, 2005). Phosphorylation plays an important role in regulating the activity of tau; balanced by kinase and phosphatase activity. In normal neurons low phosphorylation levels of tau are associated with its interaction with tubulin, promoting tubulin assembly and stabilizing the MT structure. Abnormal hyperphosphorylation of tau decreases the interaction of tau with MTs and inhibits their assembly, perturbing axonal transport (Abraha et al., 2000, Cho and Johnson, 2003, Hutton et al., 1998). When detached from MTs, tau can self-aggregate into insoluble aggregates through its hexapeptide motifs in the repeat domain (Iqbal et al., 2009). Tau deposition in the form of intraneuronal filaments is a pathological hallmark of a variety of neurodegenerative diseases known as tauopathies (Schraen-Maschke et al., 2008). Tauopathies include Alzheimer's disease (AD), fronto-temporal dementia with parkinsonism on

chromosome-17 (FTDP-17), Pick's disease and Huntington's disease (HD) (Wolfe, 2012).

The major pathological characteristics of AD are senile plaques and neurofibrillary tangles (NFT) formed of amyloid beta and tau respectively (Arriagada et al., 1992). In human brain, senile plaques are detected earlier than NFT in the neocortex of patients, suggesting amyloid beta is an upstream causative factor in the pathogenesis of AD (Hardy and Selkoe, 2002, Rapoport et al., 2002). In a mouse model of tauopathy, expression of aggregation-prone tau causes morphological and functional deficits in neurons (Mocanu et al., 2008, Sydow et al., 2011a). In addition, these mice showed impaired learning and memory, and loss of long-term potentiation (Sydow et al., 2011a, Sydow et al., 2011b). These defects were reversible after switching off the toxic tau protein. A previous study showed the levels of tau in the brain cytosol from AD cases was altered; the levels of normal tau were significantly reduced in AD brain, with increased abnormally phosphorylated tau (Khatoon et al., 1994).

A pathological link between tau degradation/aggregation and the UPS was shown by frequent co-localization and accumulation of Ub protein with NFTs (Lee et al., 2013, Chesser et al., 2013). A previous study indicated that the proteasome was responsible for degrading tau (David et al., 2002). Evidence of UPS-mediated tau degradation came from delayed tau degradation when tau was transiently overexpressed in the presence of the proteasome inhibitor lactacystin (Zhang et al., 2005). In addition, proteasome inhibition increased the accumulation and insolubility of tau independent of its phosphorylation state in rat brain (Liu et al., 2009). Tau can be degraded in a Ub-independent manner under normal conditions, but under certain stress conditions, tau is actively ubiquitinated by CHIP and removed by the 26S proteasome (Wang and Mandelkow, 2012). CHIP (C-terminus of HSC70 (heat-shock cognate 70)-interacting protein) is a tau E3 ligase and, together with the E2 UbcH5B, was found to ubiquitinate tau and

mediate its degradation (Petrucelli et al., 2004, Shimura et al., 2004). Overexpression of CHIP in the rat hippocampus enhanced tau degradation and deletion of CHIP in mice caused accumulation of hyperphosphorylated tau (Shimura et al., 2004). Additionally, it has been shown that the hyperphosphorylation status of tau makes tau a less efficient substrate of the proteasome (Ren et al., 2007).

1.3.3.3 Stathmin

Stathmin (STMN) is the most prominent member of a family of MT destabilizing proteins that play critical roles in destabilizing microtubules by binding tubulin dimers (Belmont and Mitchison, 1996). This MT destabilizer family, known also as the STMN family of proteins, which includes superior cervical ganglion protein 10 (SCG10 or STMN2), SCG10-like protein (SCLIP or STMN3), and stathmin-like protein B3 (RB3 or STMN4) (Charbaut et al., 2001, Gavet et al., 2002). Each of the four STMN family proteins expressed from separate genes and shares a homologous tubulin-binding domain in their C terminus (Charbaut et al., 2001) (Figure 1.9). STMN is thought to act by two mechanisms: as a tubulin-sequestering molecule that reduces the concentration of tubulin available for assembly; and as a catastrophe promoter that stimulates MT depolymerization (Andersen, 2000, Steinmetz et al., 2001).

STMN1 is a soluble cytosolic phosphoprotein preferentially expressed in the nervous system and a wide range of tissues (Ozon et al., 1997). However, SCG10, SCLIP, RB3 and its splice variants, RB3' and RB3" are neuron-specific homologues of STMN localized to membranes in developing neurons (SCG10 and SCLIP) and (RB3, RB3', RB3") in mature neurons (Ozon et al., 1998, Gavet et al., 2002). MT destabilizing activity of STMN was down-regulated by phosphorylation at multiple sites (Steinmetz et al., 2001).

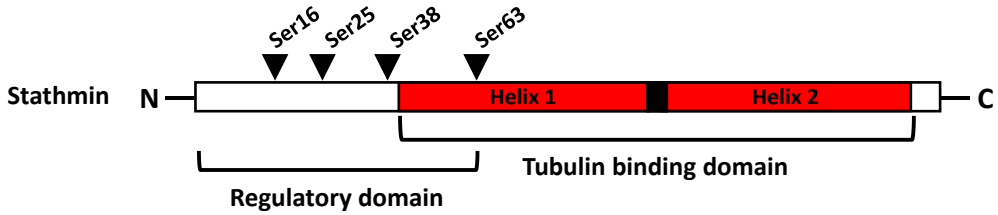


Figure 1.9 Microtubule-associated protein Stathmin

Schematic representation of domain organization of stathmin. N-terminal regulatory domain contains four serine residues as phosphorylation sites. The C-terminal interaction domain has two helical structures and interacts with two α/β-tubulin heterodimers

STMN was phosphorylated at N-terminal four serines residues (Ser 16, 25, 38 and 63; Figure 1.9) by both cell cycle-regulating and signal-transducing kinase systems (Cassimeris, 2002). All these four Ser phosphorylation sites of STMN1 are unchanged in SCG10 and SCLIP but RB3 have only one of these four sites, which corresponds to Ser 16 of STMN (Ozon et al., 1997). Phosphorylation of STMN Ser-16 or Ser-63 sites was sufficient to reduce tubulin binding and inhibits the ability of STMN to destabilize MTs in vitro (Larsson et al., 1997). However, phosphorylation of Ser25 and Ser38 have a moderate effect on destabilization of MTs and usually was a prerequisite for allowing phosphorylation of Ser16 and Ser63 in vivo (Honnappa et al., 2006). The phosphorylation of all four serine residues was required importantly to complete inhibit STMN activity in vitro (Honnappa et al., 2006). Different number of protein kinases are known to target specific STMN phosphorylation sites in vivo (Yip et al., 2014). Such as STMN Ser16 can be phosphorylate by PAK1, Calmodulin-dependent kinase II and IV and cAMP-dependent protein kinase (PKA) (Larsson et al., 1997, Stehbens and Wittmann, 2012). Whereas mitogen-activated protein kinases and cyclin-dependent kinases can phosphorylated Ser25 and Ser38 residues (Brattsand et al., 1994). The multisite phosphorylation of STMN can regulate STMN cell signalling mechanisms and MT stability (Yip et al., 2014).

STMN1 was involved in neural development, differentiation, plasticity, learning, degeneration and aging (Mori and Morii, 2002, Bohm et al., 2015). Alteration in mRNA and protein levels of STMN1 found in the developing, maturating, adult CNS of human and several species included chicken, mouse, and rat (Boekhoorn et al., 2014, Bohm et al., 2015, Chauvin and Sobel, 2015, Cheon et al., 2001, Jin et al., 1996, Liedtke et al., 2002, Saetre et al., 2011). The first evidence for an essential role of STMN in nervous system development came from RNAi silencing of the only STMN gene in Drosophila. This caused abnormal chordotonal neuron organization and loss of commissures in the ventral cord (Ozon et al., 2002).

STMN was also suggested to have a critical role in some of neurodegenerative disease pathology and in the neurofibrillary tangle (NFT) formation in the AD was associated with decreased STMN1 expression (Cheon et al., 2001, Jin et al., 1996). Reduced STMN expression was previously reported in the brain of AD and Down syndrome patients (Cheon et al., 2001), these reduced in STMN levels were suggested have accompaned AD pathology where total STMN was significantly reduced in the patient (Jin et al., 1996). These provocative findings suggest that total level of STMN and function was critical to normal brain function and reduced STMN expression can lead to dysregulation in a variety of neuropsychiatric and neurological disorders. A significant study by Liedtke and colleagues 2002 showed axonopathy of the central and peripheral nervous systems of STMN1 knockout mice with highly irregular axoplasm degeneration and dysmyelination (Liedtke et al., 2002). STMN1 was shown to play an essential role in the maintenance of axonal integrity; decreased STMN1 has a direct effect on depolymerisation of MTs, leading to the development of axonopathy (Wen et al., 2010). These studies support a role for MT changes in neurodegeneration. Moreover, a previous study in the conditional neuronal 26S proteasome knockout mouse model showed significantly decreased STMN1 levels associated with neurodegeneration and Lewy-like inclusions formation(Elkharaz et

al., 2013). In addition, previous study the effects of bortezomib on multiple myeloma cells, indicated that bortezomib-induced phosphorylation of STMN promotes cell death and that the bortezomib-induced changes in the MT stabilization can be attributed to the bortezomib-induced phosphorylation of STMN (Ge et al., 2010).

1.3.4 Stathmin regulator proteins

Along with the important role of STMN1 protein in microtubules destabilization, STMN1 was involved in cell signalling, acting as an intracellular relay of integrating diverse regulatory pathways in response to extracellular signals (Sobel et al., 1989, Chauvin and Sobel, 2015). STMN1 candidate as a downstream target of death and survival pathway whose activity could be affected by p53, p27 expression and PI3K-Akt pathway activation (Karst et al., 2011). These proteins p53, p27 and Akt were found to be degraded by the ubiquitin-proteasome pathway (Pagano et al., 1995, Shirane et al., 1999, Asher et al., 2005, Silveira et al., 2014)

1.3.4.1 p53

STMN1 is a p53-target gene (Johnsen et al., 2000, Fang et al., 2010). Previous study reported decreased STMN1 mRNA levels following induction of p53 by apoptotic insults such as UV irradiation (Murphy et al., 1999, Johnsen et al., 2000). The p53 can negatively regulate STMN1 expression at the level of both transcription and translation in a human cancer cell line (Fang et al., 2010). In addition to that decreased STMN expression can also inhibit p53 stability and its transcriptional activity as reported in a recent study in ovarian cancer (Sonego et al., 2013).

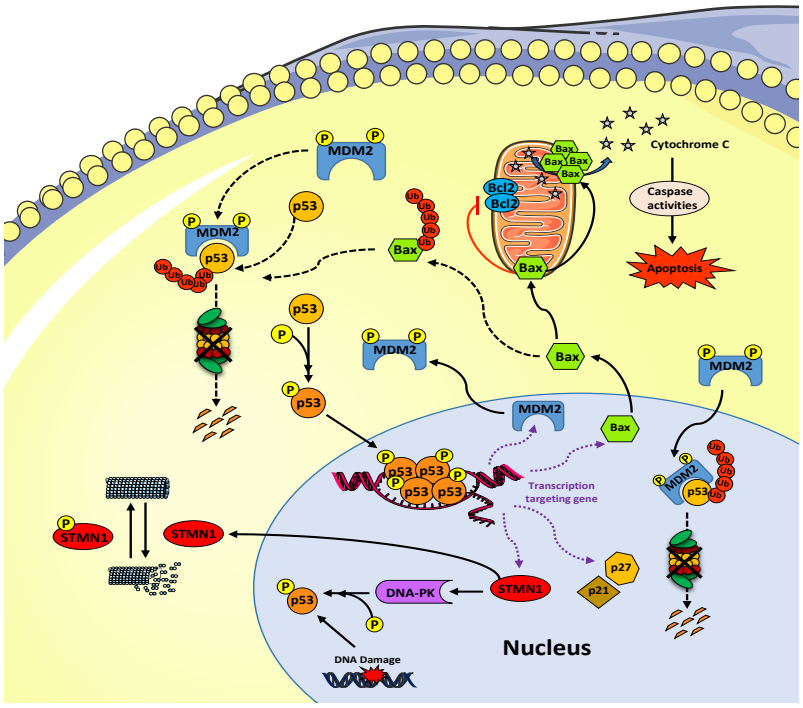


Figure 1.10 Stathmin and p53 pathway

p53 is a tumor suppressor gene that encodes a nuclear phosphoprotein and plays a key role in cell cycle regulation, and cellular apoptosis (Miller et al., 2000). In response to various types of cellular stresses including DNA damage, hypoxia, oxidative stress, p53 becomes stabilized and activated which is reflected in elevated p53 protein levels (Dai and Gu, 2010). When p53 is activated (Figure 1.10) it has ability to decide between life and death of cells by inducing cell cycle or apoptosis (Miller et al., 2000). Therefore, the amount of p53 in normal cells is tightly controlled and is kept at low levels through constant ubiquitination and proteasomal degradation (Yang et al., 2004). MDM2 (murine double minute 2) is a mediator of poly-ubiquitination that binds to the p53 protein and maintains p53 at low levels by increasing its susceptibility to proteolysis by the 26S proteasome (Haupt et al., 1997). Active p53 is no longer targeted for proteasomal degradation through dissociation of p53 from its inhibitor MDM2 and prevents MDM2-mediated degradation (Momand et al., 2000, Almond and Cohen, 2002). p53 accumulates and binds to specific sequences in DNA, initiating transcription of its target genes, such

as p21 or PUMA, resulting in growth arrest or apoptosis in a context-dependent manner (Bratton and Cohen, 2001). p53 can also induce apoptosis directly after rapid translocation to mitochondria (Mihara et al., 2003). Furthermore, a number of transcription factors, such as, FOXO3 genes were p53 negatively regulates by various mechanisms (Kruiswijk et al., 2015).

Cellular levels of p53 a play important role in pathogenesis of neurodegenerative diseases and neuronal cell death associated with enhanced levels of p53 (Chang et al., 2012). Study in post mortem brain tissue from AD patients and healthy elderly control have reported an increase in p53 immunoreactivity in AD cortical neurons especially in subpopulations undergoing neurofibrillary degeneration in the pathological temporal cortex areas (Hooper et al., 2007). Increased phosphorylation of p53 prior to the emergence of apoptotic features ,including mitochondrial membrane permeabilization, activation of caspase-3, and nuclear changes consistent, was demonstrated in both rat adrenal pheochromocytoma cells (PC12 cells) and dopaminergic neurons derived from embryonic stem cells following systemic administration of a proteasome inhibitor. This increase in p53 level was not associated with increases in p53 mRNA or change expression of PUMA or Bax mRNA and p53 co-immunoprecipitated with Bcl-xL and MDM2, suggesting that p53 was increased in a transcription-independent manner (Nair et al., 2006) (Figure 1.10).

Furthermore, increased intracellular levels of p53 was sufficient to induce apoptosis in both Rat-1 and PC12 cells following proteasome inhibitors treatment (Lopes et al., 1997). Indeed, absence of p53 disrupts apoptosis and facilitates tumorigenesis in p53 null mice (Attardi and Jacks, 1999). p53 can promote apoptosis through transcriptionally dependent and transcriptionally independent mechanisms that act in concert to ensure that the cell death program proceeds efficiently (Bates and Vousden, 1996, Fridman and Lowe, 2003). In apoptosis p53 functions as a transcription factor and promotes the transcription of several genes, which can

induce the proapoptotic members of the Bcl-2 family (such as Bax, Bad, and Bid), and inhibit antiapoptotic Bcl-2 family members (such as Bcl-2 and Bcl-XL) Bcl-2 family (Gross et al., 1999). These proteins regulate the release of cytochrome c from the mitochondria via alteration of mitochondrial membrane permeability (Figure 1.10). Cytochrome c binds with apoptotic protease activating factor 1 (Apaf-1) Apaf-1 and procaspase 9 to form the apoptosome, the formation of this complex leads to the cleavage of procaspase 9 into the functional component caspase 9. Caspase 9 starts a cascade that activates caspase 3. Caspase 3 releases caspase-activated DNase (CAD) from the inhibitor of CAD (ICAD), the ICAD-CAD complex of which is an inactive form. CAD then degrades chromosomal DNA within the nuclei and causes chromatin condensation. Caspase-3 also induces cytoskeletal reorganization and disintegration of the cell into apoptotic bodies (Elmore, 2007). However, the role of the 26S proteasome in neuronal apoptosis is poorly understood since both anti- and pro-apoptotic effects result from proteasome inhibition (Butts et al., 2005).

1.3.4.2 PI3K-Akt pathway

STMN1 expression can be the most reliable surrogate marker of PI3K-Akt pathway activation in glioblastoma and prostate cancer (Andersen et al., 2010, Saal et al., 2007, Karst et al., 2011). STMN1 the most prominently inhibited phosphoproteins following PI3K inhibitor treatment in the breast cancer cell lines (Saal et al., 2007). Therapy with the PI3K/Akt pathway inhibitor (LY294002) can decrease proliferation of pancreatic neoplasm cells through decreasing the expression and phosphorylation status of STMN1 (Schimmack et al., 2015) (Figure 1.11).

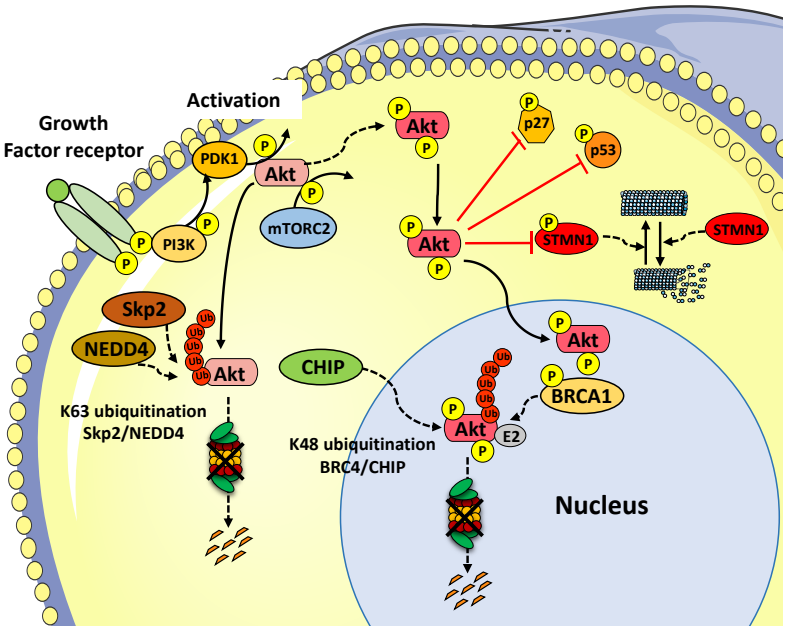


Figure 1.11 Stathmin and PI3K/Akt pathway

The kinase Akt, also called protein kinase B, is a central signaling molecule that links multiple signaling pathways to promote cell survival and prevent cell injury (Burgering and Coffer, 1995, Franke et al., 1995, Franke et al., 1997). Abnormal increase or decrease in the Akt activity has been linked to diverse diseases, including cancers and play a significant role in the onset and progression of neurodegenerative disorders (Chong et al., 2012, Rickle et al., 2004, Manning and Cantley, 2007). A different distribution of Akt and P-Akt was detected in AD temporal cortex neurons compared with control neurons, with increased activation of Akt (phosphorylated-Akt/total Akt ratio) also detected in AD neurons and may promote AD progression (Griffin et al., 2005). Akt levels and activity may regulate tau phosphorylation in the adult brain by affecting activities for PKA and GSK3α(Wang et al., 2015). Depletion of P-Akt, without altered total Akt protein levels were reported in immunostaining of post mortem dopaminergic neurons from PD patients compared with non-PD patients (Malagelada et al., 2008). Activation of Akt protected developing zebrafish neuronal cells from apoptosis induced by heat shock and UV exposure (Chen et al., 2017).

In human, there are three known PKB isoforms; Akt1, Akt2, and Akt3 encoded by separate genes. Akt3 isoforms was generally expressed in the brain, whereas Akt1 and Akt2 were expressed in multiple tissues (Yang et al., 2003a). Akt3 was importance of in brain development and Akt3-deficient brains mice have approximate 20% decrease in brain size and weight in adult mice due to decreases in cell size and number (Easton et al., 2005). Akt was tightly regulated and have three phosphorylation sites; Thr308 in the activation loop, Thr450 in the turn motif and Ser473 in the hydrophobic motif (Wu et al., 2011).

In response to growth factors stimulation, the PI3K generated phosphatidylinositol 3,4,5-trisphosphate (PIP3) that can binds to several signalling molecules through their pleckstrin (PH) homology domain (Fayard et al., 2010). One of these proteins was the phosphoinositide-dependent kinase 1 (PDK1), which essential mediator of the activation Akt by phosphorylates Akt at Thr308 (Bozulic and Hemmings, 2009). In addition to the Thr308 phosphorylation, Akt is phosphorylated at Ser473 in the HM (hydrophobic motif) by the target rapamycin complex 2 (mTORC2) kinase activity (Copp et al., 2009) Figure 1.11.

Akt promotes cell survival and prevents apoptosis by induces phosphorylates the pro-apoptotic BAD protein, which enhance the association of BAD with 14-3-3 proteins. This effectively blocks the death-inducing function of BAD then unable to interact with and antagonize the anti-apoptotic protein Bcl-2 (Datta et al., 1997, del Peso et al., 1997). Akt also activates the IκB (nuclear factor of kappa light polypeptide gene enhancer in B-cells inhibitor)/NFκB (nuclear factor-kappa B) transcription factor complex by inducing the proteasomal degradation of IκB to inhibit apoptosis. Akt also induces phosphorylation of the FOXO/forkhead family of transcription factors (Burgering and Coffer, 1995) and, consequently, reduces cellular levels of p27 (Sun et al., 2014). Akt activation can directly or indirectly reduce p53-mediated transcriptional activity, which leads to a reduction of Bax

expression and neuronal apoptosis (Yamaguchi et al., 2001) Figure 1.11.

Akt activity and stability in the neuronal cells was regulated by the UPS (Yan et al., 2006). After the establishment of neuronal polarity, Akt was enriched in axon terminals then in the dendrites, and suppressing the UPS led to the symmetric distribution of Akt and the formation of multiple axons (Yan et al., 2006). In addition, proteasome inhibitor (Bortezomib) can inhibited PI3K-Akt pathway and decreased the P-Akt expression, which can played a significant role in bortezomib-induced apoptosis in the squamous cell carcinoma cells line (Lin et al., 2012). In vitro studies in human retinal pigment epithelial cells reported that, treatment the cell with low levels of proteasome inhibitors induced resistance to oxidative injury by a pathway involving inhibition of the PI3K-Akt pathway (Tang et al., 2014). On the other hand, treatment malignant pleural mesothelioma cells with proteasome inhibitor MG132 or Bortezomib induced a limited apoptosis in these cells associated with elevated the P-Akt protein expression (Yuan et al., 2013).

1.3.4.3 p27

p27 is defined as a interacting partner to the STMN1, p27/STMN interaction plays a pivotal role in the control of cell proliferation in vivo (Berton et al., 2014). p27 can bind to C-terminal end of STMN1, and blocked its tubulin sequestering capabilities (Baldassarre et al., 2005). p27 (also known as $p27^{KIP1}$) is an atypical tumour suppressor that regulates cell cycle progression by binding and inhibition the activity of cyclin-dependent kinases (CDKs)(Nigg, 1993). In the normal cell progression of the cell cycle was controlled and maintained by the activity of serine/threonine kinases known as cyclin-dependent kinases (CDKs) (Morgan, 1995, Bloom and Pagano, 2003), and these proteins were negatively controlled by cyclin-dependent kinase inhibitors (CDKIs)(Elledge and Harper, 1994). Two groups of CDKIs, which involved in cell cycle arrest through blocking the activity of cyclin/cyclin-dependent

kinase (CDK) complexes: the Cip/Kip group whose can affected on cyclin D-, E-, and A-dependent kinases activities and these including p21 and p27. Another group is INK4 proteins act by inhibiting the activity of CDK4 and CDK6 (Cunningham et al., 2002). P27 can inhibit cell cycle transition from G1 to S phase by binding to and inhibition the activity of cyclin E–CDK2 complex (Coats et al., 1996). Decrease p27 during G1 allows cyclin E–CDK2 and cyclin A–CDK2 to activate the transcription of genes that are required for the G1–S transition and to participate in the initiation of DNA replication (Chu et al., 2008).

p27 expression in the cell is regulated by a proteasome-dependent degradation (Pagano et al., 1995) and that this mechanism plays a critical role in the regulation of p27 expression in several type of human tumors, such as in breast (Catzavelos et al., 1997) and colon cancer (Loda et al., 1997). To proteasome system degradation of p27 protein requires its phosphorylation on the threonine 187 (Thr187) (Grimmler et al., 2007). This phosphorylation is necessary for the binding of p27 to the F-Box protein Skp2 and for p27 (Figure 1.12) consequent ubiquitination and proteasome-dependent degradation (Bloom and Pagano, 2003). In addition to Thr187, there are three additional phosphorylation sites to p27, including Ser10, Thr157, and Thr198, which are effected in its cellular localization as nucleus or cytoplasm. The phosphorylation at Ser10 stabilizes the p27 protein in G1 and p27 is released from nucleus to the cytoplasm in a KPC1/2-induced ubiquitin-dependent degradation manner (Rodier et al., 2001). Based on this mechanism, p27 is phosphorylated at Ser10, which promotes (chromosome region maintenance 1) CRM1-dependent binding and nuclear export. This pathway operates in G1 cells or cells stimulated to re-enter the cell cycle from a quiescent state (He et al., 2012, Besson et al., 2006). Phosphorylation at Thr157 by protein kinase B/Akt impairs the nuclear import of p27, but does not affect its stability in breast cancer and other cell types (Shin et al., 2002). Fujita et al. 2003

indicated that p27 phosphorylation at Thr198 by p90 ribosomal protein S6 kinases promotes cytoplasmic localization (Fujita et al., 2003). These phosphorylation state of p27 is involved in signal transduction, apoptosis, and gene expression pathways (He et al., 2012). These specific mechanisms was involved in the phosphorylation regulation of p27 expression still remain unclear.

Expression of p27 in brain is important for cerebral cortex development (Lukaszewicz et al., 2005). The absence of p27 causes a general rise in cell proliferation, reflected by an increased brain size in p27 knockout mice (Fero et al., 1996). Adult CNS neurons are typically described as post-mitotic cells, which means that they permanently retract from the cell cycle. Brain neurogenesis can only take place in the subventricular and subgranular zones of the hippocampus (Eriksson et al., 1998). Re-entry of neurons into the cell cycle can induce apoptosis instead of promoting cell division and this may be another mechanism by which neurons undergo degeneration (Negis and Karabay, 2016, Rashidian et al., 2005). Studies suggest that dysregulation of cell cycle proteins may play a crucial role in the pathogenesis of Alzheimer's disease and AD pyramidal neurones shown a significant overlap of p27 with tau-positive neurofibrillary tangles (Ogawa et al., 2003). Moreover, increased gene expression of p27 was found in a cellular model of PD after acute exposure to (6-Hydroxydopamine) 6-OHDA treatment (Ryu et al., 2005).

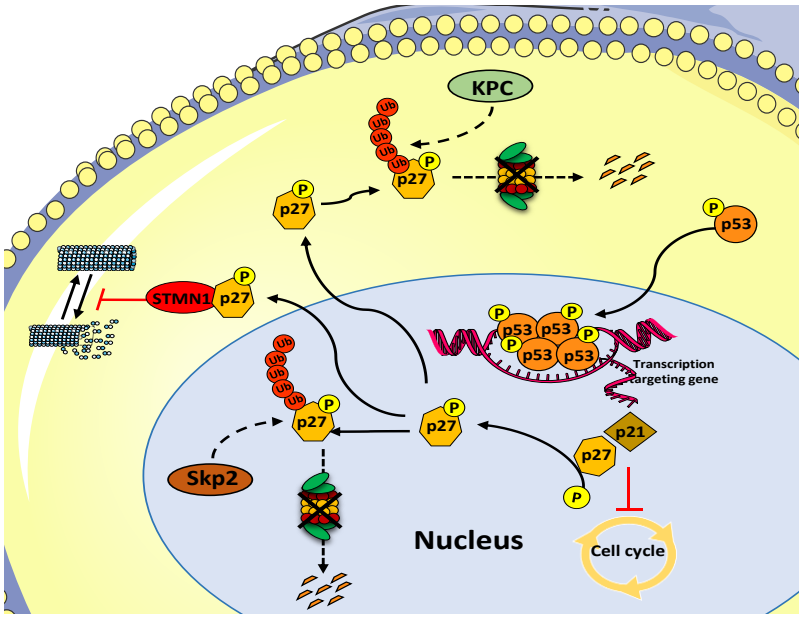


Figure 1.12 Stathmin and p27 pathway

1.3.5 Neurofilaments

Neurofilaments (NFs) are members of the intermediate filament (IF) family that are specifically expressed in neuronal cells (Friede and Samorajski, 1970). IFs are divided into five types, four found in the cytoplasm and one found in the nucleus called nuclear lamins (Liu et al., 2004). IFs are so called because their diameter (10–12 nm) is intermediate between that of microtubules (MTs) and microfilaments (MFs), with each of these make up the cytoskeleton of eukaryotic cells (Perrot and Eyer, 2009).

NFs form the backbone of axonal structure and was crucial to expand the axonal calibre in myelinated neurons and consequently increased their conduction velocity (Zhu et al., 1997). NFs have also act as a scaffold to maintain axonal mitochondrial translocation and distribution, active mitochondria for example have been shown to interact with the side-arms of phosphorylated NFs (Hirokawa, 1982, Perrot et al., 2008).

NFs also contribute to dynamic properties of the axonal during neuronal differentiation, radial axonal growth, regeneration and guidance (Zhu et al., 1997, Perrot et al., 2008, Liu et al., 2011, Dale and Garcia, 2012). In addition its play a key role in the growth

of complex dendritic trees in motor neurons (Kaufmann et al., 2000).

Abnormal accumulation of NFs in neurons is a general hallmark of neuronal dysfunction, particularly associated with axonal degeneration seen in many neurodegenerative diseases such as amyotrophic lateral sclerosis ALS, AD and PD (Liu et al., 2004, Liu et al., 2013) .

1.3.5.1 Structure and assembly of neurofilaments

NFs are composed of heteropolymers of three protein subunits; heavy (NFH, 180-200kDa), medium (NFM, 130-170kDa) and light (NFL, 60-70kDa) (Hoffman and Lasek, 1975, Griffin et al., 1978). Each subunit contains a central α-helical rod domain, edged by an N-terminal head domain and a non-α-helical C-terminal domain (Figure 1.13A). NFs produce according to a 4:2:1 ratio of NFL: NFM: NFH subunits and this ratio is continuously altered during neuronal formation (Carter et al., 1998).

The assembly of NFs occurs in many stages as seen in (Figure 1.13B); NFL subunits constitute the core of the filament on which NFM and NFH are anchored through coiled-coil interactions or rod domain around each other to form heterodimers (Dimers), which are then sorted in an anti-parallel fashion to form heterotetramers (Tetramers), two or three of heterotetramers then come together to form protofilament (Figure 1.13B), which were finally arranged in staggered, overlapping fashion to form the neurofilament (Lee et al., 1993).

NFM and NFH alone unable to form intermediate filaments in the absence of NFL (Carter et al., 1998, Elder et al., 1998). N-terminal domains all NFs have a MTs polymerization inhibitory domain that bind unassembled tubulin and regulates the number of MTs in the

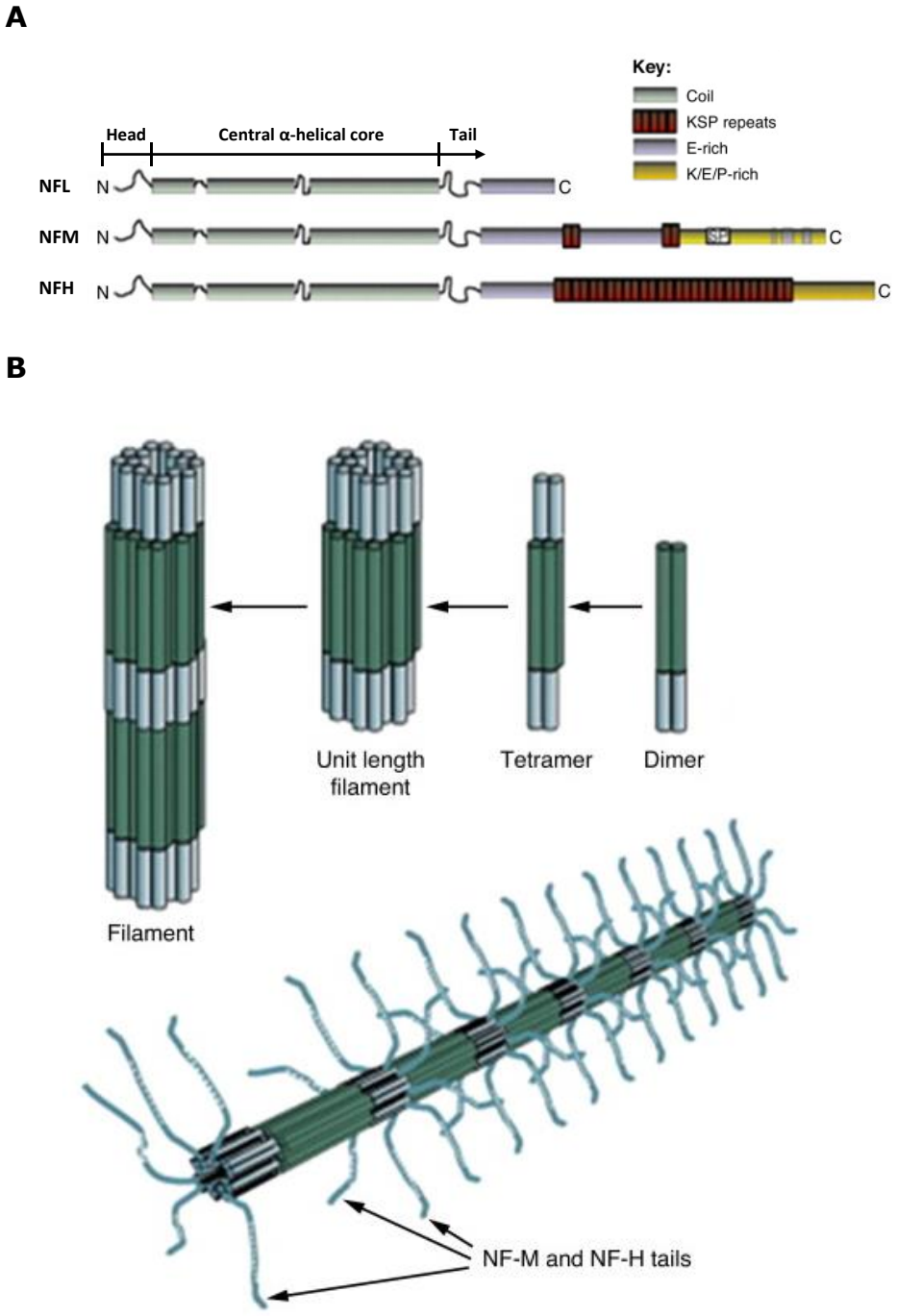


Figure 1.13 Aschematic of the structure and the assembly of neurofilament subunits into neurofilaments

(A) N-terminal head domain, a central α-helical core and a C-terminal tail domain of NFL, NFM and NFH. (B) The first step of neuronal IF formation is the dimerization of NFL with any other neuronal IF proteins through association of their conserved rod domains to form parallel, side-to-side, coiled-coil dimers. Two coiled-coil dimers line up in a half-staggered manner, forming an anti-parallel tetramer. Then, a rapid lateral aggregation of about eight tetramers occurs to form a unit-length-filament. Radial compaction then takes place resulting in close packing of the molecular filaments to constitute the final 10 nm 'bottlebrush' as neurofilaments. Adapted from (Laser-Azogui et al., 2015).

axon (Bocquet et al., 2009). The C-terminal domains of NFM and NFH form side arms that project from the filament, and are enriched in numerous Lys-Ser-Pro (KSP) repeats (Hirokawa, 1982). The phosphorylation state of KSP motifs repeated in these lateral projections was important to regulate the rate of NF transport, the radial growth of axons (Carden et al., 1987). In addition NF interactions with MTs also depend on the phosphorylation state of the C-terminal domain, as de-phosphorylation of this domain by alkaline phosphatase promotes the NFs and MTs interaction (Hisanaga and Hirokawa, 1990), while phosphorylation by the tau protein kinase II dissociates NFs from MTs (Miyasaka et al., 1993)

1.3.5.2 Transport of neurofilaments

Neurofilaments are synthesised and assembled in neuronal cell bodies then transported along axons to their sites of function and degraded at the synapse (Roy et al., 2000). NFs are transported by kinesin and dynein motors along microtubules in axonal neurons (Yuan et al., 2012). Anterograde-specific motor protein kinesin contributing in the anterograde NF axonal transport towards the growing or plus end of axonal MTs (Shea and Flanagan, 2001). The microtubule dynein-like motors mediate retrograde NF transport within axons, and also the delivery of NFs from perikarya into axons (Shea and Flanagan, 2001, Theiss et al., 2005).

Studies in NFH-NFL double knockout mice shown transport of NFs subunit does not require the formation of complete NFs (Yuan et al., 2003, Yuan et al., 2006). NFM can partner with other IF proteins than the NFH and NFL subunits in neurons to support their transport (Yuan et al., 2003).

Constantly, phosphorylation state of NFs can regulate NF transport by changing NF association with their molecular motors protein. As phosphorylation of NFH and NFM can change NF association with kinesin and dynein (Yabe et al., 2000, Motil et al., 2006) . Furthermore, increased phosphorylation of NFH can lead to

increased NFH association with the retrograde motor, dynein and NF transport towards neuronal cell bodies (Motil et al., 2006).

1.3.5.3 Degradation of neurofilaments

NF degradation is a potential mechanism for regulating the normal levels of the NFs within the axonal neurons (Gumy et al., 2010). The degradation of NFs in the axonal terminus can take place by different proteolytic pathways that include the ubiquitin–proteasome system (Gou and Leterrier, 1995), calcium-mediated protease calpain (Lopez-Picon et al., 2006) and also the lysosomal cathepsin D (Nixon and Marotta, 1984).

Treatment with proteasome inhibitors such as lactacystin was associated with a perikaryal accumulation of phosphorylated neurofilaments (Masaki et al., 2000). Furthermore, deficiency of TRIM2, which is an ubiquitin ligase that binds to and ubiquitinates NFL for NFL degeneration, leads to neurodegeneration in mice with consequent NFL accumulation in axons and impairment of axonal transport (Balastik et al., 2008). In addition to that, NFM has been identified as a target of the E3 enzyme, carboxyl-terminus of Hsc70 interacting protein CHIP which enhanced NFM ubiquitination and degradation (Wang et al., 2011, Dale and Garcia, 2012). Previous study reported that, increased NFs phosphorylation and NFs level in the cells and brain slices was treated with the phosphatase inhibitor such as okadaic acid (Shea et al., 1993, Gong et al., 2003). Furthermore, treating purified NFs with alkaline phosphatase lead to increased dephosphorylated NFs, which were degraded more rapidly by the calpain compared to phosphorylated NFs (Pant, 1988). Therefore, increased NF phosphorylation can be a mechanism for increasing NF stability and preventing NF turnover by protease-dependent mechanisms or UPS.

Calpain proteases, expressed generally in the brain, can degrade different proteins including axonal cytoskeletal proteins such as spectrin, MAP1, tau, tubulin and NFs (Stys and Jiang, 2002, Lopez-Picon et al., 2006). Calpain inhibitor can prevent NFs degradation

and protect neuronal cells from ischaemic and excitotoxic damage (Kunz et al., 2004).

In addition to that, the breakdown and turnover of NF could also represent an important feed-back mechanism regulating NF synthesis. As the structural stability of NF proteins was essential for neuronal survival, and deterioration of NF proteins could contribute to nerve cell death or failure of axonal regeneration (Yuan et al., 2012).

1.3.5.4 Neurofilaments in neurodegenerative diseases

Abnormal accumulation of NFs in neurons is a general hallmark of neuronal dysfunction and axonal degeneration seen in many neurodegenerative diseases such as amyotrophic lateral sclerosis (ALS), Alzheimer disease (AD) and Lewy bodies in Parkinson's disease (PD) (Perrot et al., 2008, Liu et al., 2011). However it is not clear whether this NF accumulation has a harmful and beneficial role in the neurons.

Previous study shown that, overexpressing of the neurofilament subunits NFL, NFM or NFH in transgenic mice led to prominent motor neuropathy and abnormal NFs accumulations resembling those found in ALS (Xu et al., 1993). Recent observation shown that plasma NFH levels increase significantly with disease progression in the mouse model of ALS and this increase in plasma NFH correlates with late stages of motor neurodegeneration of this disease (Lu et al., 2015, Lu et al., 2012). Proteomic analysis on the postmortem AD brain tissues showed presence of NFs proteins in neurites of senile plaques, may have important role in the formation of these plaques (Liao et al., 2004).

However, a beneficial role of NF proteins in ALS progression inconsistence to this hypothesis was point of out by Kong and Xu, (2000) and Couillard-Després et al (2000); the study shown overexpression of NFL and NFH proteins have a protective effect on the ALS progression in G93A mice (Kong and Xu, 2000, Couillard-Després et al., 2000). This protective effect was more obvious in

the G93A/NFH doubly transgenic mice than the G93A/NFL doubly transgenic mice (Kong and Xu, 2000). Absence of NFL subunit in NFL knockout mice lead to accumulations of NFM and NFH proteins in the cell body of motor neurons, slowed progression SOD1 mutant-mediated toxicity in motor neurons(Williamson et al., 1998).

This increase in NF expression also coincides with lack of axonal sprouting and increased dynamics instability of axonal MTs (Cifuentes-Diaz et al., 2002, Lariviere and Julien, 2004), indicating that the increased NFs and destabilization of MTs are functionally related. NFs can modulate MTs stability and thus axon caliber and MT functions in axonal transport (Millecamps and Julien, 2013). Abnormal accumulation of NFs causes neuronal degeneration by disrupting axonal transport of cargos required for axonal maintenance (Collard et al., 1995). Recent study has shown that the increase destabilizing activity of STMN1 was associated with increased NFs level and neuronal degeneration in progressive motor neuronopathy *pmn* mice (Yadav et al., 2016). In addition, depletion NFL in *pmn* mutant mice increases MTs stability and delays axon degeneration (Selvaraj et al., 2012, Yadav et al., 2016). Depletion of axonal NFL in mice deficient for NFL (-/-) and mice double transgenic upregulation of peripherin and NFL (-/-) neurons leads to improved axonal transport of mitochondria and lysosomes (Perrot and Julien, 2009).

1.4 Histological structure of cerebral cortex in mouse brain

The cerebral cortex is the neural tissue that lies as an outer covering layer of brain with 1-1.5 mm thick of the mouse neocortex (Price and Stern, 1983). Mice have a smooth-surfaced brain with no sulci (grooves) or gyri (the bulges seen on the outer surface) (Kirkcaldie, 2012). The total number of neuronal and non-neuronal cells in the mouse cerebral cortex is an average of 13.7 million neurons in the Swiss mouse (Herculano-Houzel et al., 2006).

1.4.1 The neocortex

The neocortex represents the great majority of the cerebral cortex. Staining the tissue of the neocortex for cell bodies reveals a 6 layered laminar structure of different densities (Chow and Leiman, 1970). These layers sit on top of a dense plexus of axons and glia referred to as white matter which contiguous with the corpus callosum as seen in (Figure 1.14). Cellular morphology, layer thickness, gene expression and the distribution of characteristic cellular markers vary between cortical regions (Kirkcaldie, 2012). When neurons are described as being located in a particular layer, this refers only to their soma and proximal dendrites; their distal dendrites and axons often extend across several layers, depending on the type of neuron. The neocortex layer is dominated by principal neurons, which are excitatory cells with dendrites covered in spines which receiving excitatory inputs, and giving rise to axons spreading in the cortex. In addition to these excitatory neurons, there are different types of inhibitory interneurons which coordinate cortical activity into complex patterns (Baars and Gage, 2010, Kirkcaldie, 2012). Excitatory cells (pyramidal cells (PCs) and spiny stellate cells (SSCs)) axons target dendrites of post-synaptic cells. Inhibitory cells axons have various target compartments on post-synaptic cells. Chandelier cells almost exclusively target the axon hillocks of pyramidal neurons. Large, small and nest basket cells provide most of the somatic and perisomatic inhibitory synapses for excitatory and inhibitory neurons. Dendrites are preferentially targeted by double bouquet, bitufted, bipolar, neurogliaform and Martinotti cells, with some types favoring either spines or their supporting branches (shafts).

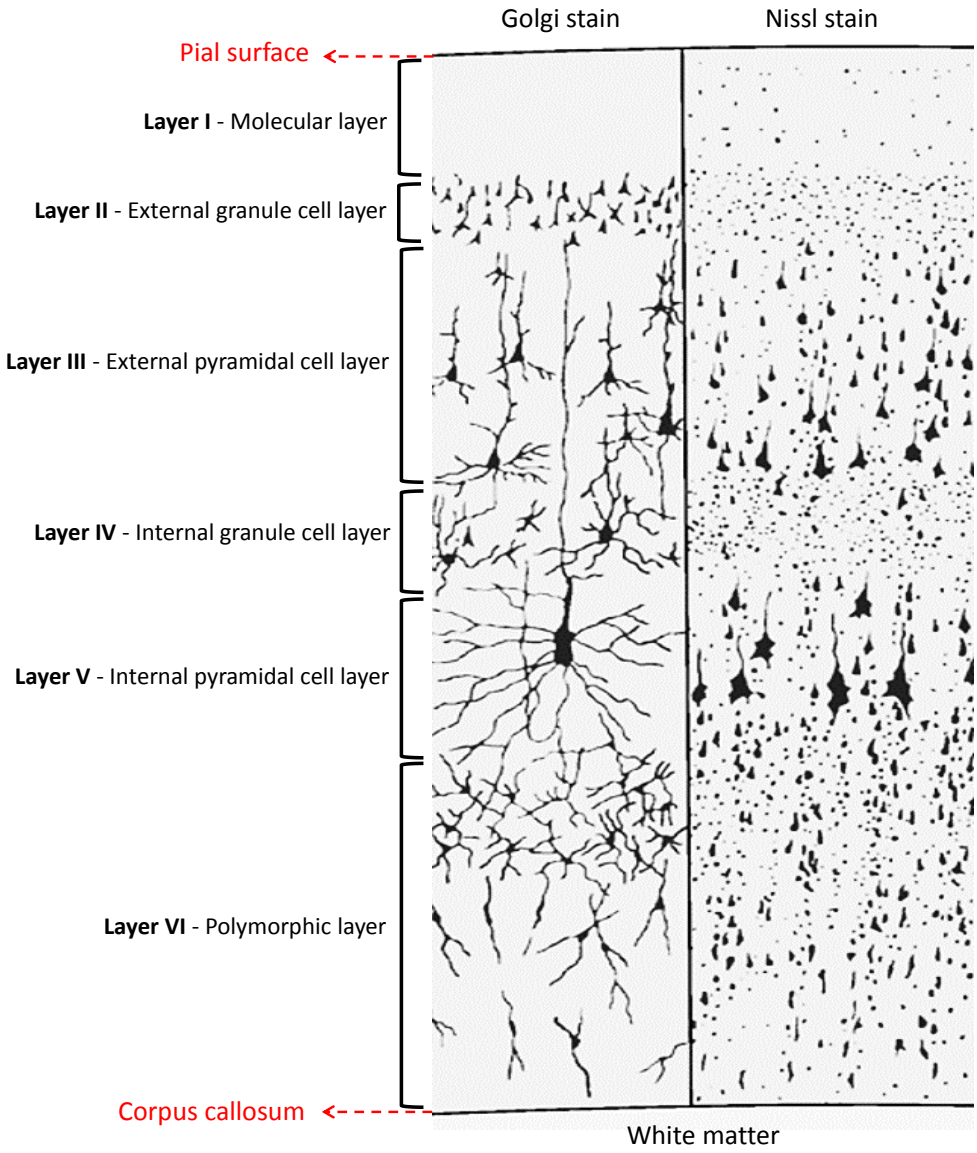


Figure 1.14 Cytoarchitecture of the neocortex in Golgi and Nissl staining-methods. Adapted from (Kirkcaldie, 2012)

Layer I, the molecular layer (Figure 1.14), is a thin plexus on the extreme rim of the cortex and sits directly below the pia mater (Hughes, 1984). It contains only a few scattered neurons (inhibitory neurons) and a limited number of glial cells (De Blas et al., 1988). Layer I consists of axons running across the cortical surface, the apical dendritic tufts of pyramidal neurons with their somata located in deeper layers (Chu et al., 2003). Dynamics in layer I are thought to be essential for learning and attention functions (Zhu and Zhu, 2004).

Layer II, the external granular layer (Figure 1.14), contains predominantly small pyramidal neurons and inhibitory neurons. It also contains apical dendrites from pyramidal cells whose cell bodies are found in layers V and VI (Hutsler et al., 2005).

Layer III, the external pyramidal layer (Figure 1.14), contains mainly small and medium-size pyramidal neurons, and few non-pyramidal neurons and is involved with local and corticocortical connectivity (Bureau et al., 2006). Layers I to III are the main targets of interhemispheric corticocortical afferents, and layer III is the principal source of corticocortical efferents (Hutsler et al., 2005). Neurons of layer II and III are notable for the expression of Cux2 a transcription factor which controls dendritic branching and synapse formation (Cubelos et al., 2010).

Layer IV, the internal granular layer (Figure 1.14). In sensory regions, layer IV is prominent, and is the main target of thalamocortical afferents from thalamus neurons(Frost and Caviness, 1980). In these regions, spiny stellate cells crowd into layer IV, forming a tightly packed band of nuclei which is named the granular cortex (Lefort et al., 2009). It also contains the apical dendrites of layer VI pyramidal neurons, enabling rapid feedback to the thalamus (Ledergerber and Larkum, 2010).

Layer V, the internal pyramidal layer (Figure 1.14), contains the largest pyramidal neurons of the cortex and project their axons to a variety of cortical and sub-cortical targets (Brown et al., 1992, Brown and Hestrin, 2009). Axons from layer V pyramidal cells target various subcortical structures, including the striatum, midbrain and pontine nuclei, the brainstem and the spinal cord (Ramos et al., 2008). On the basis of these projections, layer V is usually subdivided into layers 5a- corticostriatal and 5b- corticospinal (Anderson et al., 2010). In motor and frontal regions, layer 5b can be further divided into superficial and deep populations (Yu et al., 2008).

Layer VI, the polymorphic layer (Figure 1.14) is typically thick and often occupies a large fraction of the cortical depth in mice. It contains few large pyramidal neurons which the only neocortical pyramidal cell type whose apical dendrite terminates in layer IV rather than layer I and many small spindle-like pyramidal and multiform neurons (Ledergerber and Larkum, 2010). Layer VI has the bulk of corticothalamic fibers originates, and receives a strong thalamic projection in return (Lam and Sherman, 2010). Layer VI also contains a class of inhibitory neurons called Martinotti cells, whose axonal outputs make long projections across all layers of the neocortex (Zhang and Deschenes, 1997).

1.4.2 Neuronal cells in the neocortex

The neocortex is dominated by principal neurons, which are excitatory cells with dendrites covered in spines which receiving excitatory inputs, and giving rise to axons spreading in the cortex. Excitatory cells such as pyramidal cells (PCs) and spiny stellate cells (SSCs) as seen (Figure 1.15A). In addition to these excitatory neurons, there are different types of inhibitory interneurons (Figure 1.15B) including basket, chandelier, Martinotti, double bouquet and bitufted cells which have various target compartments on post-synaptic cells (Baars and Gage, 2010, Kirkcaldie, 2012). According to Connors and Gutnick, 1990, neurons in the neocortex can be categorised as below (Connors and Gutnick, 1990).

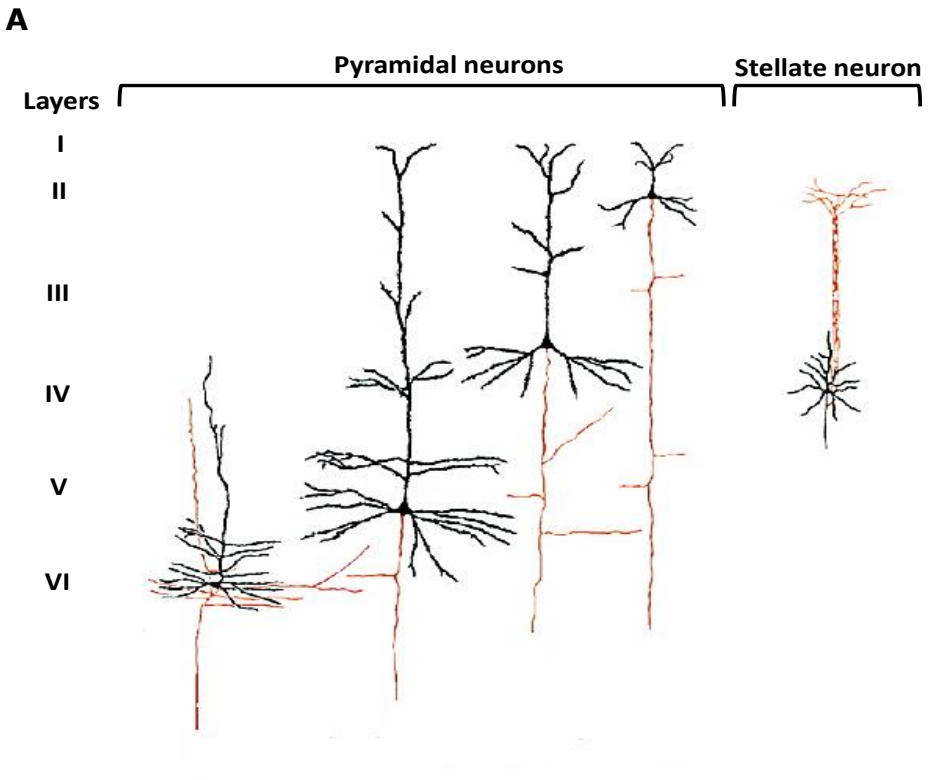
1.4.2.1 Pyramidal neurons

These consist of about 70 to 85% of the whole population of neurons in the neocortex (DeFelipe and Fariñas, 1992). The pyramidal neurons have distinct morphology (Figure 1.15A) and can vary in size throughout cortical regions and different layers of the cerebral cortex (Spruston, 2008).

Pyramidal neurons are named for their shape: typically they have pyramidal or ovoid shaped somata (Larkman, 1991). From the upper part of the soma the extending apical dendrite protrudes and directs towards pia mater (Figure 1.15A). A cluster of shorter dendrites that emerge from soma distal part called basal dendrites.

The apical dendrite of layer V pyramidal neuron forms a bifurcation and ends in layer I of the cortex forming the apical tuft of the dendritic branching, and layer VI pyramidal apical dendrites typically terminate in layer IV (Figure 1.15A). Several oblique dendrites emerge from the main apical dendrite before bifurcating at a variable distance from the soma to give rise to tuft dendrites (Molnar and Cheung, 2006). The length of the apical dendrite in the cortex of adult YFB mice from pyramidal cell bodies were visible up to ~700 µm below the pia surface (Kim et al., 2016).

The axons of pyramidal cells (Figure 1.15A) originate from the distal part of the soma, descending through and extending out of the cortex and travel through white matter to targets in other cortical or subcortical regions (Spruston, 2008).



B

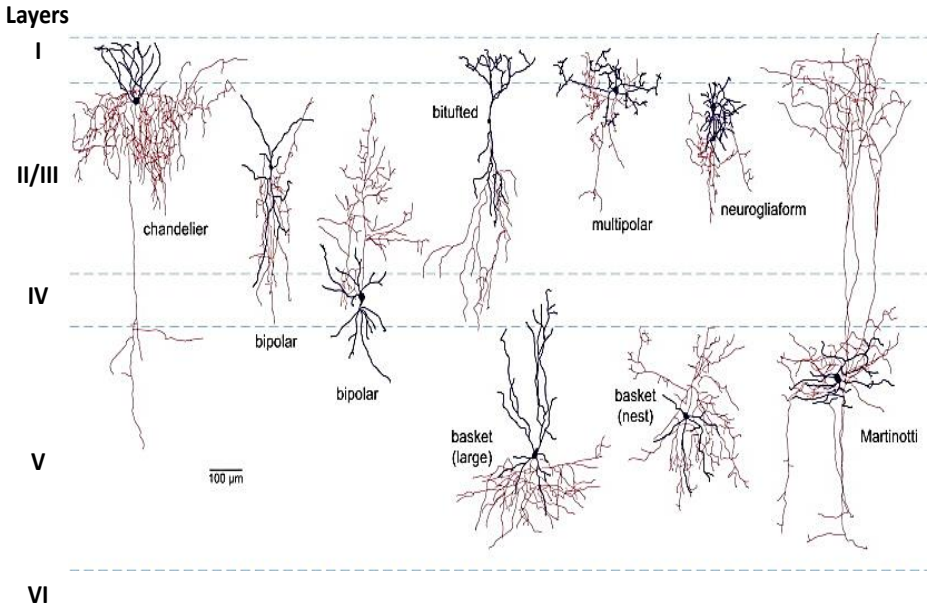


Figure 1.15 Major neuronal cell types of the adult cerebral cortex.

(A) Excitatory neurons included pyramidal and stellate neurons. (B) Inhibitory interneurons. Projection neurons display marked layer- and subtype-specific differences in the morphology of their dendrites (black) and axonal processes (red). Adapted from (Kwan et al., 2012).

1.4.2.2 Spiny stellate neurons

Spiny stellate cells resemble pyramidal cells, although they lose their apical dendrites as they mature (Figure 1.15 A). Spiny stellate cell distribution is limited to layer IV of primary sensory regions such as visual, auditory and somatosensory cortex (Spruston, 2008). Their nuclei pack together to form a "granular layer" seen in Nissl stains (Figure 1.15A)(DeFelipe and Fariñas, 1992).

Spiny stellate have a star-like shape appearance dendritic processes radiating from the cell body (Lund, 1988). Their axons emerge from the descending side of the soma and often recurve and ascend with arc-like collaterals to target more superficial layers (Figure 1.15A). These axons are primarily limited to layers II/III, IV and V and form excitatory synapses with dendrite spines and shafts of pyramidal neurons and interneurons (Staiger et al., 2004).

1.4.2.3 Inhibitory interneurons

Inhibitory interneurons consist of about 20 to 30 % of cortical neurons. These cells use gamma aminobutyric acid (GABA) as their primary neurotransmitter. Most of these neurons lack spines (Figure 1.15B). Their axons remain in the cortex and can project laterally but do not typically project down into the white matter, so they are called interneurons (Huang et al., 2007). The most common types of interneurons are:

- **Basket cells** (Figure 1.15B) represent 50% of inhibitory interneurons. They have three subtypes large, small and nest basket cells on the basis of differences in dendritic and axonal morphologies and are usually represented in layers II-VI (Markram et al., 2004).
- **Chandelier cells** (Figure 1.15B) are rare but widespread in the rodent cortex and usually found in layers II/III and V. They have local axonal clusters make numerous branching targeting the axon initial segment (axon hillock) of pyramidal neurons (Kawaguchi, 1995).
- **Double bouquet cells** (Figure 1.15B) have a fascicular axonal cylinder that can extend across all layers and make frequent branching and usually present layers II-V (Markram et al., 2004).
- **Bipolar cells** (Figure 1.15B) are relatively sparsely found in the cortex and have a narrow vertical axonal tree that crosses all layers and usually present in layers II-IV (Markram et al., 2004).
- **Bitufted cells** (Figure 1.15B) are similar to bipolar cells, and characterized by having tufts of dendrites extending from two opposite poles of the soma, which receive corticocortical and thalamocortical synapses. They primarily target pyramidal dendrites (Markram et al., 2004).
- **Martinotti cells** (Figure 1.15B) are present in all layers. They send long axons toward layer I where they inhibit pyramidal dendrites (Markram et al., 2004).

Pathogenesis of most neurodegenerative diseases such as AD, PD, DLB remains incompletely understood however, it is clear that atrophy and neuronal loss of cortical tissue are prominent features (Double et al., 1996, Regeur, 2000). Therefore histopathological and morphometric studies were used to analyse neuron numbers and densities as well as other morphologic features of neurons, including the cell body, nucleus and nucleolus diameter, for a better understanding of the pathogenesis of neurodegenerative diseases (Iacono et al., 2009, Bussiere et al., 2003, Bundgaard et al., 2001). Histopathological examination of brain tissue is required for definite diagnosis between Alzheimer's disease (AD) and frontotemporal dementia (FTD), which are usually difficult to differentiate clinically because of overlapping symptoms (Siri et al., 2001). Histopathological studies of cortical thickness reported that damage to specific cortical layers, layer II of the entorhinal cortex and layer III of the neocortex in AD, and layer III and V of frontal and temporal lobes in FTD (Kersaitis et al., 2004, Gomez-Isla et al., 1996). Increased brain cortical thickness in the sensorimotor cortex has been reported in the YAC128 mouse model of Huntington's disease (Lerch et al., 2008).

1.5 26S proteasome depletion mouse model; *Psmc1$^{fl/fl}$;CaMKIIa-Cre*

The connection between the UPS and neurodegenerative diseases began with the identification of ubiquitinated proteins in their hallmark protein inclusions (Bedford et al., 2008, Bedford et al., 2009). In most cases, these diseases are also associated with changes in cytoskeletal proteins and microtubule stability. Investigation into the levels and localisation of cytoskeletal proteins in mouse cortical neurons following 26S proteasome dysfunction (*Psmc1$^{fl/fl}$;CaMKIIa-Cre*), can provide new insights into the important role of the UPS in maintaining cytoskeletal proteins in neurodegenerative disease.

A conditional genetic mouse model with 26S proteasomal depletion in neurones was created. Cre recombinase/loxP conditional gene targeting was using to inactivation of an essential subunit of the 19 RP, ATPase Psmc1 (see section 2.1.1), which causes depletion of 26S proteasomes in forebrain neurones as described in detail previously (Bedford et al., 2008). The depletion of 26S proteasomes in neurons does not affect the formation and activity of the ubiquitin-independent 20S proteasome (Figure 1.16). Histopathological studies of 26S proteasomal depletion mouse cortical tissue showed extensive cortical neurodegeneration and intraneuronal Lewy-like protein inclusions reassembly to human PB, containing ubiquitin, α-synuclein mitochondria and fragmented dysfunctional mitochondria (Figure 1.16). Neurodegeneration in this model was associated with decreased levels of microtubule destabilizing protein stathmin and increase expression of GFAP and VIME as identified by 2D-DIGE proteomics, indicative reactive astrogliosis (Figure 1.16). Increased expression of the astrocytic antioxidant enzyme PRDX-6 (Figure 1.16) may be an important antioxidant mechanism in the mouse brain (Elkharaz et al., 2013). The 26S proteasomal depletion mouse model also showed increased levels of phosphorylated p62 and LC3B-II in *Psmc1*$^{fl/fl}$*;CaMKIIα-Cre* cortices at 3 weeks of age (Figure 1.16), suggesting early activation of autophagy. However, continued 26S proteasome dysfunction in cortical neurons leads to decreased autophagy by decreasing levels of essential autophagy proteins ATG9 and LC3B (Figure 1.16), and may ultimately lead to proteostasis collapse and cell death in *Psmc1*$^{fl/fl}$*;CaMKIIα-Cre* mice cortices at 6 weeks-old (Ugun-Klusek et al., 2017).

Behavioural studies demonstrated a deficit in learning and memory in the Morris water maze test. The mice also showed growth retardation and premature death before 12 weeks of age (Bedford et al., 2008).

Neuropathological and molecular change
following 26S proteasome dysfunction in mouse brain cortical neurons

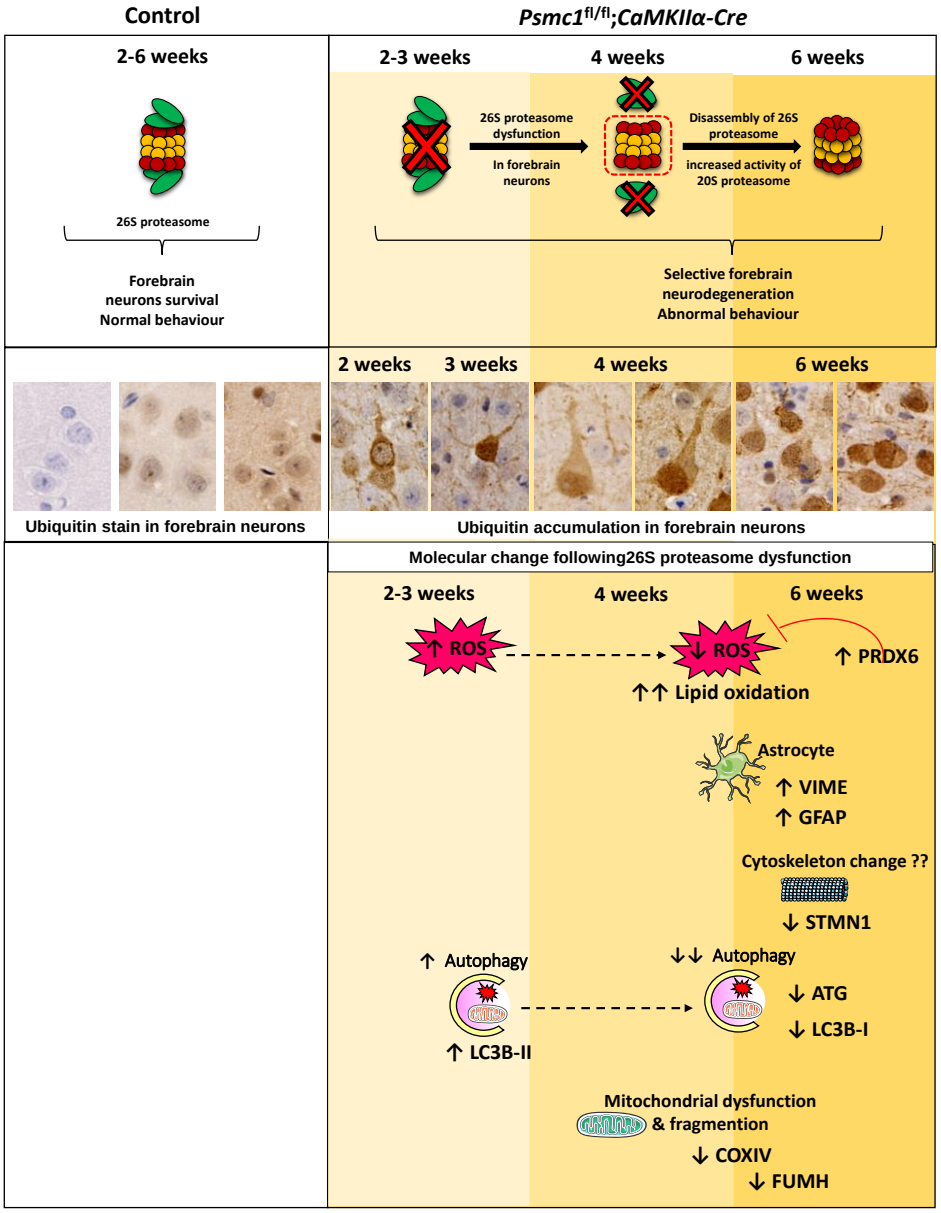


Figure 1.16 The main neuropathological and molecular changes in *Psmc1*$^{fl/fl}$*;CaMKIIα-Cre* mouse cortex (Bedford et al., 2008, Elkharaz et al., 2013, Ugun-Klusek et al., 2017).

Aims

The mechanisms involved in the cause and progression of chronic neurodegenerative diseases are still unclear. The ubiquitin proteasome system (UPS) plays an essential role in the maintenance of intracellular protein homeostasis by degrading unwanted proteins. The accumulation of ubiquitinated proteins and progressive degeneration of specific neurons are hallmarks of major neurodegenerative diseases. In most cases, these diseases are also associated with changes in cytoskeletal proteins or microtubule stability. We previously reported decreased levels of microtubule destabilizing protein stathmin following 26S proteasome dysfunction in mouse cortical neurons, associated with neurodegeneration and the formation of intraneuronal protein inclusions in surviving neurons (Elkharaz et al., 2013). This suggested a role for the 26S proteasome in maintaining the neuronal cytoskeleton. The main aims of this study are:

1. To investigate the levels and localisation of key cytoskeletal proteins, including tubulin, PTM of tubulin, microtubule-associated proteins and neurofilaments in cortical tissue with 26S proteasome dysfunction in neurons.
2. To investigate whether decreased stathmin expression following 26S proteasome dysfunction in cortical neurons is associated with changes in the levels of p53, p27 and activity of the PI3K/Akt pathway.
3. To investigate morphological changes in the cortex following disruption of the 26S proteasome in mouse cortical neurons, including cortical thickness and apical dendritic changes.

Chapter 2

Materials and Methods

2.1 Experimental animals

2.1.1 Conditional deletion of the 26S proteasome mice

Neuron-specific 26S proteasome knockout mice were created using Cre/loxP conditional gene targeting as described in detail previously (Bedford et al., 2008). A specific subunit of the base of the 19S RP, ATPase Psmc1, was inactivated by crossing floxed Psmc1 mice (*Psmc1*$^{fl/fl}$) with mice expressing Cre recombinase from the calcium calmodulin dependent protein kinase IIα promoter (*CaMKIIα-Cre*) (Figure 2.1A). This leads to the inactivation of Psmc1 in forebrain neurones in the *Psmc1*$^{fl/fl}$*;CaMKIIα-Cre* mice (Figure 2.1B and C) . Expression of CamKIIα begins approximately postnatal week 2-3 allowing normal central nervous system development before Cre-mediated recombination of Psmc1 in post-mitotic neurons. *Psmc1*$^{fl/fl}$*;CaMKIIα-Wt* and *Psmc1*$^{fl/wt}$*;CaMKIIα-Wt* littermates were used as controls(Figure 2.1B). Mice were housed under constant conditions of 12 /12 h light-dark cycle and 21 ± 2 °C room temperature. Food and water were accessible ad libitum. All procedures were carried out under personal and project licenses granted by the UK Home Office in accordance with the Animals (Scientific Procedures) Act 1986 and with ethical approval from the University of Nottingham Ethical Review Committee.

2.1.2 Extraction of genomic DNA from mouse tissue

2.1.2.1 Reagents

1) Tissue lysis buffer
   100 mM Tris-HCl pH 8.5
   5 mM Na-EDTA
   0.2% w/v SDS
   200 mM NaCl.
2) Proteinase K (10 mg /ml).
3) Isopropanol
4) 70% v/v ethanol

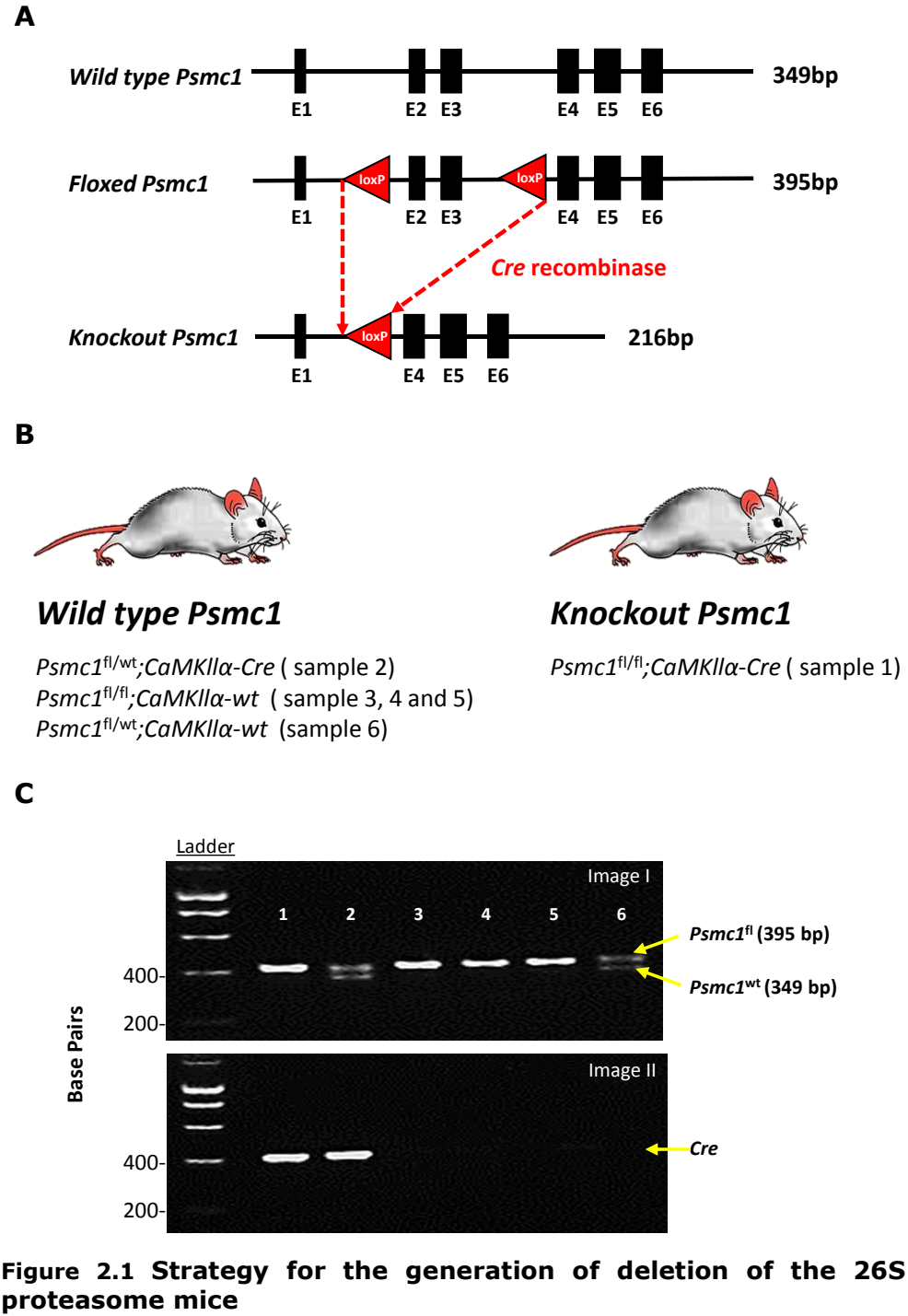


Figure 2.1 Strategy for the generation of deletion of the 26S proteasome mice

(A) LoxP sites (arrowheads) were introduced flanking exon 2 and 3 of the Psmc1 gene. Floxed mice were bred to a Cre deleter strain expressing Cre recombinase in the germline to generate null alleles. (B) Schematic diagram showing examples of mouse genotypes. (C) PCR products for Psmc1 (image I) and Cre (image II) following electrophoresis. Bands were detected using a UV trans-illuminator.

2.1.2.2 Method

Genomic DNA (gDNA) for polymerase chain reaction (PCR) was prepared from mouse tail or ear notch. Tissue was placed in a 1.5 ml eppendorf tube and incubated overnight at 55°C in tissue lysis buffer (500 µl for tail or ear notches) containing a final concentration of 0.5 mg/ml proteinase K. The sample was vortexed and the supernatant collected following centrifugation at 9300 xg for 10 min. An equal volume of isopropanol was added to precipitate the DNA, the tube inverted and centrifuged at 16100 xg for 10 min. The supernatant was discarded and the gDNA pellet washed with an equal volume of 70% v/v ethanol. Following centrifugation again at 16100 xg for 10 min the supernatant was discarded and the gDNA pellet air-dried at room temperature. After drying the gDNA pellet was re-suspended in an appropriate volume of nuclease-free water (about 60 µl for ear notches and 160 µl for tail).

2.1.3 Polymerase chain reaction

2.1.3.1 Reagents

1) Primers: 4 µM Cre (sense and antisense), 4 µM Psmc1-LB3 (sense), 4 µM Psmc1-D1360 (sense) and 4 µM Psmc1-X316 (antisense)

Table 2.1 Sequence of primers used for mice genotyping

Primer	Forward Primer (5'- 3')	Reverse Primer (5'- 3')
Cre	GGTAGCACCGCAGGTGTAG	CTAATCGCCATCTTCCAGCAG
Psmc1- LB3	TACGAACCTCCTGTCCCAAC	–
Psmc1-D1360	CAGAAATACAGCCAGTGACC	–
Psmc1- X316	–	CTGGAACTCAGTGGATTGAG

2) 10X PCR buffer containing 20 mM $MgCl_2$ (Fermentase).
3) DNA polymerase 5 U/µl (Fermentase).
4) 1 mM deoxynucleotide triphosphates (dNTPs).

2.1.3.2 Method

The final reaction volume for each PCR was 10 µl containing final concentrations: 0.5 µl of gDNA template. The PCR was performed

in a thermo-cycle PCR (Master cycle- eppendorf®) under the condition of 94°C for 3 minutes, and then for 30 cycle of 94°C for 1 minute, 60°C for 30 seconds and 72°C for 30 seconds.

2.1.4 Agarose gel electrophoresis

2.1.4.1 Reagents

1) Tris-acetate EDTA buffer (TAE)

   40 mM Tris-acetate
   1 mM EDTA pH 8 with HCl

2) 4% w/v agarose gel solution (4.5 g agarose in 150 ml TAE).
3) Ethidium bromide solution (1% w/v in water).
4) DNA Ladder 50-1350 bp

2.1.4.2 Method

The 4% w/v agarose gel solution was melted using a microwave oven. 7 µl of ethidium bromide was added to the melted agarose once cooled to approximately 55°C. The gel was poured into a gel tray pre-fitted with combs. Once the gel was set, TAE buffer was poured into the gel apparatus to cover the gel. The PCR samples and DNA ladder were loaded. A constant voltage of 150 V was applied for electrophoresis. PCR bands were detected by using a UV trans-illuminator (Figure 2.1C).

2.2 Protein analysis

2.2.1 Tissue homogenisation

2.2.1.1 Reagents

1) Protein lysis buffer

   50 mM Tris pH 7.4
   150 mM NaCl (sodium chloride)
   2 mM EDTA (Ethylene diamine tetra acetic acid)
   1 mM $MgCl_2$ (Magnesium chloride)
   100 mM NaF (sodium fluoride)
   10% v/v glycerol
   1% v/v triton X-100

1% w/v sodium deoxycholate

0.1% w/v SDS (sodium dodecyl sulphate)

125 mM sucrose

2) 1X protease inhibitor cocktail.

2.2.1.2 Method

Mouse cortices were homogenized in ice-cold protein lysis buffer using the FastPrep®-24 tissue and cell homogeniser. The homogenate was centrifuged at 16000 xg for 10 min at 4°C. The supernatant was transferred to a new tube and protein concentration determined by Bradford assay.

2.2.2 Bradford assay

2.2.2.1 Reagents

1) Bradford reagent

   100 mg of Coomassie Brilliant Blue G-250

   50 ml ethanol

   100 ml perchloric acid

   50 ml deionized water

2) Bovine serum albumin (BSA) standard solution: 1 mg /ml water

2.2.2.2 Method

A known volume of protein sample was pipetted into a 96 well plate and made up to a volume of 50 µl. A standard curve (0-50 µg standard protein) was generated using the BSA solution. All samples and standards were analyzed in duplicate. Added 150 µl of Bradford reagent (1:11 ml deionized water) into each sample and the standard. The resultant blue color was measured using a spectrophotometer at 595 nm (SPECTRA MAX 190) and the protein concentration determined from the standard curve. Concentrations of original samples were determine from the amount protein, volume/sample, and dilution factor.

2.2.3 Sodium dodecyl sulphate polyacrylamide gel electrophoresis (SDS-PAGE)

2.2.3.1 Reagents

3) Polyacrylamide gel electrophoresis

30% w/v acrylamide solution

10% w/v sodium dodecyl sulphate (SDS)

Buffer B: 1.1 M Tris, 0.1% w/v SDS, pH 8.8

Ammonium per-sulphate (AMPS): 10% w/v AMPS solution

N, N, N, N- Tetramethylene diamine (TEMED)

4) Stacking Gel

Stacking gel buffer: 0.14 M Tris, 0.1% w/v SDS, pH 6.8

Acrylamide/bis-acrylamide (30%/0.8% w/v)

10% w/v AMPS Ammonium per-sulphate solution

N, N, N, N- Tetramethylene diamine (TEMED)

5) Electrode Buffer

0.25 M Tris

1.86 M Glycine

0.1% w/v SDS

6) Gel application buffer (2x GAB)

0.15 M Tris

8 M urea

2.5% SDS

20% v/v Glycerol

10% v/v 2-mercaptoethanol

3% w/v DTT

0.1% w/v bromophenol blue

pH 6.8 and the solution made up to 50 ml with deionised water

7) Protein ladder

ColorPlus Prestained broad range (10-230 kDa)

8) Gel electrophoresis system

Table 2.2 Components of 10%, 12% and 15% SDS-PAGE gels

Components	Acrylamide percentage					
	10%		12%		15%	
	5 ml	20 ml	5 ml	20 ml	5 ml	20 ml
Acrylamide/bis-acrylamide(30%/0.8% w/v)	1.67 ml	6.67 ml	2 ml	8 ml	2.5 ml	10 ml
Buffer B (1.1 M Tris, 0.1% (w/v) SDS, pH 8.8)	1.66 ml	6.64 ml	1.66 ml	6.64 ml	1.66 ml	6.64 ml
0.1% w/v SDS-H_2O	1.67 ml	6.67 ml	1.33 ml	5.32 ml	0.85 ml	3.4 ml
10% w/v AMPS	50 µl	200 µl	50 µl	200 µl	50 µl	200 µl
N, N, N, N- Tetramethylene diamine (TEMED)	5 µl	20 µl	5 µl	20 µl	5 µl	20 µl

Table 2.3 Components of stacking gel solution

Stacking gel solution	5 ml
Stacking gel buffer	1.104 ml
Acrylamide/bis-acrylamide (30%/0.8% w/v)	0.208 ml
10% w/v AMPS	25 µl
N, N, N, N- Tetramethylene diamine (TEMED)	5 µl

2.2.3.2 Method

Samples were mixed 1:1 with gel application buffer (2x GAB) and heated at 90°C for 10 min. For each sample an equal amount of protein (30µg or 50 µg) was loaded onto a 10%, 12% or 15% w/v poly acrylamide gel (Table 2.2). Using a Pasteur pipette, a water-saturated butanol solution was layered on top whilst the gel polymerized. After polymerization, the butanol layer was decanted. The acrylamide percentage depended on the size of the protein of interest. A stacking gel was poured on top of the resolving gel (Table 2.3) and a sample comb inserted. Once the stacking gel had polymerized, the comb was removed before loading the protein samples for separation. The SDS-PAGE gel using a Mini-protean (Bio-Rad) was immersed in electrode buffer and protein samples loaded into individual wells as well as a protein standard marker. The separation was carried out at 135 V and 200 mA supplied by an electrophoresis power pack. Once the proteins were separated the gel was ready for Western blot analysis.

2.2.4 Western blotting analysis

2.2.4.1 Reagents

1) Transfer buffer

   0.025M Tris

   0.129 M glycine

   20% v/v methanol

2) Electrophoretic transfer apparatus (Bio-Rad).
3) Bio Trace™ Nitrocellulose membrane, Pall Laboratory

2.2.4.2 Method

Following separation of proteins by SDS-PAGE (described in section 2.2.3) the gel was placed onto nitrocellulose membrane that had been soaked in transfer buffer. The proteins were then wet transferred to nitrocellulose membrane in transfer buffer and cut out a piece of nitrocellulose membrane and two pieces of filter paper for the transfer. In wet transfer, the gel and membrane are sandwich assemble in the cassette in the order shown below (Figure 2.2). The sandwich is formed from: cathode (-), sponge, filter paper, gel, nitrocellulose membrane, filter paper, sponge and anode (+) and all are clamped tightly together after ensuring no air bubbles are present between the gel and membrane. The proteins were transferred at 10 V overnight. Following transfer the membrane was stained with copper stain [0.05% w/v copper phthalocyanine-3,4′,4″,4‴-tetrasulfonic acid tetrasodium salt (CPTS) and 12 mM HCl] to visualize all the separated protein bands and protein loading. Stained membrane were rinsed with deionized water and scanned using Image scanners. The membrane de-staining solution by rinsed with deionized water with one drop of 5% w/v NaOH.

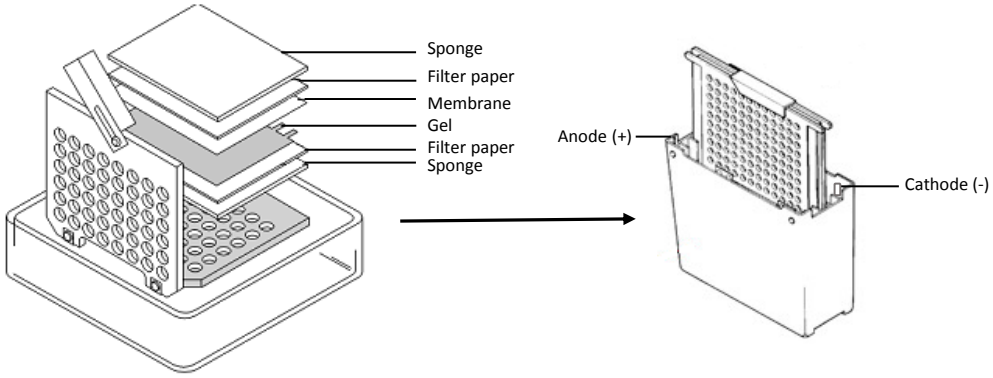


Figure 2.2 Sandwiched assemble with grey side down cathode (-)

2.2.5 Membrane blotting

2.2.5.1 Reagents

1) TBST
   Tris buffered saline
   0.1% v/v Tween
2) PBST
   Phosphate buffered saline
   0.1% v/v Tween
3) 5% w/v non-fat dry milk solution (Marvel®) in TBS-T or PBS-T
4) 5% w/v bovine serum albumin in TBS-T
5) Primary antibodies
6) LI-COR® IRDye-conjugated secondary antibodies
7) Odyssey Image Studio software
8) Secondary antibody conjugated to Horseradish Peroxidase (HRP).
9) Chemiluminescent substrate (ECL).
10) X-ray film; Lumi- Film Chemiluminescent detection film.
11) Developing solution (Calumet Photograph LTD 757314)
12) Fixative solution (Calumet Photograph LTD 2000RT)

2.2.5.2 Method

Non-specific binding of antibodies was blocked by incubating the nitrocellulose membrane for 1 hr. in 5% w/v bovine serum albumin

(BSA) or 5% dry milk Marvel blotting solution in TBS-T. The membrane was then incubated with the appropriate primary antibody in TBS-T as detailed in (Table 2.4) overnight at 4°C on a rotating machine. The membrane was then washed three times, each for 10 min with TBS-T and incubated with the appropriate secondary antibody in TBS-T as detailed in (Table 2.4) for 1 hr. at room temperature. The membrane was washed twice for 10 min each with TBS-T and once for 10 min in Tris-buffered saline (TBS). The fluorescent LI-COR IRDye conjugated secondary antibodies were detected using the Odyssey infrared imaging system at 800 nm and intensities as indicated in the results. Odyssey Image Studio software can be used to maximize the appearance of the image using a wide range of secondary antibody dilutions. The membrane was then probed for a housekeeping protein (GAPDH) as a loading control. Blots were normalized to loading control and quantified using Odyssey Image Studio software.

2.2.6 Stripping nitrocellulose membrane

2.2.6.1 Reagents

Stripping buffer

25mM glycine

2% w/v SDS, pH 2.0

2.2.6.2 Method

The membrane was washed with TBS-T once for 5 min then incubated in stripping buffer for 20 min at 65°C in a water bath followed by 5 times washes with TBS-T for 10 min each.

Table 2.4 Antibodies used throughout all protein analysis

Primary	Molecular weight (kDa)	Animal source	Dilution	Blocking solution	Manufacturing company
GAPDH	36 kDa	Rabbit	1:25,000	5% Marvel-TBST	Sigma, G9545
α-tubulin	52 kDa	Rabbit	1:1000	5% Marvel-TBST	Gene Tex, GTX102078
βIII-tubulin	55 kDa	Rabbit	1:1000	5% Marvel-TBST	Cell Signaling, D65A4
Actin	42 kDa	Rabbit	1:1000	5% Marvel-TBST	Sigma-A2066
MAP-2	250 kDa	Rabbit	1:1000	5% Marvel-TBST	Abcam, ab32454
Tau46	45-60 kDa	Mouse	1:1000	5% Marvel-TBST	Sigma-Aldrich, T9450
CP13	45-60 kDa	Mouse	1:1000	5% Marvel-TBST	Alzforum, Tau phos Ser202 (CP13)
AT8	79 kDa	Mouse	1:1000	5% Marvel-TBST	Thermo Fisher, MN1020
Acetyl-α-Tubulin (Lys40)	55 kDa	Mouse	1:2000	5% Marvel-TBST	Thermo Fisher, 6-11B-1
Anti-Tubulin Antibody, Detyrosinated	55 kDa	Rabbit	1:1000	5% Marvel-TBST	Millipore, AB3201
Anti-Tubulin antibody [YL1/2]	55 kDa	Rat	1:1000	5% Marvel-TBST	Abcam, ab6160
STMN1	17 kDa	Rabbit	1:250	5% Marvel-PBST	Gene Tex, GTX113341
p53	44 kDa	Rabbit	1:500	5% Marvel-PBST	Gene Tex, GTX118730
BAX	50 kDa	Rabbit	1:250	5% Marvel-PBST	Bioss, bs-0127R
Bcl2	24 kDa	Rabbit	1:250	5% Marvel-PBST	Bioss, bs-4563R
p27	27 kDa	Mouse	1:1000	5% Marvel-PBST	Santa Cruz Biotechnology, sc-1641
Akt	60 kDa	Rabbit	1:1000	5% BSA-TBST	Cell Signaling, 4691
p-Akt	60 kDa	Rabbit	1:1000	5% BSA-TBST	Cell Signaling, 4058
NFL	kDa	Mouse	1:1000	5% Marvel-TBST	Cell Signaling, 2835
NFM	160 kDa	Mouse	1:1000	5% Marvel-TBST	Cell Signaling, 2838
NFH	180-220 kDa	Mouse	1:500	5% Marvel-TBST	Cell Signaling, 2836

2.3 Purification of free and polymerized tubulin

According to (Jiang et al., 2006, Joshi and Cleveland, 1989, Ren et al., 2005).

2.3.1 Reagents

1) Microtuble (MT) stabilizing buffer

0.1 M N-morpholinoethanesulfonic acid (MES), pH=6.75

1 mM Magnesium sulfate $MgSO_4$

2 mM Ethylene glycol tetraacetic acid (EGTA)

0.1 mM Ethylene diamine tetraacetic acid (EDTA)

4 M glycerol

0.1% v/v Triton-X-100

1X Protease inhibitor cocktail

2) Microtuble (MT) destabilizing buffer

25 mM Tris, pH 6.8

0.5% w/v SDS

2.3.2 Method

A flow diagram of this method is shown in Figure 2.3. Mouse cortex (about 0.153g) was dissected and placed in 1.2 ml of MT stabilizing buffer. The cortex was then homogenised using eight strokes of a loosely fitting teflon pestle homogeniser and incubated at 37°C in water bath for 10 min. An aliquot of the total homogenate was taken (total tubulin). The homogenate was then centrifuged at 37°C for 1 hr at 16,000 xg using an Eppendorf 5415R. The supernatant (S1) from this centrifugation was collected and contains free tubulin. The pellet (P1) containing polymerized tubulin was re-homogenized in 1 ml of MT destabilizing buffer to depolymerize the tubulin and centrifuged at room temperature (rtp) for 1 hr at 100,000 xg using a Beckman Coulter Optima TLA-

120.2 Rotor Max Ultracentrifuge. The supernatant (S2) was collected and represents polymerized tubulin. The pellet was discarded. Protein quantification of total homogenate, S1 and S2 was performed by Bradford assay (Section 2.2.2).Equal amounts of protein were then analysed by western blotting (α-tubulin; 1:2000 GeneTex) and blots were quantified using Odyssey Image Studio software.

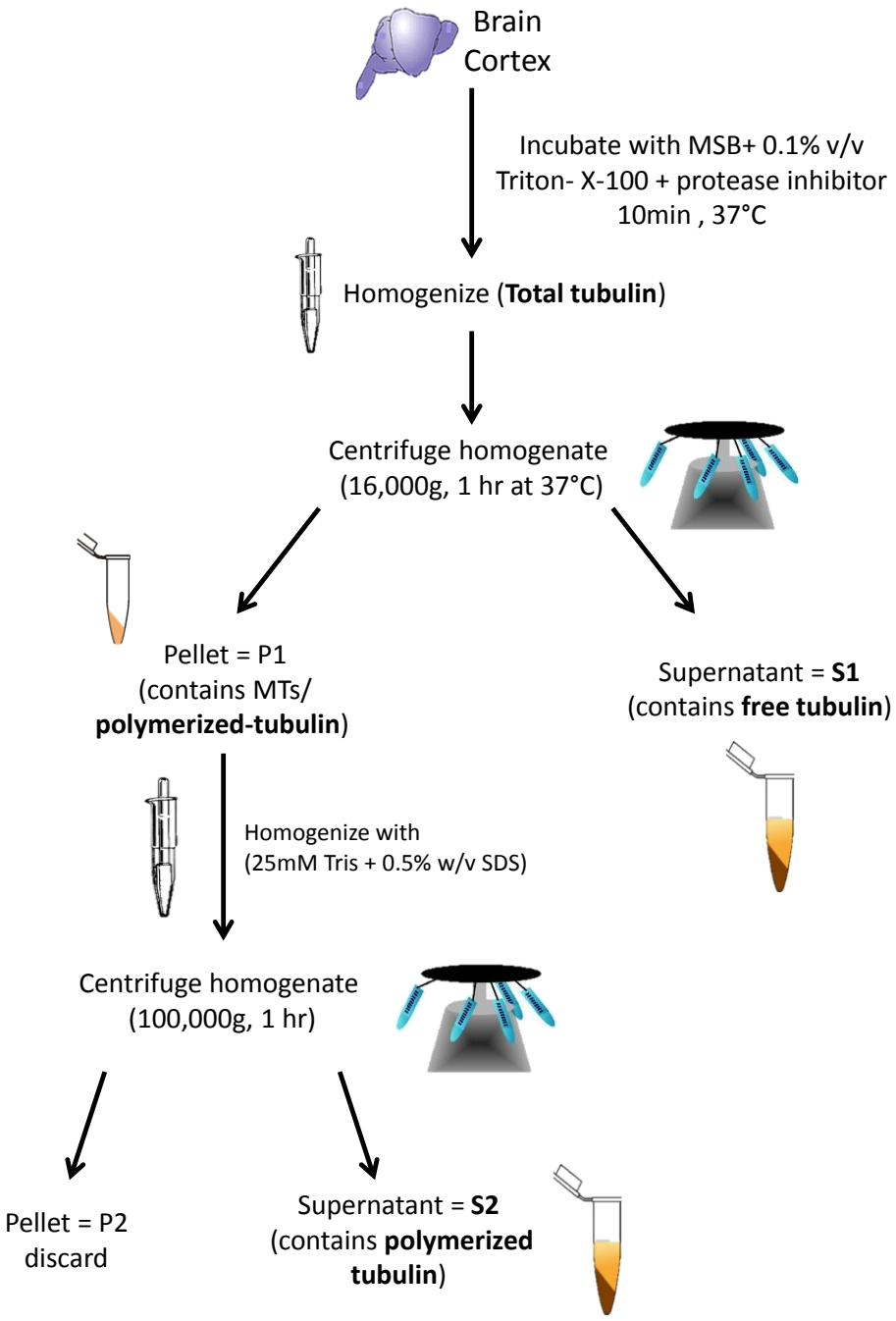


Figure 2.3 Schematic for free and polymerized tubulin protocol preparations as described in the Experimental section.

2.4 Gene expression analysis

2.4.1 RNA extraction

2.4.1.1 Reagents

1) RNeasy Lipid Tissue Mini Kit, Qiagen
2) 3 ml Ultimate Security Cryo-vial External Thread FS, alpha laboratories
3) IKA® T10 basic ULTRA-TURRAX® Homogenizer

2.4.1.2 Method

Total RNA extraction was performed using RNeasy Lipid Tissue Mini Kit. To isolate RNA, approximately 25 mg of cortical tissue, transferred to a 3 ml cryo-vial external thread tube and were homogenised in 1 ml QIAzol Lysis buffer using an IKA® T10 basic ULTRA-TURRAX® Homogenizer for 2 times for 2 sec. The homogenates were then processed in accordance with the manufacturer's protocol. Purified RNA was re-suspended in RNase-free water and RNA concentrations were measured by a NanoDrop 2000 UV-Vis Spectrophotometer (with NanoDrop 2000 software). A 260/280 nm ratio of more than 2 was considered indicative of good purity RNA. RNA samples were stored at -80°C.

2.4.2 cDNA synthesis

2.4.2.1 Reagents

SuperScript™ III Reverse Transcriptase Kit, Invitrogen

2.4.2.2 Method

1µg of total RNA was reverse transcribed using SuperScript III Reverse Transcriptase in accordance with the manufacturer's protocol. Added 1 µl of oligo (dT) (50 µM, Promega, Southampton, UK), 1 µl dNTP Mix (10 mM, Promega, Southampton, UK), 1 µg RNA and sterile distilled water together to give a total volume of 13 µl, and incubated at 65°C for 5 minutes. After adding 4µl 5×first-strand buffer, 1 µl dithiothreitol (0.1 M DTT) and 1 µl Recombinant RNase Inhibitor (40U/µl, Promega, Southampton, UK), 1µl Superscript III reverse transcriptase (200U/µl, Invitrogen,

Paisley, UK) was added and incubated at the following temperatures: 50°C for 5 minutes, following by 50°C for 60 minutes in a thermo-cycle PCR (Master cycle- eppendorf®). The reaction was terminated by heating the samples at 70°C for 15 minutes. In order to test for the presence of genomic DNA a negative control was included in which the SuperScript III enzyme was replaced with 1 µL of sterile distilled water (RT-negative samples). All cDNA samples were diluted with 1:4 µL of sterile distilled water, then placed on ice, ready to be used as a PCR template.

2.4.3 Quantitative polymerase chain reaction

mRNA quantification of genes of interest in experimental samples were measured by qPCR with TaqMan® Fast Advanced Master Mix (Applied Biosystems, Paisley, UK). 2× TaqMan® Gene Expression Master Mix

2.4.3.1 Reagents

1) TaqMan® Gene Expression Assays, Thermo Fisher Scientific
2) ABI prism 7900 sequence detector

2.4.3.2 Method

Real-time quantitative PCR (RT-PCR) assays were performed by TaqMan PCR using an ABI prism 7900 sequence detector (Applied Biosystems Inc., Foster City, CA, USA) with 2 µl of cDNA, 18 µM of each primer, 5 µM probe and Universal TaqMan 2x PCR Mastermix (Roche). Each sample was run in duplicate. Primers and MGB TaqMan probes (Thermo Fisher Scientific) were chosen where possible such that probes spanned over exon–exon boundaries to avoid genomic amplification (Table 2.5). Hydroxymethylbilane synthase (Hmbs) was used as internal control, and all genes of interest were labelled with the fluorescent reporter 5-carboxyfluorescein. All assays were performed under the following thermal cycler conditions: rapid initial heating to 95°C for 10 minutes, denaturation at 95°C for 10 seconds and annealing/extension at 60°C for 30 seconds for a total of 40 cycles.

SDS2.2.2 software was used to generate the amplification plot and determine Ct variability. All calculations of the Ct value were performed with the threshold set at 0.2.

2.4.4 Gene expression quantification

Comparative Ct method for quantification uses arithmetic calculations to determine the relative expression of a given gene in a sample of interest by comparing it to a housekeeping gene and calibrator sample. The method is based on the assumption that difference in the threshold cycles (ΔCt) between the gene of interest and the housekeeping gene is proportional to the expression level of the gene of interest (ΔCt = Ct (gene of interest) –Ct (HMBS)(Livak and Schmittgen, 2001). Next, the normalised expression of the target gene in the sample of interest relative to its expression in the calibrator sample is calculated (ΔΔCt = ΔCt (sample) - ΔCt (calibrator)). Finally, the relative fold change in gene expression in the *Psmc1*$^{fl/fl}$*;CaMKIIa-Cre* group compared with the control was calculated using the $2^{-\Delta\Delta Ct}$ method.

Table 2.5 Real-time RT-PCR Assay IDs from Thermo Fischer Scientific

Gene Symbol	Gene name	Entrez Gene ID	ThermoFisher Assay ID	Exon Boundary	Amplicon Size (bp)
Stmn1	Stathmin 1	16765	Mm01185262_m1	1 - 2	72
Nefl	Neurofilament, light polypeptide	18039	Mm01315666_m1	1 - 2	69
Nefm	Neurofilament, medium polypeptide	18040	Mm00456201_m1	2 - 3	84
Nefh	Neurofilament, heavy polypeptide	380684	Mm01191456_m1	2 - 3	71

2.5 Histology

2.5.1 Tissue processing

2.5.1.1 Reagents

1) Paraformaldehyde, P6148 Sigma-Aldrich
2) Phosphate buffered saline
3) Leica TP1020 Tissue Processor
4) Leica RM2245 Rotary Microtome

2.5.1.2 Method

Tissues were fresh collected from the animals. Mice were perfused with 0.9% saline followed by 4% w/v paraformaldehyde in PBS pH 7.4. The brain tissues were left in the fixative 4% w/v paraformaldehyde for 48 to 72 hours. Then fixed tissues were dehydrated and infiltrated with paraffin wax by processing in a Leica TP1020 Tissue Processor, program 6 as shown in Table 2.6

Table 2.6 Protocol for tissue processing

Reagent	Formalin		Alcohol						chloroform		paraffin	
			70%	80%	95%	100%						
Time	1 hr	1 hr	1:30 hr	1:30 hr	1:30 hr	1 hr	1 hr	1 hr	1:30 hr	1:30 hr	2 hr	2 hr

After the tissue processing, the tissues were manually embedded in paraffin wax, and left on ice for at least 48 hours before sectioning with a sliding microtome (Leica RM2245 Rotary Microtome) set to 7μm. The sections were floated on a preheated water bath to 37^{o}C before mounting on APES coated glass slides. The slides were then left overnight on a hot plate at 37^{o}C to dry.

2.5.2 APES (amino-propyl-tri-ethoxy-silane) coating of slides

2.5.2.1 Reagents

1) APES (amino-propyl-tri-ethoxy-silane), Sigma-Aldrich
2) Acetone, Sigma-Aldrich
3) Superfrost™ Microscope Slides, Thermo Fisher Scientific

2.5.2.2 Method

A slide is placed in the Coplin jar containing 10 mL of the APES with 500 mL acetone. (This makes a 2% solution). Then dip clean dry slides in APES solution for 2 minutes. Wash the slides in 2 changes of distilled water. Slides dry completely in oven at 50°C. Treated slides store in boxes at room temperature for used.

2.5.3 Immunohistochemistry of paraffin-embedded tissue sections

This method is based on Vector® M.O.M.™ immunodetection kit for mouse primary antibodies and the VECTASTAIN® ABC system for rabbit antibodies. Levelled horizontal brain sections from 4 and 6-weeks of age *Psmc1*$^{fl/fl}$*;CaMKIIα-Cre* and control mice were processed for immunohistochemistry (Figure 2.4).

2.5.3.1 Reagents

1) Horizontal brain sections
2) Xylene
3) Ethanol, 100%, 95% and 70% dilutions
4) Schiefferdecker staining dish (for slide washing)
5) Antigen retrieval buffer solution
   10 M sodium citrate buffer 0.05% v/v Tween-80, pH 6
6) Hydrogen peroxide solution 30% w/w in H_2O, Sigma-Aldrich
7) Vector® M.O.M™ immunodetection kit for mouse antibody, Vector Laboratories
8) VECTASTAIN® ABC system for rabbit antibodies, Vector Laboratories
9) 10% goat serum (VECTASTAIN Elite rabbit IgG, ABC kit)
10) Secondary biotinylated antibody according to the kit
11) Detection VECTASTAIN® Elite® ABC reagent according to the kit
12) DAB (3,3' Diaminobenzidine tetrahydrochloride), Sigma-Aldrich
13) DAB solution

0.1M Tris pH 7.5

0.05% w/v DAB

0.03% v/v H_2O_2

14) Shandon™ Harris Hematoxylin, Thermo Fisher scientific
15) 1% acid alcohol [HCl in 70% v/v ethanol]
16) DPX mounting medium, Fisher Scientific

2.5.3.2 Method

1) Deparaffinization and rehydration

Brain cortex sections were deparaffinized by immersion the slides in xylene for 10 min, then rehydrated in gradually decreasing concentrations of ethanol: 100%, 95% and 70% for 10 min each and then gently running tap water for 10 minutes.

2) Antigen retrieval

The slides were incubated for 20 min in pre-heated antigen retrieval solution at approximately 100°C. The slides were then removed and the breaker left on a gentle shaker at room temperature for 20 min and then rinse for 10 min with running tap water.

3) Block endogenous peroxidase

Endogenous peroxidase activity was blocked by incubating the slides in 0.3% v/v H_2O_2 hydrogen peroxide in tap water at room temperature for 10 min. The slides were then washed in gently running tap water for 10 min and then PBS on a rocking platform for 5 min.

4) Block non-specific background

To block non-specific binding, the slides were incubated with serum from the same species as the secondary antibody for 30 min in a humidified chamber at room temperature; 3% v/v goat serum in PBS (VECTASTAIN® ABC system - rabbit kit), but with mouse protocol block non-specific binding solution is 0.8% v/v Mouse on Mouse (M.O.M) Ig blocking reagent in PBS.

5) Primary antibody incubation

Primary antibodies were diluted with appropriate non-specific blocking reagent or 8% M.O.M. diluent in PBS according to (Table 2.7). The brain sections were incubated with primary antibodies using adhesive frames. Antibody solutions of 65 µl covered brain section within a frame (Frame-Seal incubation chambers). The sections were covered and incubated in humid chamber overnight at 4°C. The next morning the sections were washed extensively with 3 changes of PBS for 10 min each with gentle agitation.

Table 2.7 Antibodies used in the immunohistochemistry

Primary	Animal source	Dilution	Manufacturing company
STMN1	Rabbit	1:100	Gene Tex, GTX113341
NFL	Mouse	1:100	Cell Signaling, 2835
NFM	Mouse	1:100	Cell Signaling, 2838
NFH	Mouse	1:50	Cell Signaling, 2836
Ub UV-1	Mouse	1:100	LifeSensors, VU101
Ub-KIH	Rabbit	1:100	House made

6) Secondary antibody incubation

The appropriate amount of diluted biotinylated secondary antibody was applied according to the protocol on Vector® M.O.M™ immunodetection kit for mouse and the VECTASTAIN® ABC system for rabbit antibodies 1:200. The sections were incubated in a humidified chamber at room temperature for 1 hr. The sections were then washed 3 times for 10 min each with PBS and gentle agitation.

7) Detection

Premixed VECTASTAIN® Elite® ABC reagent: add exactly two (2) drops of reagent A to 5 ml of buffer in the ABC. Then add exactly two (2) drops of reagent B to the same mixing bottle. Mix immediately, and allow VECTASTAIN® Elite® ABC reagent to stand for about 30 minutes before use. The premixed ABC

reagent was applied to each section and incubated in a humidified chamber at room temperature for 30 min protected from light. The slides were then washed with PBS three times for 10 min each with gentle agitation.

8) DAB reaction (3,3' Diaminobenzidine tetrahydrochloride)

DAB (3, 3'-diaminobenzidine) is a substrate for peroxidase forming a brown precipitate when they react together. Therefore, when peroxidase-conjugated antibodies are bound to epitopes they can be specifically stained by incubation with DAB. It is necessary to block the endogenous peroxidase activity using H_2O_2 prior to the DAB staining. Following incubation with ABC detection reagent and washing the sections were incubated in DAB solution. When the appropriate staining was achieved, the reaction was stopped by gently running tap water for 10 min.

9) Counterstaining, dehydration and mounting

The sections were counterstained by immersing the slides in Harris hematoxylin 5 min. To obtain a better contrast of the sample. The slides were then washed in running tap water and dipped in 1% acid alcohol [HCl in 70% v/v ethanol] for 10 seconds followed by gentle washing in running tap water for 10 min. The slides were subjected to dehydration through 3 stages of ethanol (70%, 95%, and 100%) for 10-20 sec each. Finally the slides were treated with 100% v/v xylene, and then mounted with DPX (Distrene, Plasticiser, and Xylene) and covered with a cover slip to protect the tissue from shrinking. The slides were ready to be examined, preferably after 12-24 hours so the slides were completely dried.

The slides were scanned using a NanoZoomer Digital Pathology (NDP) system (Hamamatsu Photonics, Japan) and images viewed using NDP.view.2 software

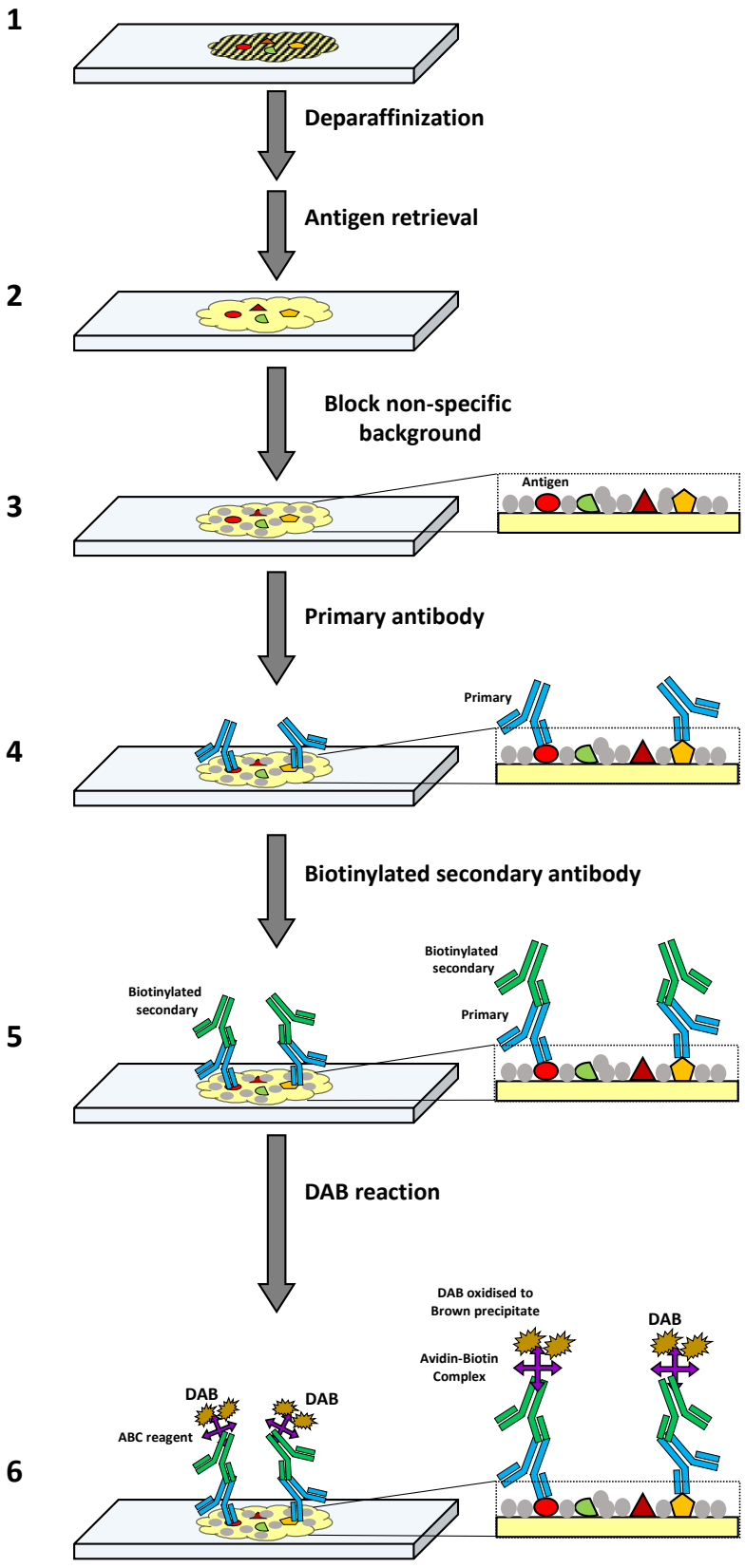


Figure 2.3 Schematic for immunohistochemistry method as described in the experimental section

2.6 Statistical analysis

Statistical analysis was done by using GraphPad Prism software 6.07. Data were collected from three or more independent samples as indicated in the results and expressed as mean ± S.E.M. Comparisons between control and *Psmc1*$^{fl/fl}$;*CaMKIIa-Cre* mice data were made using two-tailed Student`s unpaired t-test and non-parametric Mann-Whitney U test , which used to determine the statistical significance for non-normal distribution data. *p* values of less than 0.05 were taken as significant *$p < 0.05$;**$p < 0.01$; ***$p < 0.001$, ****$p \leq 0.0001$.

Chapter 3

Microtubule instability following disruption of the 26S proteasome in mouse cortical neurons

3.1 Introduction

The neuronal cytoskeleton is a highly organized polymers of protein that provide architectural support to axons and dendrites, and also provide railways for the transport of various cytoplasmic organelles (Monteiro et al., 2011). The main components of the cytoskeleton in cells are microfilaments (MFs), neurofilaments (NFs) and microtubules (MTs). This chapter will focus on MFs, MTs and microtubule-associated proteins (MAPs) following disruption of the 26S proteasome in cortical neurons and consequent neurodegeneration in the *Psmc1*$^{fl/fl}$;*CaMKIIa-Cre* mouse model. NFs will be investigated in Chapter 5.

Studies suggest cytoskeletal dysfunction is an important mechanism in the aetiology of several neurodegenerative diseases, including Alzheimer's and Parkinson's diseases (Cairns et al., 2004). Neurodegenerative disorders are characterized by selective dysfunction and loss of neurons associated with pathological accumulation of abnormal protein aggregates, including cytoskeletal proteins such as actin-depolymerizing factor (ADF) and the actin binding protein, cofilin (D'Andrea et al., 2001, Minamide et al., 2000). Direct evidence supporting the involvement of MTs in neurodegenerative disease comes from genetic studies identifying mutations in various members of the tubulin family, such as the MAP tau (Arendt et al., 2016, Franker and Hoogenraad, 2013).

Actin is the most abundant cytoskeletal protein in neurons and glia (Kollins and Davenport, 2000). Actin plays an essential role in morphological development of neurons as well as structural changes in the mature neuron (Kirkpatrick et al., 1999). Actin is also involved in specialized microdomains on the cell surface for pre- and post-synaptic morphological specializations (Kollins and Davenport, 2000, Schevzov et al., 2012). Cytoplasmic aggregations containing actin and actin-binding proteins are associated with a number of neurodegenerative diseases, including Alzheimer's disease (Bamburg and Bernstein, 2016), amyotrophic

lateral sclerosis (Griffin et al., 2014) and parkinsonism-dementia complex (Sousa et al., 2009). Tau-induced neurodegeneration in Drosophila and AD mouse model is associated with the formation of actin-rich rod-like structures, and this neurodegeneration can be attenuated by reducing actin accumulation (Fulga et al., 2007). Furthermore, under stress conditions, the actin binding protein (cofilin) becomes dephosphorylated and binds to actin leading to formation cofilin-actin rod structures in either the nucleus or cytoplasm (Munsie and Truant, 2012, Cichon et al., 2012). Persistent rods that span the diameter of the neurite disrupt MTs and cause degeneration of the distal neurite without killing the neuron. These findings suggest that cofilin-actin inclusions in mature neurons can lead to neuronal dysfunction and synaptic loss.

MTs are dynamic polymers of α/β-tubulin heterodimers (Sirajuddin et al., 2014, Howard and Hyman, 2003). These proteins are characterized by an intrinsic resistance to bending and compression and the capability to switch between destabilization (depolymerisation) and stabilization (polymerisation), which is called dynamic instability (Cartelli et al., 2013). MTs have a stable minus (-) end, where MTs initiate and anchored at a central microtubule-organizing center (MTOC). MTs also have a dynamic plus (+) end that serving as the site of tubulin addition and loss. The α-tubulin present at the (-) end contains a non-hydrolysable guanosine-5`-triphosphate (GTP). Whereas the β-tubulin capped microtubules at the (+) end have a GTP molecule which can hydrolyse to guanosine diphosphate (GDP) during MT polymerization (Quiniou et al., 2013). MT are more stable in mature than immature neurons (Zhang et al., 2012).

In normal neurons MT stability is highly regulated by the intrinsic GTPase activity of tubulins as well as MT-interacting proteins, including MAPs, MT-severing proteins, MT (+)-end tracking proteins (+TIPs), and motor proteins. The interactions between MTs and MT-interacting proteins are also influenced by post-

translational modifications (PTMs) of tubulin (Kapitein and Hoogenraad, 2015).

PTMs of tubulin, which include acetylation, tyrosination, detyrosination, palmitoylation and phosphorylation have recently gained new interest for their role in neuronal differentiation and neurodegenerative disorders (Fukushima et al., 2009). Tubulin PTMs can reflect the stability of MTs (Perdiz et al., 2011, Baas et al., 1993). Stable microtubules usually have detyrosinated and acetylated tubulin (Fukushima et al., 2009, Peris et al., 2009). In cultured rat sympathetic neurons, tyrosinated MTs were observed in the proximal and distal regions of growing axons, indicating newly assembled MTs (Brown et al., 1992). Changes in the detyrosination/tyrosination cycle affect MT dynamics and their interactions with intermediate filaments (Kreitzer et al., 1999) and MFs (Marcos et al., 2009). α-tubulin undergoes a tyrosination/detyrosination cycle. α-tubulin modified with a tyrosine residue at the C-terminus forms a heterodimer with β-tubulin and assembles into MTs (Fukushima et al., 2009). After assembly the tyrosine residue is removed from α-tubulin forming detyrosinated α-tubulin within the MTs and reattached to free α-tubulin to continue the cycle (Janke and Bulinski, 2011). Hence, detyrosinated α-tubulin is often used as an indication of how long a microtubule has been assembled, while tyrosination is associated with young neurons and the most dynamic microtubules (Poulain and Sobel, 2010, Baas et al., 1993). This modification is accomplished by the action of two enzymes, tubulin tyrosine ligase (Arce et al., 1975), which catalyses the incorporation of tyrosine, and tubulin carboxypeptidase, which removes the tyrosine residue. Most of the results obtained in vitro and in vivo indicate that the ligase acts on non-assembled tubulin whereas the carboxypeptidase acts mainly on tubulin in MTs (Arregui et al., 1991). These modifications affect the C-terminal domain of α/β-tubulins, which is located on the outside of the microtubule and forms a readable code for microtubule-associated and motor

proteins (De Forges et al., 2012). Acetylation is the reversible transfer of an acetyl group from the acetyl-coenzyme A to the ε-amino group of a lysine (Lys) residue (Ren et al., 2014). Acetylation of Lys40 on α-tubulin is unique in that it is located on the luminal surface of MTs and carried out by a conserved α-tubulin acetyltransferase (α-TAT) (Nogales et al., 1999, Friedmann et al., 2012). Two histone deacetylating (HDAC) enzymes HDAC6 and SIRT2 have been shown to be involved in de-acetylation α-tubulin both in in vitro and in vivo studies (Hubbert et al., 2002, North et al., 2003).

Alterations in MT stability have consistently been linked to pathological conditions. In hereditary spastic paraplegia MTs are hyper-stabilized. Therefore, the cytoskeletal structure becomes rigid and neurons lack plasticity (Salinas et al., 2005). By contrast, in Alzheimer's disease, MTs are destabilized; axonal trafficking is impaired and synaptic contacts collapse (Zhang et al., 2012). Recent studies suggest that disassembly of MTs is an early event in Parkinson's disease pathology, followed by degradation of other cytoskeletal components and fragmentation of the axon (Cartelli et al., 2013). Since nigral neurons have very long axons projecting to the striatum, a high degree of cooperation between MTs and MT-dependent motor proteins is required to ensure dopamine vesicle transport. Depolymerisation of MTs may lead to impairment of dopamine transport and an abnormal accumulation of dopamine vesicles in the soma, which may cause increased oxidative stress and eventually cell death (Parisiadou and Cai, 2010). Decreased tubulin acetylation is associated with more unstable microtubules and altered intracellular transport was observed in Huntington's (Dompierre et al., 2007) and Parkinson's (Outeiro et al., 2007) disease cellular models. In addition, increased detyrosinated tubulin was associated with impairment of axonal transport and mitochondrial damage as a consequence of MT dysfunction in 1-methyl-4-phenyl-1, 2, 3, 6-tetrahydropyridine (MPTP)-induced neurodegeneration in PC12 cells (Cartelli et al., 2010).

Increased MT dynamics may serve as a general indicator of neurite remodelling in health and disease states (Kleele et al., 2014). Increased destabilization of axonal MTs and impaired axonal transport is linked to motor neuron degeneration in ALS transgenic mice (Fanara et al., 2007, Sasaki and Iwata, 2007). Moreover, treatment of these mice with microtubule-modulating agent Noscapine reduced microtubule turnover, preserved spinal cord neurons, normalized axonal transport kinetics and delayed the onset of neurodegenration symptoms (Fanara et al., 2007). Previous studies in progressive motor neuronopathy (*pmn*) mutant mice, a model of motorneuron disease, showing a dramatic reduction in α and β-tubulin heterodimers was associated with unstable MTs and significantly increased the levels of tyrosinated tubulin (Martin et al., 2002). However, the levels of acetylated stable MTs were not different between *pmn* and wild-type motoneurons. Stabilization of MTs by taxol demonstated a key role in axon regeneration after spinal cord injury (Hellal et al., 2011). Increasing total polymerized tubulin and decreasing tyrosinated tubulin promoted regeneration of dorsal root sensory nerve fibers.

Regulation of MT assembly and MT stability are further dependent on MAPs (Chapin and Bulinski, 1992). There are two main types of MAPs in neurons; those that stabilize MTs such as MAP2 and tau, and those that destabilize MTs such as stathmin (STMN). MAP2 and tau have been shown to play roles in MT stabilization and facilitate tubulin polymerization in vitro. MAP2, especially high molecular MAP2 isoforms, is found in the dendrites of mature neurons, while tau is associated mainly with axonal MTs (Zhang and Dong, 2012). MAP2 and tau bind to the sides of MTs, contributing to their stabilization by forming cross-bridges between adjacent MTs (Farah and Leclerc, 2008, Al-Bassam et al., 2002). Binding of these proteins to MTs may be regulated by phosphorylation of their tubulin binding motifs within each microtubule-binding repeat. These motifs are phosphorylated by multiple protein kinases, including protein kinase A (PKA) (Ozer and Halpain, 2000, Drewes

et al., 1995), and phosphorylation appears to reduce the affinity between MAP2/tau and MTs leading to MT disassembly (Cassimeris and Spittle, 2001, Dehmelt and Halpain, 2005).

MAP2 has been shown to play an important role in maintaining dendritic structure via its interaction with MTs. Loss of MAP2 immunoreactivity across several cortical regions was closely linked to dendritic spine pathology in schizophrenia brain tissue (Shelton et al., 2015). In addition, decreased MAP2 expression led to reduced dendrite length in MAP2-deficient mice (Harada et al., 2002) and in primary cultured neurons prevents dendritic differentiation (Farah and Leclerc, 2008). Decreased MAP2 has also been reported in Alzheimer's disease (Fifre et al., 2006).

Tau and MAP2 may compensate for each other, as deletion of tau led to increased levels of MAP2 in middle-aged (8-9 months) tau knock-out mice (Ma et al., 2014). However, in aged (19-20 months) tau knock-out mice significant loss of MAP2 was reported associated with Morris Water Maze deficits and loss of hippocampal acetylated α-tubulin. Low levels of tau phosphorylation are found in normal neurons, promoting its interaction with tubulin, which stabilizes MT structure. Abnormal hyper-phosphorylation of tau can decrease the interaction between tau and MTs, inhibiting their assembly (Abraha et al., 2000, Cho and Johnson, 2003).

Stathmin (STMN1) is a member of a family of MT regulatory proteins that play important roles in destabilizing microtubules by binding tubulin dimers (Ringhoff and Cassimeris, 2009). Studies have shown an association between STMN1 and an increase in the rate of microtubule catastrophe via direct interaction of STMN1 with tubulin dimers and inhibition of tubulin polymerization (Belmont and Mitchison, 1996, Clement et al., 2005). The first evidence for an essential role of stathmin in nervous system development came from RNAi silencing of the only stathmin gene in Drosophila (Ozon et al., 2002). This caused abnormal chordotonal neuron organization and loss of commissures in the ventral cord. A significant study by Liedtke and colleagues (2002) showed

axonopathy of the central and peripheral nervous systems in STMN1 knockout mice with highly irregular axoplasm degeneration and demyelination (Liedtke et al., 2002). STMN1 was shown to play an essential role in the maintenance of axonal integrity in Drosophila; decreased STMN1 had a direct effect on depolymerisation of MTs, leading to the development of axonopathy (Wen et al., 2010).

STMN1 and MAP2-tau have opposing roles in MT stability. In STMN1 expressing cells the amount of tau phosphorylation in the MT-unbound fraction was higher than in the MT-bound fraction (Miyasaka et al., 2010). The inverse relationship of these proteins is also evident in breast cancer; low STMN1 levels and high tau levels were associated with increased microtubule stability and better prognosis (Baquero et al., 2012). In addition, downregulation of both the expression and activity of STMN1 is important for normal dendritic arborization in cultured Purkinje cells; STMN downregulation is mediated by neuronal activity and calcium/calmodulin-dependent protein kinase II (CaMKII) phosphorylation (Ohkawa et al., 2007a). Interestingly, CaMKII also phosphorylates MAP2, decreasing its binding to MTs (McVicker et al., 2015).

Taken together, these studies support a role for MT changes in neurodegeneration. Interesting, we recently showed significantly decreased STMN1 levels associated with neurodegeneration and Lewy-like inclusions following disruption of the 26S proteasome in forebrain mouse neurons (Elkharaz et al., 2013). Therefore, this chapter will focus on MFs, MTs and microtubule-associated proteins (MAPs) following disruption of the 26S proteasome in cortical neurons and consequent neurodegeneration in the *Psmc1*$^{fl/fl}$;*CaMKIIa-Cre* mouse model.

3.2 Results

3.2.1 Normalization of Western blots

Quantitative Western blot analysis was used to measure relative protein levels in control and *Psmc1*$^{fl/fl}$;*CaMKIIα-Cre* mouse cortical brain tissue in this chapter. Normalization is essential for accurate quantitation where so-called 'housekeeping proteins' are used as loading controls to correct for any loading errors (Ghosh et al., 2014). α-tubulin, β-actin and glyceraldehyde 3-phosphate dehydrogenase (GAPDH) are widely used housekeeping proteins. These proteins are found in high quantities within biological samples and remain relatively insensitive to changes in environmental conditions and treatments (Gilda et al., 2015, Eaton et al., 2014, Taylor et al., 2013). However, studies have also shown that housekeeping proteins are influenced by various physiological and pathological factors, and that α-tubulin and β-actin may not be suitable loading controls when investigating neuronal cytoskeletal changes (Ferguson et al., 2005, Dittmer and Dittmer, 2006, Castano and Kypta, 2008, Eaton et al., 2013). Therefore, normalising the data to the expression of these proteins may skew the results, leading to erroneous conclusions.

To clarify whether we could use a housekeeping protein for normalization in our studies, we compared the total density of transferred protein on the nitrocellulose membrane by copper staining and also GAPDH protein levels between control and *Psmc1*$^{fl/fl}$;*CaMKIIα-Cre* mice (Figures 3.1 and 3.2). Figure 3.1A shows copper staining of four different sets of 6 week-old cortical samples where each sample is a biological replicate, i.e. a different mouse. As expected, Figure 3.1B shows that there is no significant difference in the amount of protein loaded between control and *Psmc1*$^{fl/fl}$;*CaMKIIα-Cre* cortical samples. Having demonstrated that total protein was similar in control and *Psmc1*$^{fl/fl}$;*CaMKIIα-Cre* mouse cortices at 6 weeks-old using copper staining, we then compared GAPDH protein levels of the blots shown in Figure 3.1 (Figure 3.2). Figure 3.2 shows that the levels of GAPDH are not

significantly different between control and *Psmc1*$^{fl/fl}$;*CaMKIIα-Cre* mice. These investigations were also repeated with 4 week-old mice with similar findings (data not shown). Our results suggest that both copper staining and GAPDH may be used to normalize for protein loading in the Western analyses presented in this chapter.

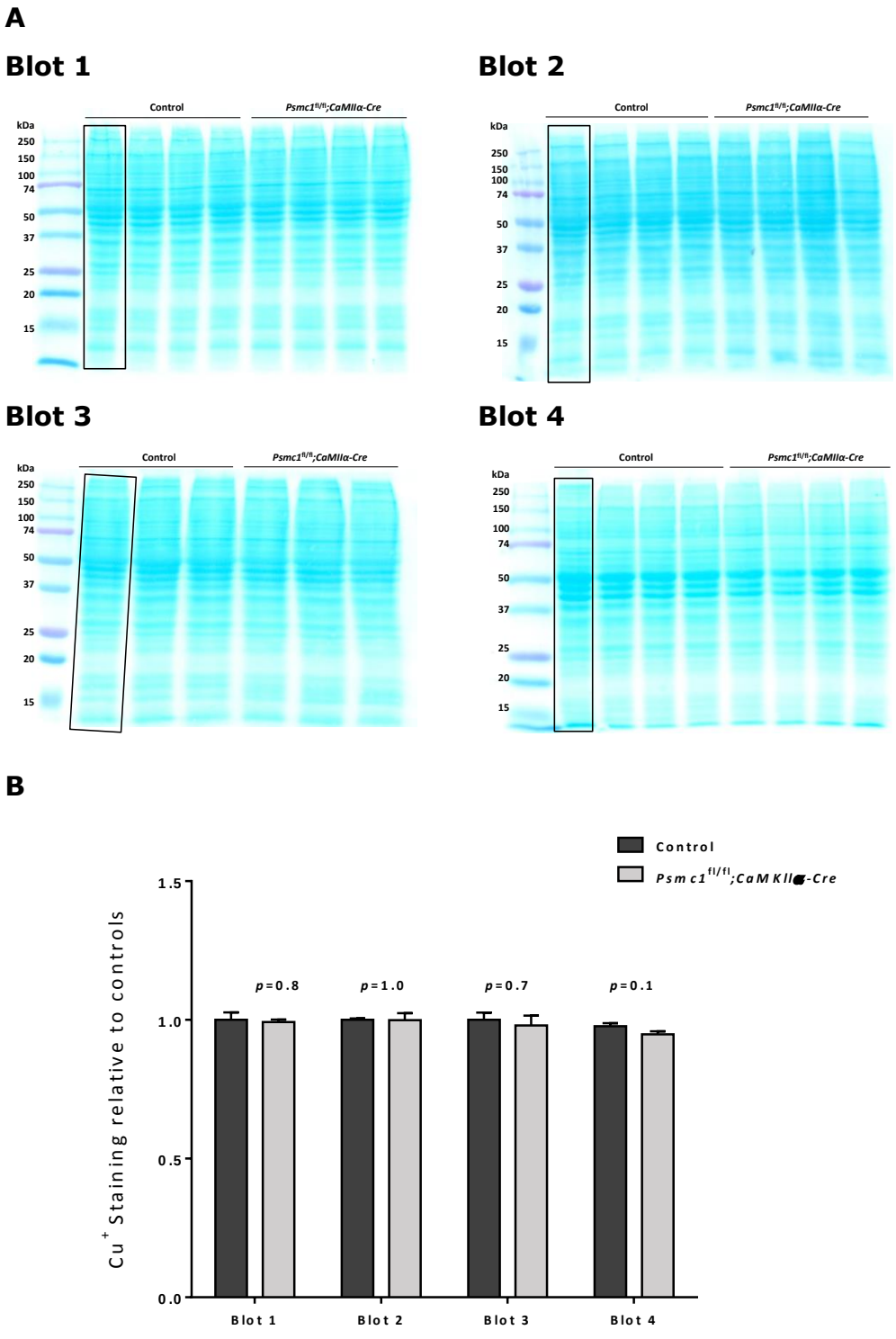
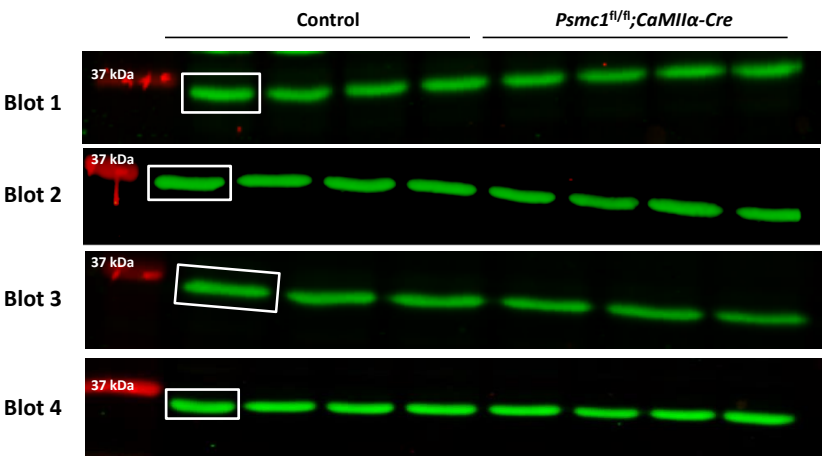


Figure 3.1 Relative levels of copper staining in 6 week-old control and *Psmc1*$^{fl/fl}$*;CaMKIIa-Cre* mouse cortical samples

(A) Copper-stained nitrocellulose membrane following SDS-PAGE on a 12% gel and transfer of 30 µg protein in protein lysis buffer per lane to visualize and quantitate total protein loading. Lanes are biological replicates. (B) Aida Image analyser software was used to quantitate total protein; an example of the area quantitated is shown by the black box. Data are presented as mean ± SEM and compared using Student's unpaired t-test. n=4 for blot 1, 2 and 4; n=3 for blot 3.

A



B

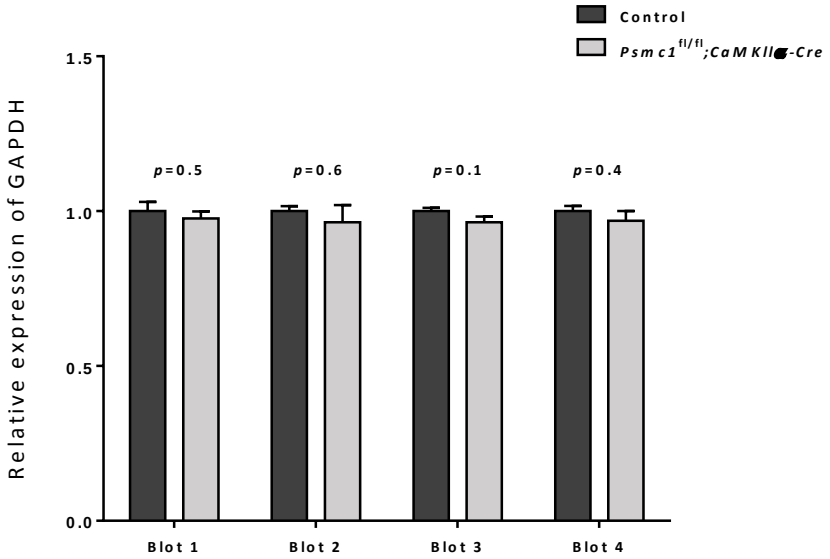


Figure 3.2 Relative levels of GAPDH in 6 week-old control and *Psmc1*$^{fl/fl}$*;CaMKIIα-Cre* mouse cortical samples

Immunoblots (A) and densitometric analysis (B) of GAPDH (38 kDa) protein levels of the blots shown in Figure 3.1. Image Studio software analysis was used for quantitation of protein bands; an example is shown by the white box. Data are presented as mean +/- SEM and compared using Student's unpaired t-test. n=4 for blot 1, 2 and 4; n=3 for blot 3.

3.2.2 Decreased cortical expression of microtubule proteins following disruption of the 26S proteasome in mouse cortical neurons

Western blotting analyses were carried out to investigate the levels of MT proteins; α-tubulin (Figure 3.3) and neuron-specific βIII-tubulin (Figure 3.4), and the MF protein; β-actin (Figure 3.5) in control and *Psmc1*$^{fl/fl}$;*CaMKIIα-Cre* mouse cortices at 4 and 6 weeks-old. Densitometric analyses showed that the total levels of α–tubulin and neuron-specific βIII- tubulin isotype were not significantly different between control and *Psmc1*$^{fl/fl}$;*CaMKIIα-Cre* cortices at 4 weeks of age (α-tubulin; p = 0.8; βIII-tubulin; p = 0.2, Figures 3.3 and 3.4 respectively). Interestingly, at 6 weeks of age expression of these MT proteins was significantly decreased in *Psmc1*$^{fl/fl}$;*CaMKIIα-Cre* mouse cortices compared to controls (α–tubulin; $p < 0.01$, βIII-tubulin; $p < 0.05$, Figures 3.3 and 3.4 respectively). The levels of MF protein β-actin did not show any significant difference between control and *Psmc1*$^{fl/fl}$;*CaMKIIα-Cre* cortices at either age studied (Figure 3.5; 4 weeks-old p = 0.5, 6 weeks-old p = 0.3). These observations suggest that decreased microtubule mass is one of the cellular events occurring as a consequence of neurodegeneration following 26S proteasome disruption in cortical neurons. Pharmacologic inhibition of the UPS in primary neurons has been shown to lead to loss of synaptic connections and reduced neuronal protein; βIII-tubulin, synaptophysin and drebrin occurred prior to any loss of mitochondrial activity or cell death (Bajic et al., 2012). However, another study using a neurotoxin-induced mouse model of Parkinson's disease showed that the levels of β-actin and α-tubulin were unchanged in the striatum and substantia nigra of 1-methyl-4-phenyl-1, 2, 3, 6-tetrahydropyridine (MPTP)-treated mice (Cartelli et al., 2013). However, β-tubulin levels were found to be decreased in the striatum of these mice and increased neuron-specific βIII-tubulin and detyrosinated tubulin was found in dopaminergic neurons.

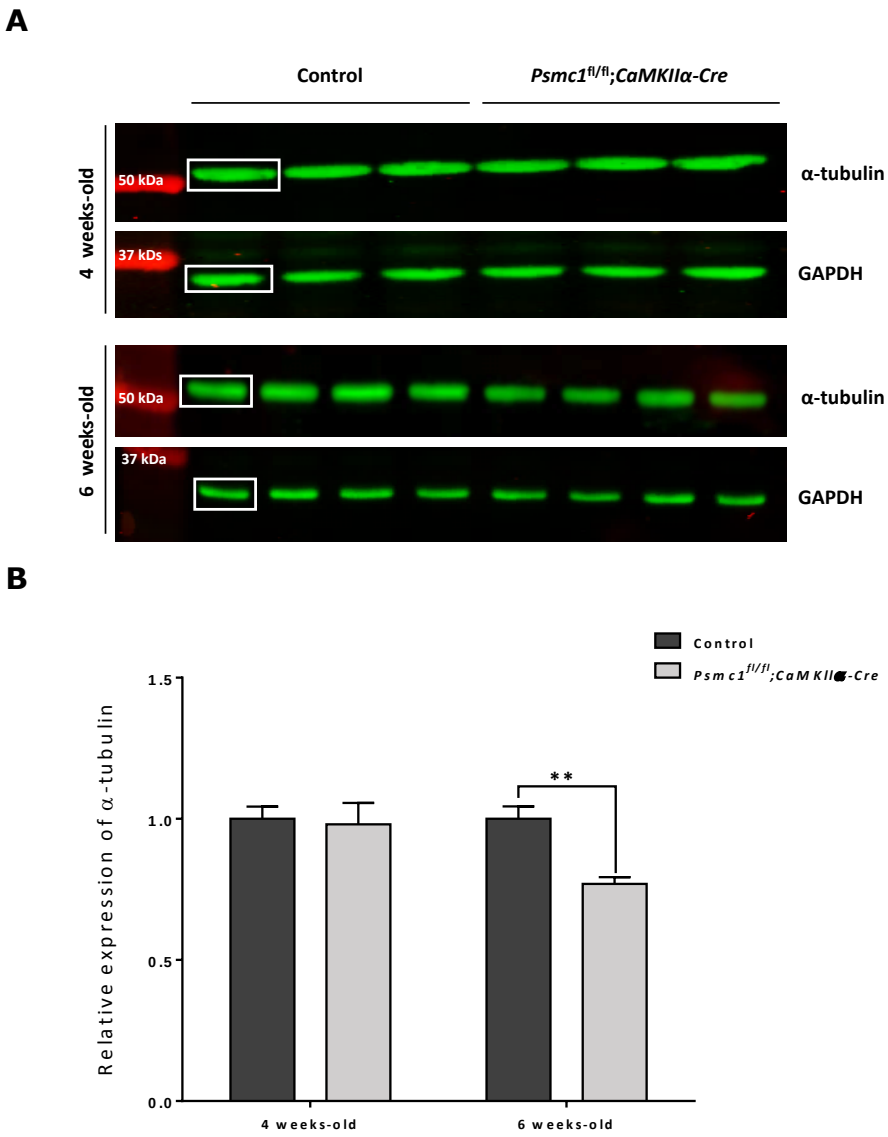


Figure 3.3 α-tubulin is significantly decreased in 6 week-old *Psmc1*$^{fl/fl}$*;CaMKIIα-Cre* compared to control mouse cortices

Immunoblots (A) and densitometric analysis (B) of α-tubulin (50 kDa) in 4 and 6 week-old control and *Psmc1*$^{fl/fl}$*;CaMKIIα-Cre* mouse cortices. 20 µg of protein per lane in protein lysis buffer was subjected to SDS-PAGE on a 12% gel and transferred to nitrocellulose membrane for Western blotting. (B) Quantitative analysis of immunoblots used Studio Image software analysis. α-tubulin level was normalised to the levels of GAPDH, used as a loading control. Data are presented as mean ± SEM and compared using Student's unpaired t-test. ** $p < 0.01$, n=4 for 6 weeks-old blot ; n=3 for 4 weeks-old blot.

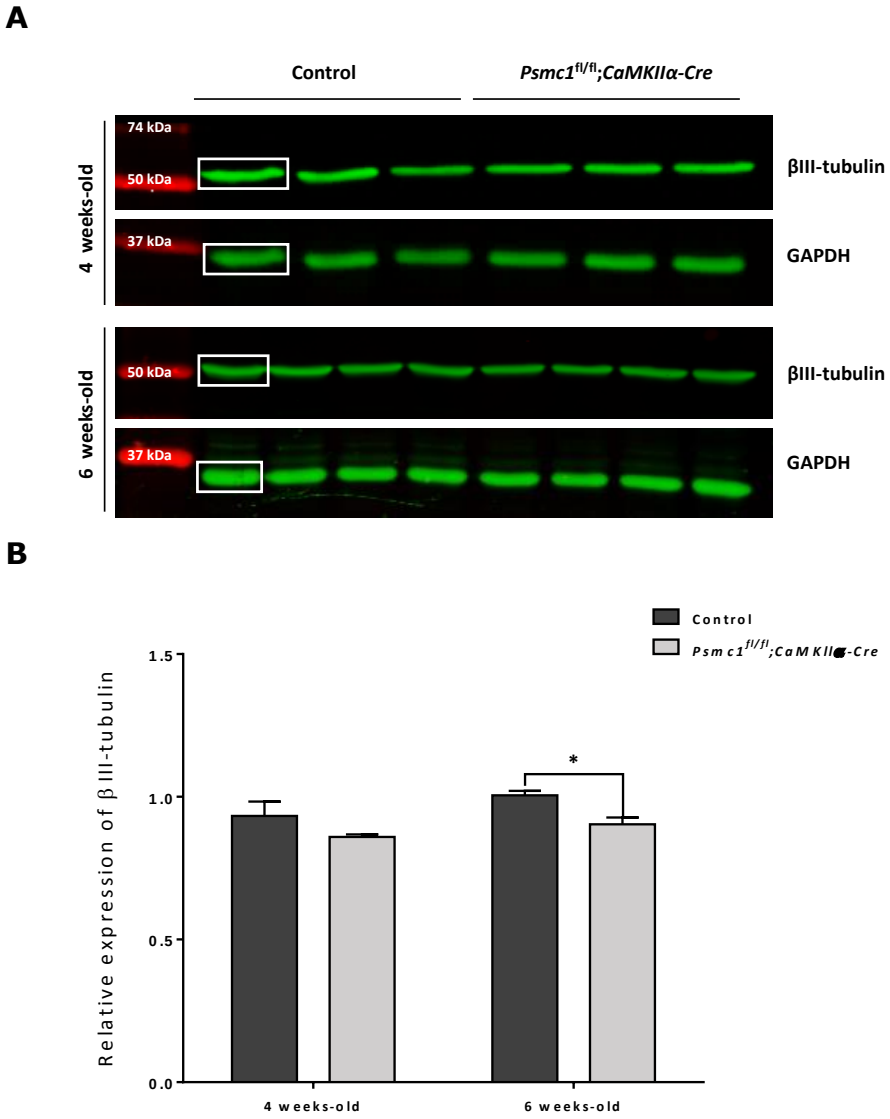


Figure 3.4 βIII-tubulin is significantly decreased in 6 week-old *Psmc1*$^{fl/fl}$*;CaMKIIα-Cre* compared to control mouse cortices.

Immunoblots (A) and densitometric analysis (B) of βIII-tubulin (50 kDa) in 4 and 6 week-old control and *Psmc1*$^{fl/fl}$*;CaMKIIα-Cre* mouse cortices. 20 µg of protein per lane in protein lysis buffer was subjected to SDS-PAGE on a 12% gel and transferred to nitrocellulose membrane for Western blotting. (B) Quantitative analysis of immunoblots used Image Studio software analysis. βIII-tubulin was normalised to the levels of GAPDH for each sample. Data are presented as mean ± SEM and compared using Student's unpaired t-test. * $p < 0.05$, n=4 for 6 week-old blot; n=3 for 4 week-old blot.

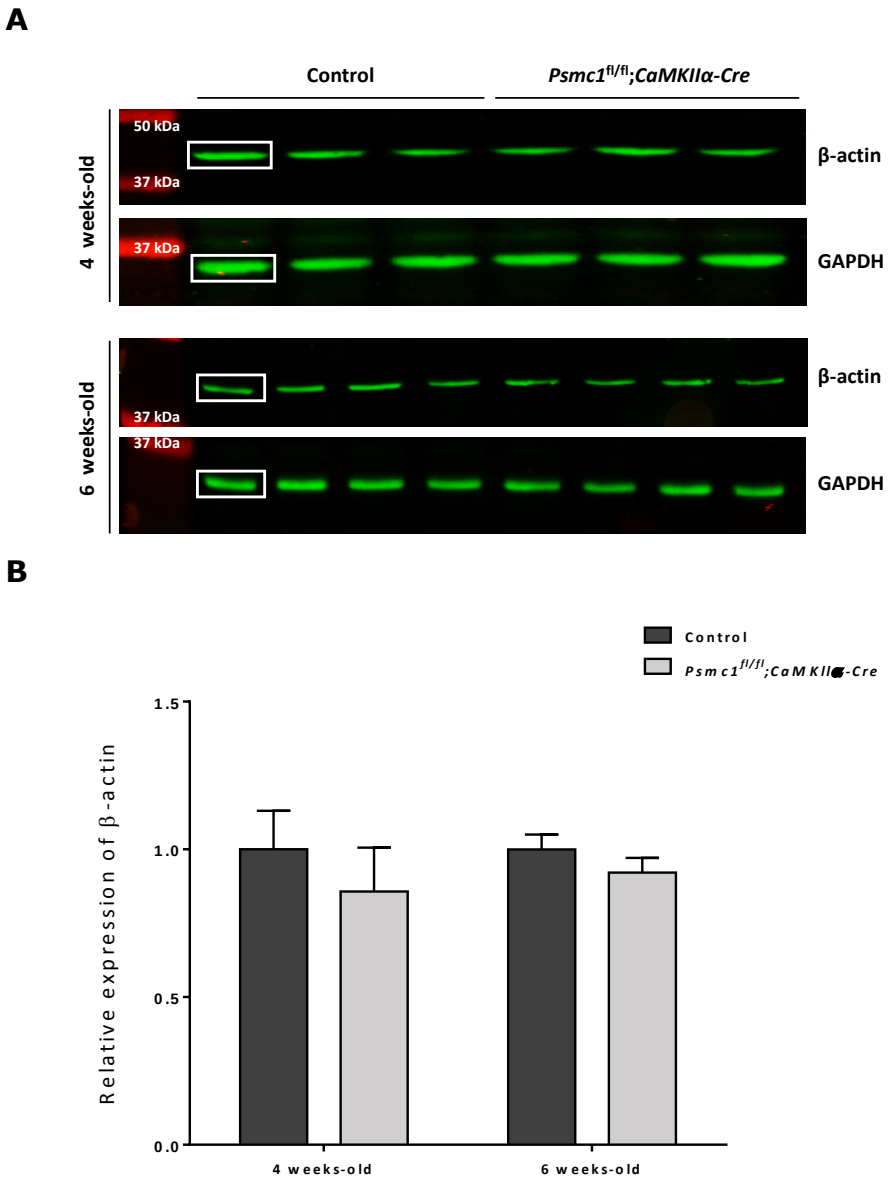


Figure 3.5 Expression of β-actin is not significantly different between control and *Psmc1*$^{fl/fl}$*;CaMKIIα-Cre* mouse cortices.

Immunoblots (A) and densitometric analysis (B) of actin (42 kDa) in 4 and 6 week-old control and *Psmc1*$^{fl/fl}$*;CaMKIIα-Cre* mouse cortices. 20 µg of protein per lane in protein lysis buffer was subjected to SDS-PAGE on a 12% gel and transferred to nitrocellulose membrane for Western blotting. (B) Quantitative analysis of immunoblots used Image Studio software analysis. β-actin was normalised to the levels of GAPDH for each sample. Data are presented as mean ± SEM and compared using Student's unpaired t-test. n=4 for 6 week-old blot; n=3 for 4 week-old blot.

3.2.3 Post-translational modifications of α-tubulin following disruption of the 26S proteasome in mouse cortical neurons

Post-translational modifications (PTMs) of α-tubulin, which include acetylation, tyrosination and detyrosination, are used as markers of MT stability (Marcos et al., 2009, Perdiz et al., 2011). Tyrosinated tubulin is found in the most dynamic MTs, whereas acetylated and detyrosinated tubulin are associated with more stable MTs (Poulain and Sobel, 2010, Baas et al., 1993). Recently, it was shown that α-tubulin PTM may play a role in neurodegenerative diseases such as Huntington's disease (Dompierre et al., 2007) and Parkinson's disease (Outeiro et al., 2007). Therefore, we evaluated PTMs of α-tubulin and MT stability in control and *Psmc1*$^{fl/fl}$;*CaMKIIα-Cre* mouse cortices at 4 and 6 weeks of age (Figures 3.6-3.8). No significant differences in the levels of detyrosinated-tubulin, tyrosinated-tubulin and acetylated-tubulin were observed between control and *Psmc1*$^{fl/fl}$;*CaMKIIα-Cre* cortices at 4 weeks of age (detyrosinated-tubulin; $p = 0.5$, tyrosinated-tubulin; $p = 0.3$ and acetylated-tubulin; $p = 0.8$, Figures 3.6, 3.7 and 3.8 respectively). However, a significant decrease in detyrosinated-tubulin (Figure 3.6; $p < 0.05$), associated with a significant increase in tyrosinated-tubulin (Figure 3.7; $p < 0.01$), was observed in *Psmc1*$^{fl/fl}$;*CaMKIIα-Cre* compared to control cortices at 6 weeks-age. In addition, the levels of acetylated–tubulin in *Psmc1*$^{fl/fl}$;*CaMKIIα-Cre* cortices showed a tendency to decrease compared to control mice at this age (Figure 3.8; $p = 0.07$). These results suggest that the significant decrease in MT proteins (Figures 3.3 and 3.4), as well as stathmin, in *Psmc1*$^{fl/fl}$*;CaMKIIα-Cre* cortices is also associated with changes in MT stability; MTs are more dynamic or unstable in *Psmc1*$^{fl/fl}$*;CaMKIIα-Cre* cortices.

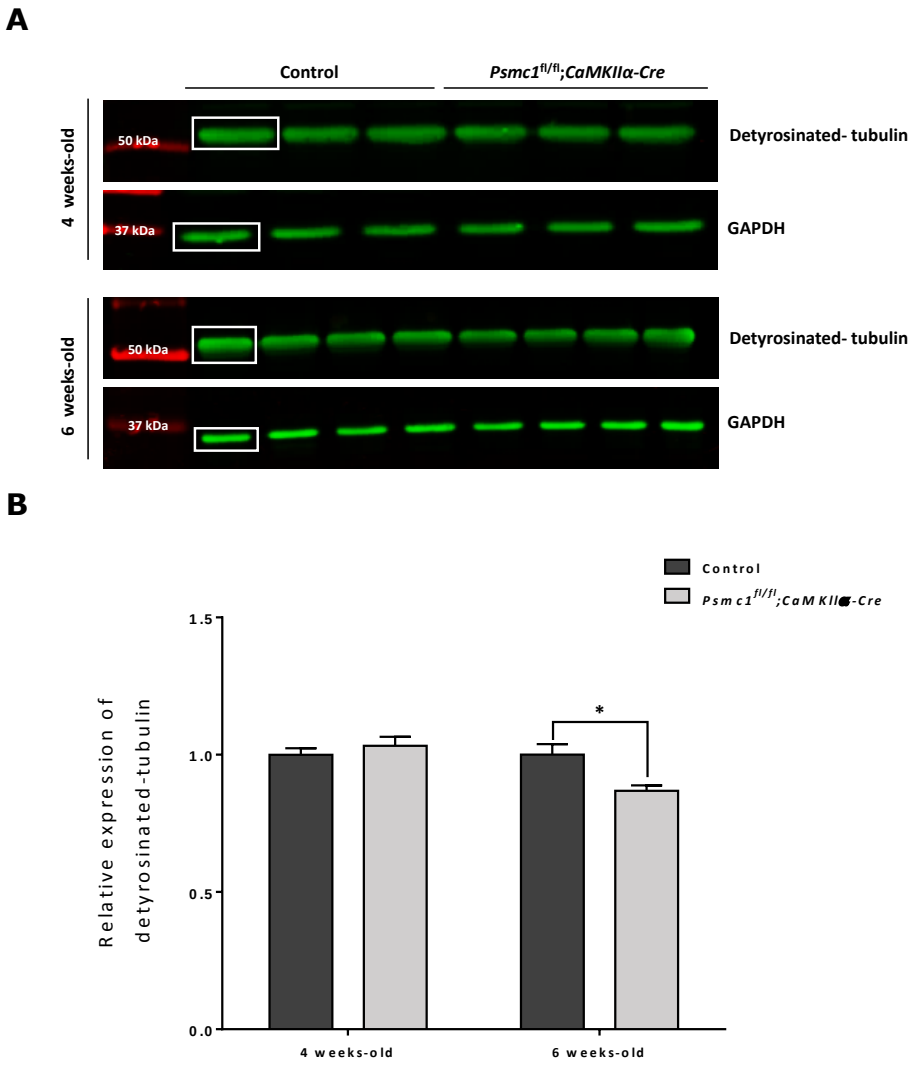


Figure 3.6 Detyrosinated-tubulin is significantly decreased in 6 week-old *Psmc1*$^{fl/fl}$*;CaMKIIα-Cre* compared to control mouse cortices

Immunoblots (A) and densitometric analysis (B) of detyrosinated-tubulin (50 kDa) in 4 and 6 week-old control and *Psmc1*$^{fl/fl}$*;CaMKIIα-Cre* mouse cortices. 20 µg of protein per lane in protein lysis buffer was subjected to SDS-PAGE on a 12% gel and transferred to nitrocellulose membrane for Western blotting. (B) Quantitative analysis of immunoblots used Image Studio software analysis. Detyrosinated-tubulin expression was normalised to the levels of GAPDH for each sample. Data are presented as mean ± SEM and compared using Student's unpaired t-test. *$p < 0.05$; n=4 for 6 week-old blot; n=3 for 4 week-old blot.

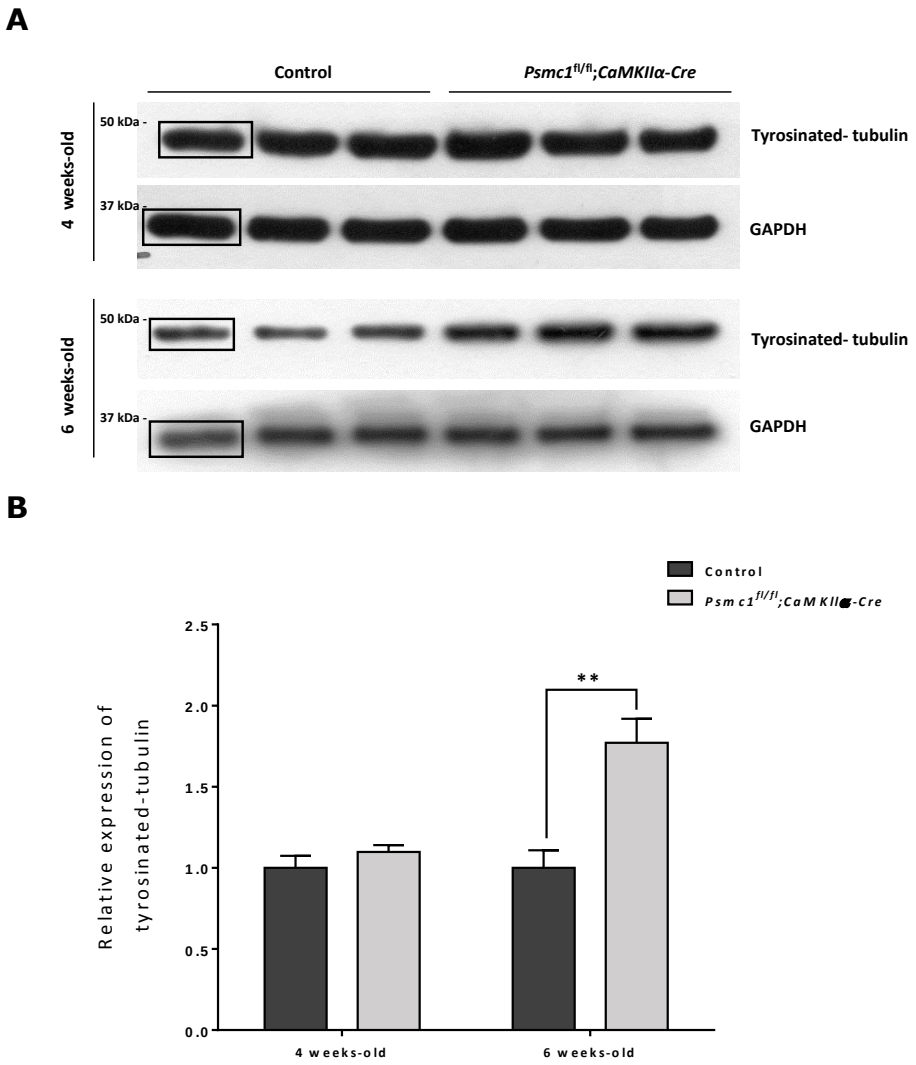


Figure 3.7 Tyrosinated-tubulin is significantly increased in 6 week-old *Psmc1*$^{fl/fl}$*;CaMKIIα-Cre* compared to control mouse cortices.

Immunoblots (A) and densitometric analysis (B) of Tyrosinated-tubulin (50 kDa) in 4 and 6 week-old control and *Psmc1*$^{fl/fl}$*;CaMKIIα-Cre* mouse cortices. 30 µg of protein per lane in protein lysis buffer was subjected to SDS-PAGE on a 12% gel and transferred to nitrocellulose membrane for Western blotting. (B) Quantitative analysis of immunoblots used Odessy Image Studio software analysis. Tyrosinated-tubulin was normalised to the levels of GAPDH for each sample. Data are presented as mean ± SEM and compared using Student's unpaired t-test. *$p < 0.05$, **$p < 0.01$, n=3.

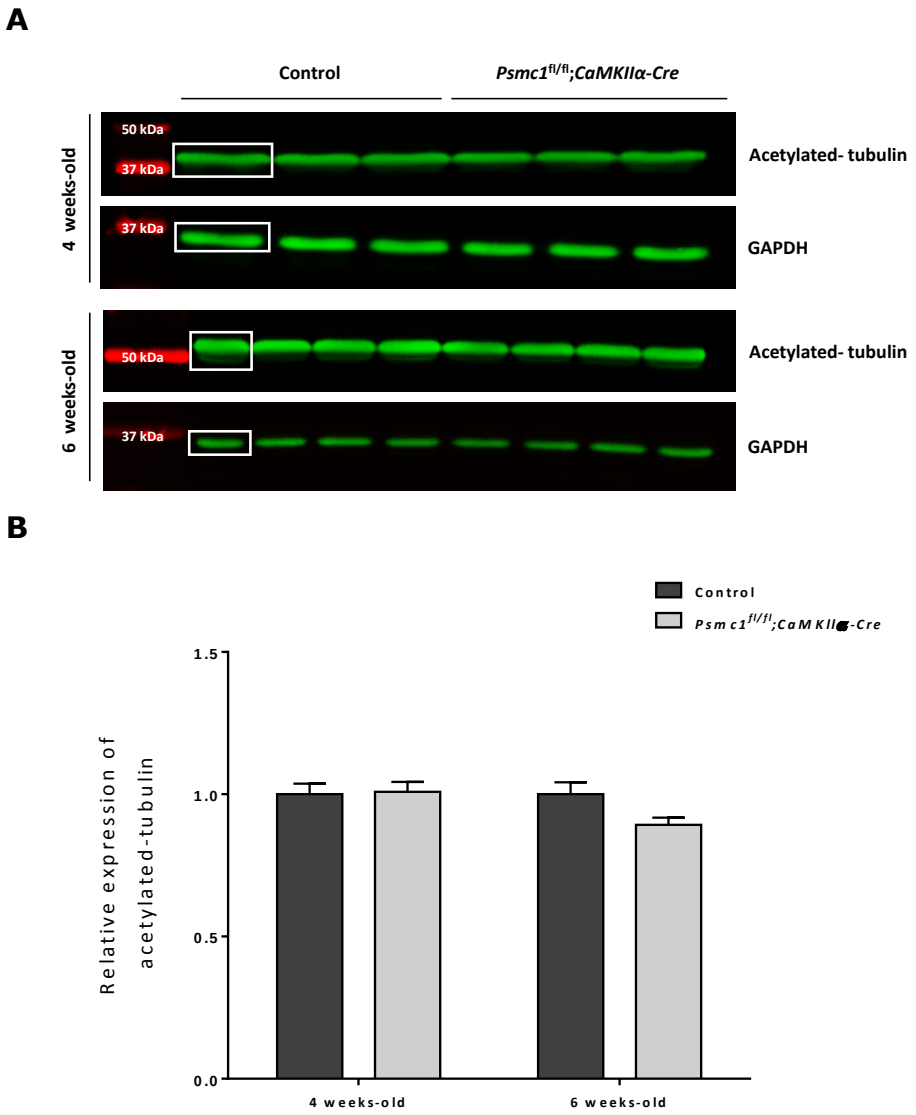


Figure 3.8 Expression of acetylated-tubulin is not significantly different in *Psmc1*$^{fl/fl}$*;CaMKIIα-Cre* mouse cortices compared to controls.

Immunoblots (A) and densitometric analysis (B) of acetylated-tubulin (50 kDa) in 4 and 6 week-old control and *Psmc1*$^{fl/fl}$*;CaMKIIα-Cre* mouse cortices. 20 µg of protein per lane in protein lysis buffer was subjected to SDS-PAGE on a 12% gel and transferred to nitrocellulose membrane for Western blotting. (B) Quantitative analysis of immunoblots used Image Studio software analysis. Acetylated-tubulin was normalised to the levels of GAPDH for each sample. Data are presented as mean ± SEM and compared using Student's unpaired t-test. n=4 for 6 week-old blot; n=3 for 4 week-old blot.

3.2.4 Increased free/polymerised tubulin ratio following disruption of the 26S proteasome in mouse cortical neurons

Proteasome inhibitors are known to promote tubulin polymerization in a variety of cell lines (Poruchynsky et al., 2008) and in vivo studies (Meregalli et al., 2014). In respect to dynamic MTs, tyrosinated MTs are more resistant to MT polymerization; hence, increased tubulin tyrosination in the forebrain following disruption of the 26S proteasome in neurons (Section 2.3) may lead to changes in MT polymerization. To investigate this we used Western blot analyses to measure the relative levels of tubulin associated with cytosolic dimers (soluble) and polymerized (P) MTs in *Psmc1*$^{fl/fl}$;*CaMKIIα-Cre* and control mouse cortices (Figures 3.9 and 3.10). Although total α-tubulin levels were significantly decreased at 6 weeks-old in *Psmc1*$^{fl/fl}$;*CaMKIIα-Cre* mice, there were no significant differences in the expression of acetylated-tubulin levels. Therefore, acetylated-tubulin was used in addition to total α-tubulin to evaluate the ratio of free/polymerized α-tubulin as well as the percentage of α-tubulin polymerization in mouse brain cortical samples at 4 and 6 weeks-old.

GAPDH expression was significantly different between soluble (S) and polymerized (P) α-tubulin fractions, as well as between the control and *Psmc1*$^{fl/fl}$;*CaMKIIα-Cre* cortices in the polymerized fraction, suggesting less GAPDH is associated with the polymerized fraction (Figures 3.9 and 3.10). Therefore, quantification was normalized to copper staining.

GAPDH activity has been shown to be differentially regulated by its interaction with either soluble or polymerized tubulin (Parker et al., 2014). A previous study has also shown that protein-protein interactions between GAPDH and tubulin are affected by the ionic strength of the buffer and whether tubulin is soluble or polymerized (Muronetz et al., 1994). Studies suggest tubulin can moderate the catalytic activity of the immobilized GAPDH, suggesting that glycolytic flux is regulated by microtubule polymer levels, but that

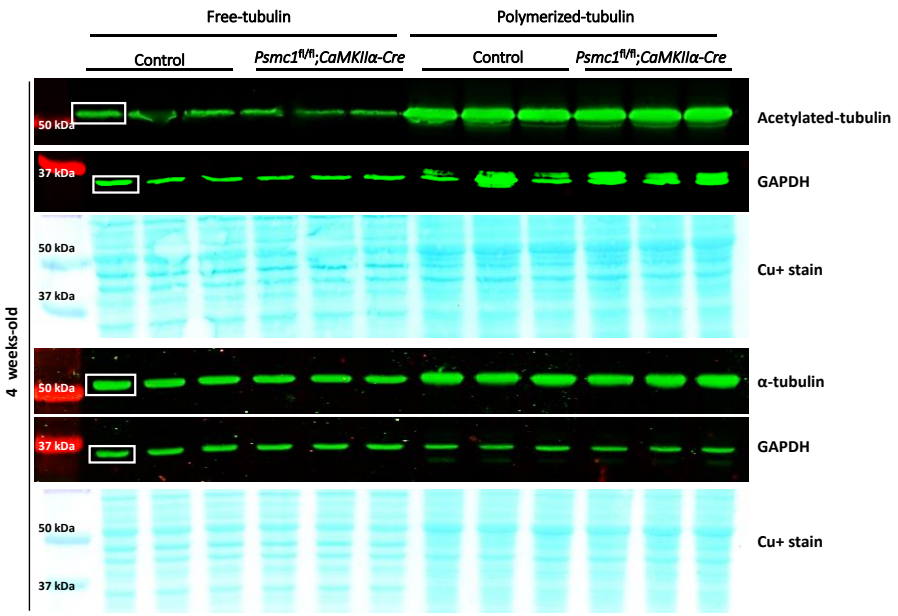
soluble-tubulin had no effect on this catalytic activity of GAPDH (Aon and Cortassa, 2002).

Soluble and polymerised tubulin from 4 and 6 week-old cortical samples were obtained as described in section 2.3. Immunoblotting analyses using acetylated-tubulin and α-tubulin showed that most α-tubulin is associated with the polymerized fraction (Figure 3.9A). Figure 3.9B shows that total tubulin levels are not significantly different at 4 weeks-old between controls and *Psmc1*$^{fl/fl}$;*CaMKIIα-Cre* cortices (acetylated-tubulin $p = 0.6$; α-tubulin $p = 0.2$). However, the levels of free tubulin were significantly decreased in *Psmc1*$^{fl/fl}$;*CaMKIIα-Cre* cortices at 4 weeks of age compared to controls (Figure 3.9C; acetylated-tubulin $p < 0.001$, α-tubulin $p < 0.01$). This was accompanied by an increase in polymerized tubulin using acetylated-tubulin immunoblotting, but no significant change was evident using α-tubulin (Figure 3.9C; acetylated-tubulin $p < 0.05$, α-tubulin; $p = 0.7$). This led to a significant decrease in the free/polymerized acetylated-tubulin ratio and similar increase in the percentage polymerised acetylated-tubulin in *Psmc1*$^{fl/fl}$;*CaMKIIα-Cre* cortices (Figure 3.9D and 3.9E; $p < 0.05$). Figures 3.9D and 3.9E also show a tendency for the ratio of free/polymerised α-tubulin ratio to decrease ($p = 0.14$) and the % polymerised α-tubulin to increase ($p = 0.17$) in *Psmc1*$^{fl/fl}$;*CaMKIIα-Cre* cortices compared to controls, supporting the acetylated α-tubulin observations.

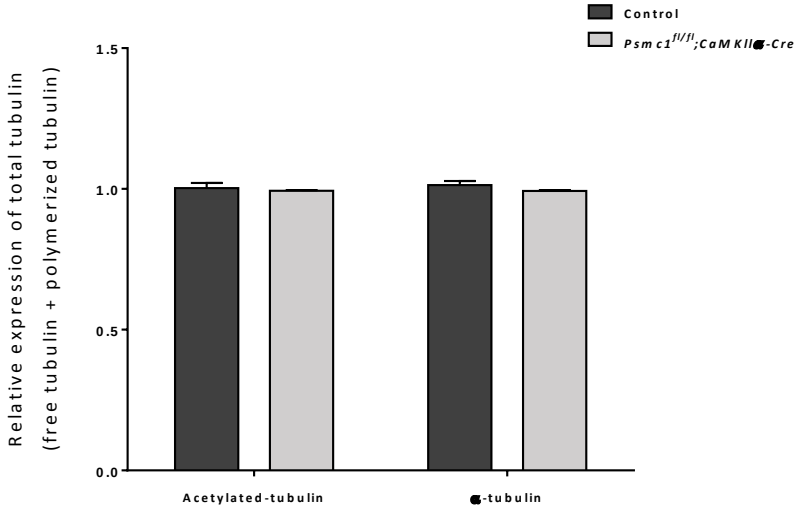
Similar analyses were performed at 6 weeks of age. Figure 3.10B shows that the total levels of both acetylated-tubulin and α-tubulin were significantly decreased at this time point in *Psmc1*$^{fl/fl}$;*CaMKIIα-Cre* cortices (acetylated-tubulin, $p < 0.001$; α-tubulin, $p < 0.001$). Figure 3.10C shows a marked decrease in polymerised tubulin and a decrease free tubulin in *Psmc1*$^{fl/fl}$;*CaMKIIα-Cre* cortices compared to controls (Figure 3.10C; polymerised acetylated-tubulin $p < 0.001$; free acetylated-tubulin $p < 0.05$; polymerised tubulin $p < 0.001$; free α-tubulin $p < 0.01$). Therefore, at 6 weeks of age, the free/polymerized tubulin

ratio is significantly increased in *Psmc1*$^{fl/fl}$;*CaMKIIα-Cre* cortices (Figure 3.10D; acetylated-tubulin $p < 0.01$; α-tubulin $p < 0.001$). There was a corresponding decrease in the percentage of α-tubulin and acetylated-tubulin polymerization (Figure 3.10E; acetylated-tubulin $p < 0.01$; α-tubulin $p < 0.01$). Interestingly, despite the significant decrease in STMN1 expression following 26S proteasome disruption in *Psmc1*$^{fl/fl}$;*CaMKIIα-Cre* mice (Elkharaz et al., 2013), we show here increased MT destabilization.

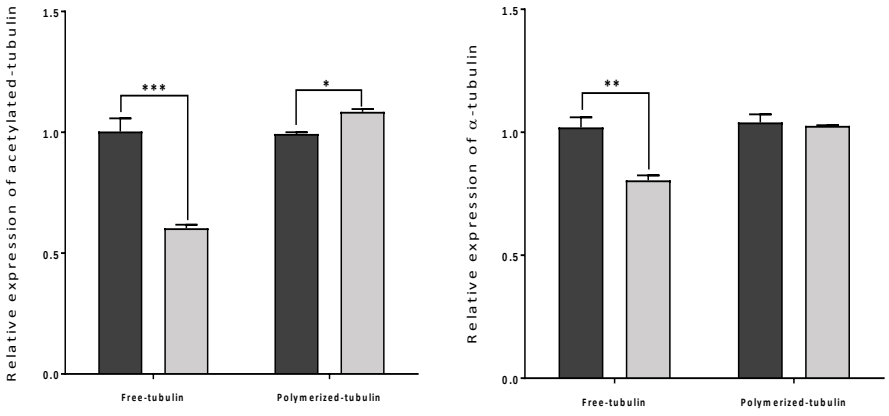
A


Free-tubulin
Polymerized-tubulin
Control
Psmc1fl/fl;CaMKIIα-Cre
Control
Psmc1fl/fl;CaMKIIα-Cre
4 weeks-old
50 kDa
37 kDa
Acetylated-tubulin
GAPDH
Cu+ stain
α-tubulin
GAPDH
Cu+ stain

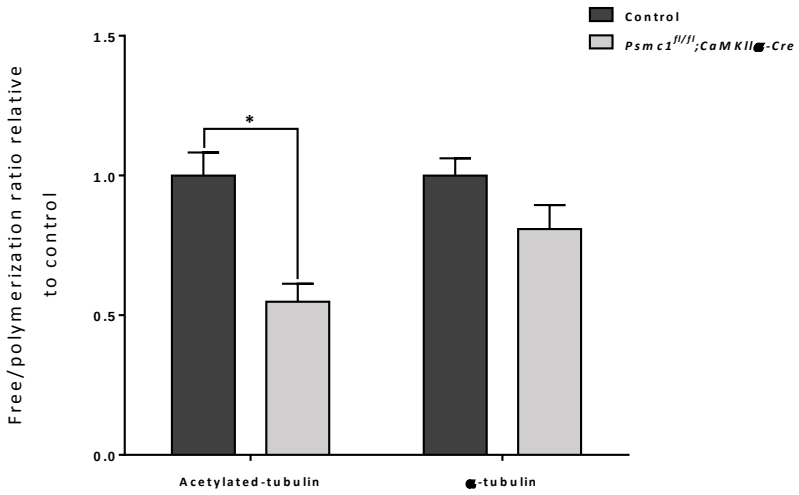
B


Control
Psmc1fl/fl;CaMKIIα-Cre
Relative expression of total tubulin
(free tubulin + polymerized tubulin)
1.5
1.0
0.5
0.0
Acetylated-tubulin
α-tubulin

C


Relative expression of acetylated-tubulin
1.5
1.0
0.5
0.0
***
*
Free-tubulin
Polymerized-tubulin
Relative expression of α-tubulin
1.5
1.0
0.5
0.0
**
Free-tubulin
Polymerized-tubulin

D



E

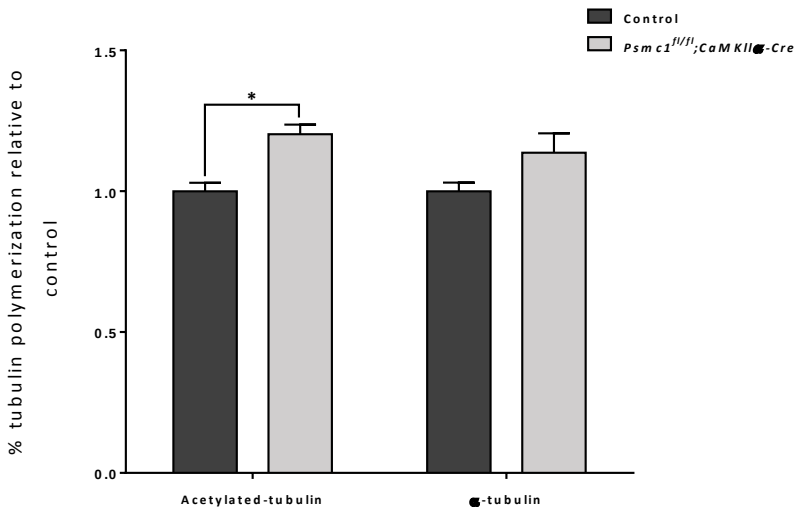
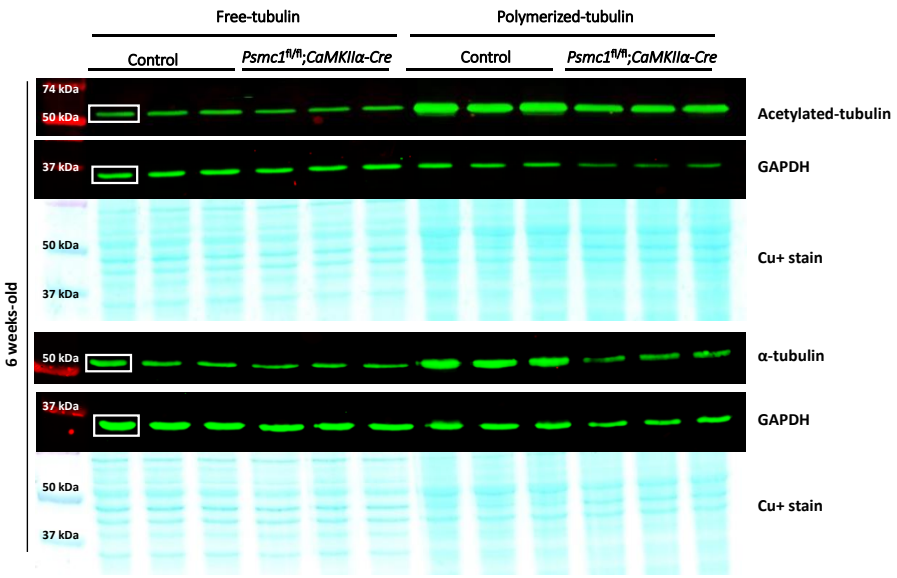


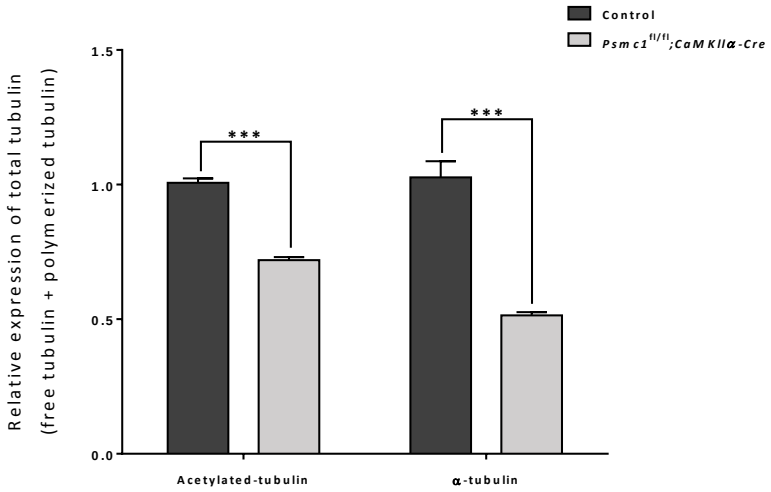
Figure 3.9 Free/polymerized tubulin ratio and % tubulin polymerization in 4 week-old *Psmc1*$^{fl/fl}$*;CaMKIIα-Cre* mouse cortices

(A) Immunoblots and densitometric analyses of soluble (free) and MT-bound (polymerized) tubulin using α-tubulin and acetylated α-tubulin (50 kDa) in 4 week-old control and *Psmc1*$^{fl/fl}$*;CaMKIIα-Cre* cortical samples. GAPDH (38 kDa) is shown, but copper staining was used as a loading control. 10 µg protein per lane was subjected to SDS-PAGE on a 12% gel and transferred to nitrocellulose membrane for Western blotting. Quantitative analysis of immunoblots used Image S software and normalised copper staining. (B) Total tubulin expression (free tubulin + polymerized tubulin) relative to controls. (C) Acetylated and α-tubulin expression in free and polymerized tubulin fractions relative to controls. (D) Values represent the ratio free/polymerized tubulin. (E) Percentage tubulin polymerization calculated as % P/P+S (P=polymerized tubulin fraction and S=soluble or free tubulin fraction). Data are presented as mean ± SEM and compared using Student's unpaired t-test. * p = 0.05, ** p < 0.01, *** p < 0.001, n = 3.

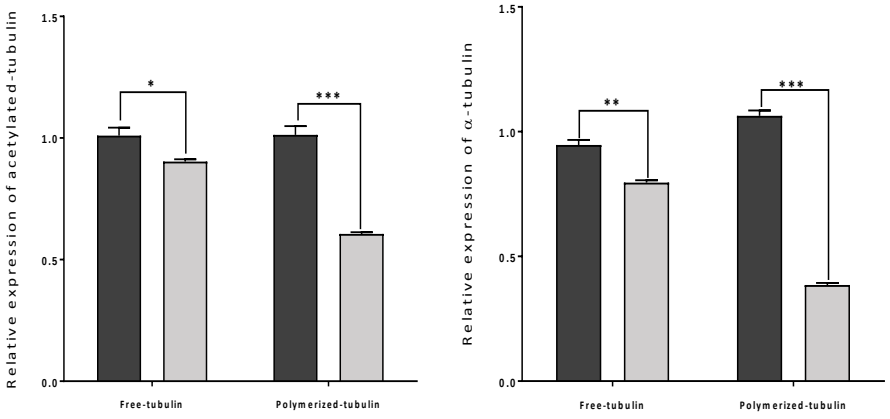
A


Free-tubulin
Polymerized-tubulin
Control
Psmc1fl/fl;CaMKIIα-Cre
Control
Psmc1fl/fl;CaMKIIα-Cre
6 weeks-old
74 kDa
50 kDa
37 kDa
Acetylated-tubulin
GAPDH
50 kDa
37 kDa
Cu+ stain
50 kDa
α-tubulin
37 kDa
GAPDH
50 kDa
37 kDa
Cu+ stain

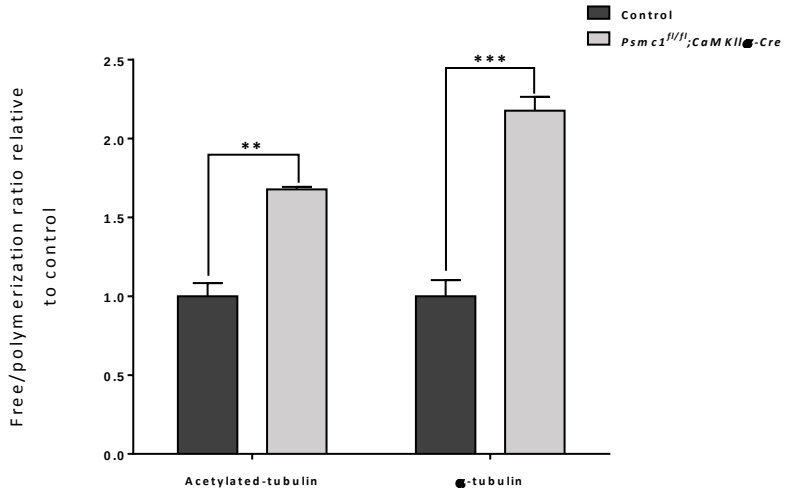
B


Control
Psmc1fl/fl;CaMKIIα-Cre
Relative expression of total tubulin
(free tubulin + polymerized tubulin)
1.5
1.0
0.5
0.0
***
***
Acetylated-tubulin
α-tubulin

C


Relative expression of acetylated-tubulin
1.5
1.0
0.5
0.0
*
***
Free-tubulin
Polymerized-tubulin
Relative expression of α-tubulin
1.5
1.0
0.5
0.0
**
***
Free-tubulin
Polymerized-tubulin

D



E

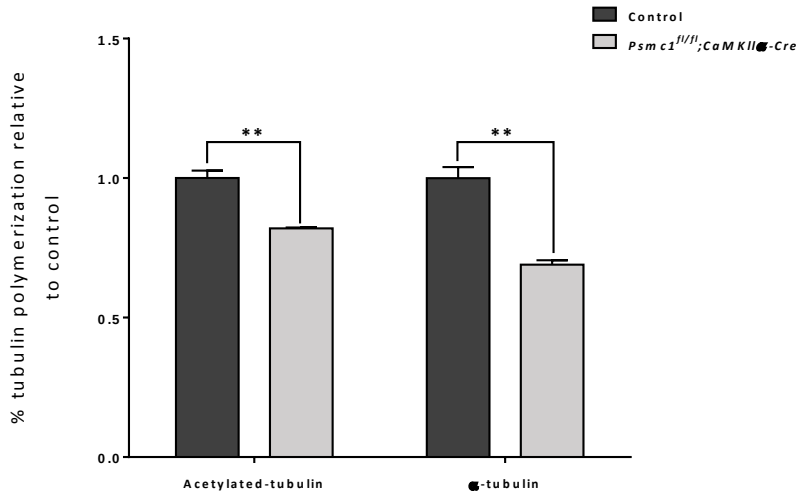


Figure 3.10 Increased free/polymerized tubulin ratio and decreased % tubulin polymerization in 6 week-old *Psmc1*$^{fl/fl}$*;CaMKIIα-Cre* mouse cortices.

(A) Immunoblots and densitometric analyses of soluble (S; free) and MT-bound (P; polymerized) tubulin using α-tubulin and acetylated α-tubulin (50 kDa) in 6 week-old control and *Psmc1*$^{fl/fl}$*;CaMKIIα-Cre* cortical samples. GAPDH (38 kDa) is shown, but copper staining was used as a loading control. 10 µg of protein per lane was subjected to SDS-PAGE on a 12% gel and transferred to nitrocellulose membrane for Western blotting. Quantitative analysis of immunoblots used Image S software. (B) Total tubulin expression (free tubulin + polymerized tubulin) relative to controls. (C) Acetylated and α-tubulin expression in free and polymerized tubulin fractions relative to controls. (D) Values represent the ratio free/polymerized tubulin. (D) Values represent the ratio free/polymerized tubulin. (E) Percentage tubulin polymerization was calculated as % P/P+S (P=polymerized tubulin fraction and S=soluble free tubulin fraction). Data are presented as mean ± SEM and compared using Student's unpaired t-test. ** $p < 0.01$, *** $p \leq 0.001$, n = 3.

3.2.5 Microtubule-associated protein expression following disruption of the 26S proteasome in mouse cortical neurons

MT arrangement, polymerization and stabilization can be modulated by interactions with microtubule-associated proteins (MAPs). These include both microtubule stabilizing proteins such as MAP2 and tau, and microtubule destabilizing proteins like STMN1 (Zhang and Dong, 2012). MAP2 and tau are found in neurons and interact with tubulin to promote its assembly into microtubules, stabilizing the microtubule network (Dehmelt and Halpain, 2005).

Since cellular functions require a critical balance between microtubule stabilizers and destabilizers, and we had previously observed decreased STMN1 expression, that there may also be changes in MAP2 and tau protein expression. Therefore, we examined the levels of MAP2 and tau in control and *Psmc1*$^{fl/fl}$*;CaMKIIa-Cre* cortices at both 4 and 6 weeks of age (Figure 3.11 and 3.12). Figure 3.11 shows that the total levels of MAP2 were not significantly different between control and *Psmc1*$^{fl/fl}$*;CaMKIIa-Cre* cortices either age (4 weeks p = 0.9, 6 weeks p = 0.7). We also investigated tau levels in control and *Psmc1*$^{fl/fl}$*;CaMKIIa-Cre* cortices using the tau 46 antibody, which detects total tau levels. Figure 3.12 shows several bands following tau immunoblotting, suggesting numerous sites for phosphorylation and posttranslational modifications of the tau protein (Orr et al., 2012). Although the total levels of tau 46 were not significantly different between control and *Psmc1*$^{fl/fl}$*;CaMKIIa-Cre* cortices at 4 weeks-old (4 weeks p = 0.23; Figure 3.12B), there was a significant decrease in total tau at 6 weeks of age in *Psmc1*$^{fl/fl}$*;CaMKIIa-Cre* cortices (Figure 3.12B; $p < 0.01$). This is suggestive of unstable microtubules following 26S proteasome dysfunction. Given our previous observation of decreased STMN1 and also destabilised microtubules it may have been expected to see an increased in stabilising microtubule proteins such as tau. It is also possible that decreasing a destabilising protein such as STMN may be an attempt to stabilize microtubules. Our

observations are interesting given that tau and STMN1 play opposite roles in MT stability. A previous study in a breast cancer cohort showed an inverse relationship between these proteins in a subset of cases (Baquero et al., 2012). They found low STMN1 and high tau was associated with increased microtubule stability and better prognosis.

A previous in vitro study in COS-7 cells revealed that increased STMN expression released tau from MTs via its phosphorylation and led to MT instability (Miyasaka et al., 2010). The authors also found that the amount of tau phosphorylation in the MT-unbound (free) fraction from STMN-expressing cells was higher than that in the MT-bound fraction (polymerized). Significantly decreased α-tubulin and acetylated α-tubulin expression in the polymerized fraction was observed, suggesting that α-tubulin subunits are released into the soluble fraction. To examine the effects of decreased STMN1 expression and MT instability on the ability of tau and MAP2 to bind MTs following 26S proteasome dysfunction in cortical neurons Western blot analyses were performed on the free and polymerized tubulin from 4 and 6 week-old *Psmc1*$^{fl/fl}$*;CaMKIIα-Cre* and control mouse cortices (Figures 3.13 and 3.14). Multiple MAP2 bands were detected following immunoblotting, which correspond to different isoforms expressed in neurons as a result of alternative splicing: high molecular weight MAP2 (200-250 kDa, HMWMAP2) consists of MAP2a and MAP2b, and low molecular weight MAP2 (70-75 kDa, LMWMAP2), consists of MAP2c and MAP2d (Lewis et al., 1988). Figure 3.13A shows multiple bands between 150-260 kDa following MAP2 immunoblotting. This suggests detection of the HMWMAP2, but also may reflect some protein degradation has occurred during sample preparation. MAP2 is rich in proline, glutamic acid, serine and threonine (PEST) sequences, which are putative signals for rapid proteolytic degradation (Friedrich and Aszodi, 1991). A previous study has shown that MAP2 isolated from rat brain was extremely sensitive to hydrolysis by calpain, resulting in significantly altered electrophoretic mobility by SDS-PAGE (Billger

et al., 1988). It is possible that multiple bands are not observed in the previous total cell lysates analyses (Figure 3.11A) because of different homogenisation buffers used.

At 4 weeks-old the % MAP2 associated with polymerized-tubulin between control and *Psmc1*$^{fl/fl}$*;CaMKIIα-Cre* mice showed a tendency to increase, but this was not statistically significant (Figure 3.13; 4 weeks $p = 0.07$). However, at 6 weeks-old the % MAP2 associated with polymerization of tubulin was significantly decreased in *Psmc1*$^{fl/fl}$*;CaMKIIα-Cre* mice (Figure 3.13; 6 weeks $p < 0.01$). These observations suggest that MT instability in *Psmc1*$^{fl/fl}$*;CaMKIIα-Cre* mice is connected to less MAP2 in the polymerized fraction. Investigations of tau 46 showed that there were no significant differences in the % of this protein in the polymerized fraction at 4 and 6 weeks-old in *Psmc1*$^{fl/fl}$*;CaMKIIα-Cre* cortices (Figure 3.14; 4 weeks $p = 0.3$, 6 weeks $p = 0.4$). Figure 3.14A shows that the expression of tau is predominantly in the polymerized tubulin fraction, as expected.

Our results suggest that tau may be more susceptible to becoming dephosphorylated and bound to polymerize MTs because we observe decreased STMN and increased MTs instability following 26S proteasome dysfunction in mouse cortical neurons. Given that tau phosphorylation affects its association with MTs we used anti-phospho-tau antibodies CP13 and AT8, which react with phospho-Ser202 and phospho-Ser199, -Ser202 and -Thr205 respectively. Phosphorylation at Ser202 showed a significant decrease in *Psmc1*$^{fl/fl}$*;CaMKIIα-Cre* cortices compared to controls at 6 weeks of age (Figure 3.15; $p < 0.02$). Figure 3.15 also shows that the phosphorylation of Ser-199, -Ser202 and -Thr205 was not significantly different between control and *Psmc1*$^{fl/fl}$*;CaMKIIα-Cre* cortices (Figure 3.15; AT8 $p = 0.1$).

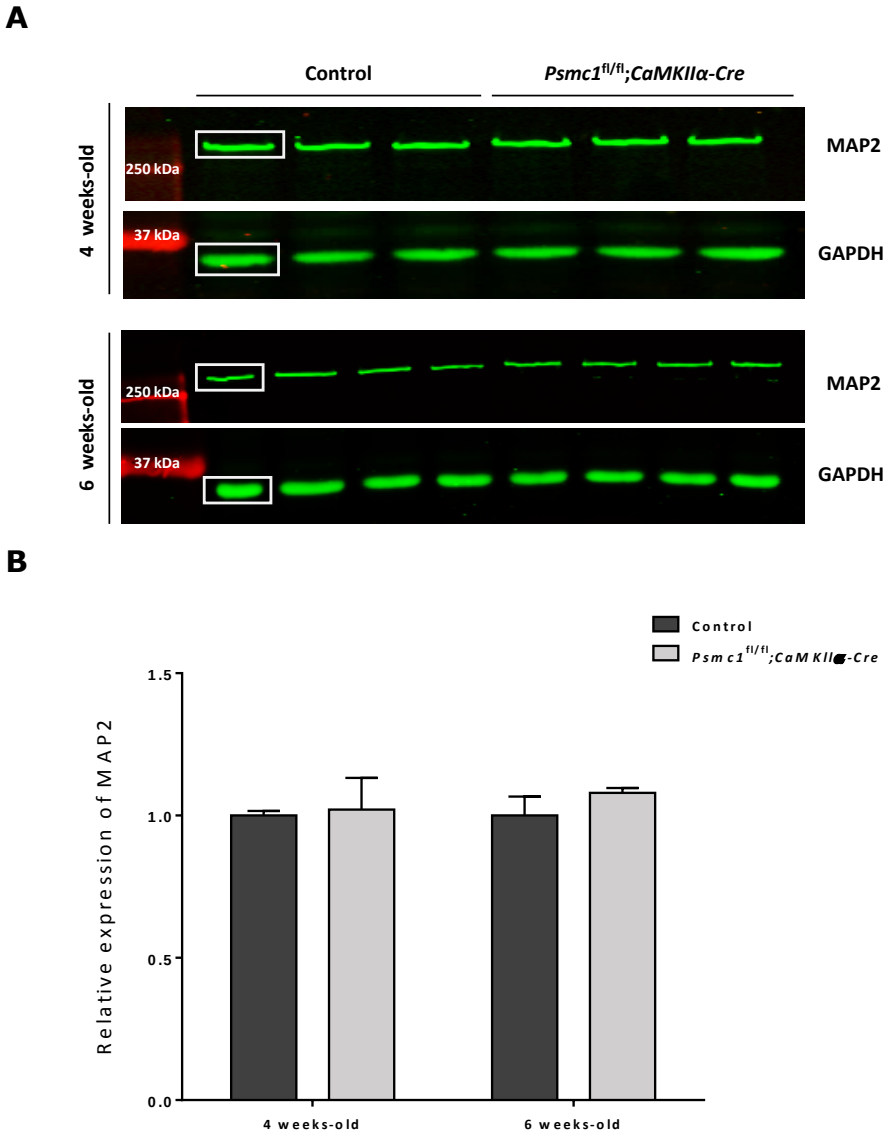


Figure 3.11 MAP2 expression is not significantly different in control and *Psmc1*$^{fl/fl}$*;CaMKIIα-Cre* mouse cortices.

Immunoblots (A) and densitometric analysis (B) of MAP2 (280 kDa) in 4 and 6 week-old control and *Psmc1*$^{fl/fl}$*;CaMKIIα-Cre* mouse cortices. 20 µg of protein per lane in protein lysis buffer was subjected to SDS-PAGE on a 8% gel and transferred to nitrocellulose membrane for Western blotting. (B) Quantitative analysis of immunoblots used Image Studio software analysis. MAP2 was normalised to the levels of GAPDH for each sample. Data are presented as mean ± SEM and compared using Student's unpaired t-test. n=4 for 6 week-old; n=3 for 4 week-old.

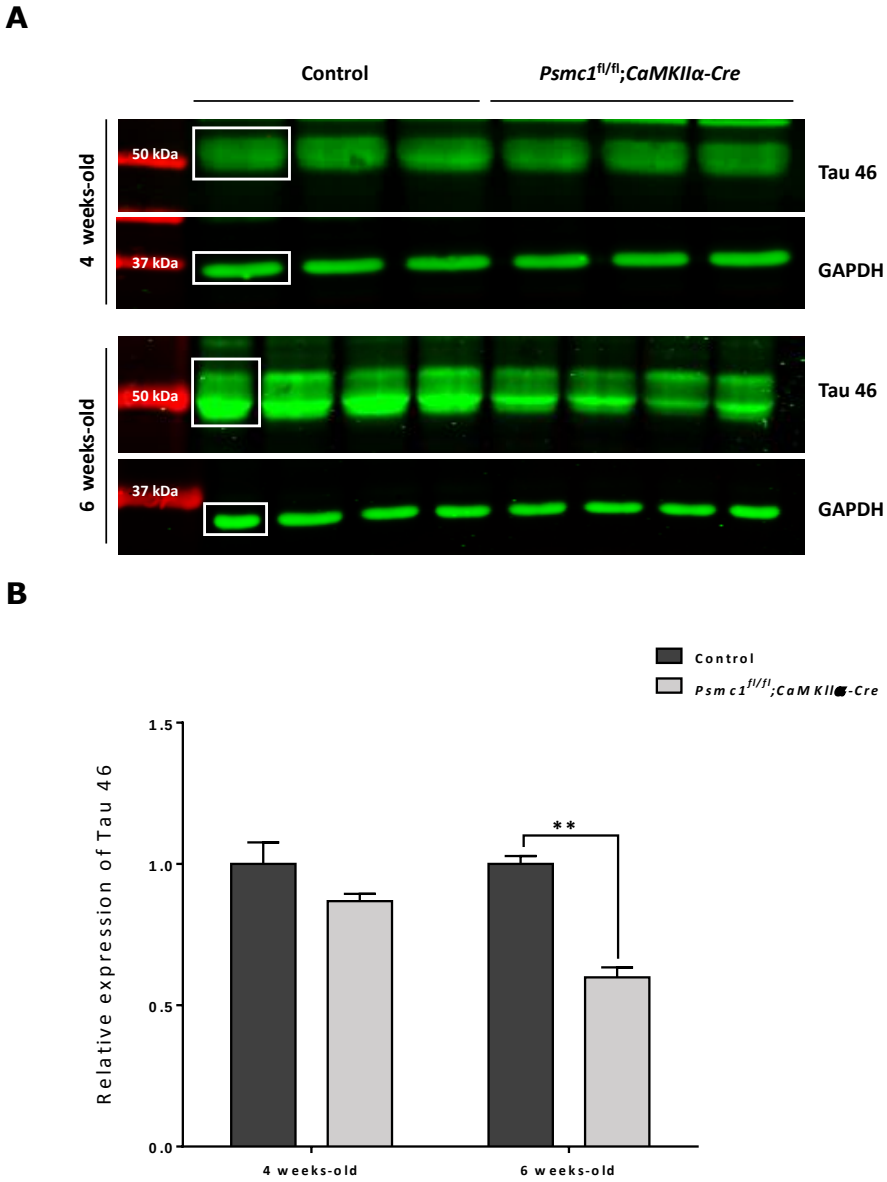


Figure 3.12 Total tau protein is significantly decreased in 6 week-old *Psmc1*$^{fl/fl}$*;CaMKIIα-Cre* compared to control mouse cortices.

Immunoblots (A) and densitometric analysis (B) of total Tau (Tau 46; 50 kDa) in 4 and 6 week-old control and *Psmc1*$^{fl/fl}$*;CaMKIIα-Cre* mouse cortices. 20 µg of protein per lane in protein lysis buffer was subjected to SDS-PAGE on a 12% gel and transferred to nitrocellulose membrane for Western blotting. (B) Quantitative analysis of immunoblots used Image Studio software analysis. Total Tau level was normalised to the levels of GAPDH for each sample. Data are presented as mean ± SEM and compared using Student's unpaired t-test. ** $p < 0.01$; n=4 for 6 week-old; n=3 for 4 week-old.

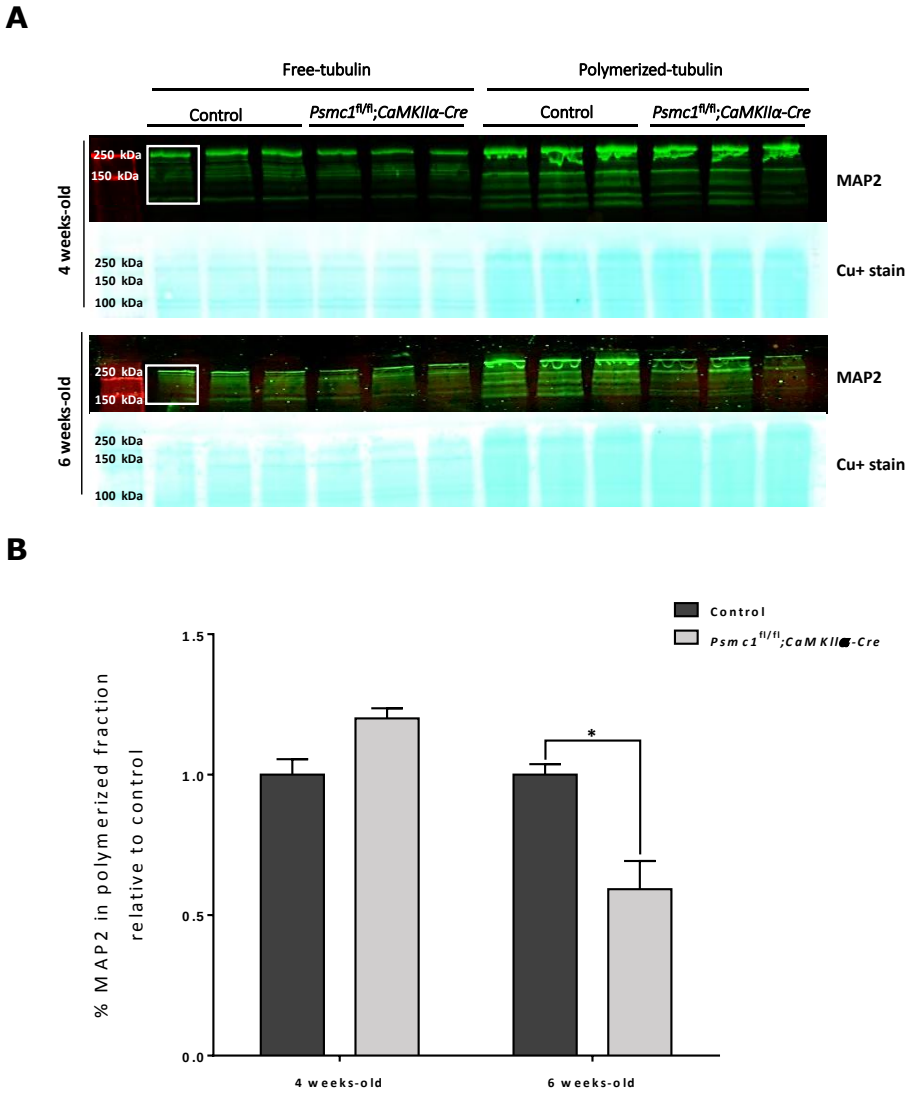


Figure 3.13 % MAP2 in the polymerized fraction is significantly decreased in 6 week-old *Psmc1*$^{fl/fl}$*;CaMKIIa-Cre* compared to control mouse cortices

(A) MAP2 (280 kDa) immunoblots and densitometric analyses of soluble (free) and polymerized-tubulin fractions at 4 and 6 weeks-old in control and *Psmc1*$^{fl/fl}$*;CaMKIIa-Cre* mouse cortices. Copper staining was used as a loading control for each sample. 20 µg of protein per lane was subjected to SDS-PAGE on a 12% gel and transferred to nitrocellulose membrane for Western blotting. (B) Quantitative analysis of immunoblots used Image Studio software analysis. % MAP2 associated with polymerized-tubulin was calculated as % MAP2 in P/P+S (P=polymerized; S=soluble). Data are presented as mean ± SEM and compared using Student's unpaired t-test. ** $p < 0.01$, n = 3.

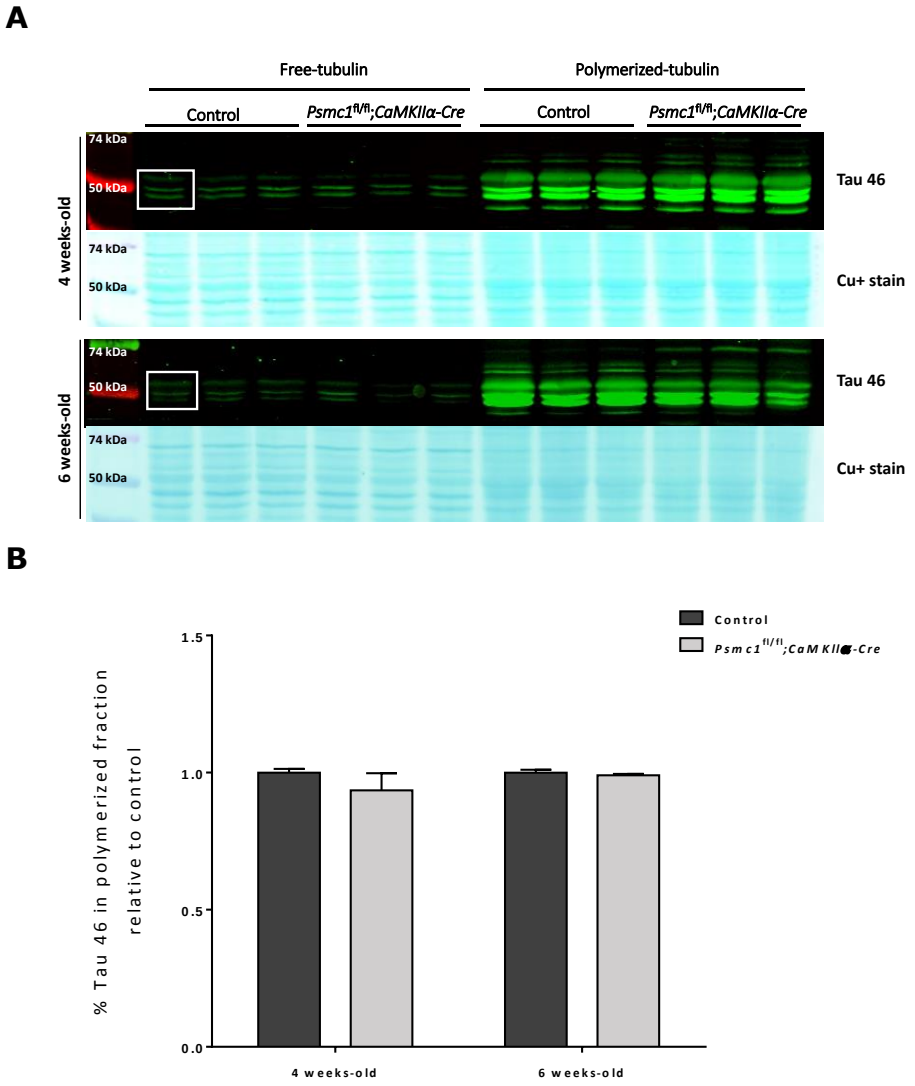


Figure 3.14 Tau 46 in the polymerized tubulin fraction is not significantly different in control and *Psmc1*$^{fl/fl}$*;CaMKIIα-Cre* mouse cortices.

(A) Tau 46 (50-75 kDa) immunoblots and densitometric analyses of soluble (free) and polymerized-tubulin fractions at 4 and 6 weeks-old in control and *Psmc1*$^{fl/fl}$*;CaMKIIα-Cre* mouse cortices. Copper staining was used as a loading control for each sample. 20 µg of protein per lane was subjected to SDS-PAGE on a 12% gel and transferred to nitrocellulose membrane for Western blotting. (B) Quantitative analysis of immunoblots used Image Studio software analysis. % Tau 46 associated with polymerized-tubulin was calculated as % Tau 46 in P/P+S (P=polymerized; S=soluble). Data are presented as mean ± SEM and compared using Student's unpaired t-test. n = 3.

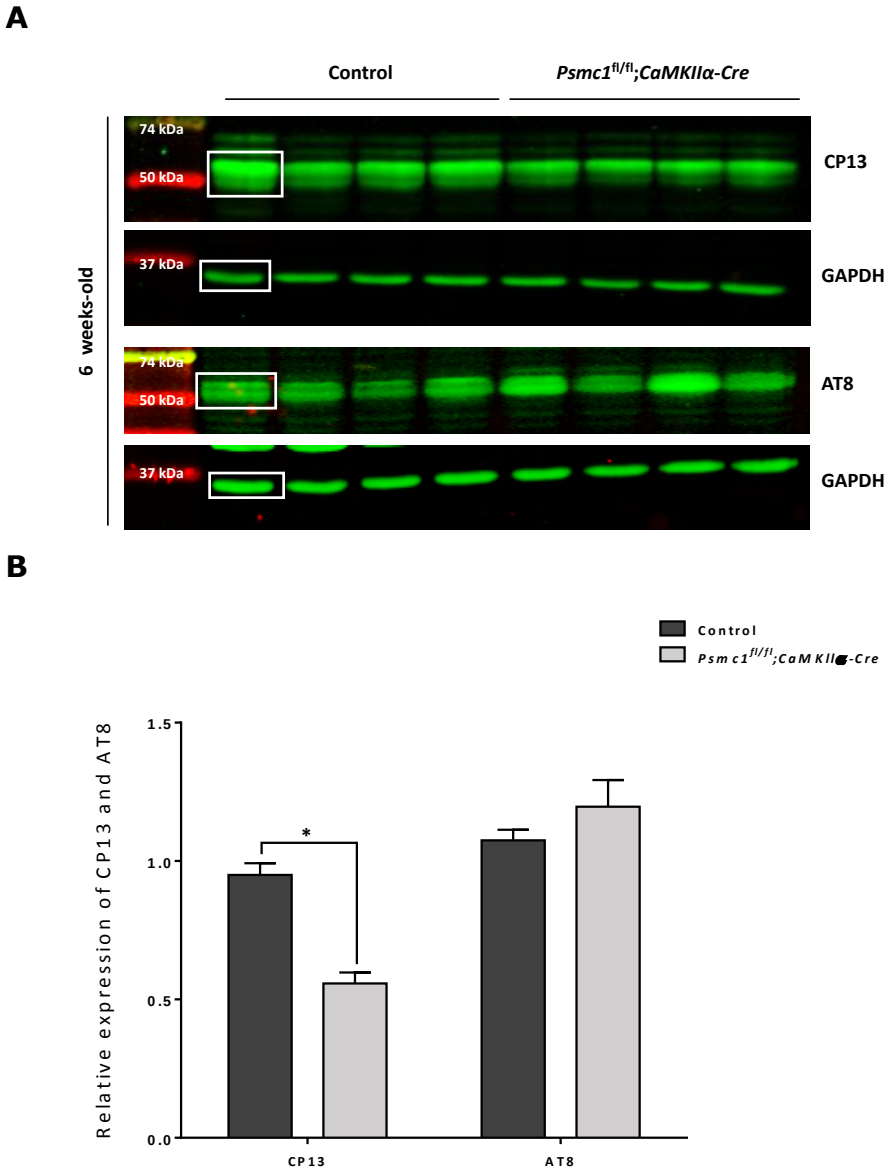


Figure 3.15 Expression of phosphorylated tau in 6 week-old control and *Psmc1*$^{fl/fl}$*;CaMKIIa-Cre* mouse cortices

Immunoblots (A) and densitometric analysis (B) of CP13 (pSer^{202}) and AT8 (pSer^{199}/pSer^{202}/pThr^{205}) in 6 week-old control and *Psmc1*$^{fl/fl}$*;CaMKIIa-Cre* mouse cortices. 20 µg of protein per lane in protein lysis buffer was subjected to SDS-PAGE on a 12% gel and transferred to nitrocellulose membrane for Western blotting. (B) Quantitative analysis of immunoblots used Image Studio software analysis. CP13 and AT8 were normalised to the levels of GAPDH for each sample. Data are presented as mean ± SEM and compared using Student's unpaired t-test, * $p < 0.05$, n=4.

3.3 Discussion

26S proteasome dysfunction in mouse forebrain neurons has been implicated in neurodegeneration and intraneuronal protein inclusion formation resembling Lewy body dementia (Bedford et al., 2008). The underlying mechanisms involved in neuroprotection and neurodegeneration in this mouse model have not been confirmed. Abnormal MT dynamics have been connected to several neurodegenerative disorders, including Alzheimer's disease (AD), Parkinson's disease (PD) and Amyotrophic Lateral Sclerosis (ALS) (Cartelli et al., 2013, Dubey et al., 2015). MTs form important cytoskeletal structures within neurons, which can be both stable and dynamic to establish and maintain neuronal polarity (Witte et al., 2008), regulate neuronal morphology (Jaworski et al., 2009) and transport cargo (Maday et al., 2014). MAPs and PTMs of tubulin are known to influence both stable and dynamic pools of MTs within the cell.

We previously reported decreased levels of microtubule destabilizing protein STMN1 following 26S proteasome dysfunction in mouse brain cortical neurons (Elkharaz et al., 2013). This suggested changes in MT dynamics following 26S proteasome dysfunction and/or the 26S proteasome has a role in maintaining MTs in neurons. In this study we have found significantly decreased expression of MT proteins α-tubulin and neuron-specific βIII-tubulin, associated with microtubule instability evident by decreased and increased expression of detyrosinated-tubulin and tyrosinated-tubulin respectively following 26S proteasome dysfunction. These observations are supported by an increased free/polymerized tubulin ratio. Here we also show significantly decreased expression of total tau, but not MAP2, in *Psmc1*$^{fl/fl}$*;CaMKIIα-Cre* mice. This is interesting since tau and STMN play opposing, but complimentary roles in MT stability (Figure 3.16).

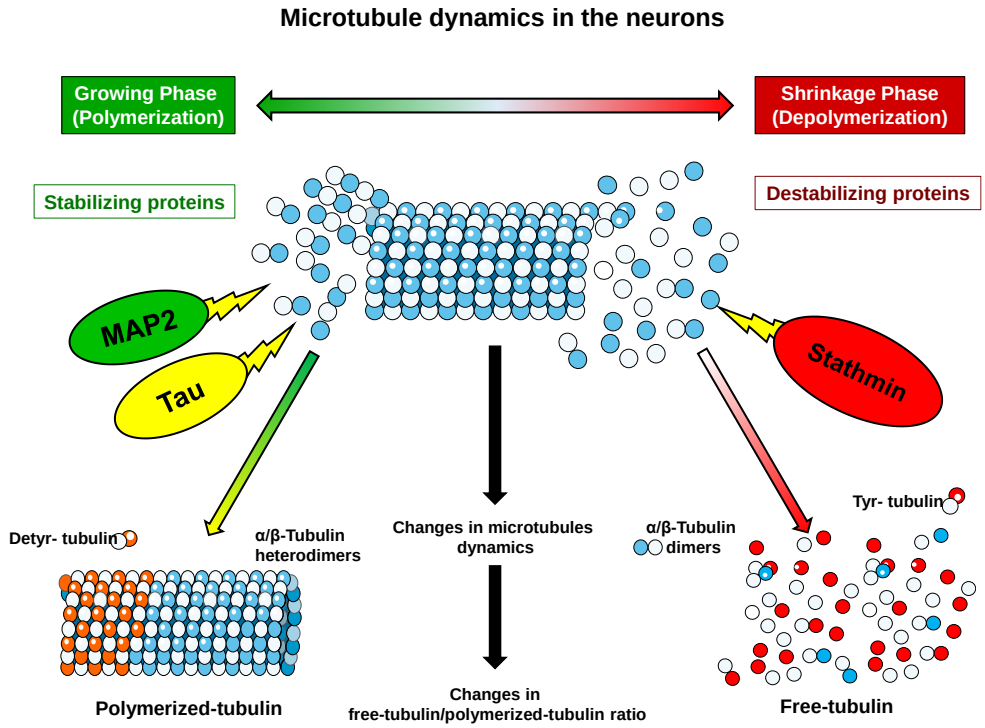


Figure 3.16 Schematic representation of microtubule dynamics in *Psmc1*$^{fl/fl}$*;CaMKIIα-Cre* mouse cortical neurons

3.3.1 Decreased α-tubulin and βIII-tubulin levels following disruption of the 26S proteasome in mouse cortical neurons

Ultrastructural analysis showed that both the total length of MTs and their number were significantly reduced in pyramidal neurons from AD patients in comparison to control cases (Cash et al., 2003). Decreased total expression of α-tubulin associated with reduced PTMs such as polyglutamylation, tyrosination, and detyrosination are also reported in AD brains, suggesting that decreased α-tubulin expression could contribute to the pathogenesis of AD (Zhang et al., 2015a).

Interestingly, we found significantly decreased levels of α-tubulin and neuron-specific βIII-tubulin in *Psmc1*$^{fl/fl}$*;CaMKIIα-Cre* compared to control cortices at 6 weeks of age. These observations suggest decreased microtubule mass is one of the cellular events occurring as a consequence of neurodegeneration following 26S proteasome dysfunction in cortical neurons. Tubulin is an abundant and stable protein in neurons and its levels are tightly regulated by

protein synthesis (Cleveland et al., 1983) and proteasome-dependent proteolysis (Ren et al., 2003). Parkin is an E3 ubiquitin ligase responsible for the ubiquitination of α-tubulin and β-tubulin, and increased Parkin expression in HEK293 cells can lead to increased α- and β-tubulin degradation (Ren et al., 2003).

Pharmacological inhibition of proteasome activity is generally associated with increased MT stability. A study using the neural cell lines HCN1A and HCN2 found dramatically decreased tubulin levels in HCN2 cells after treatment with microtubule-depolymerizing agent Vincristine was rescued by the proteasome inhibitor MG132 (Huff et al., 2010). In embryonic fibroblasts decreased STMN expression lead to increased MT polymers, but the levels of β-tubulin and total tubulin pool were not affected (Ringhoff and Cassimeris, 2009). Therefore, STMN expression may not have a direct effect on tubulin levels. Our results in mouse forebrain neurons in vivo showing decreased STMN1 and tubulin expression are not consistent with previous observations.

It is possible that tubulin synthesis is affected in our mouse model where decreased tubulin expression is associated with increased MT instability. MT disassembly can lead to a dramatic increase in tubulin monomers, which may selectively destabilize tubulin mRNA and subsequently decrease tubulin protein synthesis (Pachter et al., 1987). Previous studies have shown that tubulin synthesis decreases rapidly in response to MT inhibitors that increase the monomer pool (Cleveland et al., 1981). This decrease in synthesis was associated with a decline in the amounts of both α- and β-tubulin mRNAs.

βIII-tubulin is neuron-specific in mammalian brain and is widely used to identify neurons in developmental studies (Lee et al., 1990). The expression of βIII-tubulin is usually associated with differentiation and decreased cell proliferation of neurons (Katsetos et al., 2009). Decreased βIII-tubulin expression can lead to neurodevelopmental abnormalities, and fewer and shorter neurites

were found in neural stem cells from a spinal muscular atrophy (SMA) mouse model (Shafey et al., 2008) and SMA patient motor neurons (Fuller et al., 2015).

A study using differentiating neuroblastoma cells found βIII-tubulin expression could protect neurons against free radicals and reactive oxygen species (Guo et al., 2010). The expression of neuron-specific βIII-tubulin was previously linked to hypoxia, and hypoxia via HIF-1α was able to increase βIII-tubulin expression in Glioblastoma Multiforme (Katsetos et al., 2009) and A2780 cells (Raspaglio et al., 2014). In addition, the anti-oxidative activity of curcumin against hypoxia decreased βIII-tubulin in rat prefrontal cortex (PFC) neurons (Shen and Yu, 2008). These studies agree with our previous data showing oxidative stress in the brain following 26S proteasome dysfunction in cortical neurones (Elkharaz et al., 2013). Decreased βIII-tubulin levels in *Psmc1*$^{fl/fl}$*;CaMKIIα-Cre* cortex may be part of an anti-oxidant protective mechanism during neurodegeneration. It is also possible that decreased βIII-tubulin levels in *Psmc1*$^{fl/fl}$*;CaMKIIα-Cre* cortex may be due to increased neuronal cell death.

Levels of β-actin were not significantly different in *Psmc1*$^{fl/fl}$*;CaMKIIα-Cre* mice despite significant neuropathology at 6 weeks of age. A recent study by Cartelli (2013) showed that the levels of actin, α-tubulin and β-tubulin were unchanged in the striatum and substantia nigra of mice with 1-methyl-4-phenyl-1,2,3,6-tetrahydropyridine (MPTP)-induced experimental parkinsonism (Cartelli et al., 2013). However, a study in Alzheimer's disease (AD) patients showed a significant decrease in β-actin in AD cases compared to controls (Gebhardt et al., 2010). Post mortem studies of schizophrenia patients reported no differences in β-actin expression between schizophrenia and comparison groups (Bauer et al., 2009).

3.3.2 Increased tyrosinated-tubulin and decreased detyrosinated-tubulin suggest decreased MT stability following 26S proteasome dysfunction in mouse cortical neurons.

PTMs of tubulin are involved in regulating the stability of MTs. These modifications form a readable code on MTs for MAPs (De Forges et al., 2012). PTMs of tubulin, including acetylation, tyrosination, detyrosination, polyglutamylation and phosphorylation have gained new interest for their role in neuronal differentiation and neurodegenerative disorders (Fukushima et al., 2009). In particular, α-tubulin acetylation takes place at the ends of MTs and is mostly associated with stable MTs. Detyrosinated α-tubulin is often used as an indication of how long a MT has been assembled, while tyrosination is associated with young neurons and the most dynamic MTs (Poulain and Sobel, 2010, Baas et al., 1993).

In the current study decreased α-tubulin and neuron-specific βIII-tubulin expression at 6 weeks-old in *Psmc1*$^{fl/fl}$*;CaMKIIα-Cre* cortices is associated with MT instability. This was evident by a significant increase in tyrosinated and decrease in detyrosinated α-tubulin following 26S proteasome dysfunction in cortical neurons, suggesting that the MTs are more dynamic or unstable. Disruption of the 26S proteasome function had no significant effect on acetylated α-tubulin levels compared to control mice. Acetylation is enriched in stable and long-lived MTs; soluble tubulin dimers are rapidly deacetylated when released from MTs (Perdiz et al., 2011). This mechanism may explain tendency to decreased to the acetylated α-tubulin expression was noted at 6 weeks-age in *Psmc1*$^{fl/fl}$*;CaMKIIα-Cre*.

The tyrosination/detyrosination cycle in neurons is also involved in MT interaction with MAPs (Peris et al., 2009). In normal neurons, tyrosinated tubulin supports dynamic MTs and allowing rapid remodelling of the cytoplasm (Peris et al., 2009). The C-terminal tyrosine residue of newly synthesized α-tubulin can undergo a

regulated cycle in which it is removed by an unknown carboxypeptidase then re-added back by tubulin-tyrosine ligase (TTL) (Ersfeld et al., 1993). TTL and STMN each form stable complexes with tubulin and inhibit tubulin polymerization in vitro and in vivo (Belmont and Mitchison, 1996, Szyk et al., 2011). As TTL and STMN compete for binding on tubulin dimers, it is possible that STMN can inhibit the tyrosination of tubulin due to partially overlapping binding sites, (Szyk et al., 2013). Since STMN1 expression is significantly decreased following 26S proteasome dysfunction, this mechanism may explain the significant increase in tyrosinated-tubulin.

The presence or absence of the C-terminal tyrosine residue of α-tubulin has been implicated in the regulation of motor proteins and microtubule (+)-end binding proteins (+TIPs) (Peris et al., 2009). A recent study demonstrated that axon injury rapidly increases tyrosinated α-tubulin levels in peripheral sensory neurons in a TTL-dependent manner (Song et al., 2015). Injury-induced tyrosinated α-tubulin promotes axon regeneration by facilitating the retrograde transport of injury signals by +TIPs, which is required for retrograde organelle transport (Lloyd et al., 2012). However, in Purkinje cell degeneration (*pcd*) mice increased levels of tyrosinated α-tubulin are associated with adult-onset degeneration of Purkinje and retinal neurons (Wang and Morgan, 2007).

It is unclear whether the increased tyrosinated α-tubulin in cortices following 26S proteasome dysfunction is involved in regeneration or degeneration of neurons without further investigations. It is possible that increased tyrosinated α-tubulin is involved in retrograde transport given that continued 26S proteasome dysfunction causes paranuclear accumulation of proteins and fragmented dysfunctional mitochondria (Ugun-Klusek et al., 2017).

Significantly decreased levels of α-tubulin in AD was associated with decreased levels of tyrosinated and detyrosinated tubulin, but increased acetylated α-tubulin expression. These changes in tubulin modification in AD brain may represent a compensatory

response to microtubule destabilization in susceptible neurons (Zhang et al., 2015a). In addition, pharmacological proteasome inhibition is usually associated with increased tubulin polymerization. Treatment of dorsal root ganglia neurons in vitro and in vivo with Bortezomib increased tubulin polymerisation (Meregalli et al., 2014). Also, a significant increase in acetylated α-tubulin in whole cell lysates from HCN1A and HCN2 cells was found following treatment with proteasome inhibitors (Poruchynsky et al., 2008).

3.3.3 Decreased MT polymerization following disruption of the 26S proteasome in mouse cortical neurons

MT stability requires a balanced equilibrium between polymerized and free tubulin. We found α-tubulin polymerization was significantly decreased at 6 weeks-old in *Psmc1*$^{fl/fl}$*;CaMKIIα-Cre* mouse cortices compared to controls. This was reflected by an increased free/polymerized α-tubulin ratio and decreased % α-tubulin polymerization. In support of our results, reduced MT stability has been observed in several neurodegenerative diseases, including Alzheimer's disease (AD), Parkinson's disease (PD) and Amyotrophic Lateral Sclerosis (ALS) (Dubey et al., 2015). A marked decrease in MT dynamics and accumulation of mitochondria along the axon was observed in cultured neurons treated with Parkinsonism-inducing neurotoxin 1-methyl-4-phenylpiridinium (MPP^+) (Cartelli et al., 2013, Cartelli et al., 2010). A further study showed that MT instability increased very early, before observable impairment of axonal transport, in a mouse model of ALS, and drug-induced stabilization of MT was able to restore normal axonal transport, suggesting that axonal transport defects in this model are a consequence of increased MT dynamics (Fanara et al., 2007).

MT stabilization or destabilization may play an important role in the regulation of intracellular transport of mitochondria as well as interaction with other organelles within the axon. Interestingly, MT instability following 26S proteasome dysfunction is associated with

the formation of paranuclear protein inclusions contained aggregated proteins and fragmented dysfunctional mitochondria (Bedford et al., 2008, Ugun-Klusek et al., 2017). Interestingly, MT instability does not appear to be affected by decreased STMN1 expression in this model, which may be a compensatory response to changing MT dynamics.

3.3.4 Decreased tau and MAP2 associated with polymerized-tubulin following disruption of the 26S proteasome in mouse cortical neurons

Microtubule-associated proteins (MAPs) are a series of phospho-proteins and their interaction with MTs depends on their phosphorylation state (Mollinedo and Gajate, 2003). MAP2 and tau are brain specific MAPs involved in the maintenance of MT dynamics in dendrites and axons, respectively (Drewes et al., 1998). MAP2 and tau play roles in stabilization of MTs and oppose the action of STMN, which is a MT destabilizing protein. Increased STMN expression in COS-7 cells can lead to MT instability and release tau from MTs via increasing tau phosphorylation, reducing its affinity to MTs. This study also found that in STMN-expressing cells tau phosphorylation in the MT-unbound fraction was higher than in the MT-bound fraction (Miyasaka et al., 2010). An inverse relationship between MAP-tau expression and that of STMN was seen in a subset of cases of a breast cancer cohort. The study found that low STMN and high MAP-tau were associated with increased microtubule stability and better prognosis in breast cancer (Baquero et al., 2012).

We found that the protein levels of MAP2 and tau were not significantly different at 4 weeks of age in control and *Psmc1*$^{fl/fl}$*;CaMKIIa-Cre* mice. At 6 weeks-old a significant decrease in total tau was observed when obvious neurodegeneration is evident in this mouse model. These data suggest that changes in the expression of total tau at 6 weeks-old may be secondary to neurodegenerative processes that are occurring following 26S proteasome dysfunction in cortical neurons.

The significant decrease in total tau at 6 weeks-old in *Psmc1*$^{fl/fl}$*;CaMKIIα-Cre* mice did not affect its binding affinity to MTs. The % tau associated with the polymerized fraction was not different between control and *Psmc1*$^{fl/fl}$*;CaMKIIα-Cre* mice. However, there was a significant reduction in tau phosphorylation at this age.

A previous study indicated that the 20S proteasome was responsible for degrading tau protein under normal conditions (Grune et al., 2010). Under stress conditions, phosphorylated tau may be ubiquitinated by CHIP and degraded by 26S proteasomes (Shimura et al., 2004). Increased 20S proteasome assembly and activity promotes life span and resistance to proteotoxicity in the nematode Caenorhabditis elegans (Chondrogianni et al., 2015). A hyperactive 20S proteasome also has potentially beneficial effects in the cell by protecting against ROS-mediated oxidative stress (Pickering and Davies, 2012). It is possible that the 20S proteasome is more resistant to oxidative stress than the 26S proteasome, maintaining its activity even upon treatment with moderate to high concentrations of H_2O_2 (Ben-Nissan and Sharon, 2014). 20S proteasome activity is increased at 4 and 6 weeks-old in *Psmc1*$^{fl/fl}$*;CaMKIIα-Cre* mice; ubiquitin-independent proteasomal degradation is not affected in this mouse model (Bedford et al., 2008). Therefore, decreased total tau expression in *Psmc1*$^{fl/fl}$*;CaMKIIα-Cre* mice seen in the analyses here might be a consequence of increased 20S proteasome activity following 26S proteasome dysfunction. This is supported by a recent study showing reduced levels of tau protein and its aggregates in mammalian cells with open-gated proteasomes (Choi et al., 2016). A recent study revealed that tau knockout in the prefrontal cortex (PFC) of mice prevents stress-induced dendritic atrophy and spine loss in PFC neurons, by changing proteins involved in mitochondrial transport and oxidative phosphorylation as well as in the synaptic localization of mitochondria. These findings provide evidence for a causal role of tau in mediating stress-elicited neuronal atrophy and

cognitive impairment, and indicate that tau may exert its effects through synaptic mitochondria (Lopes et al., 2016)

We also showed a significant decrease in the amount of MAP2 associated with polymerized MTs in *Psmc1*$^{fl/fl}$*;CaMKIIα-Cre* mice. An explanation for the decreased binding affinity of MAP2 to MTs may be a deregulation of the activity of kinases in *Psmc1*$^{fl/fl}$*;CaMKIIα-Cre* mice. Several kinases have been identified that phosphorylate MAP2 at different sites, including protein kinase A (PKA), protein kinase C (PKC) and microtubule-affinity-regulating kinase (MARKs); phosphorylation of MAP2 causes its dissociation from microtubules (Zhang and Dong, 2012).

MAP2/tau and STMN play opposite, but complimentary roles in MT stability. Therefore, it is possible that decreased binding affinity of MAP2 and decreased total tau expression leads to disruption of the MT structure, increased destabilization of the MT network and impairment of axonal transport, eventually triggering death in neurons. Decreased STMN1 expression at 6 weeks of age can provide a negative feedback loop to stabilizing the MTs following 26S proteasome disruption in neurons, compensating for MT instability.

Chapter 4

Stathmin and its regulators following disruption of the 26S proteasome in mouse cortical neurons

4.1 Introduction

Stathmin (STMN) is a microtubule destabilizing protein that binds α-tubulin/β-tubulin heterodimers, decreasing the availability of tubulin dimers for polymerization and increasing catastrophe (Sobel et al., 1989, Belmont and Mitchison, 1996, Rubin and Atweh, 2004). STMN is regulated by phosphorylation at four serine residues; Ser-16, -25, -38 and -63, which reduces its binding affinity for tubulin heterodimers (Beretta et al., 1993, le Gouvello et al., 1998, Di Paolo et al., 1997). Phosphorylation of STMN leads to more stable MTs and MT dynamics (Belmont and Mitchison, 1996, Budhachandra et al., 2008).

STMN1 is the most abundant member of a family of MT destabilizing proteins (Chauvin and Sobel, 2015). It is selectively expressed in the adult mammalian brain, including the dentate gyrus of the hippocampus, amygdala and cortex (Amat et al., 1991, Shumyatsky et al., 2005). Alterations in STMN1 mRNA expression and protein levels are evident during development and maturation of the CNS and STMN1 has been shown to be involved in neural development, differentiation, plasticity, learning, degeneration and aging (Mori and Morii, 2002, Bohm et al., 2015).

Besides the importance of STMN1 in the healthy nervous system (Ohkawa et al., 2007a, Boekhoorn et al., 2014, Bohm et al., 2015, Duncan et al., 2013), changes in STMN1 expression have been found in pathological neurons (Mori and Morii, 2002, Ohkawa et al., 2007b). A potential link between STMN1 accumulation and MT defects was reported in spinal muscular atrophy (SMA) and SOD1-linked amyotrophic lateral sclerosis, showing decreased levels of polymerized tubulin correlated with disease severity (Wen et al., 2010). Genetic knockout of STMN1 in a SMA mouse model lead to improved neuromuscular function through enhanced MT stabilization, underlining the pathogenic relevance of STMN1 upregulation (Bellouze et al., 2016). However, decreased STMN1 protein and mRNA was found in Alzheimer's disease neocortex, where decreased STMN1 expression was correlated with

neurofibrillary tangle-bearing neurons and disease severity (Cheon et al., 2001, Jin et al., 1996). Decreased STMN1 expression in STMN1-deficient mice is associated with axonopathy of the central and peripheral nervous systems, suggesting STMN1 may also be important for the maintenance of axonal integrity (Liedtke et al., 2002). Together, these studies highlight the critical role of STMN1 in the nervous system as well as the need for further studies to understand its function in diverse pathological conditions.

Along with the important role of STMN1 in microtubule destabilization, STMN1 is involved in cell signalling and acts as an intracellular relay (=''stathmos'' in Greek), integrating diverse regulatory pathways in response to extracellular signals (Sobel et al., 1989, Chauvin and Sobel, 2015). STMN1 can function in both cellular growth and death pathways (Rubin and Atweh, 2004, Okazaki et al., 1995). The function of STMN1 in proliferation is thought to explain its frequent overexpression in human cancer and has been shown to be required for the survival of several cancer cell lines, including bone marrow, acute myeloid leukaemia U937 and breast cancer cell lines (Carney and Cassimeris, 2010, Wen et al., 2013). However, STMN1 depletion in a number of cell lines slows cell proliferation and ultimately leads to apoptosis and cell death (Carney et al., 2012, Wen et al., 2013). In colon cancer cell lines a slowing of cell proliferation caused by a block in G2 was observed, which led to increased apoptosis in colon cancer cell lines (Carney et al., 2012). STMN1 is a downstream target of cell death and survival pathways and its activity could be affected by p53, p27 and the PI3K/Akt pathway (Karst et al., 2011).

We previously identified STMN1 as significantly decreased following 26S proteasome disruption in mouse cortical neurons (Elkharaz et al., 2013). Given that we have now shown microtubule instability following 26S proteasome disruption (section 3.2.4), it is possible that decreased STMN1 is part of a negative feedback loop attempting to stabilize the MTs. This is particularly important in neurons where the microtubule network provides structural

support and allows for the movement of organelles (Monteiro et al., 2011). Cytoskeletal dysfunction has been proposed to contribute to the aetiology of several neurodegenerative diseases (D'Andrea et al., 2001). To further investigate the role of STMN1 following 26S proteasome disruption and associated cortical neurodegeneration we investigate in this chapter proteins and pathways that have been linked to STMN1, namely p53, p27 and the PI3K/Akt pathway. Degradation of p53, p27 and Akt proteins are regulated by UPS; and dysfunction of this system has been shown to upregulate these proteins (Pagano et al., 1995, Shirane et al., 1999, Asher et al., 2005, Silveira et al., 2014).

4.1.1 Stathmin and p53

STMN1 is a p53-target gene (Johnsen et al., 2000, Fang et al., 2010). It has been shown that STMN1 mRNA levels decrease following induction of p53 by apoptotic insults such as UV irradiation and doxorubicin treatment (Murphy et al., 1999). p53 can negatively regulate STMN1 expression at both transcriptional and translational levels in the lung cancer cell line A549 (Fang et al., 2010). In a study of ovarian cancer, decreased STMN1 expression also inhibited p53 stability and its transcriptional activity (Sonego et al., 2013).

In normal cells, low p53 levels are maintained by a negative-feedback loop whereby p53 promotes MDM2 expression, which tags p53 for proteasomal degradation (Yang et al., 2003b). For apoptotic events, p53 must accumulate in the cell and transcriptionally regulate genes that control the cell fate. For example, p53 can induce the expression of p21 and p27, cyclin-dependent kinase inhibitors, which leads to cell cycle arrest (Bratton and Cohen, 2001). p53 can also activate both death-receptor and mitochondrial apoptotic pathways by inducing the expression of various pro-apoptotic genes such as Bax and Noxa (Mihara et al., 2003).

Increased cellular levels of p53 play an important role in the pathogenesis of neurodegenerative diseases (Chang et al., 2012). Increased p53 levels and activity were observed in PD patient brains as well as in PD animal and cellular models (Mogi et al., 2007). Studies in post-mortem brain tissue from AD patients and healthy elderly controls reported an increase in p53 immunoreactivity in AD cortical neurons, particularly in subpopulations that were undergoing neurofibrillary degeneration in the temporal cortex (Hooper et al., 2007). An involvement of p53 in HD pathogenesis has been reported; huntingtin expression was upregulated at the transcriptional level following activation of p53 in lung epithelial H1299 cells (Feng et al., 2006). Deletion of the p53 gene in mouse brain dopaminergic neurons during late developmental stages, protected both the striatum and substantia nigra from neuronal death following acute MPTP treatment through blocking MPTP-induced Bax and PUMA upregulation (Qi et al., 2016).

Increased p53 levels were demonstrated in both PC12 cells and dopaminergic neurons derived from embryonic stem cells following administration of the proteasome inhibitor PSI. This increase in p53 level was not associated with an increase in p53 mRNA or change expression of Puma or Bax mRNA. p53 co-immunoprecipitated with Bcl-xL and MDM2, suggesting that p53 was increased in a transcription-independent manner (Nair et al., 2006). In human cancer cell lines, cell death induced by proteasome inhibitors MG-132, bortezomib and thiostrepton was correlated with p53-independent induction of pro-apoptotic protein Noxa, but not with p53-dependent upregulation of pro-apoptotic PUMA. Furthermore, increased intracellular levels of p53 was sufficient to induce apoptosis in both Rat-1 and PC12 cells following MG115 proteasome inhibitor treatment (Lopes et al., 1997). Despite studies using pharmacological inhibitors of the 20S proteasome in diverse cell types and animal models, the role of the 26S proteasome system in neuronal apoptosis is poorly understood

since changes in both anti- and pro-apoptotic proteins have been reported following proteasome inhibition (Butts et al., 2005).

4.1.2 Stathmin and PI3K/Akt pathway

STMN1 is a downstream target of the PI3K/Akt pathway, and activity of the PI3K/Akt pathway can measured by STMN1 expression and its phosphorylation status (Saal et al., 2007). Increased expression of STMN1 following treatment of cervical and gastric cancer cells by arsenic trioxide can be inhibited by PI3K inhibitors (Gao et al., 2014, Wang et al., 2010). Moreover, inhibitors of PI3K decreased proliferation of pancreatic neuroendocrine neoplasm cells through decreasing expression and phosphorylation of STMN1 (Schimmack et al., 2015).

In the developing nervous system, the phosphorylation and activation of Akt is both necessary and sufficient for survival of different neuronal types. Akt can also mediate the neuronal survival-promoting activities of a variety of neurotrophic factors, including neurotrophin brain-derived neurotrophic factor (BDNF), nerve growth factor (NGF) and neurotrophin-3 (NT3) (Datta et al., 1997, Crowder and Freeman, 1998, Orike et al., 2001, Brunet et al., 2001, Duronio, 2008). The PI3K/Akt pathway has been linked to promoting neurite outgrowth and enhancing the diameter of processes in the brain (Rickle et al., 2004, Kwon et al., 2006, Read and Gorman, 2009). In primary neuronal cultures, studies have shown the PI3K pathway regulates cell survival, neurite growth, dendritic arborisation and axonal branching (Grider et al., 2009). Activation of this pathway was also found in the amygdala during synaptic plasticity and memory consolidation in fear-conditioned rats (Lin et al., 2001).

An abnormal increase or decrease in Akt activity has been linked to diverse diseases, including cancers and may play a significant role in the onset and progression of neurodegenerative disorders (Chong et al., 2012, Rickle et al., 2004, Manning and Cantley, 2007). Immunostaining of post-mortem brains indicated that Akt

phosphorylation was significantly decreased in dopaminergic neurons of PD patients compared with non-PD patient controls (Greene et al., 2011, Malagelada et al., 2008, Timmons et al., 2009). In addition, decreased immunostaining of total Akt protein was reported in dopaminergic neurons of PD patients (Timmons et al., 2009). A different distribution of Akt and phosphorylated Akt was detected in AD temporal cortex neurons compared with controls, with increased activation of Akt (phosphorylated-Akt/total-Akt) which may promote AD progression (Griffin et al., 2005).

Akt activity and stability in neuronal cells has been shown to be regulated by the UPS (Yan et al., 2006). After establishment of neuronal polarity, Akt was enriched in axon terminals then in the dendrites. Suppressing the UPS led to symmetric distribution of Akt and the formation of multiple axonal branches (Yan et al., 2006). In addition, the proteasome inhibitor Bortezomib can inhibit the PI3K/Akt pathway and decrease phosphorylated-Akt expression, which may play a significant role in Bortezomib-induced apoptosis in head and neck squamous cell carcinoma (HNSCC) cells (Lin et al., 2012). However, treatment of malignant pleural mesothelioma cells with proteasome inhibitor MG132 or Bortezomib led to limited apoptosis associated with elevated phosphorylated-Akt expression (Yuan et al., 2013).

Activated Akt can promote cell survival by inhibiting or promoting the activity of various pro- and anti-apoptotic factors (Burgering and Coffer, 1995, Franke et al., 1995, Franke et al., 1997). In addition, Akt can regulate the proteasomal degradation of p27 (Prasad et al., 2015) and affect p53 protein levels through phosphorylation, inhibiting their activity (Yamaguchi et al., 2001).

4.1.3 Stathmin and p27

The interaction of p27 with STMN plays a pivotal role in the control of cell proliferation in vivo (Berton et al., 2014). p27 can bind to the C-terminal end of STMN1, blocking its tubulin sequestering

capabilities (Baldassarre et al., 2005). Baldassarre et al. (2005) reported that STMN1 bound to p27 in the cytoplasm of sarcoma cells and that high STMN1-expressing and low p27-expressing cells demonstrate increased proliferation and invasion ability (Baldassarre et al., 2005). In vitro STMN1 knockdown led to significantly increased p27 expression in extrahepatic cholangiocarcinoma (EHCC) cells. Moreover, high STMN1 expression was associated with low nuclear and high cytoplasmic p27 expression in clinical EHCC samples and STMN1 suppression regulated proliferation and paclitaxel sensitivity in an EHCC cell line (Watanabe et al., 2014). STMN1 was shown to directly interact with p27 in the cytoplasm of HuCCT1 cells in vitro (Wang et al., 2017). Recent studies raise the possibility that p27 might also control STMN1 expression by an indirect pathway (Adam et al., 2015, Berton et al., 2014, Atweh and Iancu-Rubin, 2014). It is possible that p27 inhibits the phosphorylation of the retinoblastoma (Rb) protein by inhibition of cyclin-dependent kinase (CDK) (Adams et al., 1999). Phosphorylated Rb is no longer able to inhibit the activity of the transcription factor E2F1 (Harbour and Dean, 2000, Hiebert et al., 1992), and E2F1 can trans-activate the STMN1 gene (Chen et al., 2013).

In addition to the interactions between STMN1 and p27, the PI3K/Akt pathway has been shown to regulate p27, where Akt activation downregulates p27 by increasing p27 proteolysis or repressing p27 expression through Akt phosphorylation of a forkhead transcription factor (Brazil et al., 2004). p27 expression in the cell is regulated by proteasome-dependent degradation (Pagano et al., 1995). A recent study by Prasad et al. (2015) showed p27 down-regulation in cervical cancer cells was primarily regulated through PI3K/Akt-mediated proteasomal degradation. The authors found treatment of cervical cancer-derived cell lines with the PI3K inhibitor LY294002 resulted in reduced Akt1 activity. Subsequent treatment of these cell lines with proteasome inhibitor MG132 caused decreased nuclear and increased cytoplasmic p27

expression. The synergistic effect of MG132 and LY294002 resulted in a sub-G1 cell cycle arrest and apoptosis induction through poly (ADP-ribose) polymerase (PARP) cleavage (Prasad et al., 2015).

Expression of p27 in brain is important for cerebral cortex development (Lukaszewicz et al., 2005). The absence of p27 causes a general rise in cell proliferation, reflected by an increased brain size in p27 knockout mice (Fero et al., 1996). Adult CNS neurons are typically described as post-mitotic cells, which means that they permanently retract from the cell cycle. In the adult human brain neurogenesis can only take place in the subventricular and subgranular zones of the hippocampus (Eriksson et al., 1998). Increasing studies have shown that post-mitotic neurons attempt to reactivate the cell cycle, which leads to uncoordinated expression of cell cycle proteins in neurons (Wang et al., 2009, Yang and Herrup, 2007). Progression of attempted cell cycle reactivation is closely associated with the phosphorylation of Rb, its inability to bind to E2F1, and the degradation of the Rb protein. Inhibition of Rb phosphorylation by cyclin dependent kinase inhibitors such as p27 can maintain the integrity of the E2F1/Rb complex (Chong et al., 2006).

Re-entry of neurons into the cell cycle can induce apoptosis instead of promoting cell division and this may be another mechanism by which neurons undergo degeneration (Negis and Karabay, 2016, Rashidian et al., 2005). Studies suggest that dysregulation of cell cycle proteins may play a crucial role in the pathogenesis of Alzheimer's disease. Immunostaining of both p27 and phosphorylated p27 (Thr187) was markedly increased in the cytoplasm of hippocampal pyramidal neurones in AD in comparison with controls (Ogawa et al., 2003). In AD pyramidal neurones a significant overlap of p27 with tau-positive neurofibrillary tangles was found. Moreover, increased gene expression of p27 was found in a cellular model of PD after acute exposure to 6-OHDA treatment (Ryu et al., 2005).

This chapter will therefore investigate whether decreased STMN1 expression is associated with changes in the p53, p27 and the PI3K/Akt pathways following 26S proteasome disruption in cortical mouse neurons. This will lead to a discussion on how these pathways may interact in the context of neurodegeneration in this model.

4.2 Results

4.2.1 Decreased stathmin expression following 26S proteasome dysfunction in mouse cortical neurons

Previous 2D-DIGE (2-Dimensional Difference In Gel Electrophoresis) analyses by our group showed significantly decreased STMN1 expression in *Psmc1*$^{fl/fl}$*;CaMKIIα-Cre* mouse cortices compared to controls at 6 weeks-old (Elkharaz et al., 2013). Since altered 26S proteasome activity is evident in *Psmc1*$^{fl/fl}$*;CaMKIIα-Cre* cortices at 4 weeks-old, we further investigated this observation here by Western blotting at 4 weeks-old and immunohistochemistry at 4 and 6 weeks-old (Figures 4.1-4.3) (Bedford et al., 2008).

4.2.1.1 Stathmin protein expression is decreased at 6 weeks-of-age

Investigations of STMN1 protein expression by Western blotting showed no significant differences between control and *Psmc1*$^{fl/fl}$*;CaMKIIα-Cre* mice at 4 weeks-old (Figure 4.1; $p = 0.7$), and we confirmed significantly decreased STMN1 at 6 weeks-old (Figure 4.1; $p < 0.001$). Therefore, there is an obvious decrease in STMN1 protein expression between 4 and 6 weeks-old in *Psmc1*$^{fl/fl}$*;CaMKIIα-Cre* cortices compared to controls.

To determine whether the decreased STMN1 expression in *Psmc1*$^{fl/fl}$*;CaMKIIα-Cre* cortices was associated with altered distribution of the protein, we performed immunohistochemical studies on control and *Psmc1*$^{fl/fl}$*;CaMKIIα-Cre* mouse brain sections (Figures 4.2 and 4.3). The results presented in this chapter show pyramidal neurons in the somatosensory and auditory cortical areas of the brain. In control neurons STMN1 immunoreactivity was mainly focused in the cell body, including the nucleus and soma, and proximal dendrites of neurons (Figure 4.2A-D, 4 weeks-old; Figure 4.3A-D, 6 weeks-old). Enlarged nuclei and protein inclusions are evident in cortical neurons in *Psmc1*$^{fl/fl}$*;CaMKIIα-Cre* mice (Bedford et al., 2008) (Figure 4.2E-H, 4 weeks-old; Figure 4.3E-H, 6 weeks-old). In *Psmc1*$^{fl/fl}$*;CaMKIIα-Cre* mice at 4 weeks of age

STMN1 immunoreactivity was found predominantly in the cell body similar to control neurons and was also detected in protein inclusions of affected neurons in *Psmc1*$^{fl/fl}$*;CaMKIIα-Cre* mice (Figures 4.2F and H, arrows). However, in neurons with altered morphology, i.e. enlarged nuclei, the nucleus appeared to be devoid of STMN1 staining (Figure 4.2H). At 6 weeks of age, STMN1 staining was not detected in affected cortical neurons or protein inclusions (Figures 4.3F and H), suggesting decreased STMN1 expression in these neurons and supporting the Western blotting observations.

Some neurons in *Psmc1*$^{fl/fl}$*;CaMKIIα-Cre* cortices showed similar STMN1 immunoreactivity as control neurons and are likely non-targeted neurons (Figure 4.2E-H, 4 weeks-old; Figure 4.3E-H, 6 weeks-old; arrowheads).

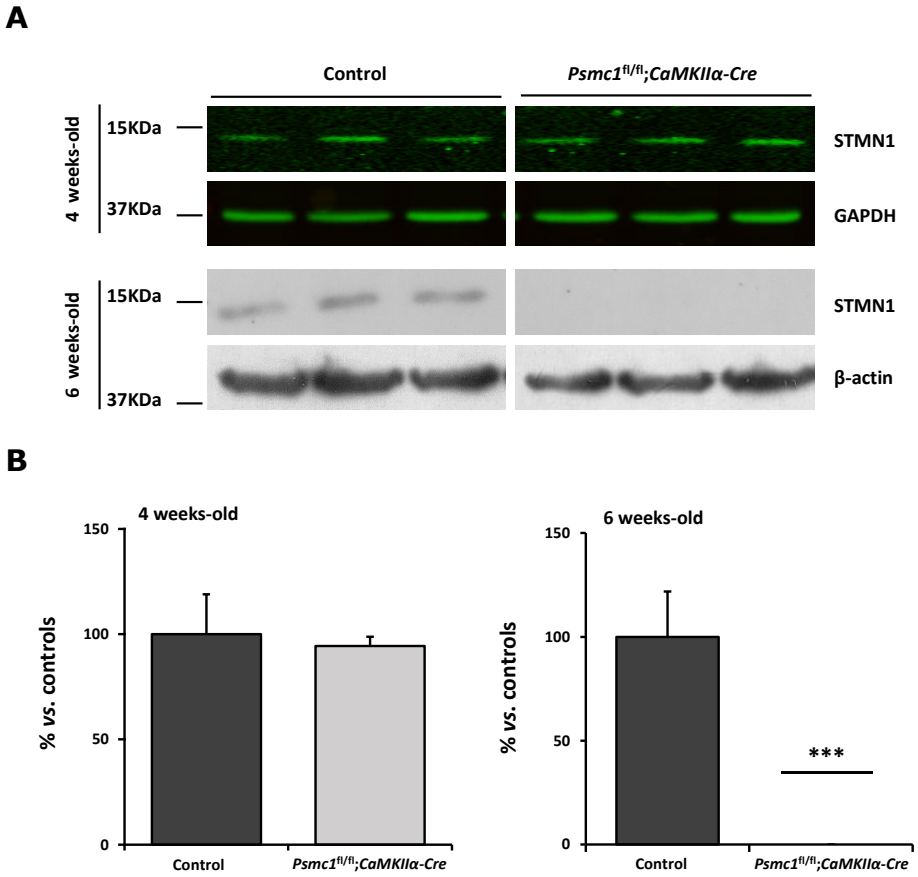


Figure 4.1 STMN1 is significantly decreased in 6 week-old *Psmc1*$^{fl/fl}$*;CaMKIIα-Cre* mouse cortices.

Immunoblots (A) and densitometric analysis (B) of STMN1 (16 kDa) in 4 and 6 week-old (Elkharaz et al., 2013) control and *Psmc1*$^{fl/fl}$*;CaMKIIα-Cre* mouse cortices. 20 µg of protein per lane homogenized in protein lysis buffer was subjected to SDS-PAGE on a 12% gel and transferred to nitrocellulose membrane for Western blotting. (B) Quantitative analysis of immunoblots used Odessy Studio Image software. STMN1 levels was normalised to the level of GAPDH at 4 weeks-old and actin at 6 weeks-old. Data are presented as % vs. controls. Error bars represent mean ± SEM, Student's unpaired t-test. *** $p < 0.001$, n=3.

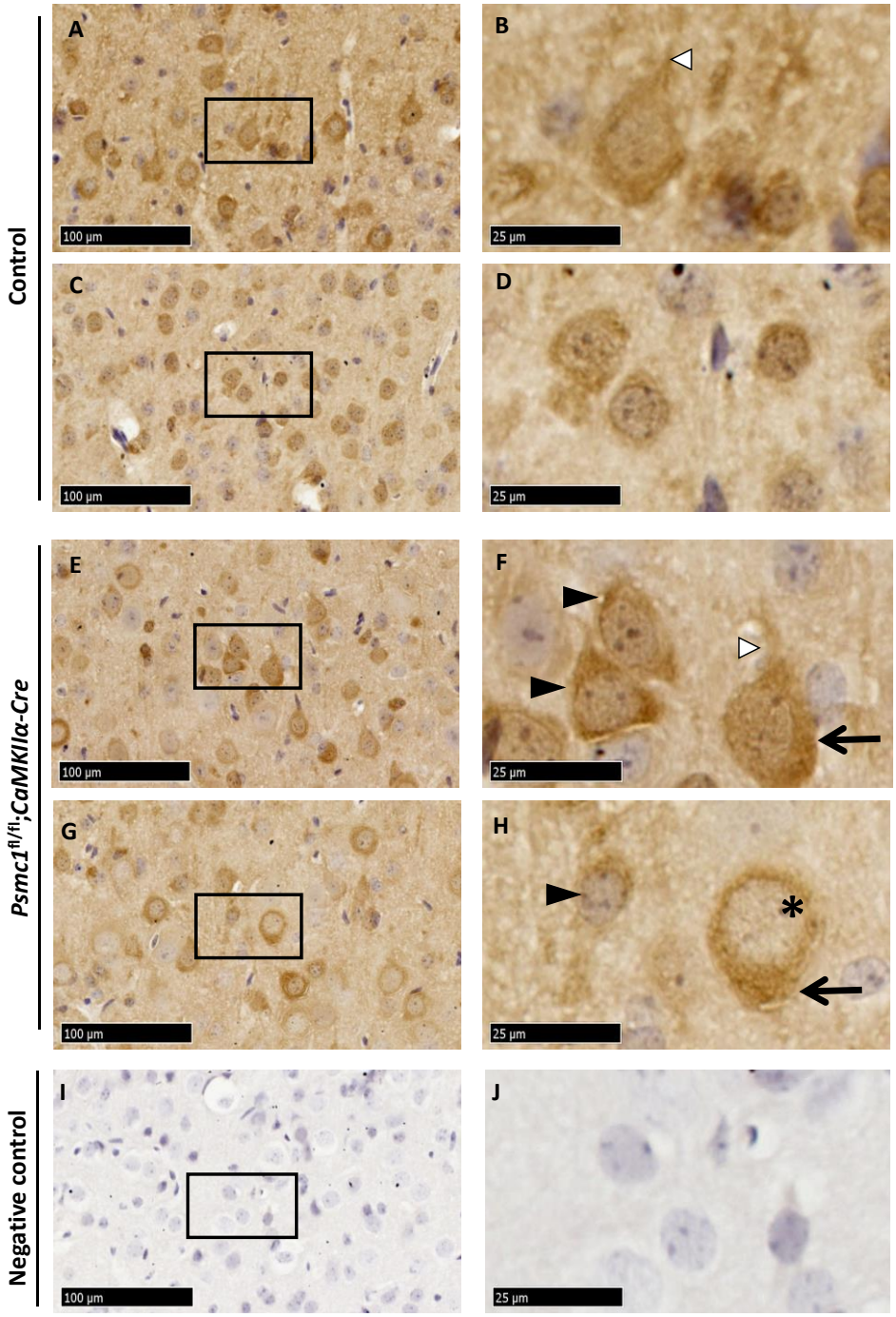


Figure 4.2 STMN1 immunostaining in 4 week-old cortical neurons

Immunohistochemical staining of 7 µm horizontal brain sections from control (A-D) and *Psmc1*$^{fl/fl}$*;CaMKIIα-Cre* (E-H) mice at 4 weeks-old. B, D, F and H show higher magnification images of the boxed areas A, C, E and G respectively. Arrowheads indicate neurons in *Psmc1*$^{fl/fl}$*;CaMKIIα-Cre* mice that show similar morphology to control neurons (F and H). White arrowhead indicated to proximal dendrites of neurons (B and F). Asterisk indicates an enlarged nucleus with decreased STMN1 immunostaining (H). Arrows indicate protein inclusions (F and H). (I and J) Negative control horizontal brain sections from control mice at 4 weeks-old without primary antibody. J higher magnification image of the boxed area I.

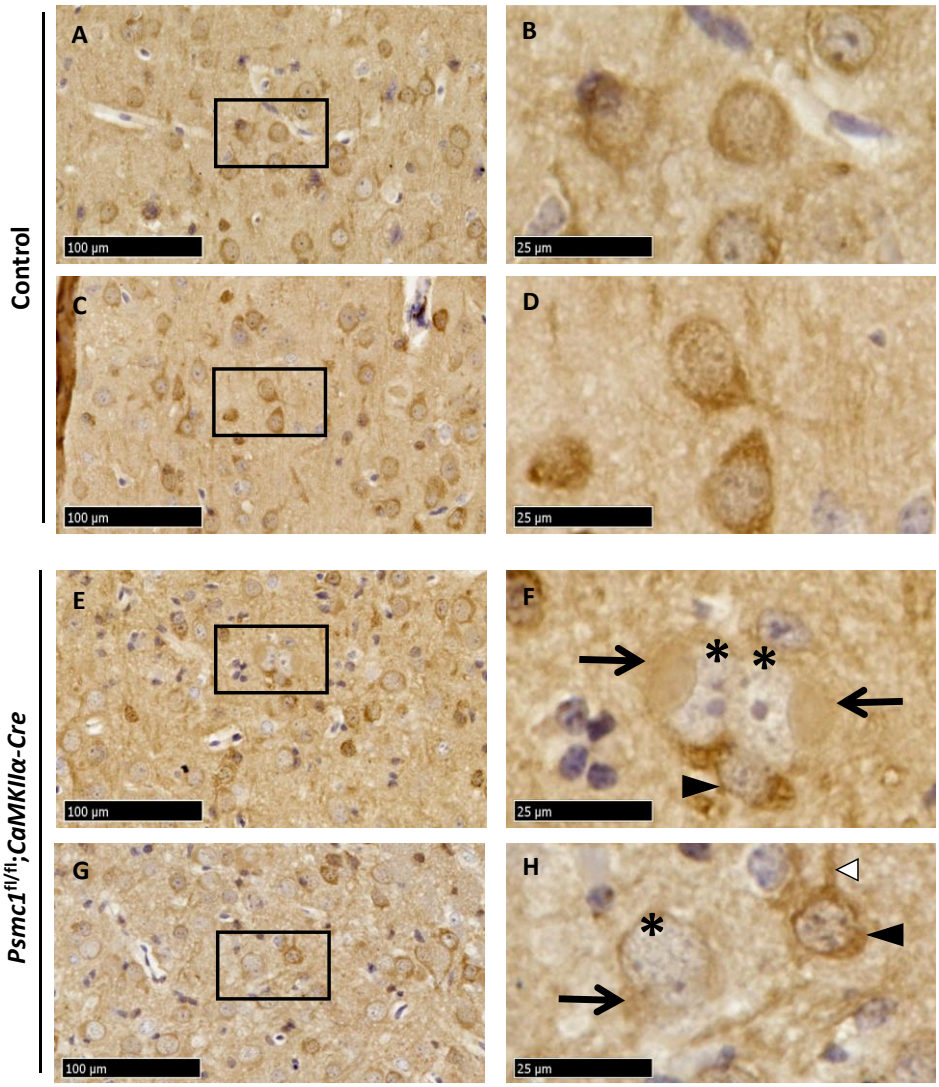


Figure 4.3 STMN1 immunostaining in 6 week-old cortical neurons.

Immunohistochemical staining of 7 µm horizontal brain sections from control (A-D) and *Psmc1*$^{fl/fl}$*;CaMKIIα-Cre* (E-H) mice at 6 weeks-old. B, D, F and H show higher magnification images of the boxed areas in A, C, E and G respectively. Arrowheads indicate neurons in *Psmc1*$^{fl/fl}$*;CaMKIIα-Cre* mice that show similar morphology to control neurons (F and H). White arrowhead indicated to proximal dendrites of neurons (H). Asterisks indicate enlarged nuclei with no STMN1 immunostaining (F and H). Arrows indicate protein inclusions (F and H).

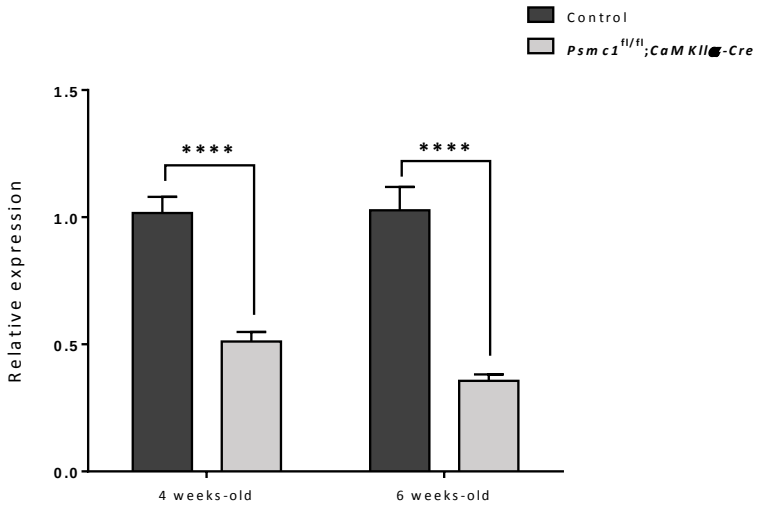
4.2.1.2 Stathmin gene expression is decreased following disruption of the 26S proteasome in mouse cortical neurons

Given that we observed significantly decreased levels of STMN1 protein in *Psmc1*$^{fl/fl}$*;CaMKIIα-Cre* cortices we decided to clarify this observation by investigating the levels of STMN1 mRNA using real-time quantitative RT-PCR at 4 and 6 weeks-old. Table 4.1 and Figure 4.4 show that STMN1 mRNA is significantly decreased at both 4 and 6 weeks of age in *Psmc1*$^{fl/fl}$*;CaMKIIα-Cre* cortices compared to controls ($p < 0.0001$ by Student's unpaired t-test). STMN1 mRNA was decreased approximately to 2- and 2.8-fold in *Psmc1*$^{fl/fl}$*;CaMKIIα-Cre* mice at 4 and 6 weeks-old respectively (Table 4.1).

Table 4.1 STMN1 gene expression in 4 and 6 week-old control and *Psmc1*$^{fl/fl}$*;CaMKIIα-Cre* mouse cortices. Levels of STMN1 mRNA are normalized to the Hmbs housekeeping gene. The normalized relative expression of STMN1 mRNA is shown based on the ΔΔCT calculation. Data are presented as mean ± SEM of n = 8 mice.

Gene symbol	Age	ΔΔCT	$2^{-\Delta\Delta CT}$	Animal ID	Student`s unpaired *t*-test	
					Mean ± SEM	*p* value
STMN1	4 weeks	0.99	0.50	Control	-8.078 ± 0.1052, n=8	< 0.0001
				Psmc1$^{fl/fl}$*;CaMKII α-Cre*	-7.084 ± 0.1195, n=8	****
	6 weeks	1.51	0.35	Control	-7.533 ± 0.1252, n=8	< 0.0001
				Psmc1$^{fl/fl}$*;CaMKII α-Cre*	-6.021 ± 0.1032, n=8	****

A



B

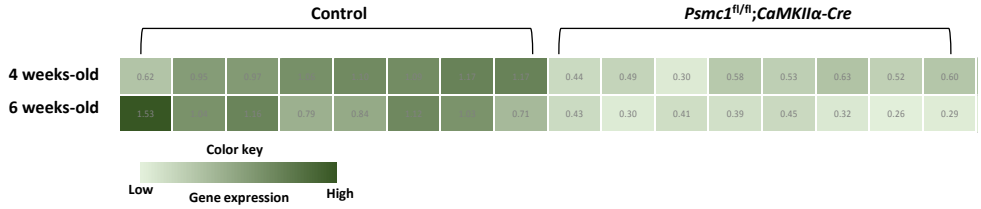


Figure 4.4 STMN1 mRNA expression is decreased in *Psmc1*$^{fl/fl}$*;CaMKIIα-Cre* mouse cortices.

Real-time RT-PCR analysis of STMN1 mRNA expression in cortices from 4 and 6 week–old control and *Psmc1*$^{fl/fl}$*;CaMKIIα-Cre* mice (n = 8). Levels of STMN1 mRNA are normalized to the Hmbs housekeeping gene. (A) The normalized relative expression of STMN1 mRNA is shown based on the ΔΔCT calculation (Table 1). Data are shown as mean ± SEM. ****$p < 0.0001$ by Student's unpaired t-test vs. controls (B) Heat map generated using excel to demonstrate low (light green) and high (dark green) gene expression.

4.2.2 Stathmin regulatory proteins

In order to investigate mechanisms affecting STMN1 expression in cortical neurons, we took a candidate approach and identified proteins known to be involved in regulating STMN1. STMN1 is a downstream target of many signalling pathways whose activity may be regulated by p53, p27 and PI3K/Akt pathway (Karst et al., 2011). Ubiquitin-mediated protein degradation is a well-established negative regulatory mechanism that switches off diverse cellular activities such as the cell cycle and signal transduction (Ciechanover, 2005). p53, p27 and Akt are degraded by the ubiquitin-proteasome pathway and therefore were of interest in these investigations (Pagano et al., 1995, Shirane et al., 1999, Asher et al., 2005, Silveira et al., 2014).

4.2.2.1 Increased p53, but no change in the Bcl2 family, following 26S proteasome disruption in mouse cortical neurons

STMN1 is a p53-target gene (Johnsen et al., 2000, Fang et al., 2010). Studies have shown decreased STMN1 mRNA levels following induction of p53 by apoptotic insults, such as UV irradiation and doxorubicin treatment (Murphy et al., 1999). In addition, p53 negatively regulates STMN1 expression at both the transcriptional and translational levels in the lung cancer cell line A549 (Fang et al., 2010). This study indicated transcriptional repression of STMN1 by p53 activation. p53 is a well characterised substrate of the UPS and studies have shown its accumulation in response to proteasome inhibition (Vogelstein et al., 2000, Bedford et al., 2008).

p53 is associated with the MT cytoskeleton and, in response to DNA damage, is transported towards the nucleus via the minus-end MT-associated motor protein dynein (Giannakakou et al., 2000). MT-targeting compounds such as paclitaxel and vincristine can enhance the nuclear accumulation of p53 and induce activation of the p53-dependent gene mdm2. Nuclear accumulation of p53 was dependent on the ability of the MT-targeting compound to bind to

tubulin (Giannakakou et al., 2002). It is possible that decreased STMN1 expression in *Psmc1*$^{fl/fl}$*;CaMKIIα-Cre* mice may be connected to changes in the expression of p53 as part of a p53-regulated apoptotic process connected and Bcl2 family of proteins.

Western blotting analyses were carried out to evaluate the protein levels of p53 and Bcl2 family proteins Bax and Bcl2 in 4 and 6 week-old control and *Psmc1*$^{fl/fl}$*;CaMKIIα-Cre* mouse cortices (Figures 4.5 and 4.6). Figure 4.5 shows significantly increased expression of p53 at both ages examined in *Psmc1*$^{fl/fl}$*;CaMKIIα-Cre* cortices compared to control mice (Figure 4.5; $p < 0.001$). In contrast, there were no significant differences in levels of Bcl2 family proteins Bax and Bcl2 between control and *Psmc1*$^{fl/fl}$*;CaMKIIα-Cre* cortices at 4 or 6 weeks of age (Figure 4.6: Bax; 4 weeks-old $p = 0.9$, 6 weeks $p = 0.9$; Bcl2 4 weeks $p = 0.4$, 6 weeks $p = 0.6$).

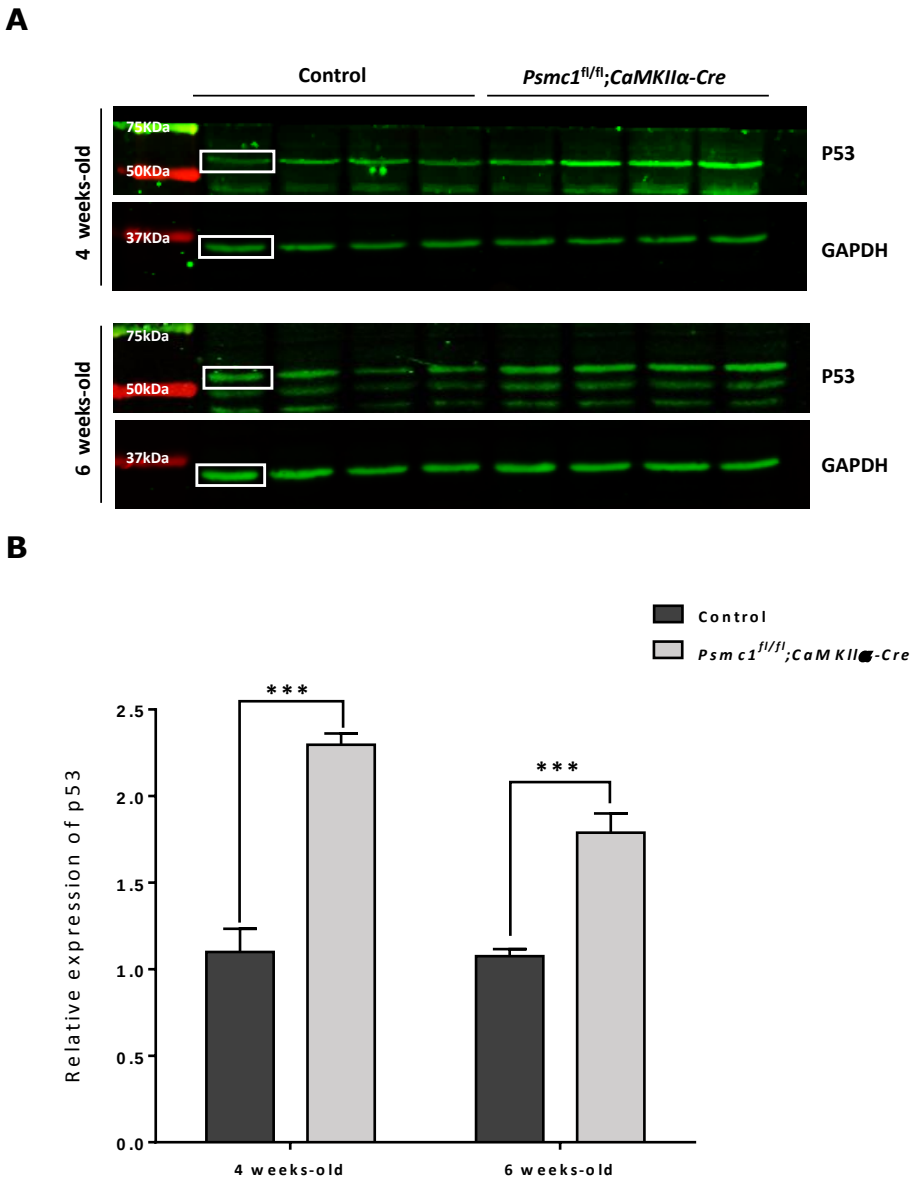


Figure 4.5 Increased p53 protein expression in *Psmc1*$^{fl/fl}$*;CaMKIIα-Cre* mouse cortices

Immunoblots and densitometric analysis of p53 (55 kDa) in 4 and 6 week-old control and *Psmc1*$^{fl/fl}$*;CaMKIIα-Cre* mouse cortices. (A) 60 µg of protein per lane homogenized in protein lysis buffer was subjected to SDS-PAGE on a 12% gel and transferred to nitrocellulose membrane for Western blotting. (B) Quantitative analysis of immunoblots used Odessy Studio Image software analysis. GAPDH was used as a loading control for normalisation. Data are presented as relative expression to controls. Error bars are mean ± SEM. Student's unpaired t-test, ***$p < 0.001$, n=4.

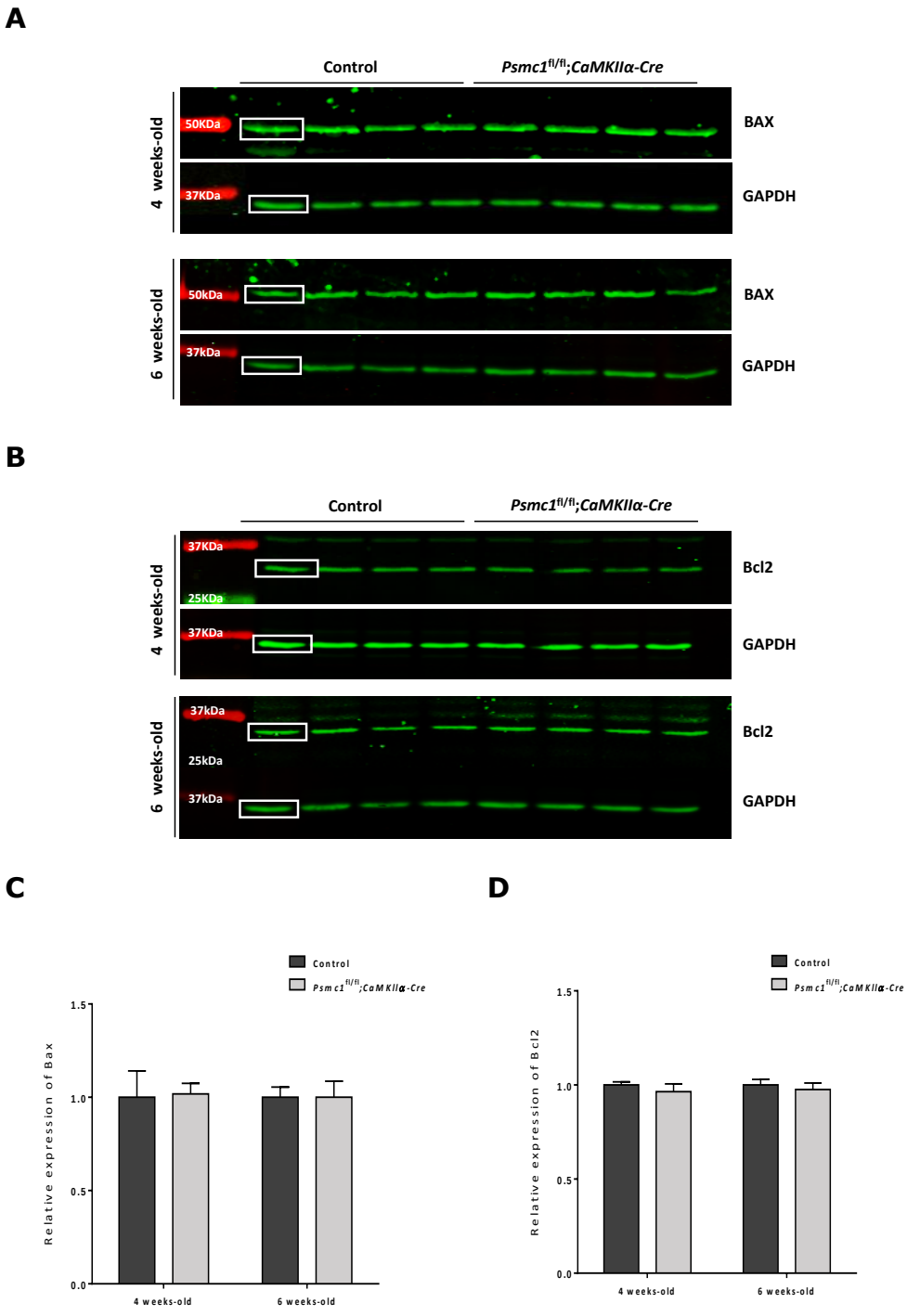


Figure 4.6 Expression of Bcl2 family proteins does not change in *Psmc1*$^{fl/fl}$*;CaMKIIa-Cre* mouse cortices

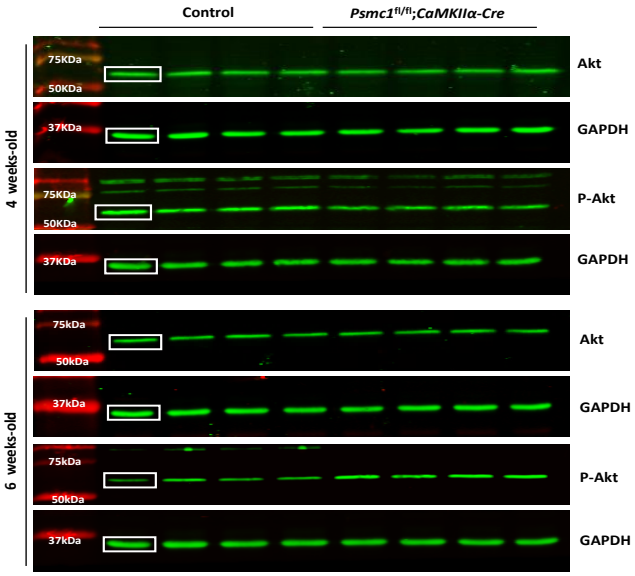
Immunoblots and densitometric analysis of Bcl2 family proteins Bax (A and B; 50 kDa) and Bcl2 (C and D; 26 kDa) in 4 and 6 week-old control and *Psmc1*$^{fl/fl}$*;CaMKIIa-Cre* mouse cortices. (A and C) 50 µg of protein per lane homogenized in protein lysis buffer was subjected to SDS-PAGE on a 12% gel and transferred to nitrocellulose membrane for Western blotting. (B and D) Quantitative analysis of immunoblots used Odessy Studio Image software analysis. GAPDH was used as a loading control for normalisation. Data are presented as relative expression to controls. Error bars represent as mean ± SEM. Student's unpaired t-test, n=4.

4.2.2.2 Changes in the PI3K/Akt pathway following 26S proteasome disruption in mouse cortical neurons

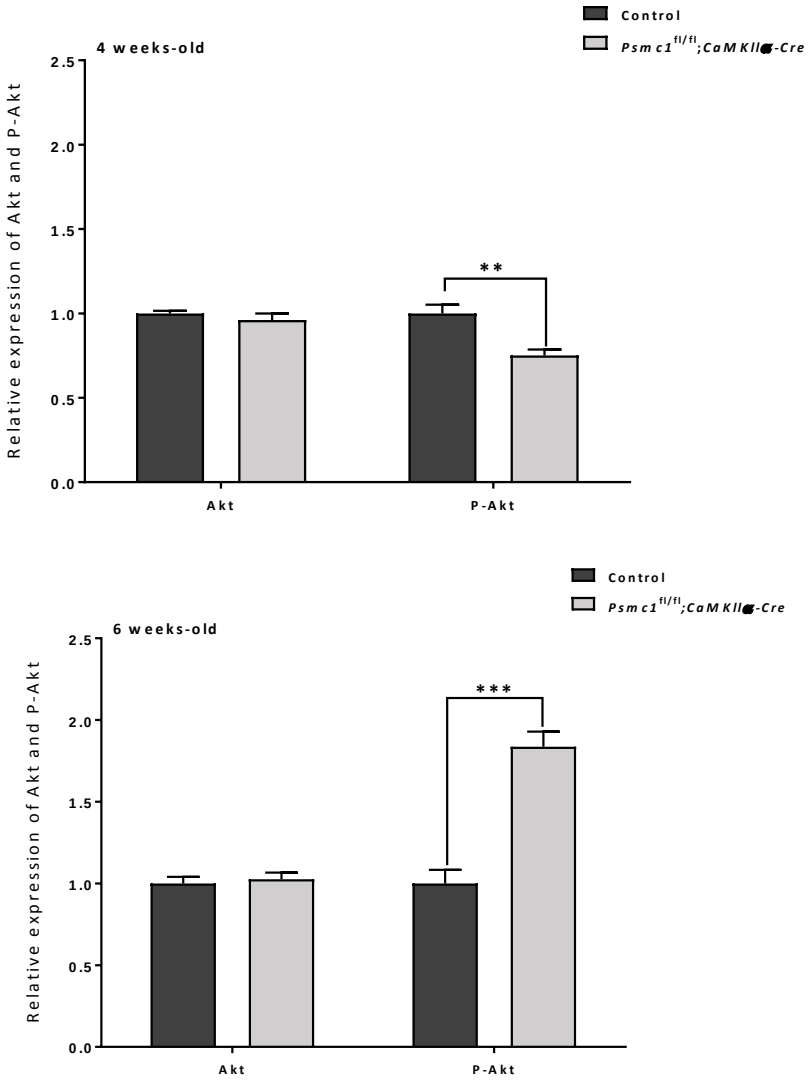
STMN1 depletion is sufficient to increase cell death in cancer cell lines, but the underlying mechanism is unclear (Fang et al., 2010, Carney and Cassimeris, 2010, Zhang et al., 2006). Recent studies have highlighted a strong correlation between phosphorylated (P)-Akt and STMN1 expression (Wang et al., 2010, Schimmack et al., 2015, Belletti and Baldassarre, 2011). In 2007, Saal et al. showed that STMN1 was a downstream target of the PI3K pathway, and that the activity of this pathway could be measured by STMN expression. This study reported that down-regulation of P-Akt (S473) by inhibition of the PI3K pathway using LY294002 was associated with reduced STMN1 levels in three different PTEN-mutant breast cancer cell lines (Saal et al., 2007). Akt is activated by phosphorylation at Thr308 and Ser473 by PDK1 and mTORC2 kinases respectively following activation of the PI3K pathway (Burgering and Coffer, 1995, Franke et al., 1997, Griffin et al., 2005). Akt activation is commonly measured as the ratio of phosphorylated-Akt (Ser473) to total Akt. To investigate whether downregulation of STMN1 expression following 26S proteasome disruption in mouse cortical neurons was associated with changes in the PI3K pathway activity, we investigated Akt and P-Akt (Ser473) by Western blotting at 4 and 6 weeks-old.

Figure 4.7 shows a significant decrease in P-Akt and the P-Akt/Akt ratio at 4 weeks-old in *Psmc1*$^{fl/fl}$*;CaMKIIα-Cre* cortices relative to controls (P-Akt p <0.01; P-Akt/Akt ratio p <0.05). However, at 6 weeks-old the levels of P-Akt and the ratio of P-Akt/Akt significantly increased in *Psmc1*$^{fl/fl}$*;CaMKIIα-Cre* cortices (Figures 4.7B and C; P-Akt p < 0.001; P-Akt/Akt ratio p < 0.001). It is possible that the changes in phosphorylation of Akt may be a protective response to ongoing neurodegeneration between 4 and 6 weeks-old in *Psmc1*$^{fl/fl}$*;CaMKIIα-Cre* mice.

A


Control
Psmc1fl/fl;CaMKIIα-Cre
4 weeks-old
6 weeks-old
75KDa
50KDa
37KDa
Akt
GAPDH
P-Akt
GAPDH
75kDa
50kDa
37kDa
Akt
GAPDH
P-Akt
GAPDH

B


Control
Psmc1fl/fl;CaMKIIα-Cre
4 weeks-old
Relative expression of Akt and P-Akt
2.5
2.0
1.5
1.0
0.5
0.0
**
Akt
P-Akt
Control
Psmc1fl/fl;CaMKIIα-Cre
6 weeks-old
Relative expression of Akt and P-Akt
2.5
2.0
1.5
1.0
0.5
0.0
***
Akt
P-Akt

C

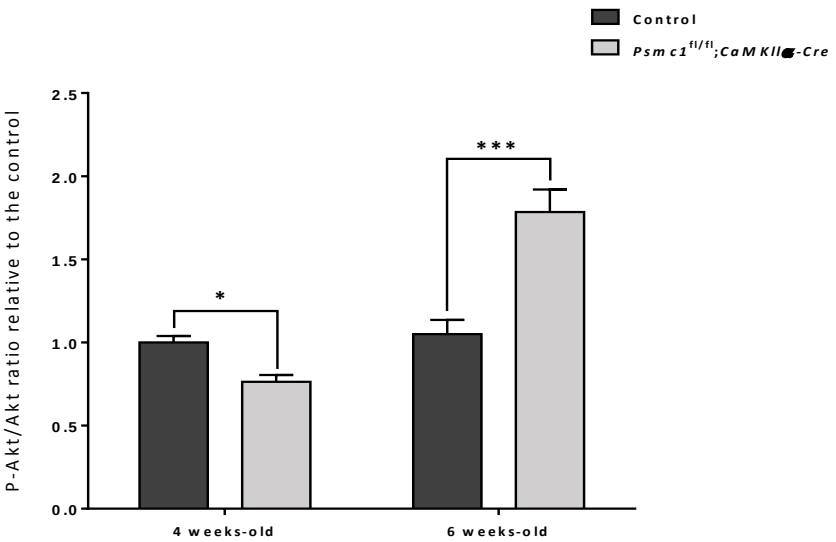


Figure 4.7 Changes in the PI3K pathway in *Psmc1*$^{fl/fl}$*;CaMKIIa-Cre* mouse cortices at 4 and 6 weeks-old

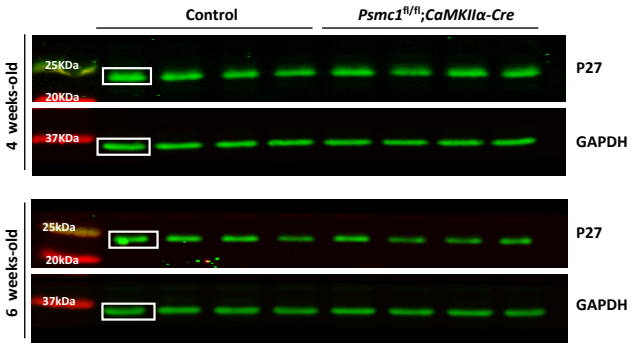
Immunoblots and densitometric analysis of the PI3K/Akt pathway; Akt and P-Akt (60 kDa) in 4 and 6 week-old control and *Psmc1*$^{fl/fl}$*;CaMKIIa-Cre* mouse cortices. (A) 20 µg of protein per lane homogenized in protein lysis buffer was subjected to SDS-PAGE on a 12% gel and transferred to nitrocellulose membrane for Western blotting. (B and C) Quantitative analysis of immunoblots used Odessy Studio Image software analysis. Akt and P-Akt were normalised to GAPDH as a loading control. Data are presented as mean ± SEM relative to control mice. Student's unpaired t-test; *$p < 0.05$, **$p < 0.001$, ***$p < 0.0001$, n=4.

4.2.2.3 p27 expression does not change following 26S proteasome disruption in mouse cortical neurons

The tumour suppressor protein p27 was originally identified as a cyclin/cyclin-dependent kinase (CDK) inhibitor, blocking the activity of cyclin/CDK complexes and G1/S arrest (Vidal and Koff, 2000, Hengst et al., 1994). p27 is an interacting partner of STMN1, which interferes with the ability of STMN1 to sequester tubulin and leads to increased microtubule polymerization (Baldassarre et al., 2005). The p27/STMN1 interaction plays a pivotal role in the control of cell proliferation in vivo (Berton et al., 2014).

Western blot and densitometric analysis here (Figure 4.8) show that the expression levels of p27 protein were not significantly different between control and *Psmc1*$^{fl/fl}$*;CaMKIIα-Cre* cortices at 4 and 6 weeks of age (Figure 4.8B; 4 weeks-old $p = 0.6$, 6 weeks-old $p = 0.3$).

A



B

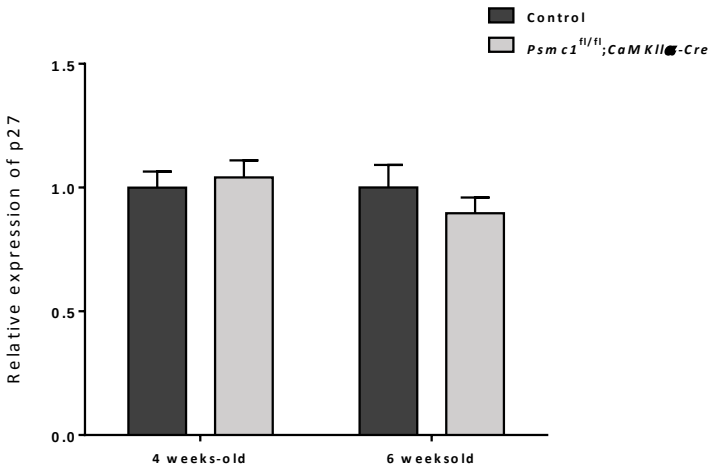


Figure 4.8 No change in p27 expression in *Psmc1*$^{fl/fl}$*;CaMKIIα-Cre* mouse cortex.

Immunoblots and densitometric analysis of p27 (26 kDa) in 4 and 6 week-old control and *Psmc1*$^{fl/fl}$*;CaMKIIα-Cre* mouse cortices. (A) 50 µg of protein per lane homogenized in protein lysis buffer was subjected to SDS-PAGE on a 12% gel and transferred to nitrocellulose membrane for Western blotting. (B) Quantitative analysis of immunoblots used Odessy Studio Image software analysis. p27 level was normalised to GAPDH as a loading control. Error bars represent mean ± SEM. Student's unpaired t-test, n=4.

4.3 Discussion

The work described in this chapter expands our understanding of the molecular events during neurodegeneration following 26S proteasome dysfunction in cortical neurons. The aim was to investigate known cellular pathways involved in regulating STMN1 expression. In this chapter we have shown that changes in p53 and the PI3K/Akt pathway may be involved in regulating the expression of STMN1 following 26S proteasome dysfunction in this model.

4.3.1 Stathmin expression decreases following disruption of the 26S proteasome in mouse cortical neurons

Stathmin (STMN1) is a member of a family of MT regulatory proteins that play critical roles in destabilizing microtubules by direct interaction with tubulin dimers and inhibition of tubulin polymerization (Belmont and Mitchison, 1996, Clement et al., 2005). Previous studies from our lab showed significantly decreased STMN1 protein levels associated with neurodegeneration following disruption of the 26S proteasome in forebrain mouse neurons (Elkharaz et al., 2013). These studies were performed at 6 weeks-of-age and extending these observations; here we show that there are no significant differences in the STMN1 protein levels at 4 weeks-of-age. Interestingly, analyses of STMN1 gene expression show that STMN1 mRNA is significantly decreased at 4 and 6 weeks-old in *Psmc1*$^{fl/fl}$*;CaMKIIa-Cre* cortices compared to controls. This suggests that the dramatic decrease in STMN1 protein levels at 6 weeks-of-age may be caused by down-regulation of STMN1 mRNA during the progression of neurodegeneration in this context. STMN1 mRNA, but not protein, is decreased at 4 weeks-old, and this may reflect the turnover of the STMN protein.

In general, decreased STMN1 levels correlate with decreasing 26S proteasome activity causing progressive neurodegeneration in *Psmc1*$^{fl/fl}$*;CaMKIIa-Cre* cortical neurons. Our observations in general are in agreement with previous studies, which found decreased STMN1 expression with aging and more so in

Alzheimer's disease cases (Saetre et al., 2011, Jin et al., 1996, Cheon et al., 2001, Hayashi et al., 2006, Uchida and Shumyatsky, 2015). Moreover STMN-deficient mice develop an aging axonopathy (Liedtke et al., 2002).

STMN1 is expressed at high levels in the brain, including expression in neurons and glia (Bohm et al., 2015). Studies have shown that the distribution of STMN1 immunostaining in the neuron is restricted to the somata and proximal dendrites (Boekhoorn et al., 2014, Bohm et al., 2015, Liedtke et al., 2002). Interestingly, we demonstrate that STMN1 was localized to the nucleus, cytoplasm and part of dendrites of cortical neurons in control mice. In targeted *Psmc1*$^{fl/fl}$*;CaMKIIa-Cre* cortical neurons, characterised by the presence of protein inclusions and enlarged nuclei, STMN1 immunostaining was localized to the cytoplasm and protein inclusions, with decreased staining in the nucleus associated with aging. At 6 weeks-of-age, we did not detect STMN1 immunostaining in soma and proximal dendrites of targeted *Psmc1*$^{fl/fl}$*;CaMKIIa-Cre* neurons. This observation may be explained by decreased transcription of STMN1 in neurons in response to decreased 26S proteasome activity with increasing age.

Our data suggest that STMN1 may be regulated at the transcriptional level in *Psmc1*$^{fl/fl}$*;CaMKIIa-Cre* mice. In order to identify mechanisms that may be involved in this regulation, we investigated proteins and pathways that are known to regulate or interact with STMN1. Expression of STMN1 has been shown to be affected by p53 (Karst et al., 2011, Fang et al., 2010) and the PI3K/Akt pathway (Wang et al., 2010), and STMN1 is a binding partner of p27 (Berton et al., 2014).

4.3.2 Increased p53, but no change in the Bcl2 family, following 26S proteasome disruption in mouse cortical neurons

p53 is a tumor suppressor protein that regulates many cellular processes through gene transcription (Sionov and Haupt, 1999). Studies have shown that p53 can downregulate the transcription of STMN1, and, in lung cancer cells, this was via the transcription factor Egr1 (Johnsen et al., 2000, Fang et al., 2010). Further studies show p53/p73-mediated negative regulation of STMN may occur through the induction of p21/CDKN1A (Lohr et al., 2003, Asher et al., 2005). STMN can also effect p53 stability and transcriptional activity via the catalytic subunit of the DNA-dependent protein kinase (DNA-PKCS). Inhibition of STMN or DNA-PKCS effects p53-dependent transcription of several M phase regulators, leading to the failure of M phase and death of epithelial ovarian carcinomas (EOC) cells (Sonego et al., 2013). Our results show a correlation between decreased protein and transcript levels of STMN1 and increased p53 expression following 26S proteasome disruption in forebrain neurons, suggesting that p53 may be transcriptionally regulating STMN1 in this context.

It is also possible that increased p53 may lead to activation of p53-regulated apoptotic signalling processes, which contribute to neuronal cell death in this context. The role of the p53 in apoptosis induced by treatment of human cancer cells with proteasome inhibitors has been the subject of considerable debate. Some authors suggest that cell death induced by proteasome inhibitors is p53-dependent (MacLaren et al., 2001, Ding et al., 2007, Yu et al., 2007, Vaziri et al., 2009). Treatment of colon cancer cells with MG132 or bortezomib induced a significant accumulation of p53 and PUMA associated with Bax activation, cytochrome c release and apoptosis (Ding et al., 2007). Other studies have indicated that inhibition of proteasome activity by bortezomib is associated with enhanced apoptosis by p53-dependent and NF-κB independent

mechanisms in in vitro models of renal cell carcinoma (Vaziri et al., 2009).

However, others suggest that proteasome inhibitors can induce apoptosis by a p53-independent mechanism (Kitagawa et al., 1999, Asher et al., 2005, Perez-Galan et al., 2006, Pandit and Gartel, 2011, Zhuang et al., 2016). Previously it has been shown that one of the p53 targets, Noxa, is induced by proteasome inhibitors such as MG132, bortezomib, and thiostrepton in human cancer cells of different origins by a p53-independent mechanism (Pandit and Gartel, 2011).

We show a significant increase in p53 in *Psmc1*$^{fl/fl}$;*CaMKIIα-Cre* cortices at both 4 and 6 weeks-of-age. Since p53 is degraded by the UPS, our observations suggest that p53 is stabilized due to decreased degradation in this model. However, we cannot exclude that p53 is transcriptionally activated in the brain following 26S proteasome dysfunction. Inhibition of the proteasome complex can lead to stabilization of proteins that induce cell cycle arrest and apoptosis, including p53 (An et al., 2000). Stabilized p53 may induce apoptosis and cell cycle arrest by increasing p53 transcriptional activity. Rashidian et al. (2005) suggests that cell cycle regulators such as cyclin-dependent kinases are abnormally activated in neuropathological conditions, including stroke and neurodegenerative disease and may have an important role in neuronal death mechanisms (Rashidian et al., 2005).

p53 accumulation in the nucleus following stress is important to its activity, which involves binding to p53-target genes. Consistent with this view, we previously showed expression of p53 protein predominantly in nuclei of *Psmc1*$^{fl/fl}$;*CaMKIIα-Cre* cortical neurons (Bedford et al., 2008). Consequently, we suggest decreased expression of STMN1 following 26S proteasome dysfunction in neurons may be a consequence of increased p53 and its associated transcriptional activity.

Pro-apoptotic and anti-apoptotic members of the Bcl-2 family proteins, such as Bax and Bcl-2, may be affected by changes in expression of p53. Here we did not detect any significant differences in the expression of these proteins at 4 and 6 weeks-of-age between control and *Psmc1*$^{fl/fl}$;*CaMKIIα-Cre* mouse cortices. This result is consistent with a previous study investigating mechanisms of apoptosis induced by the proteasome inhibitor Bortezomib in cancer cell lines with differing p53 status. The study found that expression of the death gene Bik/Nbk was rapidly up-regulated by Bortezomib, but the levels of other Bcl-2 family members (Bax, Bak, Bcl-2 and Bcl-XL) did not change at any Bortezomib concentration or time point (Zhu et al., 2005). Applying pharmacological proteasome inhibitors to cultured neonatal mouse sympathetic neurons led to apoptotic death, which was accompanied by caspase 3 activation, release of cytochrome c and increased Bcl-2 expression, but no change in Bax (Lang-Rollin et al., 2004). Further investigations of apoptosis and Bcl-2 family members may provide insight into the mechanisms following 26S proteasome dysfunction in neurons in this model. It is possible that the lack of significant change in pro and anti-apoptotic Bcl-2 family members may be a result of activation or suppression of other pathways not analysed here.

4.3.3 Changes in the PI3K/Akt pathway following 26S proteasome disruption in mouse cortical neurons

The PI3K/Akt signaling pathway plays a critical role in anti-apoptotic signal transduction and can block cell death by either blocking the cell death machinery, or regulating expression of genes involved in cell death, protecting cells from several apoptotic stimuli (Kennedy et al., 1997, Brunet et al., 2001).

A strong correlation between P-Akt and STMN1 expression has been highlighted by many research studies. Increased Akt activity and STMN1 levels are closely related with tumour progression and patient outcome (Pérez-Tenorio and Stål, 2002, Ying et al., 2013, Li et al., 2015). Recent studies have demonstrated that PI3K

pathway activation in clinical tissue from prostate cancer was directly correlated with P-Akt and STMN1 immunohistochemical staining (Martin et al., 2015). STMN1 expression has been closely linked to the PI3K-mediated signal transduction pathway by a study identifing STMN1 as a biomarker of PI3K pathway activation and fallopian tube epithelial transition from benign to malignant mucosa (Karst et al., 2011).

In 2007, Saal et al. showed that STMN1 was a downstream target of the PI3K pathway because down-regulation of P-Akt (S473) by PI3K pathway inhibition using LY294002 was associated with reduced STMN1 levels in the three different PTEN-mutant breast Cancer cell lines (Saal et al., 2007). Further studies showed that decreased P-Akt expression or inactivation of Akt may be involved in the cell death induced by arsenic trioxide (As_2O_3) treatment in gastric cancer cells (Gao et al., 2014). In contrast, treatment of cervical cancer cells with As_2O_3 induced STMN1 up-regulation, which was mediated by the PI3K/Akt pathway, and co-treatment of As_2O_3 with the LY294002 PI3K/Akt pathway inhibitor led to a significant decrease in STMN1 expression (Wang et al., 2010). In pancreatic neuroendocrine neoplasm, pathological parameters were associated with overexpression of STMN1, and PI3K inhibitory therapy can decreased proliferation of these tumour cells through decreasing expression and phosphorylation status of STMN1 (Schimmack et al., 2015).

Our studies show a relationship between STMN1 expression and activation of the PI3K/Akt pathway following 26S proteasome disruption in cortical mouse brain neurons. STMN1 expression was significantly decreased at the transcriptional level at both 4 and 6 weeks-of-age in *Psmc1*$^{fl/fl}$*;CaMKIIα-Cre* mice, but STMN1 protein was only significantly decreased at 6 weeks-of-age. P-Akt/Akt ratio at 4 week-old showed a tendency to decrease, which is suggestive of inactivation of this pathway. Previous literature suggested decreased activity of the PI3K/Akt pathway decreases STMN1

expression and this is supported by our observation of decreased STMN1 mRNA.

At 6 weeks-of-age P-Akt and the P-Akt/Akt ratio is dramatically increased in *Psmc1*$^{fl/fl}$*;CaMKIIα-Cre* cortices compared to the controls, suggestive of activation of this pathway. This is interesting given the significant decrease in STMN1 mRNA and protein expression observed at this age. Furthermore, we have also shown significantly increased free/polymerized-tubulin ratio at 6 weeks-old in *Psmc1*$^{fl/fl}$*;CaMKIIα-Cre* cortices, which is associated with increased tyrosinated tubulin; found in the most dynamic MTs, suggesting more dynamic or unstable microtubules. In the context of our results, therefore, we would expect STMN1 to increase. It is possible that decreased STMN1 expression at 6 weeks-old is a negative feedback loop attempting to stabilize MT following 26S proteasome disruption in neurons.

Increased P-Akt expression and Akt activity has been shown protect substantia nigra dopaminergic neurons from oxidative stress in a mouse MPTP model of PD (Aleyasin et al., 2010, Salinas et al., 2001). Study of the PI3K/Akt/mTOR pathway in human post-mortem brain from late AD, amnestic mild cognitive impairment (MCI) and pre-clinical AD (PCAD) patients found hyperactivation of PI3K/Akt/mTOR pathway in MCI and late AD, but not in PCAD. Activation was positively correlated with decreased autophagy activation and increased amounts of Aβ (Tramutola et al., 2015).

There is evidence to suggest that increased P-Akt expression or elevation of Akt activity as we have found at 6 weeks-old may be a neuroprotective response from affected neurons in an attempt to promote survival. Proteasome inhibitor (YSY01A), a potential treatment for breast cancer, has been shown to affect various regulatory proteins in the MCF-7 tumor cell line, including cell cycle associated proteins and the PI3K/Akt pathway. Inhibition of the proteasome led to increases in p53, p21 and p27, but decreased P-Akt (Xue et al., 2015). The anti-tumor effect of YSY01A is mediated by cell cycle arrest at the G2/M stage (Zhang et al., 2015b), via

decreased activity of the PI3K/Akt pathway (Xue et al., 2015). Additionally, proteasome inhibitor Bortezomib can also inhibit Akt activity in a dose-dependent manner and down-regulation of P-Akt played a significant role in Bortezomib-induced apoptosis in head and neck squamous cell carcinoma (HNSCC) cells (Lin et al., 2012). These studies are in contrast to our findings showing increased activity of the PI3K/Akt pathway following genetic inactivation of the 26S proteasome in neurons. However, treatment of malignant pleural mesothelioma (MPM) cells with proteasome inhibitor MG132 or Bortezomib induced limited apoptosis in MPM cells associated with elevated P-Akt protein levels (Yuan et al., 2013), supporting our findings.

Apoptosis is positively regulated by the tumor-suppressor p53 and negatively regulated by the pro-survival PI3K/Akt pathway. Increased transcriptional activity of p53 increases the expression of many pro-apoptotic genes, including death receptors and multiple pro-apoptotic Bcl-2 family members. p53 also represses the expression of anti-apoptotic genes such as Bcl-2 and Bcl-xL (Wang and Scadden, 2015). Activation of the PI3K/Akt pathway can suppress apoptosis either directly by phosphorylating and inactivating pro-apoptotic proteins such as Bad and Bax or indirectly by activating downstream pro-survival targets such as FOXO, NF-κB and GSK signaling cascades (Zhang et al., 2011).

The results show that decreased STMN1 mRNA level at 4 weeks-old in *Psmc1*$^{fl/fl}$*;CaMKIIα-Cre* cortices may be a response to increased p53 at this age since STMN1 is a p53-target gene (Johnsen et al., 2000, Fang et al., 2010). Moreover, at 4 weeks of age the levels of P-Akt in *Psmc1*$^{fl/fl}$*;CaMKIIα-Cre* cortices also decrease, which promotes neurodegeneration. These observations may explain the significantly decreased STMN expression and increased apoptotic neurons evident at 6 weeks-old in *Psmc1*$^{fl/fl}$*;CaMKIIα-Cre* cortex.

In vitro studies in human retinal pigment epithelial cells reported that treatment with low levels of proteasome inhibitors induced

resistance to oxidative injury by a pathway involving inhibition of the PI3K/Akt-mTOR pathway and activation of autophagy (Tang et al., 2014). In addition, inhibition of Akt phosphorylation and its downstream signalling resulted in activation of autophagy via decreased mTORC1 activity in cancer cells (Makhov et al., 2014). 26S proteasome dysfunction in cortical neurons was associated with increased levels of phosphorylated p62 and OPTN, and LC3B-II in *Psmc1*$^{fl/fl}$;*CaMKIIa-Cre* cortices at 3 weeks of age, supporting early autophagy induction (Ugun-Klusek et al., 2017). It is possible that this may explain the decreased P-Akt levels at 4 weeks-old following 26S proteasome dysfunction. However, continued 26S proteasome dysfunction in cortical neurons leads to decreased autophagy by decreasing levels of essential autophagy proteins ATG9 and LC3B, in *Psmc1*$^{fl/fl}$*;CaMKIIa-Cre* mice cortices at 6 weeks-old (Ugun-Klusek et al., 2017). A previous study reported that the PI3K/Akt/mTOR signaling pathway has a critical role in the negative regulation of autophagy activity. Interferon regulatory factor-4 binding protein (IBP) can inhibit autophagy via activating the PI3K/Akt/mTOR signaling pathway in breast cancer cells (Han et al., 2013).

The activity of the PI3K/Akt/mTOR pathway is also linked to autophagic processes and may be related to neuroprotective effects in neurons (Young et al., 2009). P-Akt can activate mTOR a major repressor of autophagy, suggesting that activation of Akt 6 weeks-old may be involved in the downregulation of autophagy following 26S proteasome dysfunction. Another study suggested that enhanced activation of Akt may be involved in inhibition of lethal autophagy-induced neuronal death caused by Ginsenoside rb1 (Luo et al., 2014).

We have previously shown evidence of a neuroprotective response to increased ROS following 26S proteasome disruption, showing increased antioxidant peroxiredoxin 6 (PRDX6) and phospholipase A2 (PLA_2) activities in response to elevated ROS (Elkharaz et al., 2013). In vitro studies in human lung cancer cells showed a

correlation between increased P-Akt and increased PRDX6, supporting our observations. PRDX6 induced lung cancer cell invasiveness by generating arachidonic acid via its PLA_2 activity; arachidonic acid enhanced invasiveness by stimulating signalling components such as p38 kinase, PI3K and Akt (Sloss et al., 2008).

An in vitro study showed a role for active phosphorylated Akt in promoting neurite outgrowth and enhancing dendritic branching in cultured hippocampal mature neurons (7–14 Days IV). This dendritic complexity was reduced by inhibition of PI3K and Akt activity. There is also evidence that increased activity of Akt can increase axonal branching and soma size in primary sensory neurons via activation of mTOR (Grider et al., 2009). These results are in agreement with our data in chapter 5, showing significantly increased apical dendrite length and dendritic arborisations by NFH and NFL immunostaining of 6 weeks-old pyramidal neurons following 26S proteasome dysfunction. Therefore, the increase in P-Akt at 6 weeks-of-age may be promoting neuronal protection and repair.

4.3.4 p27 expression does not change following 26S proteasome disruption in mouse cortical neurons

p27 is a cyclin-dependent kinase inhibitor (CDKI) that regulates cell cycle progression by binding to and inhibiting the activity of cyclin-dependent kinases (CDKs) (Nigg, 1993). STMN1 is an interacting partner of p27. The p27/STMN interaction plays a pivotal role in the control of cell proliferation in vivo (Berton et al., 2014). p27 can bind to the C-terminal end of STMN1, and block its tubulin sequestering capability (Baldassarre et al., 2005). Baldassarre et al. (2005) reported that STMN1 bound to p27 in the cytoplasm of sarcoma cells and that high STMN1-expressing and low p27-expressing cells demonstrate increased proliferation and invasion ability (Baldassarre et al., 2005). Recent studies raise the possibility that p27 might also control STMN1 expression by an indirect pathway (Adam et al., 2015, Berton et al., 2014, Atweh and Iancu-Rubin, 2014). The possibility is that p27 can inhibit

phosphorylation of the retinoblastoma (Rb) protein by inhibition of CDK (Adams et al., 1999). Phosphorylated Rb protein is no longer able to inhibit the activity of the transcription factor E2F1 (Harbour and Dean, 2000, Hiebert et al., 1992), and STMN1 gene is transactivated by the E2F1 protein (Chen et al., 2013).

p27 was investigated at both 4 and 6 weeks-of-age in control and *Psmc1*$^{fl/fl}$*;CaMKIIa-Cre* mouse cortices. No significant differences in p27 protein expression were observed at either age. These results suggest that decreased STMN1 expression following 26 proteasome disruption in cortical neurons may be regulated by other signalling pathways independent of p27. The PI3K/Akt pathway had been shown to directly and indirectly regulate CDKIs p21 and p27, allowing cell cycle progression (Chang et al., 2003). Akt activation can downregulate p27 by increasing p27 proteolysis or repressing p27 expression through Akt phosphorylation of a forkhead transcription factor (Brazil et al., 2004). We previously reported that decreased 26S proteasome activity in primary mouse embryonic fibroblasts (*Psmc1*$^{+/-}$) did not affect the expression of p21, but was associated with a prominent G2/M cell cycle arrest (Rezvani et al., 2012). Further immunohistochemical studies are required to further investigate any changes in the cellular localization of p27 in these mice.

Chapter 5

Morphological and neurofilament changes following disruption of the 26S proteasome in mouse cortical neurons

5.1 Introduction

5.1.1 Morphological insights into neurodegenerative diseases

Cortical thickness has been used as an important morphological feature in the diagnosis and prognostication of neurodegenerative diseases. For instance, Alzheimer's disease (AD) and frontotemporal dementia (FTD) are difficult to differentiate clinically because of overlapping symptoms and histopathological examination of brain tissue is required for definite diagnosis (Siri et al., 2001). However, histopathological studies of cortical thickness have reported damage to specific cortical layers in these diseases; layer II of the entorhinal cortex and layer III of the neocortex in AD and layers III and V of the frontal and temporal lobes in FTD (Kersaitis et al., 2004, Gomez-Isla et al., 1996). Cortical thinning has been shown to be associated with disease severity and progression in neurodegenerative diseases. Patients with PD have significant cortical thinning in the temporal, inferior parietal, rostral frontal and orbitofrontal cortical regions, and this was associated with disease duration (Lyoo et al., 2010). A magnetic resonance imaging (MRI) study of cortical thickness showed thinning of the cortex in regions including the medial temporal lobe, frontal and parietal lobes in patients with AD when compared to normal patients (Badhwar et al., 2013, Lerch et al., 2005).

Although the pathogenesis of most neurodegenerative diseases remains incompletely understood, neurodegeneration and associated atrophy is the main feature of disease (Double et al., 1996, Regeur, 2000). Morphometric studies have been used to analyse neuron numbers and densities as well as other features, including the cell body and nucleus, for a better understanding of the pathogenesis of degenerative diseases (Ihara et al., 2010, Iacono et al., 2009, Iacono et al., 2008, Everall et al., 1997, Bussiere et al., 2003, Bundgaard et al., 2001). Previous morphometric analysis of AD brain sections showed a significant

loss of large neurons in the nucleus basalis, associated with a reduction in the perikaryon and nuclear diameter (Rinne et al., 1987). The number of nerve cells and volume of their nucleoli were decreased in both the temporal cortex and hippocampus of AD patients (Mann et al., 1985). Another study reported decreased neuronal volumes in the neocortex of AD patients (Bussiere et al., 2003). More recent studies detected no difference in neuronal nucleus diameter in the dentate gyrus and CA4 region of the hippocampus between AD, DLB and control patients (Gagyi et al., 2012).

However, other studies have shown the mean nuclear volume of large neocortical neurons is significantly higher in AD patients than controls, while the perikaryal volume was not significantly different (Bundgaard et al., 2001). Increased neuronal nucleus volume, referred as nuclear hypertrophy, was observed in the anterior cingulate gyrus and hippocampal CA1 region in asymptomatic AD patients in comparison to mild cognitive impairment AD and controls (Riudavets et al., 2007). This may represent an early compensatory mechanism that prevents the progression of disease (Iacono et al., 2008, Iacono et al., 2009). The differences observed in morphology between studies may be due to evaluation of different brain regions and stages of the neurodegenerative process.

5.1.2 Neurofilament proteins in neurodegenerative disease

Neurofilaments (NFs) are the major intermediate filament proteins found in neurons (Friede and Samorajski, 1970), where they form the backbone of the axonal cytoskeleton during neuronal differentiation, radial axonal growth, regeneration and guidance (Zhu et al., 1997, Perrot et al., 2008, Liu et al., 2011, Dale and Garcia, 2012).

In mature neurons, NFs are heteropolymers of three protein subunits; heavy (NFH, 180-200kDa), medium (NFM, 130-170kDa) and light (NFL, 60-70kDa) (Hoffman and Lasek, 1975, Griffin et al.,

1978). Each subunit contains a central α-helical rod domain, edged by an N-terminal head domain and a non-α-helical C-terminal domain. NFL subunits constitute the core of the filament on which NFM and NFH subunits are anchored through coiled-coil interactions or rod domains. NFM and NFH subunits alone are unable to form intermediate filaments in the absence of NFL (Carter et al., 1998, Elder et al., 1998). The N-terminal domain of NFs has a MT polymerization inhibitory domain that binds unassembled tubulin and regulates the number of MTs in the axon (Bocquet et al., 2009). The C-terminal domain of NFM and NFH forms side arms that project from the filament and are enriched in Lys-Ser-Pro (KSP) repeats (Hirokawa, 1982). The phosphorylation state of KSP motifs repeated in these lateral projections is important in regulating the rate of NF transport and radial growth of axons (Carden et al., 1987). In addition, NF interactions with MTs also depends on the phosphorylation state of the C-terminal domain; de-phosphorylation of this domain by alkaline phosphatase promotes NF and MT interaction (Hisanaga and Hirokawa, 1990), while phosphorylation by tau protein kinase II dissociates NFs from MTs (Miyasaka et al., 1993).

Abnormal accumulation of NFs in neurons is a hallmark of neuronal dysfunction and axonal degeneration seen in many neurodegenerative diseases, such as amyotrophic lateral sclerosis (ALS), Alzheimer's (AD) and Parkinson's (PD) diseases (Perrot et al., 2008, Liu et al., 2011). Increased NFs coincides with lack of axonal sprouting and increased dynamic instability of axonal MTs (Cifuentes-Diaz et al., 2002, Lariviere and Julien, 2004), suggesting that increased NFs and destabilization of MTs are functionally related. NFs can modulate MT stability and thus axon caliber and axonal transport (Millecamps and Julien, 2013). Increased NF accumulation has been shown to cause neurodegeneration by disrupting axonal transport of cargos required for axonal maintenance (Collard et al., 1995). A recent study showed that the destabilizing activity of STMN1 was

enhanced when NFs were increased in progressive motor neuronopathy (*pmn*) pathology and probably in other neurodegenerative disorders, and this may explain axonal degeneration (Yadav et al., 2016). In addition, depletion of NFL in *pmn* mice increased microtubule stability and delayed axon degeneration by increasing the interaction between Stat3 and STMN1 (Selvaraj et al., 2012, Yadav et al., 2016). Depletion of axonal NFL in NFL knockout mice and in double transgenic mice with overexpression of peripherin leads to improved axonal transport of mitochondria and lysosomes (Perrot and Julien, 2009).

Increased MT instability and altered axonal transport have been suggested as underlying mechanisms that lead to accumulation of NFs in degenerating neurons (Perrot and Eyer, 2009, Perrot and Julien, 2009). Upregulation of NFs in neurodegenerative diseases could be a consequence of increased NF synthesis (Szaro and Strong, 2010) or their defective degradation. Increased NF protein synthesis was ruled out in degenerating neurons of ALS and AD patients, where significantly decreased NFL mRNA levels were found (Strong, 2010, Bergeron et al., 1994, Kittur et al., 1994), while NFM and NFH mRNA levels remained unchanged in ALS (Wong et al., 2000).

NFs have been reported as a target of the ubiquitin-proteasome pathway and calpain (Gou and Leterrier, 1995, Lopez-Picon et al., 2006). Inhibition of NF degradation was noted following the inhibition of calpain and proteasomal activity during axonal degeneration in injured peripheral nerves (Park et al., 2013). In addition, TRIM2 deficiency can lead to neurodegeneration in mice by altering NFL metabolism with consequent NFL accumulation in axons and impairment of axonal transport. TRIM2 is an E3 ubiquitin ligase that ubiquitinates NFL for degeneration (Balastik et al., 2008). TRIM2 deficiency led to axonopathy with axonal accumulation of NFs in human cell lines and a mouse model (Ylikallio et al., 2013). NFM has been identified as a target of the E3 enzyme carboxyl-terminus of Hsc70 interacting protein CHIP,

which enhances NFM ubiquitination and degradation (Wang et al., 2011, Dale and Garcia, 2012).

Immunohistochemical studies reported accumulation of phosphorylated NFH and NFM subunits in the perikarya and tangle-bearing neurons in AD brain (Wang et al., 2001). NFs are synthesized and assembled in the cell body and their phosphorylation occurs upon entry into the axon, suggesting the importance of NF phosphorylation in its transport and interaction with cytoskeletal proteins (Wang et al., 2001, Liu et al., 2011). The phosphorylated form of NF subunits are found in the axoplasm, while the non-phosphorylated form is located in the neuronal perikarya and dendrites (Nixon et al., 1994). Non-phosphorylated NF subunits are rapidly degraded by the UPS and increased NF phosphorylation prevents their turnover by UPS (Dale and Garcia, 2012). In vitro studies using cultured rat pheochromocytoma subcloned (PC12h) cells showed that the proteasome inhibitor lactacystin can induce neuropathological features associated with perikaryal accumulation of phosphorylated NFs (Masaki et al., 2000). Accumulation of phosphorylated NF proteins in the neuronal soma was associated with neuronal dysfunction and degeneration in MS patients (Gray et al., 2012). Furthermore, transgenic mice overexpressing NFM show NF accumulation with filamentous swellings in perikarya and proximal axons of motor neurons (Wong et al., 1995). An in vitro study revealed that disordered NFH and NFM phosphorylation in neurons could lead to blockage of axonal transport and neuronal cell death (Shea et al., 2004). Aberrant phosphorylation of neuronal NFM and NFH proteins has been shown to be involved in AD (Rudrabhatla et al., 2010). Qualitative and quantitative studies have shown that accumulation of NFH subunit in the neuronal perikarya and spheroids has an important role in the ALS pathogenesis (Mendonca et al., 2005).

NFs play an important role in the structural integrity of neurons and in neuronal development (Mendonca et al., 2005). In the mammalian brain, NFs are present in the perikarya, dendrites and

proximal segment of axons of pyramidal neurons within cortical layers II/III and V, and this has been useful in delineating subpopulations of neurons and characterizing the cytoarchitectonic organization of cortical areas (Hof et al., 1992, Kirkcaldie et al., 2002, Van der Gucht et al., 2007, Mellott et al., 2010, Paulussen et al., 2011).

Pyramidal neurons are found in most mammalian forebrain structures, including the cerebral cortex, the hippocampus and the amygdala (Pestronk, 1997). Neocortical pyramidal neurons are the major excitatory neuron in all cortical layers except layer I, representing 70–85% of the total population of neurons in the cortex (Romand et al., 2011). Typical pyramidal neurones are characterized by their pyramidal or ovoid shaped soma and long apical dendrite, ascending from the apex of the soma and ending in a terminal tuft near the pial surface. In addition, there are four to five dendritic domains emerging from the base of the soma, directed laterally or downward (Larkman et al., 1992, Ito, 1992, DeFelipe and Fariñas, 1992). Therefore, the length of the apical dendrite depends on the depth of the cell soma from which it emerges. However, there are many exceptions to this as the majority of layer VI and some layer V pyramidal neurons apical dendrites do not reach layer I (DeFelipe and Fariñas, 1992).

Dendrites play important roles in neuronal function (Yuste and Tank, 1996). However, the cellular mechanism for the growth and maintenance of dendritic arborization is unclear (Kong et al., 1998). The abundance of NFs in dendrite trees in many types of neurons suggests that they may play a role in the growth and maintenance of elaborate dendritic trees (Spruston, 2008). During neuronal development, the expression of NFL and NFM significantly increases at the earliest stages of neuronal process growth (Undamatla and Szaro, 2001) and during neuronal differentiation (Carden et al., 1987). However, the expression of NFH is delayed until 10 days after birth (Shaw and Weber, 1982, Pachter and Liem, 1984), which helps to stabilize neuronal processes and plays a role

in modulating axonal events, such as the slowing of cytoskeletal transport and the growth of axonal calibre (Kong et al., 1998).

Studies of the dendritic architecture of spinal cord neurons in NFL knockout mice showed a significant reduction in dendritic arborisation and diameter in large motor neurons; medium neurons were mildly effected, but no effect was seen in small neurons. The study also revealed that decreased NFL led to reduced NFM and NFH content in dendrites and axons, and their accumulation in cell bodies (Zhang et al., 2002). Maintaining a lower ratio of NFH and NFM to NFL plays a critical role in the development of complex dendritic trees in motor neurons because NFL antagonizes NFH and NFM in organizing the NF network (Zhu et al., 1997). A previous study found that increasing NFH and/or NFM inhibited dendritic arborisation (Kong et al., 1998). However, these changes were reversed by elevating the level of NFL with either NFH or NFM. On the other hand, overexpression of NFL together with NFH may have a protective role in ALS pathology (Couillard-Després et al., 2000, Meier et al., 1999). Crossing of the SOD1 ALS mouse model with NFL or NFH overexpressing mice led to delayed ALS symptoms and extended life span (Kong and Xu, 2000).

5.2 Image processing and data analysis

Images were acquired of 3 control and 3 *Psmc1*$^{fl/fl}$*;CaMKIIα−Cre* horizontal brain sections at 4 and 6 weeks of age. Image acquisition used NanoZoomer whole-slide scanning microscopy at 40X magnification (NanoZoomer Digital Pathology RS, Hamamatsu Photonics), which is capable of capturing wide-field images over entire brain sections at high resolution. The resulting image was viewed using NDP.view.2 software (Figure 5.1A and B). Using the Mouse Brain Atlas: DBA/2J Horizontal Section 14 (http://www.mbl.org/atlas247/atlas247_frame.html); the auditory and somatosensory cortex, was identified (Figure 5.1C).

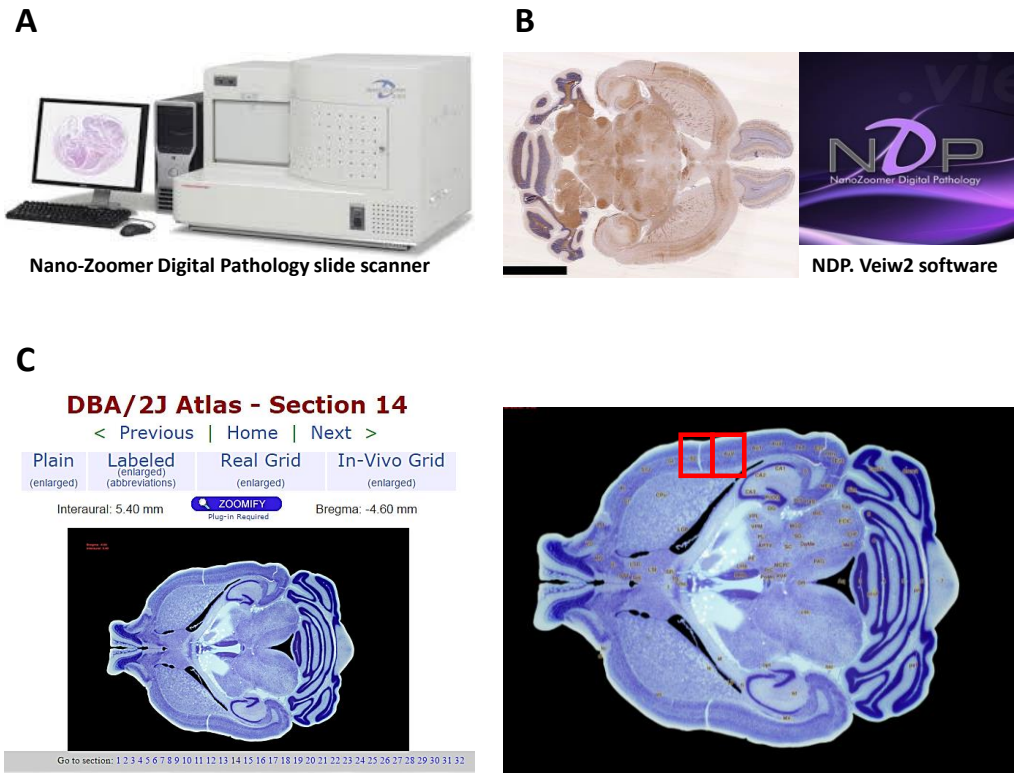


Figure 5.1 Image processing

(A) Image acquisition used a C9600–01 NanoZoomer Digital pathology Slide Scanner. (B) Scanned sections were viewed using NDP.view.2 software. (C) Low magnification whole brain horizontal sections from the Mouse Brain Atlas: DBA/2J Horizontal Section 14; the auditory and somatosensory cortex is highlighted by the red box.

Using annotation tools in NDP.view.2 software, a rectangular box (area = 1.28 mm^2 and perimeter = 4.5 mm) was drawn manually

to include all cortical layers of the auditory (AU) and somatosensory (SS) cortex at 5X magnification (Figure 5.2).

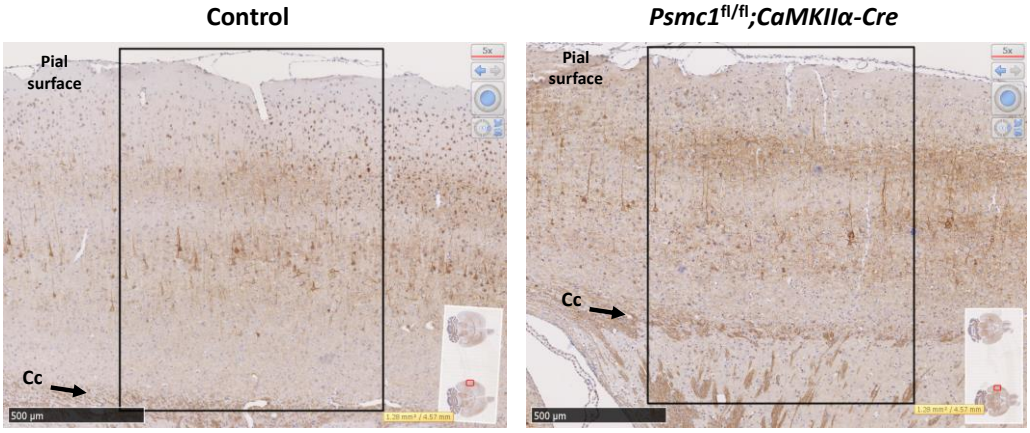


Figure 5.2 NFH immunostaining

NFH immunostaining of the auditory cortex (AU) from representative 6 week-old control and *Psmc1*$^{fl/fl}$;*CaMKIIα-Cre* mice at 5X magnification. A rectangular box (area = 1.28 mm^2 and perimeter = 4.5 mm) was drawn manually to include all cortical layers of the auditory (AU), extending from the pial surface to the border line of corpus callosum (Cc).

The *Psmc1*$^{fl/fl}$*;CaMKIIα-Cre* mice display intraneuronal protein inclusions and extensive neurodegeneration in forebrain regions, accompanied by behavioural changes (Bedford et al., 2008). In this chapter we will focus on morphometric changes in the auditory (AU) and somatosensory (SS) cortex, which are regions linked to neurodegenerative disease (Lenka et al., 2016, Maatuf et al., 2016). The apical dendrites of pyramidal neurons in cortical layers III and layer V are clearly visible by NF immunostaining of mouse brain horizontal sections.

The temporal lobe is recognised as a major site of pathology in a number of neurodegenerative diseases, including AD, PD and DLB (Armstrong, 2012, Martin et al., 2009, Tam et al., 2005). Temporal lobe grey and white matter play an important role for understanding memory changes in PD (Tanner et al., 2015). The temporal lobe accommodates 17% of the cerebral cortex and includes areas with auditory, olfactory, vestibular, visual and linguistic functions (Kiernan, 2012). The auditory cortex is the part of the temporal lobe that processes auditory information (Baars

and Gage, 2010). A previous study found that separable stages of auditory object analysis and profiles of impaired auditory object cognition in different dementia syndromes such as AD, DLB (Goll et al., 2011). Abnormalities of auditory hedonic processing are a significant issue in common dementia (Fletcher et al., 2015). In addition to the AU cortex, the somatosensory (SS) cortex is also affected by dementia syndromes. The SS cortex is affected early in the progression of AD and may have some consequence on behavioural and functional measures (Stephen et al., 2010). In the mouse cerebral cortex most neurons are concentrated in the primary somatosensory cortex, which contains 25% of all cortical neurons. This distribution is consistent with a predominance of somatosensory function in mouse behaviour (Kiernan, 2012).

5.2.1 Cortical thickness

Cortical thickness was defined as the vertical distance from the pial boundary to the border line of the corpus callosum (Carpentier et al., 2013, Cardinale et al., 2014). AU and SS cortical thickness was measured for control and *Psmc1*$^{fl/fl}$*;CaMKIIa-Cre* mice at 4 and 6 weeks-old (Table 5.1). Neurofilament H (NFH) staining was used as a marker to identify cortical layers III and V in the horizontal brain sections (Van der Gucht et al., 2007, Mellott et al., 2010, Paulussen et al., 2011). Figure 5.3 shows the clear demarcation of layer IV, which is almost devoid of NFH staining, as well as layers I, II and VI.

Table 5.1 Total thickness of the AU cortex (Ctx) and all cortical layers in 4 and 6 week-old control and *Psmc1*$^{fl/fl}$*;CaMKIIα-Cre* mice. Data are expressed as mean ± standard error of the mean, n = 3. *p < 0.05, **p < 0.01, ***p < 0.001, ****p < 0.0001 by Student's unpaired t-test.

Cortical layers		4 weeks-old				6 weeks-old			
		Control	*Psmc1*$^{fl/fl}$*;CaMKIIα-Cre*	*t*-test		Control	*Psmc1*$^{fl/fl}$*;CaMKIIα-Cre*	*t*-test	
		Mean ± SEM (µm)	Mean ± SEM (µm)	*p* value	*Sign.*	Mean ± SEM (µm)	Mean ± SEM (µm)	*p* value	*Sign.*
AU	I & II	314.7 ± 3.8	262.0 ± 2.0	0.0003	***	307.7 ± 6.1	223.7 ± 3.8	0.0003	***
	III	216.0 ± 2.3	234.7 ± 0.8	0.002	**	214.0 ± 2.3	166.0 ± 3.0	0.0002	***
	IV	110.7 ± 2.3	111.7 ± 2.1	0.8	ns	102.7 ± 1.4	89.33 ± 2.0	0.006	**
	V	302.7 ± 2.7	335.7 ± 6.5	0.01	**	304.7 ± 3.1	254.0 ± 3.6	0.0005	***
	VI	225.3 ± 4.7	159.0 ± 4.5	0.0005	***	150.3 ± 2.9	89.00 ± 4.5	0.0004	***
	Ctx	1169 ± 12.8	1103 ± 7.0	0.01	*	1079 ± 3.3	822.0 ± 10.0	< 0.0001	****

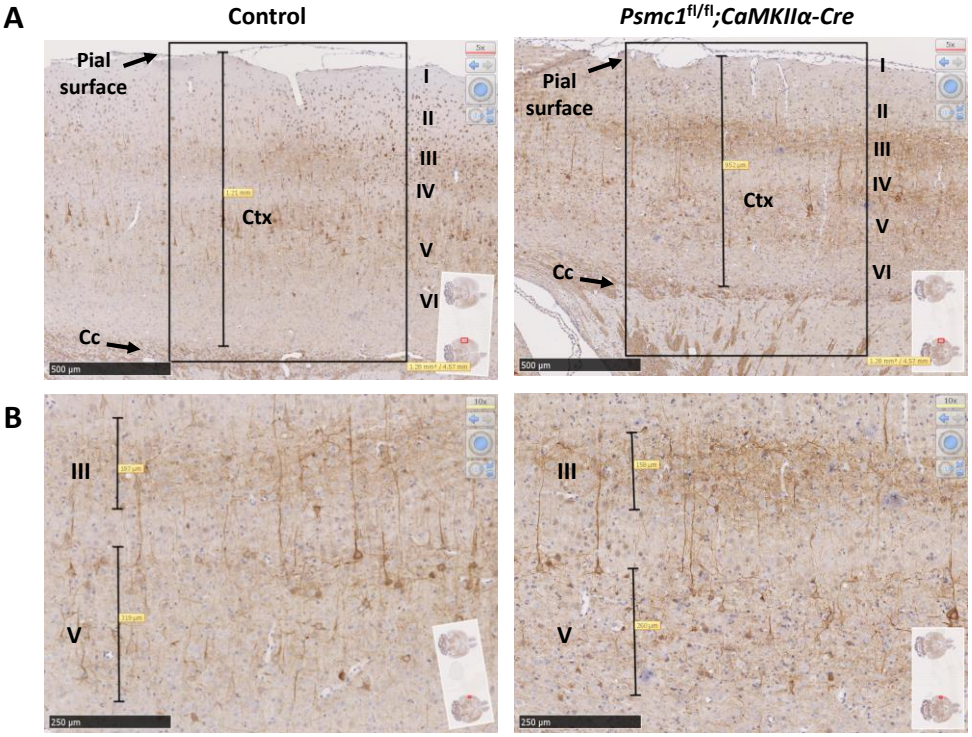


Figure 5.3 Cortical thickness

(A) NFH immunostaining of representative 6 week-old control and *Psmc1*$^{fl/fl}$*;CaMKIIα-Cre* mouse AU cortices (layers I–VI). Total cortical thickness (Ctx) was measured by drawing a vertical line extending from the pial surface to the border line of the corpus callosum (Cc). (B) Higher magnification of (A) shows obvious NFH staining in layers III & V, and clear demarcation of layer IV. The thickness of layers III & V was measured by drawing a vertical line using the NFH staining as shown.

5.2.2 Neuronal number and nuclear size

26S proteasome dysfunction in *Psmc1*$^{fl/fl}$*;CaMKIIα−Cre* mice was confirmed by accumulation of polyubiquitinated proteins and increased ubiquitin (Ub) immunostaining in the cortex with increasing age (Bedford et al., 2008). We can use Ub immunostaining to identify neurons with 26S proteasome dysfunction, allowing morphometric analysis of neurons in the AU cortex of *Psmc1*$^{fl/fl}$*;CaMKIIα−Cre* mice compared to controls. Morphometric analyses included counting the number of Ub-positive neurons and measuring their nuclear size.

Quantitative data was collected from layers III and V of the AU cortex for control and *Psmc1*$^{fl/fl}$*;CaMKIIα-Cre* mice at 4 and 6 weeks-old (Figure 5.4). Cortical layers were identified using NFH staining as described in Section 5.2 Using annotation tools in NDP.view.2, two counting boxes of 0.07mm^2 and perimeter 1.16mm were marked in layer III of the AU cortex (annotated 1 and 2; Figure 5.4B). In layer V, two counting boxes of 0.15mm^2 with a perimeter of 1.5mm were used (annotated 3 and 4; Figure 5.4B). Images were acquired at 10X magnification and saved as uncompressed Tiffs with a calibrated scale bar. Counting of Ub-positive neurons and measurement of their nuclear size used ImageJ (freeware: http://rsb.info.nih.gov/ij/) (Figure 5.4C). Neurons were counted if their nucleus bisected either the left or upper boundary of the counting frame, whereas those where the nucleus bisected the right or lower boundary were not counted. For quantification of nuclear size, a line was drawn manually around haematoxylin-stained nuclei of Ub-positive neurons using the oval selection tool in Image J (Figure 5.4D). Furthermore, we noted neurons with Lewy-like inclusions during our analysis to allow further processing of the data.

Most studies characterising morphometric changes associated with declining neuronal function in normal aging and AD have employed semi-quantitative methods (Bundgaard et al., 2001, Andrade-Moraes et al., 2013, Gagyi et al., 2012).

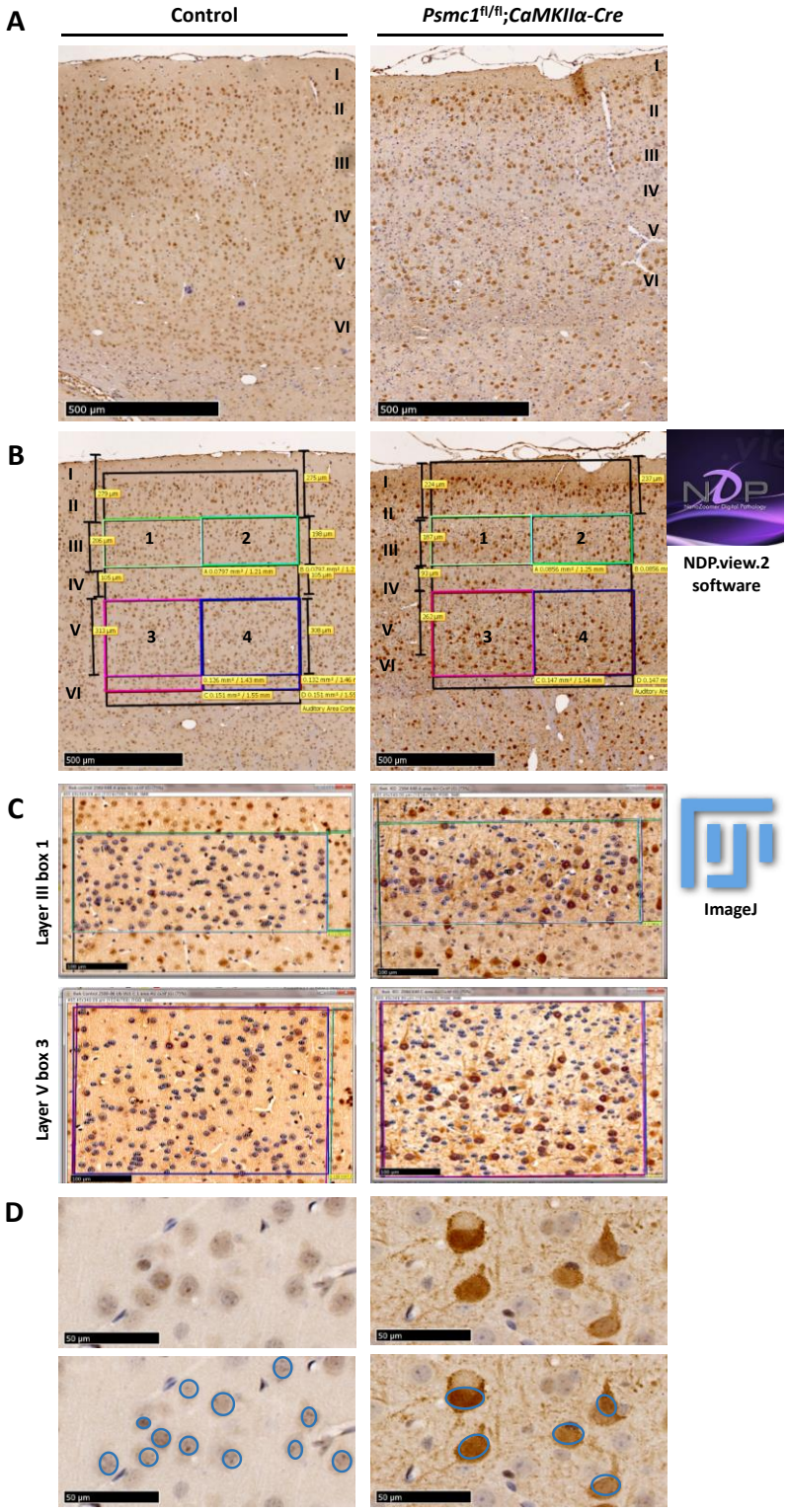


Figure 5.4 Neuronal number and nuclear size in the AU cortex

(A) Representative ubiquitin immunostaining (brown) of 6 week-old control and *Psmc1*$^{fl/fl}$*;CaMKIIα-Cre* mouse AU cortices. (B) Sections annotated using NDP.view.2 software to show layers III and V, and boxes 1, 2, 3 and 4 used for quantification. (C) Cortical layers III (box 1) and V (box 3) of control and *Psmc1*$^{fl/fl}$*;CaMKIIα-Cre* AU cortices in Image J used for quantification. (D) Nuclear size of Ub-positive neurons using the oval selection tool in Image J.

5.2.3 Apical dendrite length

Neocortical pyramidal neurons are the major excitatory neuron in all cortical layers except layer I, representing 70–85% of the total population of neurons in the cortex (Romand et al., 2011). Typical pyramidal neurons are characterized by their pyramidal or ovoid shaped soma and long apical dendrite ascending from the apex of the soma, ending in a terminal tuft near the pial surface. In addition, four to five dendritic domains emerge from the base of the soma directed laterally or downward (Larkman et al., 1992, Ito, 1992, DeFelipe and Fariñas, 1992). Typical pyramidal neurons are most commonly found in layers II, III and V (Garey et al., 1998). Following NFH and NFM staining, apical dendrites of pyramidal neurons in cortical layers III and layer V are clearly visible (Figure 5.5). Therefore, we chose to measure the length of individual apical dendrites in these layers of the auditory (AU) and somatosensory (SS) cortices. Image data used for quantification of apical dendrites was aquired at 10X magnification and stored as uncompressed Tiff files. Individual images were then exported to ImageJ (freeware: http://rsb.info.nih.gov/ij/). Apical dendrite length was measured manually using ImageJ using the segmented line tool as cortical surface (Figures 5.5A and B). Using NFH staining, we found that the apical dendrites of NFH-positive neurons in layers III and V had a perpendicular orientation to the cortical layers (Figures 5.4A and B). Single apical dendrites were identified extending from the superior pole of the soma towards the pial surface, often as far as layer I, where it ramified (Figures 5.4A and B). In some cases, the apical dendrite branched earlier, with branches ascending almost parallel to the main apical trunk (Figure 5.5C). Several basal dendrites typically formed a skirt around the inferior pole of the soma (Figure 5.5C). Apical dendrite length was measured in neurons that met the following criteria:

- Neurons with a visible undamaged apical dendritic arbor emerging from the top of cell soma.
- Exclusion of neurons where apical dendrites travel in the oblique direction to the cortical layers or are cut-off.

Immunostaining analyses with markers such as the calcium binding protein parvalbumin (PV) and calbindin D-28k (CB), and the non-phosphorylated neurofilament protein (SMI-32) have been used previously to investigate the cytoarchitecture, including cortical layers and thickness (Cipelletti et al., 2002). All quantification was repeated twice by the same researcher, but at a different time. We acknowledge that this method is not a typical approach to measure the dendrite length of pyramidal neurons. Sholl analyses are more often used to quantify dendritic complexity, apical dendritic segment lengths and basal dendritic arbors. This method generates concentric rings radiating from the soma centre and at each ring the number of dendrites is counted based on difference in contrast between the arbour and the background (Binley et al., 2014). We acknowledge that the length of the apical dendrite may be limited by tissue sectioning and it is possible that neurons with significantly lengthened or shortened dendrites processes could bias the results. Despite this, statistically significant differences were found in apical dendrite length between control and *Psmc1*$^{fl/fl}$;*CaMKIIα-Cre* mice (Section 5.3.7). All statistical comparisons were done using a Mann Whitney U test.

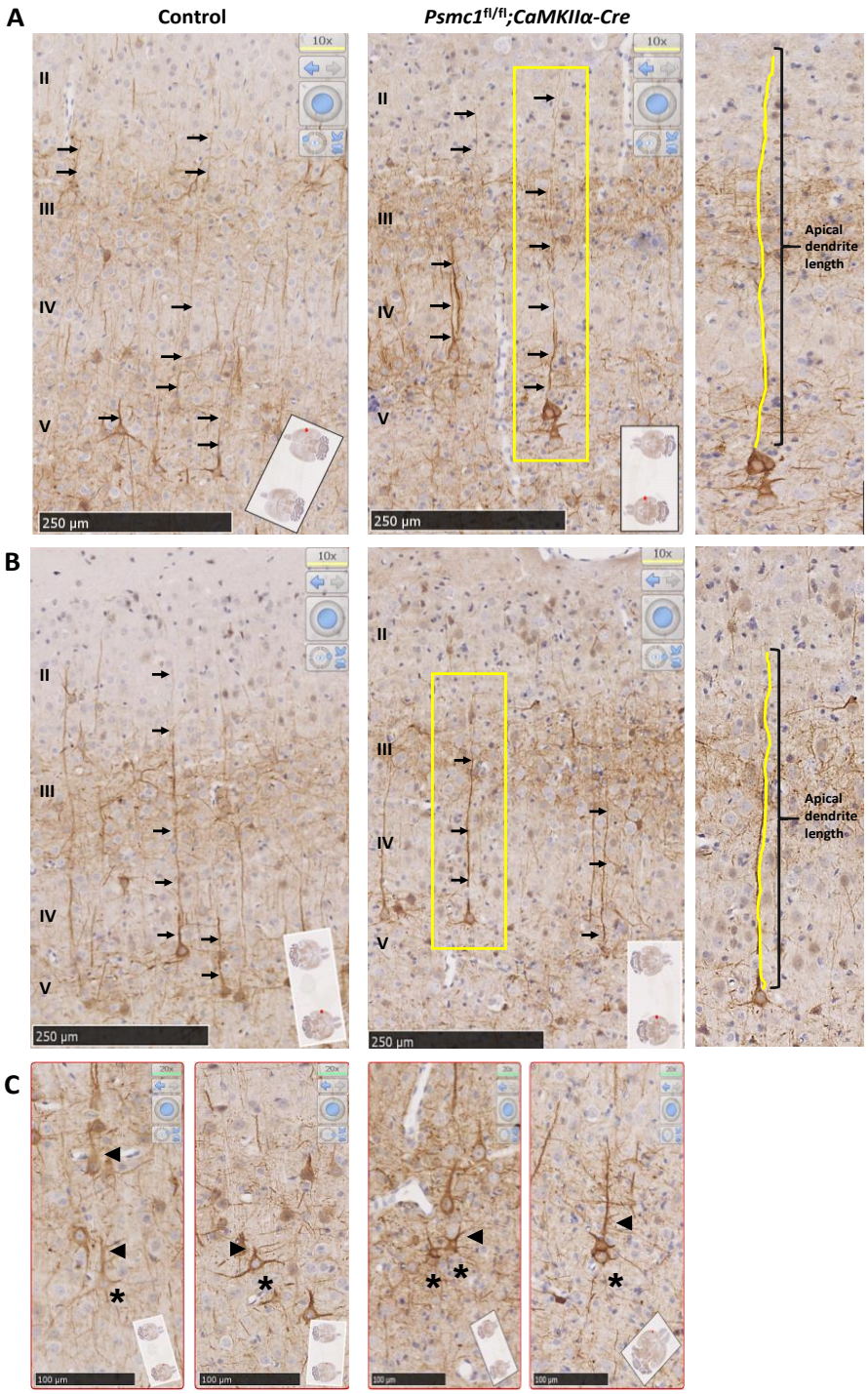


Figure 5.5 Apical dendrite length

(A and B) NFH immunostaining of the AU cortex from representative 6 week-old control and *Psmc1*$^{fl/fl}$;*CaMKIIα-Cre* mice. Pyramidal neurons of layers III (A) and V (B) are shown with apical dendrites extending from the superior pole of the soma towards layer I (arrows). High magnification of the yellow box in A and B shows how apical dendrite length was measured in control and *Psmc1*$^{fl/fl}$;*CaMKIIα-Cre* mice pyramidal cortical neurons. (C) Arrowheads indicate apical dendrites that branched earlier with branches ascending parallel to the main apical trunk. Asterisks indicate basal dendrites forming a skirt around the inferior pole of the soma.

5.3 Results

5.3.1 Decreased cortical thickness following disruption of the 26S proteasome in mouse cortical neurons

NFH-stained horizontal brain sections from 4 and 6 week-old *Psmc1*$^{fl/fl}$*;CaMKIIα-Cre* and control mice were used to measure cortical thickness of the AU and SS areas (Figure 5.6). NFH immunostaining is prominent in pyramidal neurons of cortical layers III and V, while layers I, II, IV and VI show weaker staining (Figure 5.6B). Cortical thickness was measured as the linear distance from the pial surface to the dorsal surface of the corpus callosum as described in Section 5.2.1 (Carpentier et al., 2013, Cardinale et al., 2014). Quantitative measurements revealed that the cortical thickness of AU and SS areas was significantly decreased in *Psmc1*$^{fl/fl}$*;CaMKIIα-Cre* compared to control mice at 4 weeks-old (Figure 5.6C and Table 5.2; $p < 0.05$ and $p < 0.01$ in the AU and SS cortices respectively). The decrease in cortical thickness was more obvious in *Psmc1*$^{fl/fl}$*;CaMKIIα-Cre* relative to control mice at 6 weeks-old showing 1.3- and 1.2- fold decreases in the AU and SS cortices respectively (Figure 5.6C and Table 5.2; $p < 0.0001$ and $p < 0.001$ in the AU and SS cortices respectively).

The thickness of individual cortical layers in the AU and SS cortices was also assessed in control and *Psmc1*$^{fl/fl}$*;CaMKIIα-Cre* mouse brain sections at 4 and 6 weeks-old (Figure 5.7C). We found that the thickness of layers I&II and VI in the AU and SS cortices was significantly decreased in *Psmc1*$^{fl/fl}$*;CaMKIIα-Cre* compared to control mice at 4 and 6 weeks-old (Figure 5.7A and B; Table 5.2). Whilst layers III and V were significantly increased at 4 weeks of age in *Psmc1*$^{fl/fl}$*;CaMKIIα-Cre* cortices, these were significantly decreased at 6 weeks of age compared to control mice (Figure 5.7A and B; Table 5.2). The thickness of layer IV was not different between control and *Psmc1*$^{fl/fl}$*;CaMKIIα-Cre* mice at 4 weeks-old, but was also significantly decreased at 6 weeks-

old in *Psmc1*$^{fl/fl}$*;CaMKIIa-Cre* cortices (Figure 5.7A and B; Table 5.2). Taken together, the data shows that the AU and SS cortices of *Psmc1*$^{fl/fl}$*;CaMKIIa-Cre* mice are significantly thinner than those of controls. Furthermore, cortical thinning is more significant with increasing age consistent with progressive neurodegeneration in *Psmc1*$^{fl/fl}$*;CaMKIIa-Cre* mice. Measurement of cortical thickness in PD patients has been useful in assessing disease stage, identifying dementia and cognitive impairment in these patients (Zarei et al., 2013).

Table 5.2 Total cortical (Ctx) thickness and thickness of the individual cortical layers of the AU and SS cortices in 4 and 6 week-old control and *Psmc1*$^{fl/fl}$*;CaMKIIa-Cre* mice. Data are expressed as mean ± standard error of the mean, n = 3. *$p < 0.05$, **$p < 0.01$, ***$p < 0.001$, ****$p < 0.0001$ by Student's unpaired t-test.

Cortical layers		4 weeks-old				6 weeks-old			
		Control	*Psmc1*$^{fl/fl}$*;CaMKIIa-Cre*	*t*-test		Control	*Psmc1*$^{fl/fl}$*;CaMKIIa-Cre*	*t*-test	
		Mean ± SEM (µm)	Mean ± SEM (µm)	*p* value	*Sign.*	Mean ± SEM (µm)	Mean ± SEM (µm)	*p* value	*Sign.*
AU	I & II	314.7 ± 3.8	262.0 ± 2.0	0.0003	***	307.7 ± 6.1	223.7 ± 3.8	0.0003	***
	III	216.0 ± 2.3	234.7 ± 0.8	0.002	**	214.0 ± 2.3	166.0 ± 3.0	0.0002	***
	IV	110.7 ± 2.3	111.7 ± 2.1	0.8	ns	102.7 ± 1.4	89.33 ± 2.0	0.006	**
	V	302.7 ± 2.7	335.7 ± 6.5	0.01	**	304.7 ± 3.1	254.0 ± 3.6	0.0005	***
	VI	225.3 ± 4.7	159.0 ± 4.5	0.0005	***	150.3 ± 2.9	89.00 ± 4.5	0.0004	***
	Ctx	1169 ± 12.8	1103 ± 7.0	0.01	*	1079 ± 3.3	822.0 ± 10.0	< 0.0001	****
SS	I & II	284.3 ± 3.5	249.7 ± 4.7	0.004	**	286.3 ± 3.1	213.3 ± 2.9	< 0.0001	****
	III	213.3 ± 2.1	229.0 ± 0.5	0.002	**	202.0 ± 1.7	167.3 ± 1.8	0.0002	***
	IV	105.0 ± 3.2	105.7 ± 2.0	0.9	ns	106.3 ± 4.0	90.67 ± 1.7	0.02	*
	V	296.7 ± 3.8	318.7 ± 1.4	0.006	**	308.0 ± 2.6	260.7 ± 1.2	< 0.0001	****
	VI	253.7 ± 4.2	156.0 ± 3.7	< 0.0001	****	148.3 ± 6.1	91.67 ± 4.3	0.002	**
	Ctx	1153 ± 15.7	1059 ± 3.6	0.004	**	1051 ± 15.0	823.7 ± 9.9	0.0002	***

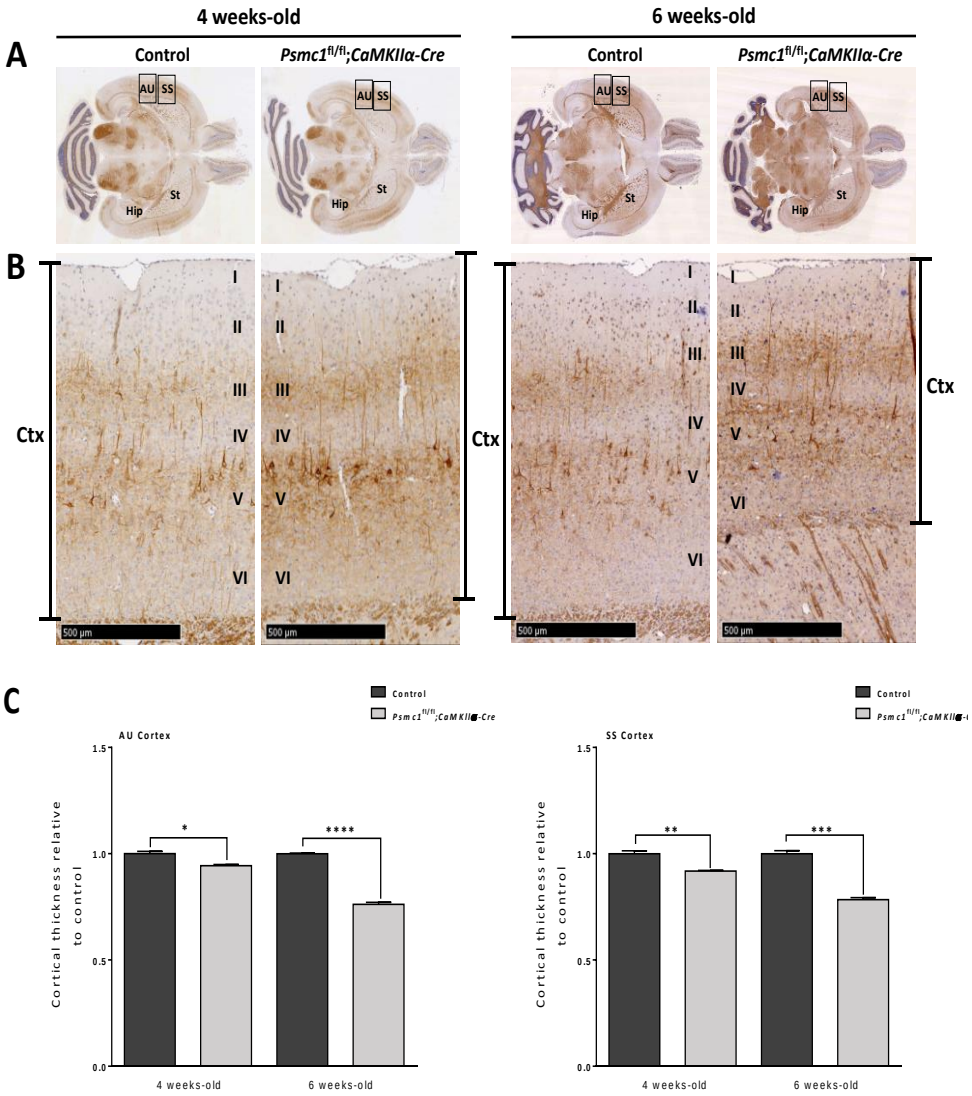


Figure 5.6 Decreased cortical thickness in *Psmc1*$^{fl/fl}$*;CaMKIIα-Cre* compared to control mouse cortices at 4 and 6 weeks-old.

(A) Whole brain 7 µm horizontal brain sections from representative 4 and 6 week-old control and *Psmc1*$^{fl/fl}$*;CaMKIIα-Cre* mice immunostained with NFH. (B) Higher magnification images of the AU cortex boxed in A; also indicating the individual cortical layers and how cortical thickness was measured as the linear distance from the pial surface to the dorsal surface of the corpus callosum. (C) AU and SS cortical thickness in *Psmc1*$^{fl/fl}$*;CaMKIIα-Cre* mice relative to controls. Data are expressed as mean ± SEM of n = 3 mice. *p < 0.05, **p < 0.01, ***p < 0.001, ****p < 0.0001 by Student's unpaired t-test. SS, somatosensory cortex; AU, auditory cortex; Ctx, cortex; Hip, hippocampus; St, striatum.

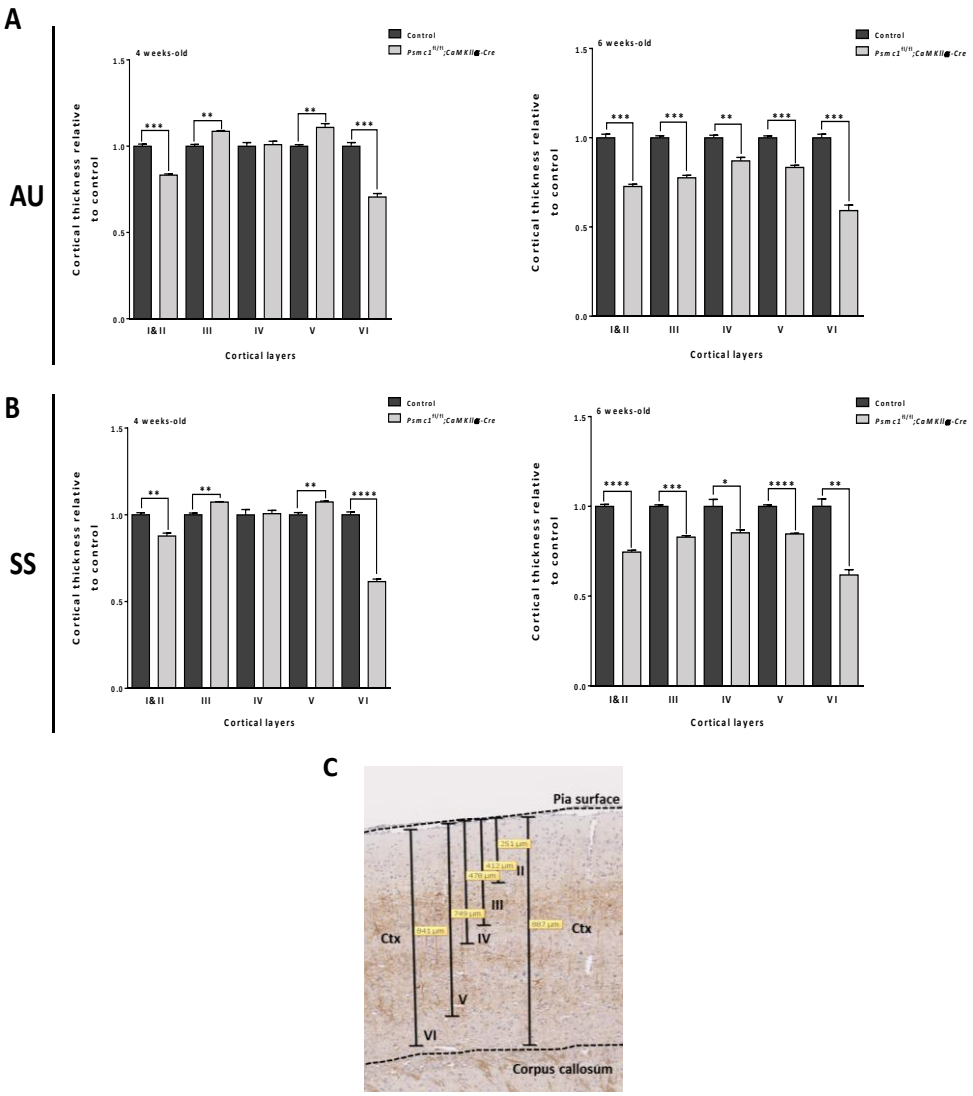


Figure 5.7 Thickness of individual cortical layers in *Psmc1*$^{fl/fl}$*;CaMKIIa-Cre* compared to control mouse cortices.

(A and B) Thickness of the individual AU and SS cortical layers in 4 and 6 week-old *Psmc1*$^{fl/fl}$*;CaMKIIa-Cre* mice relative to controls. (**C**) Schematic representation showing how the cortical layers were delineated for measurement using NFH staining and NDP.view2 software. Data are expressed as mean ± SEM of n = 3 mice. *p < 0.05, **p < 0.01, ***p < 0.001, ****p < 0.0001 by Student's unpaired t-test. Ctx, cortex.

5.3.2 The number of neurons is decreased following disruption of the 26S proteasome in mouse cortical neurons

In this section we evaluate the total number of haematoxylin-positive and Ub-positive neurons in layers III and V of the AU cortex of control and *Psmc1*$^{fl/fl}$*;CaMKIIα-Cre* mice as described in Section 5.2.2. In control neurons ubiquitin immunostaining is diffuse compared to strong immunostaining evident in *Psmc1*$^{fl/fl}$*;CaMKIIα-Cre* neurons, and particularly in neurons in layers II-III and V-VI (Figures 5.8 and 5.9). Ub immunostaining is less evident in cortical layer IV and may be a consequence of the conditional gene targeting used in this model (Bedford et al., 2008). Figure 5.9 shows a significant increase in Ub-immunostaining in the nucleus, soma and proximal part of the apical dendrite in *Psmc1*$^{fl/fl}$*;CaMKIIα-Cre* neurons compared to controls (Figure 5.9). We also noted Ub-positive intraneuronal in neurons with 26S proteasome dysfunction (Figure 5.9; arrows).

The total number of haematoxylin-positive and Ub-positive neurons in layers III and V of the AU cortex were counted. When using haematoxylin-staining as a counting measure, neurons were distinguished from glia using nuclear size data (Section 5.2.2). The nuclear size of GFAP-positive astrocytes was previously measured in control and *Psmc1*$^{fl/fl}$*;CaMKIIα-Cre* mouse AU cortex at 4 and 6 weeks-old using horizontal brain sections immunostained with GFAP. We found that the nuclear size of glia ranged from 29.9 - 16.4 μm in control mice, and from 39.3 - 20.7 μm in *Psmc1*$^{fl/fl}$*;CaMKIIα-Cre* mice. Therefore, only haematoxylin-positive cells with a nuclear size ≥24.27 μm and ≥29.9 μm in controls and *Psmc1*$^{fl/fl}$*;CaMKIIα-Cre* mice were included in the neuron morphometry analysis.

Figure 5.10 shows that the total number of neurons in layers III and V is not significantly different between control and *Psmc1*$^{fl/fl}$*;CaMKIIα-Cre* mice at 4 weeks-old. At 6 weeks-old, a significant decrease in the total number of neurons of 1.7- and

1.3-fold in layers III and V respectively was found in *Psmc1*$^{fl/fl}$*;CaMKIIa-Cre* mice compared to controls, suggestive of significant neuronal loss at this age (Figure 5.10 and Table 5.3; $p < 0.01$ and $p < 0.05$ in the layers III and V respectively).

Evaluation of Ub-positive neurons showed a significant increase in *Psmc1*$^{fl/fl}$*;CaMKIIa-Cre* compared to control cortices at 4 and 6 weeks-old (Figure 5.10 and Table 5.3). In layer III, a 1.4- and 1.3-fold increase in Ub-positive neurons was observed in *Psmc1*$^{fl/fl}$*;CaMKIIa-Cre* compared to control mice at 4 and 6 weeks-old respectively. In layer V, Ub-positive neurons showed 1.2- and 1.3-fold increases at 4 and 6 weeks-old respectively.

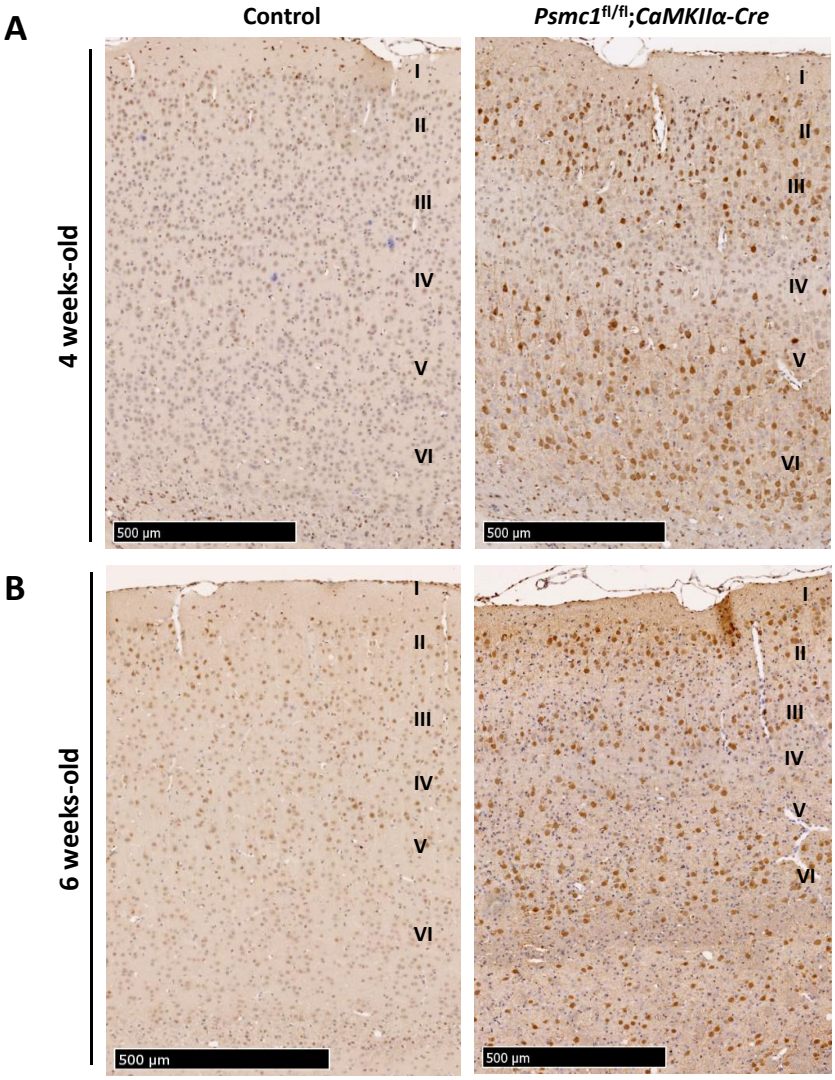


Figure 5.8 Ubiquitin immunostaining of the AU cortex of control and *Psmc1*$^{fl/fl}$*;CaMKIIα-Cre* mice at 4 and 6 weeks-old.

(A and B) Representative ubiquitin (brown) immunostained 7 µm horizontal brain sections at 4 (A) and 6 (B) weeks-old showing the AU cortical layers.

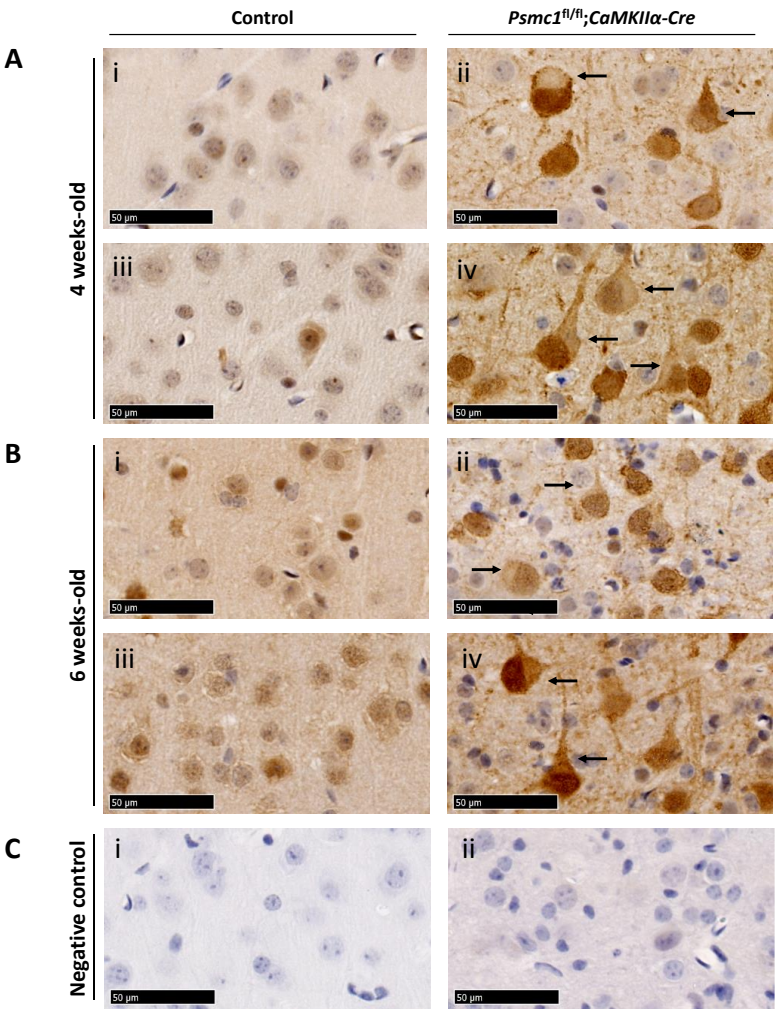


Figure 5.9 Ubiquitin immunostaining of AU cortical neurons from control and *Psmc1*$^{fl/fl}$*;CaMKIIα-Cre* mice at 4 and 6 weeks-old.

(A and B) Representative ubiquitin (brown) immunostained neurons in 7 µm horizontal brain sections at 4 (A) and 6 (B) weeks-old. (C) Representative negative control brain section. Arrows indicate intraneuronal protein inclusions in *Psmc1*$^{fl/fl}$*;CaMKIIα-Cre* cortices.

Table 5.3 Number of haematoxylin-positive and Ub-positive neurons in AU cortex layers III and V of control and *Psmc1*$^{fl/fl}$*;CaMKIIα-Cre* mice at 4 and 6 weeks-old. Data are expressed as mean ± SEM of n = 3 mice. *p < 0.05, **p < 0.01 by Student's unpaired t-test.

Age of mice								
Number of neurons	4 weeks-old				6 weeks-old			
	Control	*Psmc1*$^{fl/fl}$*;CaMKIIα-Cre*	*t* -test	*Sign.*	Control	*Psmc1*$^{fl/fl}$*;CaMKIIα-Cre*	*t* -test	*Sign.*
	Mean ± SEM	Mean ± SEM	*p* value		Mean ± SEM	Mean ± SEM	*p* value	
Layer III	246.0 ± 15.4	226.3 ± 0.8	0.2	ns	251.0 ± 13.7	147.0 ± 10.8	0.004	**
Layer V	364.7 ± 10.6	330.3 ± 10.2	0.08	ns	402.7 ± 22.8	305.0 ± 24.9	0.04	*
Ub-positive neurons in layer III	81.00 ± 6.1	117.0 ± 2.5	0.005	**	78.00 ± 4.6	101.7 ± 3.7	0.02	*
Ub-positive neurons in layer V	138.0 ± 6.0	164.3 ± 2.3	0.02	*	133.7 ± 2.9	171.7 ± 9.1	0.02	*
Ub-positive neuron with intraneuronal inclusions	95				158			

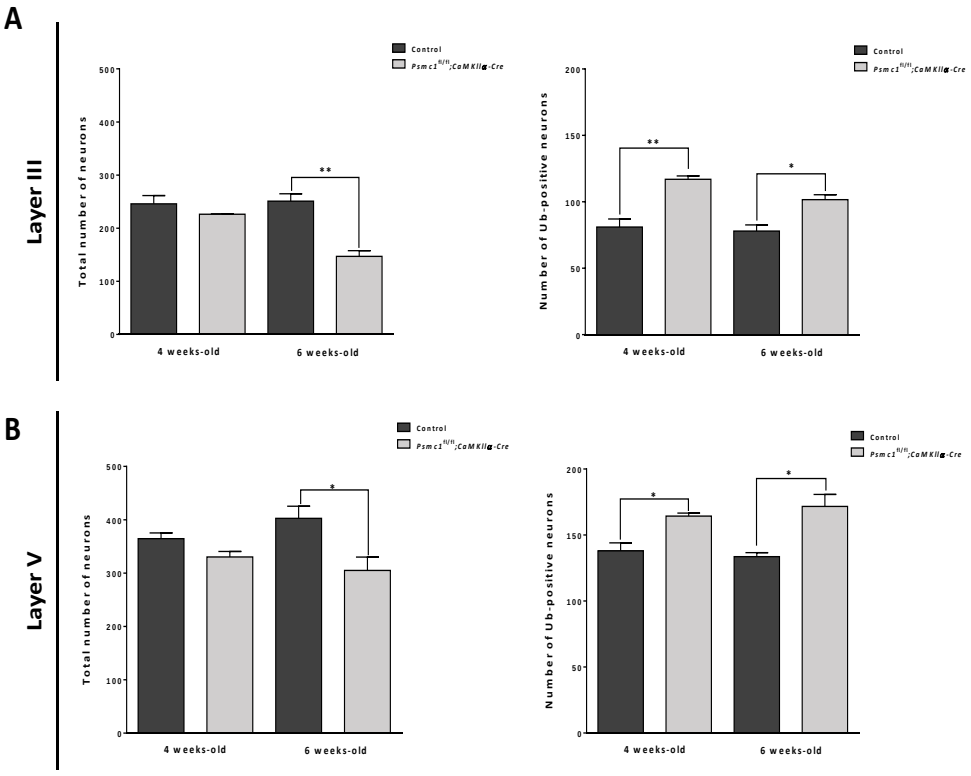


Figure 5.10 The total number of neurons is decreased, but the number of Ub-positive neurons increased in *Psmc1*$^{fl/fl}$*;CaMKIIα-Cre* mouse AU cortex compared to controls.

(A and B) Total number of neurons and Ub-positive neurons in layers III and V of the AU cortex in 4 and 6 week-old control and *Psmc1*$^{fl/fl}$*;CaMKIIα-Cre* mice. Data are expressed as mean ± SEM of n = 3 mice. *p < 0.05, **p < 0.01 by Student's unpaired t-test.

5.3.3 Nuclear size is increased following disruption of the 26S proteasome in mouse cortical neurons

To investigate the nuclear size of neurons we used neighbouring 7μm brain sections, allowing identification of the nuclei that appear in the upper section ('top') that do not appear in a lower section separated by a known distance (Abercrombie, 1946). This method provides an estimate of particle size without assuming a specific shape. Nuclear size was measured in Ub-positive neurons in layers III and V as described in Section 5.2.2; by drawing a line manually around the nuclei using the oval selection tool in Image J (Figure 5.11A). The nuclear size of control and *Psmc1*$^{fl/fl}$*;CaMKIIα-Cre* neurons was measured at 4 and 6 weeks-old. We found the nuclear size data did not show a normal distribution determined by the Kolmogorov-Smirnov normality test. Quantitation therefore used the Mann-Whitney U test.

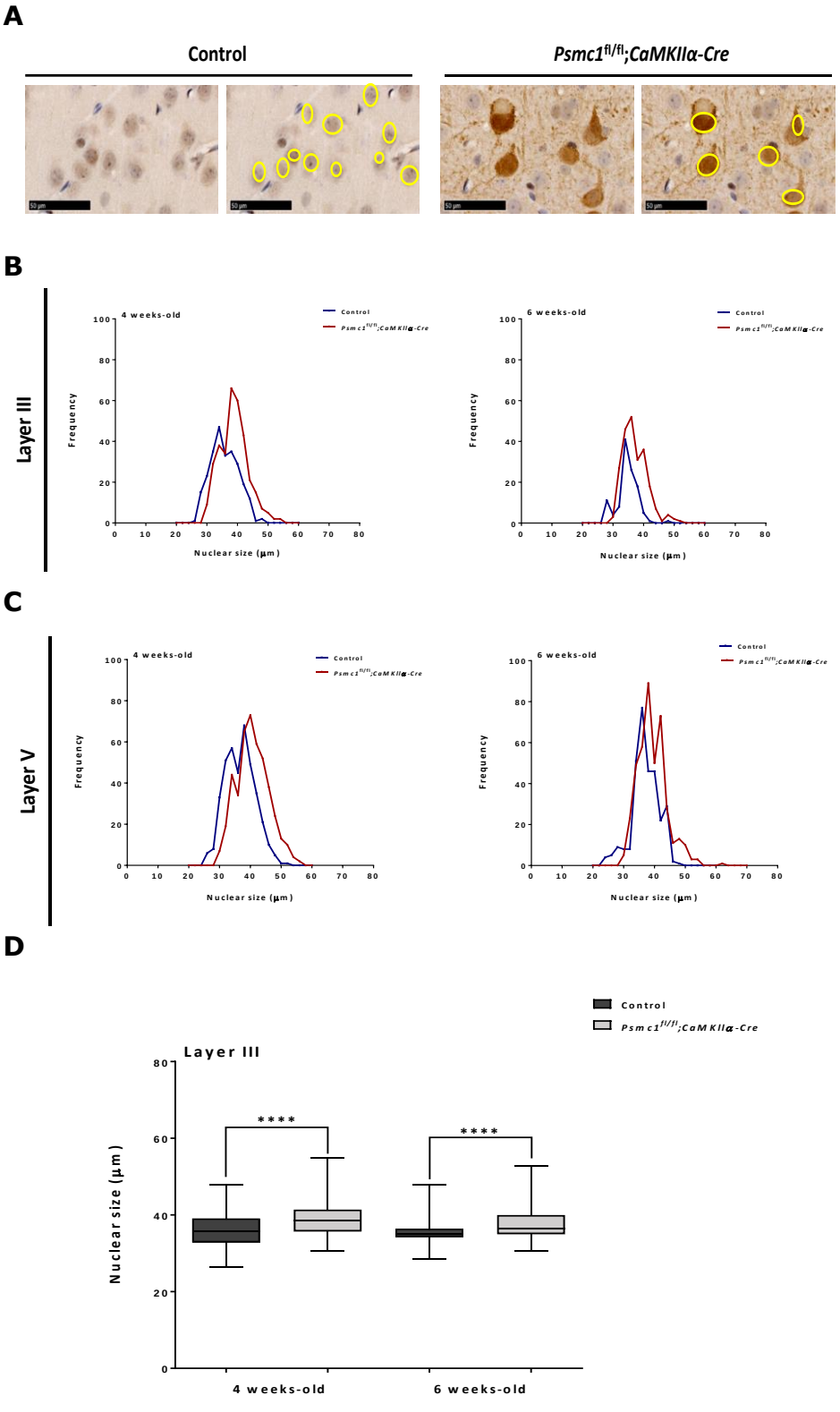
Frequency distribution histograms in Figures 5.11 show the distribution of nuclear size in control and *Psmc1*$^{fl/fl}$*;CaMKIIα-Cre* mice, highlighting the increased nuclear size of neurons in *Psmc1*$^{fl/fl}$*;CaMKIIα-Cre* mice. The nuclear size of control neurons was not significantly different at 4 and 6 weeks-old in either layer of the AU cortex examined (Figures 5.11B and C; Table 5.4). Nuclear size was significantly increased in layers III and V at both ages in *Psmc1*$^{fl/fl}$*;CaMKIIα-Cre* mice compared to controls (Figures 5.11B and C; Table 5.4).

We also found the median nuclear size of Ub-positive neurons in the *Psmc1*$^{fl/fl}$*;CaMKIIα-Cre* mice at 4 weeks-old was significantly larger than that at 6 weeks-old (Figures 5.11; Table 5.4). At 4 weeks of age the median nuclear size was 38.56 μm (n = 351 neurons) and 40.7 μm (n = 493 neurons) in layers III and V of the *Psmc1*$^{fl/fl}$*;CaMKIIα-Cre* AU cortex respectively. At 6 weeks of age median nucleus size was 36.41 μm (n = 305 neurons) and 38.51 μm (n = 515 neurons) in layers III and V of the AU cortex (Table 5.4). Interestingly, these differences were also detected when Ub-positive neurons with intraneuronal inclusions neurons

were analysed (Table 5.4). Overall, the changes in nuclear size observed in *Psmc1*$^{fl/fl}$*;CaMKIIa-Cre* neurons are part of a spectrum of morphological changes associated with neurodegeneration following 26S proteasome dysfunction.

Table 5.4 Nuclear size of Ub-positive neurons in control and *Psmc1*$^{fl/fl}$*;CaMKIIa-Cre* mice at 4 and 6 weeks-old. Data are expressed as the median nuclear size of n = 3 mice. *p < 0.05, **p < 0.01 ***p < 0.001 ****p < 0.0001 by Mann-Whitney U test.

Age of mice								
Nuclear size (µm)	4 weeks-old				6 weeks-old			
	Control	*Psmc1*$^{fl/fl}$*;CaMKIIα-Cre*	Mann–Whitney U test	*Sign.*	Control	*Psmc1*$^{fl/fl}$*;CaMKIIα-Cre*	Mann–Whitney U test	*Sign.*
	Median	Median	*p* value		Median	Median	*p* value	
Ub-positive neurons in layer III	35.7 n=243	38.56 n=351	< 0.0001	****	34.99 n=232	36.41 n=305	< 0.0001	****
Ub-positive neurons in layer V	36.41 n=414	40.7 n=493	< 0.0001	****	36.41 n=401	38.51 n=515	< 0.0001	****
Ub-positive neurons with intraneuronal inclusions in layer III		38.2 n=28				35.7 n=35	0.005	**
Ub-positive neurons with intraneuronal inclusions in layer V		41.41 n=67				37.13 n=123	< 0.0001	****


A
Control
Psmc1fl/fl;CaMKIIα-Cre
B
Layer III
4 weeks-old
6 weeks-old
Control
Psmc1fl/fl;CaMKIIα-Cre
Frequency
Nuclear size (µm)
C
Layer V
4 weeks-old
6 weeks-old
Control
Psmc1fl/fl;CaMKIIα-Cre
Frequency
Nuclear size (µm)
D
Control
Psmc1fl/fl;CaMKIIα-Cre
Layer III
Nuclear size (µm)
****
****
4 weeks-old
6 weeks-old

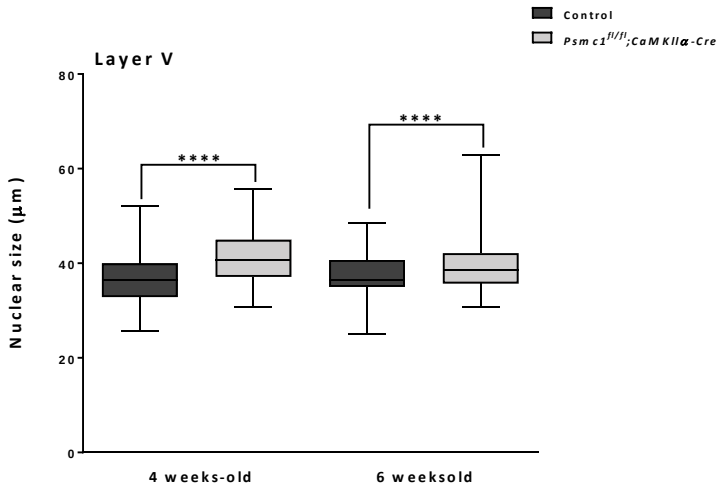


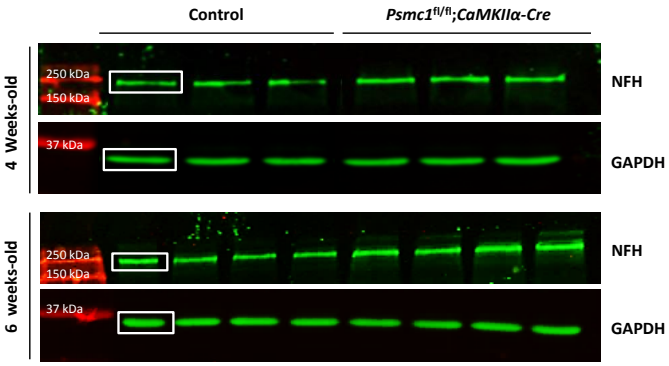
Figure 5.11 Increased nuclear size of layer III and layer V AU cortical neurons in *Psmc1*$^{fl/fl}$*;CaMKIIα-Cre* mice

(A) Nuclear size was measured in Ub-positive neurons by drawing a line manually around the nuclei using the oval selection tool in Image J. (B-C) Frequency histograms of nuclear size of Ub-positive neurons in layers III (B) and V (C) at 4 and 6 weeks-old in control and *Psmc1*$^{fl/fl}$*;CaMKIIα-Cre* mouse AU cortex. (D) Box-whisker plot of nuclear size of Ub-positive neurons in layers III and V of the AU cortex in 4 and 6 week-old control and *Psmc1*$^{fl/fl}$*;CaMKIIα-Cre* mice. Data are expressed as the median nuclear size of n = 3 mice. *p < 0.05, **p < 0.01, ***p < 0.001, ****p < 0.0001 by Mann-Whitney U test.

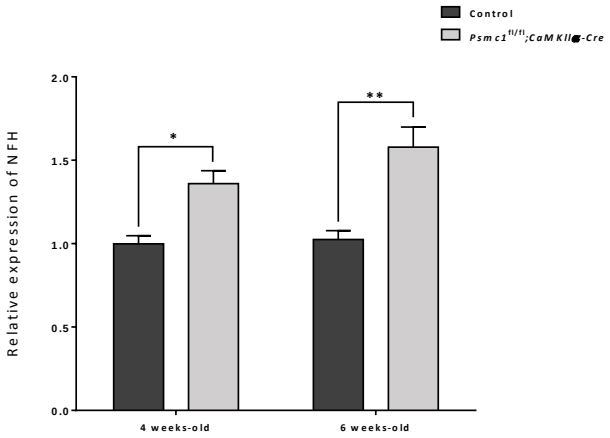
5.3.4 Increased neurofilament expression following disruption of the 26S proteasome in mouse cortical neurons

To investigate the levels of NF proteins in mouse brain cortical neurons with 26S proteasome dysfunction we carried out Western blotting of 4 and 6 week-old *Psmc1*$^{fl/fl}$*;CaMKIIα-Cre* and control cortices for NF heavy (NFH; 180–200kDa), NF middle (NFM; 130–170kDa) and NF light (NFL; 60–70kDa) chain proteins (Figure 5.12). Figures 5.12A and B show that NFH levels were significantly increased at 4 and 6 weeks-old in *Psmc1*$^{fl/fl}$*;CaMKIIα-Cre* cortices compared to controls (4 weeks-old $p = 0.01$, 6 weeks-old $p < 0.01$). NFM did not show any differences between control and *Psmc1*$^{fl/fl}$*;CaMKIIα-Cre* mice at 4 weeks-old, but was significantly increased at 6 weeks-old in *Psmc1*$^{fl/fl}$*;CaMKIIα-Cre* cortices (Figure 5.12C and D; 4 weeks-old $p = 0.24$, 6 weeks-old $p < 0.001$). The levels of NFL were significantly increased at 4 and 6 weeks-old in *Psmc1*$^{fl/fl}$*;CaMKIIα-Cre* cortices compared to control mice (Figure 5.12E and F; 4 weeks-old $p < 0.01$, 6 weeks-old $p < 0.0001$). Increased NF expression has been linked to neuronal dysfunction and axonal degeneration by numerous studies and is observed in neurodegenerative diseases such as amyotrophic lateral sclerosis (ALS), Alzheimer disease (AD) and Lewy body demetia (Perrot et al., 2008, Liu et al., 2011).

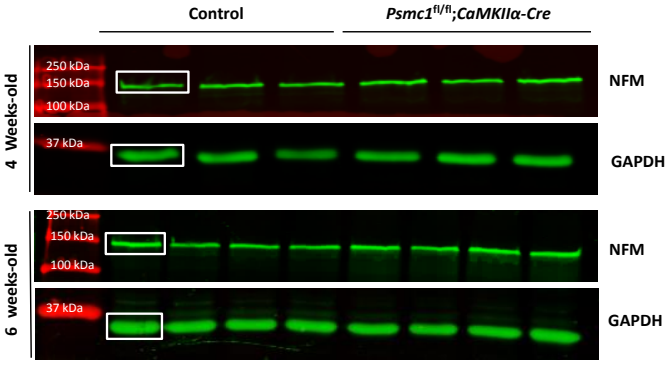
A


Control
Psmc1fl/fl;CaMKIIα-Cre
4 Weeks-old
250 kDa
150 kDa
NFH
37 kDa
GAPDH
6 weeks-old
250 kDa
150 kDa
NFH
37 kDa
GAPDH

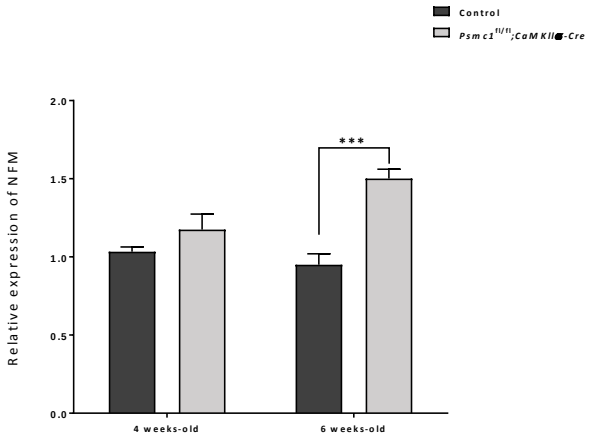
B


Control
Psmc1fl/fl;CaMKIIα-Cre
Relative expression of NFH
2.0
1.5
1.0
0.5
0.0
*
**
4 weeks-old
6 weeks-old

C


Control
Psmc1fl/fl;CaMKIIα-Cre
4 Weeks-old
250 kDa
150 kDa
100 kDa
NFM
37 kDa
GAPDH
6 weeks-old
250 kDa
150 kDa
100 kDa
NFM
37 kDa
GAPDH

D


Control
Psmc1fl/fl;CaMKIIα-Cre
Relative expression of NFM
2.0
1.5
1.0
0.5
0.0
***
4 weeks-old
6 weeks-old

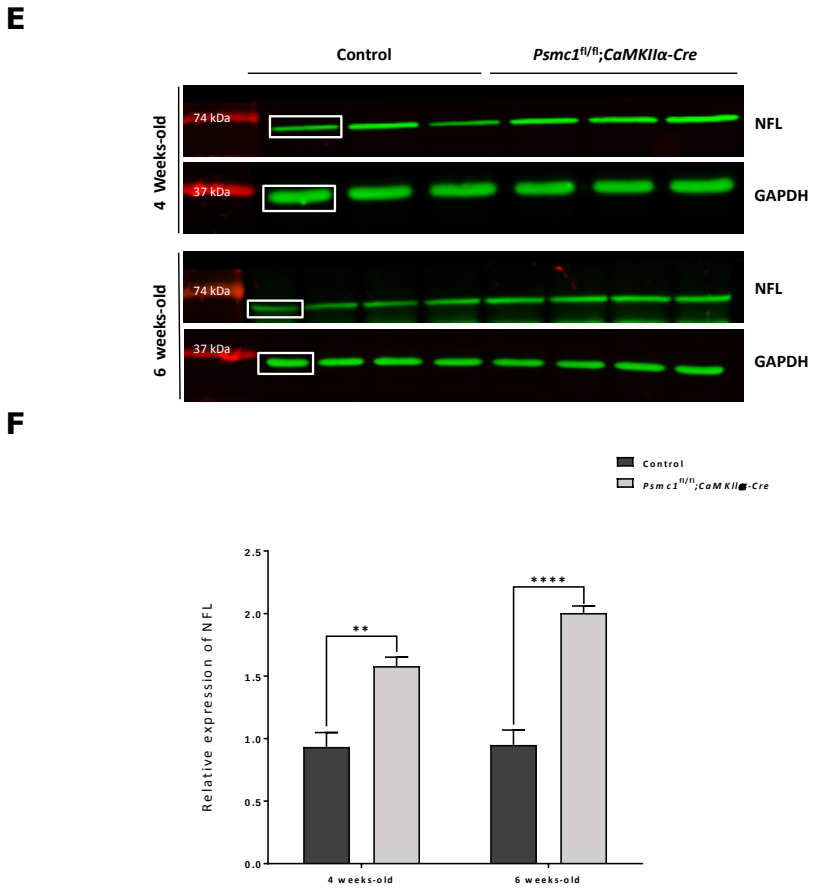


Figure 5.12 Increased NF protein expression in *Psmc1*$^{fl/fl}$*;CaMKIIa-Cre* compared to control mouse cortices.

Immunoblots and densitometric analysis of NFH (A and B), NFM (C and D) and NFL (E and F) in 4 and 6 week-old control and *Psmc1*$^{fl/fl}$*;CaMKIIa-Cre* mouse cortices. 20 µg of protein per lane in protein lysis buffer was subjected to SDS-PAGE on a 12% gel and transferred to nitrocellulose membrane for Western blotting. (B, D and F) Quantitative analysis of immunoblots (A, C and E) used Odessy Image Studio software analysis. NFH, NFM and NFL were normalised to the levels of GAPDH for each sample. Data are presented as mean ± SEM. n = 3 and n = 4 mice for 4 and 6 weeks-old respectively; *p < 0.05, **p < 0.01, ***p < 0.001, ****p < 0.0001 by unpaired Student's t-test.

5.3.5 Decreased neurofilament gene expression following disruption of the 26S proteasome in mouse cortical neurons

To determine whether changes in NF protein expression were associated with changes in transcription, we used real-time quantitative RT-PCR to examine the mRNA expression of NFH, NFM and NFL in control and *Psmc1*$^{fl/fl}$*;CaMKIIα-Cre* cortices at 4 and 6 weeks-old. The only significant difference in NF mRNA expression at 4 weeks-old was for NFM, which increased in *Psmc1*$^{fl/fl}$*;CaMKIIα-Cre* cortices (Figure 5.13A and Table 5.5). At 6 weeks-old we found a significant decrease in all the NF mRNAs investigated (Figure 5.13B and Table 5.5; NFH $p < 0.01$, NFM $p < 0.05$, NFL $p < 0.0001$). Interestingly, the expression of NFL mRNA also showed a tendency to decrease at 4 weeks-old in *Psmc1*$^{fl/fl}$*;CaMKIIα-Cre* cortices compared to controls (Figure 5.13A and Table 5.5; $p = 0.07$). Decreased NFH and NFL mRNA levels have been reported to contribute to degeneration of substantia nigra pars compacta neurons in Parkinson's disease and correlate with severity of this disease (Hill et al., 1993).

Table 5.5 NF gene expression in 4 and 6 week-old control and *Psmc1*$^{fl/fl}$*;CaMKIIα-Cre* mouse cortices. Levels of NF mRNA are normalized to the Hmbs housekeeping gene. The normalized relative expression of NF mRNA is shown based on the ΔΔCT calculation. Data are presented as mean ± SEM of n = 8 mice. *p < 0.05, **p < 0.01, ***p < 0.001, ****p < 0.0001 by Student's unpaired t-test.

Gene symbol	Age of mice	ΔΔct	$2^{-\Delta\Delta ct}$	Animal type		*t* -test	
				Control	*Psmc1* $^{fl/fl}$*;CaMKII α -Cre*		
				Mean ± SEM	Mean ± SEM	*p* value	*sign*
NEFH	4 weeks	-0.21	1.25	1.028 ± 0.09	1.254 ± 0.16	0.1	ns
	6 weeks	0.91	0.56	1.030 ± 0.098	0.5593 ± 0.07	0.002	**
NEFM	4 weeks	-0.55	1.56	1.021 ± 0.07	1.559 ± 0.19	0.02	*
	6 weeks	0.59	0.68	1.034 ± 0.11	0.6838 ± 0.06	0.01	*
NEFL	4 weeks	0.57	0.75	1.019 ± 0.07	0.7488 ± 0.11	0.07	ns
	6 weeks	1.61	0.34	1.008 ± 0.04	0.3450 ± 0.04	< 0.0001	****

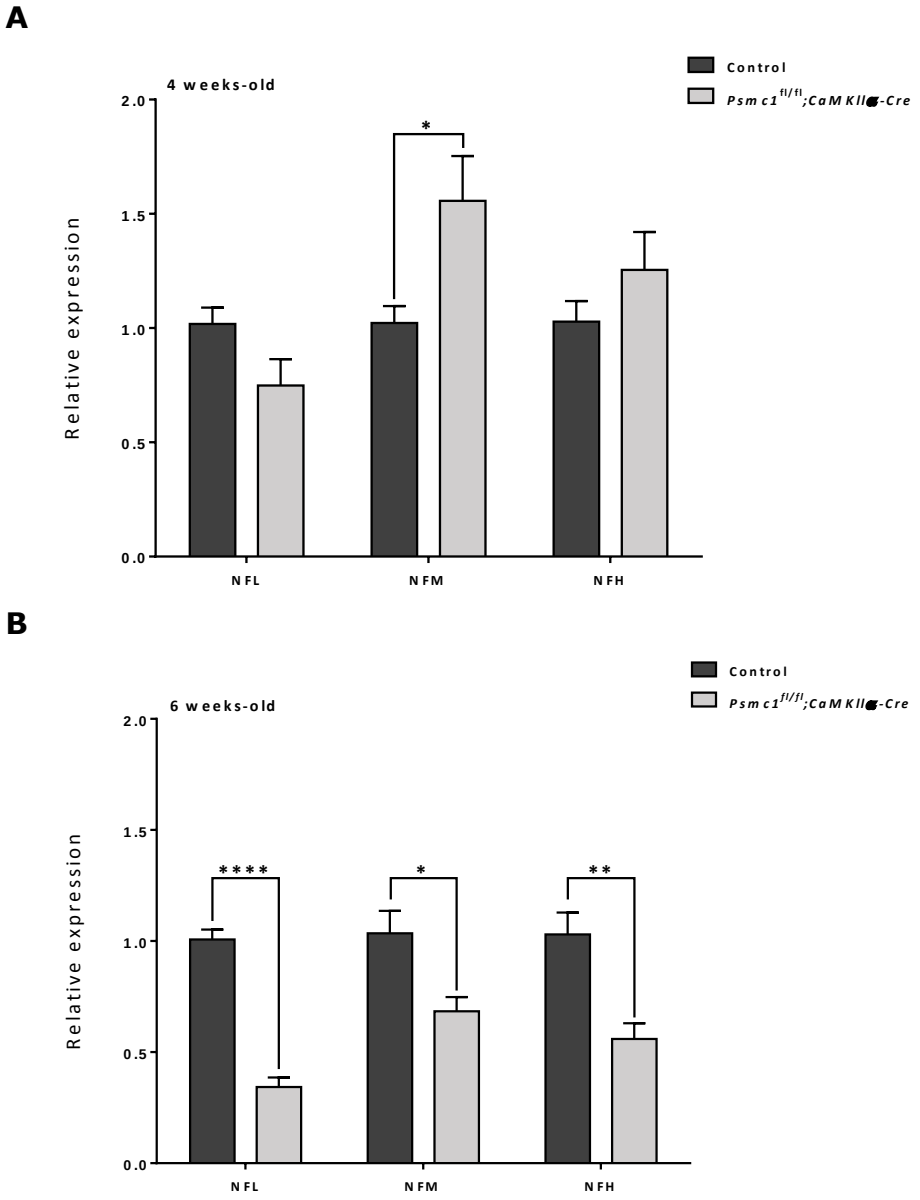


Figure 5.13 Decreased NF mRNA expression in 6 week-old *Psmc1*$^{fl/fl}$*;CaMKIIa-Cre* compared to control mouse cortices

Real-time qRT-PCR analysis of NFH, NFM and NFL in cortical tissue at 4 (A) and 6 (B) weeks-old from control and *Psmc1*$^{fl/fl}$*;CaMKIIa-Cre* mice. The levels of NFH, NFM and NFL mRNA were normalized to the Hmbs housekeeping gene. Data are presented as the mean ± standard error of the mean (SEM) of n = 8 mice. *p < 0.05, **p < 0.01, ***p < 0.001 ****p ≤ 0.0001 by unpaired Student's t-test.

5.3.6 NF immunoreactivity following disruption of the 26S proteasome in mouse cortical neurons

NF protein immunoreactivity is often used to delineate subpopulations of pyramidal neurons in cortical layers III and V and characterize the cytoarchitectonic organization of cortical areas in mammalian brain (Hof et al., 1992, Kirkcaldie et al., 2002, Van der Gucht et al., 2007, Mellott et al., 2010, Paulussen et al., 2011). To investigate further the increased NF protein expression in neurons with 26S proteasome dysfunction we performed immunohistochemical studies on control and *Psmc1*$^{fl/fl}$*;CaMKIIα-Cre* mouse brain sections at 4 and 6 weeks-old. NF antibodies used in this section detect both phosphorylated and non-phosphorylated NF proteins.

We examined neuronal structural changes within the auditory (AU) and somatosensory (SS) cortices, where the apical dendrites of pyramidal neurons in layers III and layer V are clearly visible. The length of individual apical dendrites was also measured as described in Section 5.2.3.

We show that NF proteins are predominantly expressed in pyramidal neurons of layers III and V of the somatosensory (SS) and auditory (AU) mouse cortex (Figures 5.14-5.20; Appendix Figures 1-5). NFH and NFL immunostaining was evident in the cell body, apical and basal dendritic processes (Figures 5.14-5.18; Appendix Figures 1-4). NFM immunostaining was not as obvious as NFH and NFL, and mostly found in the neuronal soma (Figures 5.19 and 5.20; Appendix Figure 5). At 4 weeks-old NFM was found in the cell body of control and *Psmc1*$^{fl/fl}$*;CaMKIIα-Cre* pyramidal neurons (Figures 5.19 and 5.20; asterisks), but at 6 weeks-old NFM immunostaining revealed large, rounded cell bodies (Figures 5.20I-L; asterisks), protein inclusions (Figures 5.20K; arrowheads), and part-labelling of apical dendrites with absent basal dendritic processes in *Psmc1*$^{fl/fl}$*;CaMKIIα-Cre* neurons (Figures 5.20K; arrows).

In control mice, NFH and NFL immunostaining of pyramidal neurons of the SS and AU cortical layers III and V revealed a triangular-shaped cell body with a single, thin apical dendrite and two or three basal dendrites (Figures 5.14-5.18). In general, the NF immunostaining appeared stronger in *Psmc1*$^{fl/fl}$*;CaMKIIa-Cre* than control cortices. NFH- and NFL-stained neurons in *Psmc1*$^{fl/fl}$*;CaMKIIa-Cre* mice at 4 and 6 weeks-old could be divided into three populations according to their cell body shape, apical dendrite length and dendritic arborisation (Figure 5.18). The first population had triangular-shaped cell bodies similar to control neurons with thick, long apical dendrites extending from the superior pole of the soma towards layer I (Figures 5.14J; 5.15I; 5.16J; 5.17L and 5.18). Their basal dendrites appeared as a network of fine processes from the soma (Figure 5.14-5.18; asterisks). This population of neurons was mostly evident in layer III compared to layer V in both cortical areas. Data for AU cortex neurons is shown in the Appendix Figures 1-4.

The second and third populations of neurons in *Psmc1*$^{fl/fl}$*;CaMKIIa-Cre* cortices were characterised by the presence of protein inclusions and large, rounded cell bodies. Protein inclusions are a consequence of 26S proteasome dysfunction in this mouse model and resemble human Pale bodies (Paine et al., 2013, Bedford et al., 2008). NFH and NFL immunostaining clearly encircled the protein inclusion in both populations (Figure 5.14-5.17; arrowheads). The second population of neurons had thick, long apical dendrites (Figures 5.14K; 5.15K; 5.16K; 5.17L and 5.18E; arrows), whereas the third population had thick, short, branched apical dendrites (Figures 5.14K; 5.15K; 5.16I; 5.17J; 5.18F and G). Again, the dendritic processes of these neurons had extensive fine branches. The second population was found mostly in cortical layer V compared to layer III.

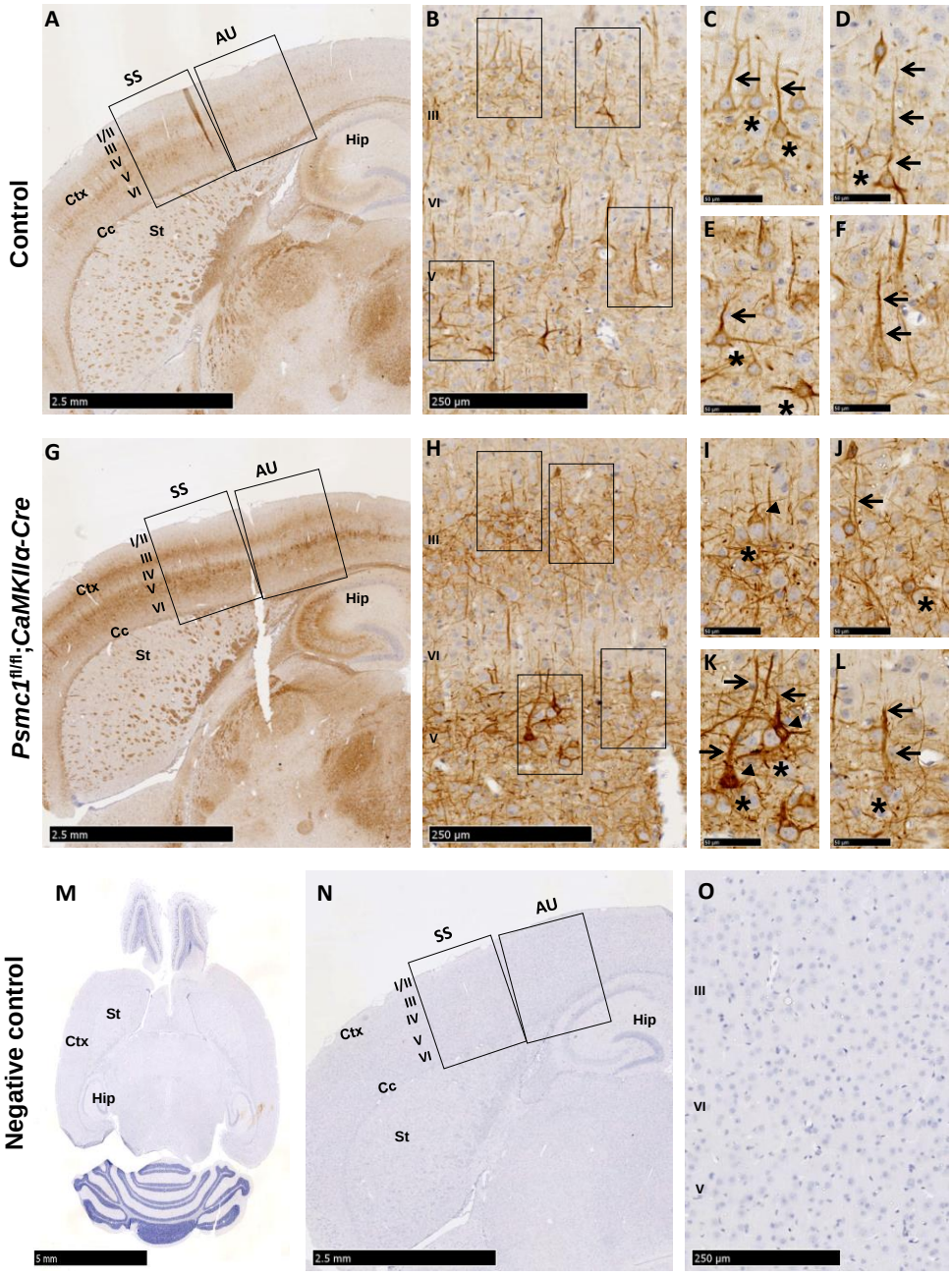


Figure 5.14 NFH immunoreactivity in 4 week-old *Psmc1*$^{fl/fl}$*;CaMKIIα-Cre* mouse cortical neurons

(A, G, M and N) Low magnification images of NFH immunostaining of 7 µm horizontal brain sections from 4 week-old control (A-F) and *Psmc1*$^{fl/fl}$*;CaMKIIα-Cre* mice (G-O) showing obvious staining of cortical layers III and V, and more intense staining in *Psmc1*$^{fl/fl}$*;CaMKIIα-Cre* mice compared to controls. Higher magnification images of the boxed SS areas in A, G and M are shown in B, H and O respectively. Enlarged views of individual neurons in the boxed areas in layers III and V (B and H) are shown in C-F and I-L respectively. Immunostaining is evident in the cell body, apical and basal dendrites in both control and *Psmc1*$^{fl/fl}$*;CaMKIIα-Cre* neurons. Arrows, Asterisks and Arrowheads indicate apical dendrites, basal dendritic processes and targeted neurons containing protein inclusions respectively. SS, somatosensory cortex; AU, auditory cortex; Ctx, cortex; Hip, hippocampus; Cc, corpus callosum; St, striatum.

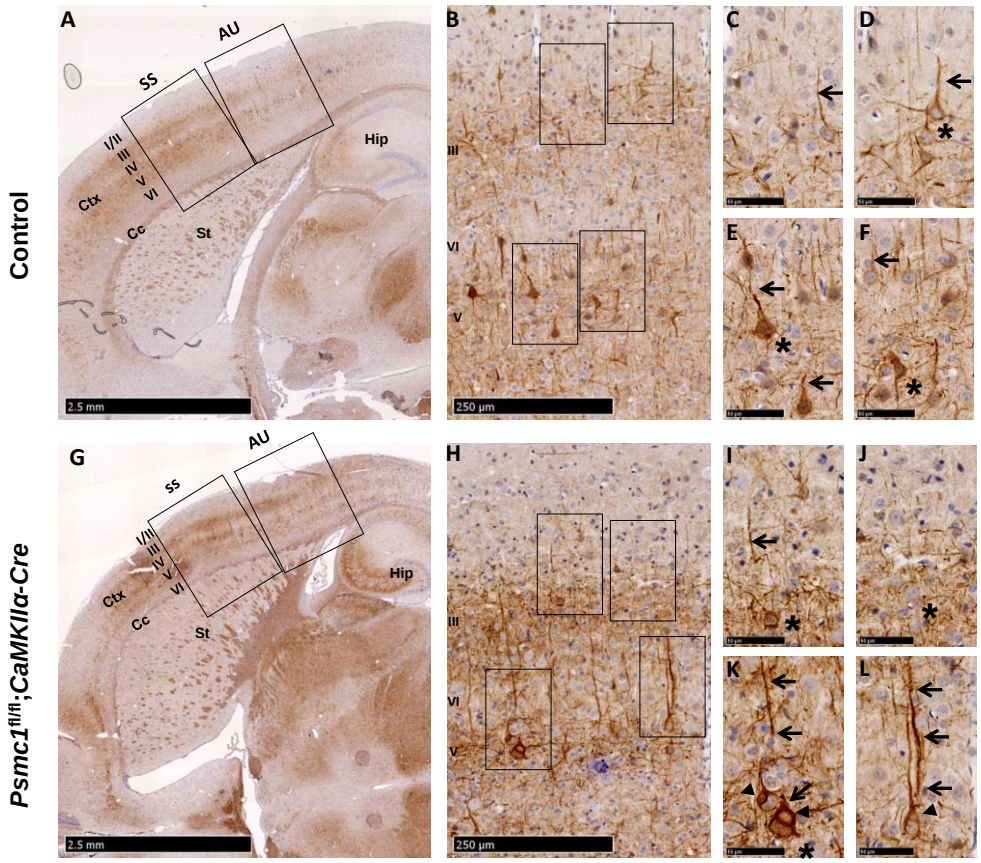


Figure 5.15 NFH immunoreactivity in 6 week-old *Psmc1*$^{fl/fl}$*;CaMKIIa-Cre* mouse cortical neurons.

(A and G) Low magnification images of NFH immunostaining of 7 µm horizontal brain sections from 6 week-old control (A-F) and *Psmc1*$^{fl/fl}$*;CaMKIIa-Cre* mice (G-L) showing clear staining of cortical layers III and V, and more intense staining in *Psmc1*$^{fl/fl}$*;CaMKIIa-Cre* mice compared to controls. Higher magnification images of the boxed SS areas in A and G are shown in B and H respectively. Enlarged views of individual neurons in the boxed areas of cortical layers III and V (B and H) are shown in C-F and I-L respectively. Immunostaining is evident in the cell body, apical and basal dendrites in both control and *Psmc1*$^{fl/fl}$*;CaMKIIa-Cre* neurons. Arrows, Asterisks and Arrowheads indicate apical dendrites, basal dendritic processes and targeted neurons containing protein inclusions respectively SS, somatosensory cortex; AU, auditory cortex; Ctx, cortex; Hip, hippocampus; Cc, corpus callosum; St, striatum.

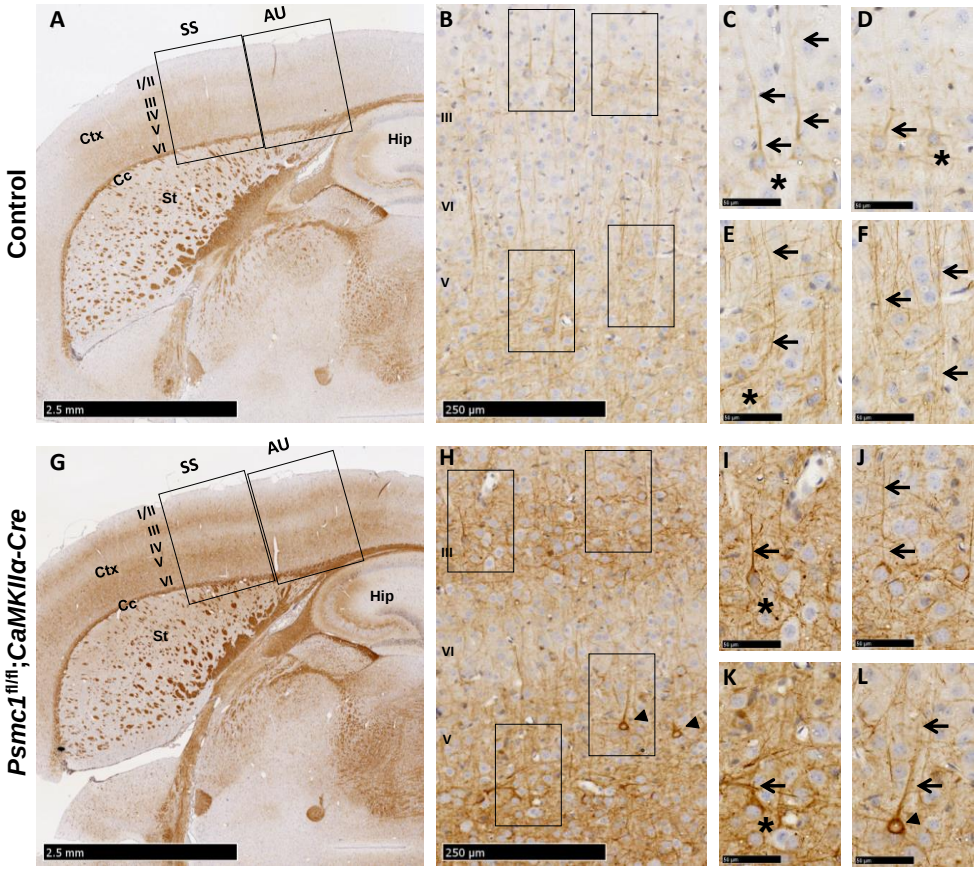


Figure 5.16 NFL immunoreactivity in 4 week-old *Psmc1*$^{fl/fl}$*;CaMKIIa-Cre* mouse cortical neurons

(A and G) Low magnification images of NFL immunostaining of 7 µm horizontal brain sections from 4 week-old control (A-F) and *Psmc1*$^{fl/fl}$*;CaMKIIa-Cre* (G-L) mice, showing clear staining of pyramidal neurons in cortical layers III and V, and more intense staining in *Psmc1*$^{fl/fl}$*;CaMKIIa-Cre* mice compared to controls. Higher magnification images of the boxed SS areas in A and G are shown in B and H respectively. Enlarged views of individual neurons in the boxed areas of cortical layers III and V (B and H) are shown in C-F and I-L respectively. Immunostaining is evident in the cell body, apical and basal dendrites in both control and *Psmc1*$^{fl/fl}$*;CaMKIIa-Cre* neurons. Arrows, Asterisks and Arrowheads indicate apical dendrites, basal dendritic processes and targeted neurons containing protein inclusions respectively. SS, somatosensory cortex; AU, auditory cortex; Ctx, cortex; Hip, hippocampus; Cc, corpus callosum; St, striatum.

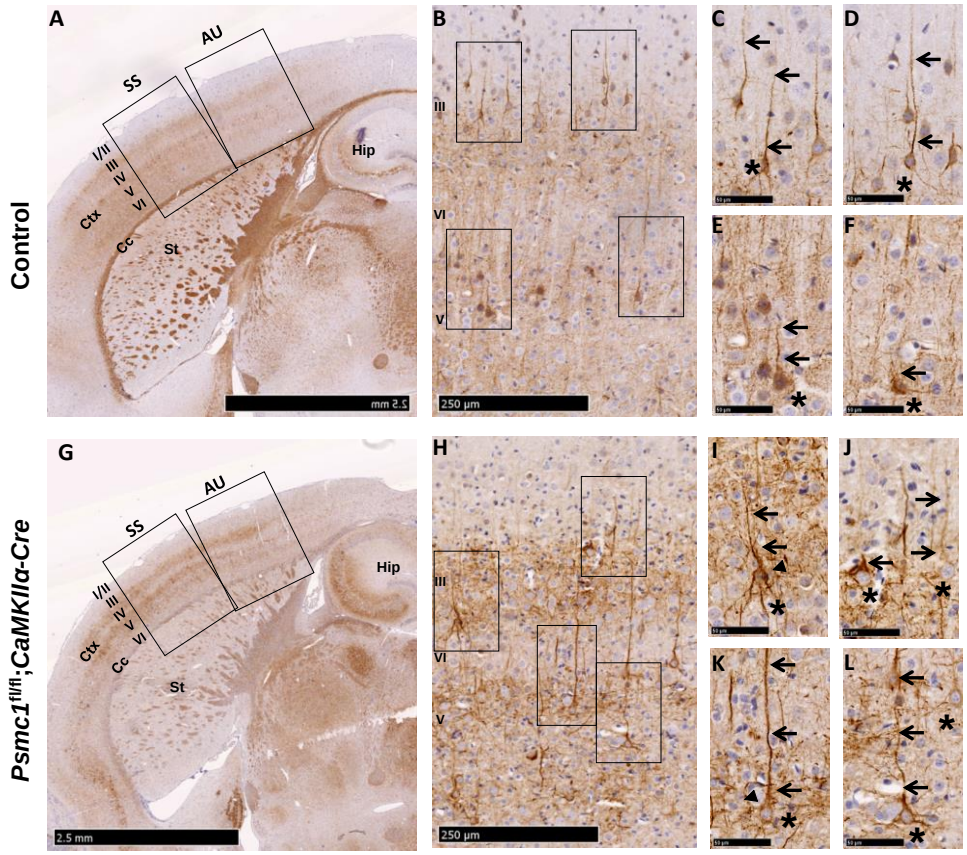


Figure 5.17 NFL immunoreactivity in 6 week-old *Psmc1*$^{fl/fl}$*;CaMKIIα-Cre* mouse cortical neurons

(A and G) Low magnification images of NFL immunostaining of 7 µm horizontal brain sections from 6 week-old control (A-F) and *Psmc1*$^{fl/fl}$*;CaMKIIα-Cre* (G-L) mice, showing clear staining of pyramidal neurons in cortical layers III and V, and more intense staining in *Psmc1*$^{fl/fl}$*;CaMKIIα-Cre* mice compared to controls. Higher magnification images of the boxed SS areas in A and G are shown in B and H respectively. Enlarged views of individual neurons in the boxed areas of cortical layers III and V (B and H) are shown in C-F and I-L respectively. Immunostaining is evident in the cell body, apical and basal dendrites in both control and *Psmc1*$^{fl/fl}$*;CaMKIIα-Cre* neurons. Arrows, Asterisks and Arrowheads indicate apical dendrites, basal dendritic processes and targeted neurons containing protein inclusions respectively. SS, somatosensory cortex; AU, auditory cortex; Ctx, cortex; Hip, hippocampus; Cc, corpus callosum; St, striatum. Ctx, cortex; Hip, hippocampus; Cc, corpus callosum; St, striatum.

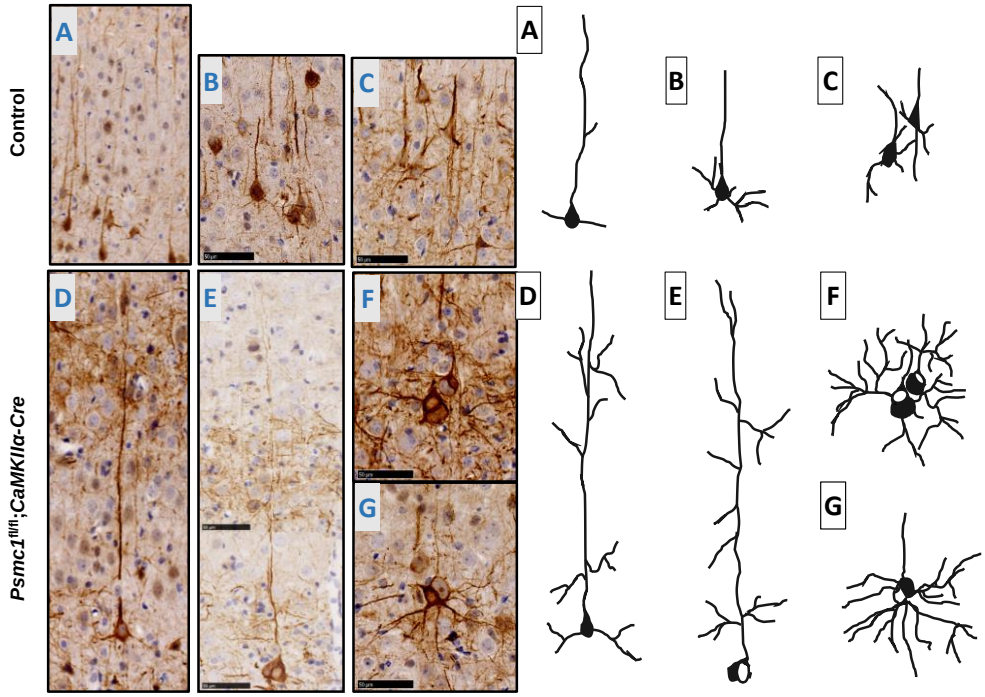


Figure 5.18 Types of pyramidal neurons

Schematic representations of the types of pyramidal neurons evident in the AU and SS areas of control and *Psmc1*$^{fl/fl}$*;CaMKIIα-Cre* mice. All neurons were self-draw from 40X images of NFH immunostaining. (A, B, D and E) show pyramidal neurons with long apical dendrites from control and *Psmc1*$^{fl/fl}$*;CaMKIIα-Cre* mice. (C, F and G) show pyramidal neurons with short apical dendrites. Most *Psmc1*$^{fl/fl}$*;CaMKIIα-Cre* pyramidal neurons have increased dendritic arborisations compared to the control neurons.

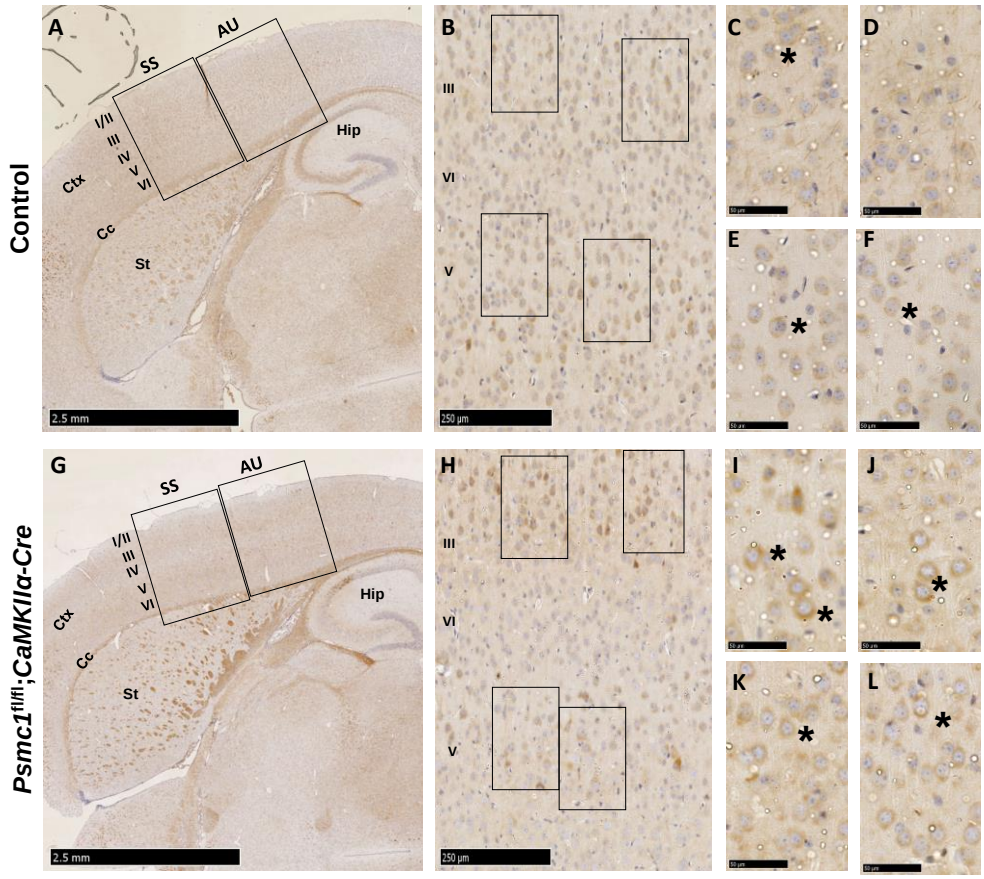


Figure 5.19 NFM immunostaining in 4 week-old mouse cortical pyramidal neurons.

(A and G) Low magnification images of NFM immunostaining of 7 µm horizontal brain sections from 4 week-old control (A-F) and *Psmc1*$^{fl/fl}$*;CaMKIIα-Cre* (G-L) mice. Higher magnification images of the boxed SS areas in A and G are shown in B and H respectively. Enlarged views of individual neurons in the boxed areas of cortical layers III and V (B and H) are shown in C-F and I-L respectively. Asterisks indicate NFM immunostaining in the cell body of both control and *Psmc1*$^{fl/fl}$*;CaMKIIα-Cre* mice. SS, somatosensory cortex; AU, auditory cortex; Ctx, cortex; Hip, hippocampus; Cc, corpus callosum; St, striatum. Ctx, cortex; Hip, hippocampus; Cc, corpus callosum; St, striatum.

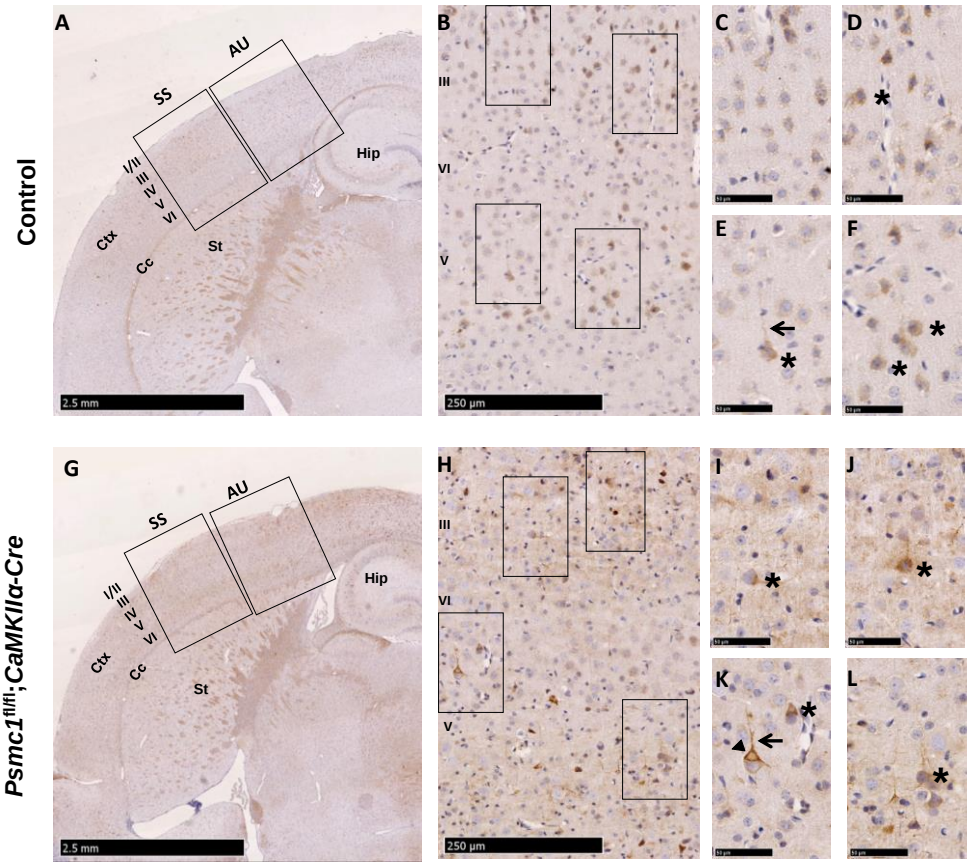


Figure 5.20 NFM immunostaining in 6 week-old mouse cortical pyramidal neurons.

(A and G) Low magnification images of NFM immunostaining of 7 µm horizontal brain sections from 6 week-old control (A-F) and *Psmc1*$^{fl/fl}$*;CaMKIIa-Cre* (G-L) mice. Higher magnification images of the boxed SS areas in A and G are shown in B and H respectively. Enlarged views of individual neurons in the boxed areas of cortical layers III and V (B and H) are shown in C-F and I-L respectively. Asterisks indicate NFM immunostaining in the cell body. Arrows indicate part-labelling of apical dendrites with absent basal dendritic processes. Arrowheads indicate targeted neurons containing protein inclusions in *Psmc1*$^{fl/fl}$*;CaMKIIa-Cre* mice. SS, somatosensory cortex; AU, auditory cortex; Ctx, cortex; Hip, hippocampus; Cc, corpus callosum; St, striatum. Ctx, cortex; Hip, hippocampus; Cc, corpus callosum; St, striatum.

5.3.7 Increased apical dendrite length following disruption of the 26S proteasome in mouse cortical neurons

In this section we measured the length of NFH- and NFL-immunostained apical dendrites in control and *Psmc1*$^{fl/fl}$*;CaMKIIα-Cre* mouse cortices. Apical dendrite length of layer III and V pyramidal neurons was quantified as described in Section 5.2.3, combining the SS and AU cortical areas. Apical dendrite length was manually measured by using ImageJ software, as the maximum distance from the apex of a soma along dendritic tree toward the cortical surface (Figure 5.21A). Since NFM immunostaining was mostly evident in the cell body of neurons this was not used for the analysis. In both control and *Psmc1*$^{fl/fl}$*;CaMKIIα-Cre* mice the staining intensity of apical dendrites varied among individuals neurons. Therefore, neurons were quantified when they were several shades darker than the background, the shape of the soma was easily identified and apical dendrites were clearly projecting from the cell body.

Apical dendrite length did not show a normal distribution using the Kolmogorov-Smirnov normality test for control and *Psmc1*$^{fl/fl}$*;CaMKIIα-Cre* mice. Therefore, a Mann-Whitney U test was used to compare *Psmc1*$^{fl/fl}$*;CaMKIIα-Cre* with control data (Table 5.6). In general, median apical dendrite length (μm) was significantly increased in *Psmc1*$^{fl/fl}$*;CaMKIIα-Cre* layer III and V pyramidal neurons compared to age-matched controls (Table 5.6 and Figure 5.21B). Frequency histograms of apical dendrite length from NFL- and NFH-immunostained neurons clearly show the increased apical length of pyramidal neurons in *Psmc1*$^{fl/fl}$*;CaMKIIα-Cre* mice compared to controls (Figure 5.21B). Interestingly, apical dendrite length was decreased between 4 and 6 weeks-old in control and *Psmc1*$^{fl/fl}$*;CaMKIIα-Cre* mice, which may be a result of changes in NF expression with aging (Table 5.6).

Table 5.6 Median apical dendrite length of pyramidal neurons in 4 and 6 week-old control and *Psmc1*$^{fl/fl}$*;CaMKIIα-Cre* mice. Data expressed as median in cortical layers III and V of AU and SS cortices. Statistics used Mann-Whitney U test.

Age of mice									
Antibody	Cortical layers	4 weeks-old				6 weeks-old			
		Control	*Psmc1*$^{fl/fl}$*;CaMKIIα-Cre*	Mann Whitney test		Control	*Psmc1*$^{fl/fl}$*;CaMKIIα-Cre*	Mann Whitney test	
		Median (µm)	Median (µm)	*P* value	*sign*	Median (µm)	Median (µm)	*P* value	*sign*
NFH	III	90.92, n=407	191.9, n=354	< 0.0001	****	59.54, n=551	98.94, n=358	< 0.0001	****
	V	149.1, n=498	254.3, n=380	< 0.0001	****	70.80, n=572	114.3, n=397	< 0.0001	****
NFL	III	94.60, n=614	162.4, n=306	< 0.0001	****	75.21, n=605	133.6, n=324	< 0.0001	****
	V	124.5, n=516	243.8, n=282	< 0.0001	****	101.0, n=657	187.5, n=288	< 0.0001	****

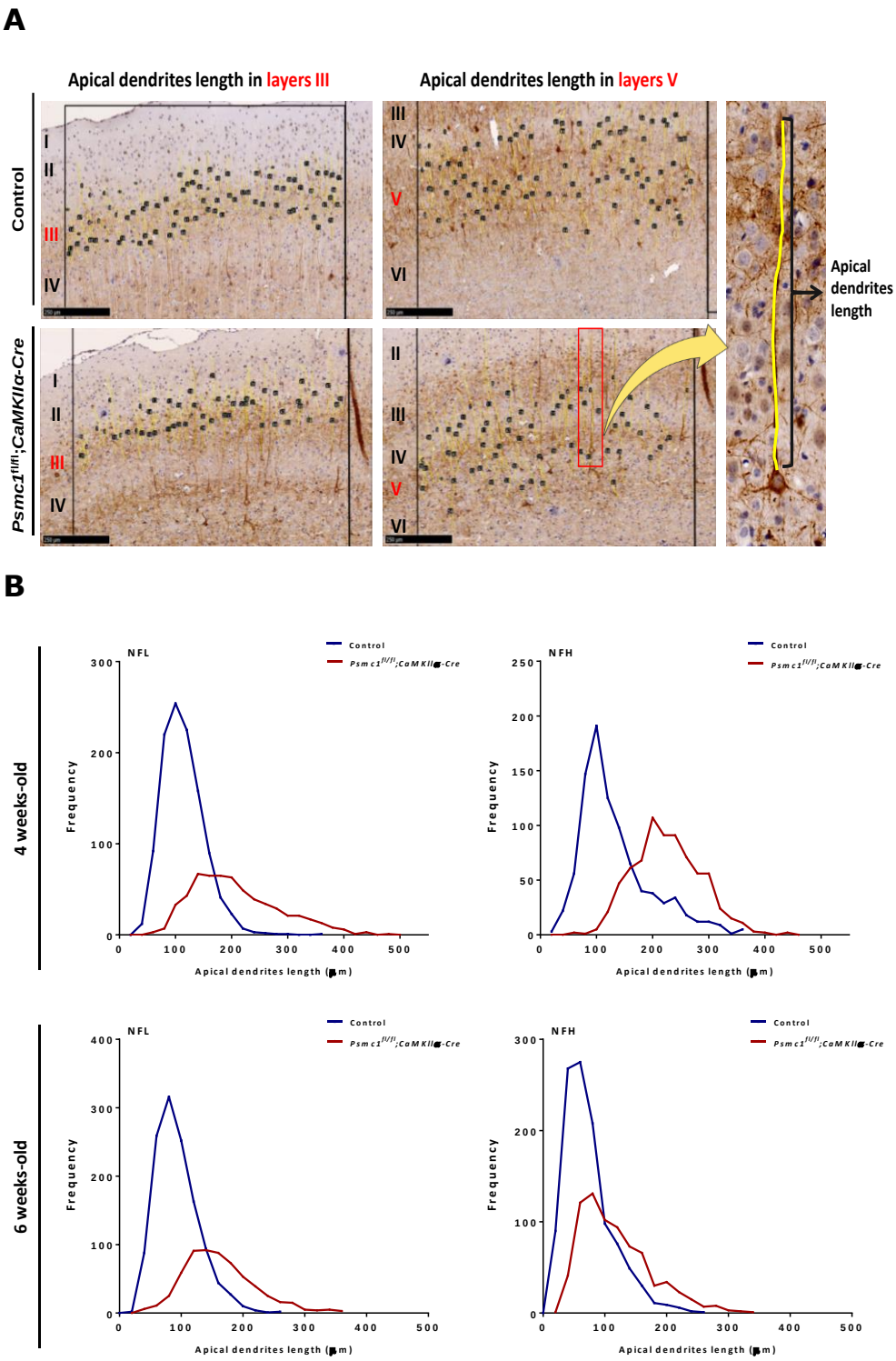


Figure 5.21 Increase apical dendrites length in the *Psmc1*$^{fl/fl}$*;CaMKIIa-Cre* mice pyramidal neurons

(A) Representation of pyramidal apical apical dendrite length measurement using ImageJ software. (B) Frequency histograms of the apical dendrite length of NFL- and NFH-immunostained pyramidal neurons at 4 and 6 weeks-old in control and *Psmc1*$^{fl/fl}$*;CaMKIIa-Cre* mice.

5.4 Discussion

5.4.1 Cortical thickness decreases following disruption of the 26S proteasome in mouse cortical neurons

Cortical thickness has been used as an important morphological feature in many brain studies. AD and DLB are characterized by significant cortical thinning in the frontal and parietal cortical regions and this longitudinal cortical thinning may be used to differentiate DLB from AD by imaging (Mak et al., 2015). Early regional cortical thickness changes was indicative of predisposition to later β-amyloid pathology in a transgenic AD mouse model (Grand'Maison et al., 2013). A recent study showed that measuring cortical thickness could be useful in assessing disease stage and identifying cognitive impairment in PD patients (Zarei et al., 2013). Furthermore, in PD patients, the presence of dementia was associated with extensive thinning of the dorsal and medial frontal cortex as well as the temporal and posterior parietal cortex (Pellicano et al., 2012). Other studies suggest that defects in cortical functions are responsible for the development of dementia in PD patients (Pagonabarraga et al., 2008, Williams-Gray et al., 2007).

Here we measured the thickness of the AU and SS cortices and show that cortical thickness significantly decreases at 4 and 6 weeks-old following disruption of the 26S proteasome compared to controls. Interestingly, at 4 weeks of age, neocortical thickness was reduced approximately 10% in the AU and SS areas in *Psmc1*$^{fl/fl}$*;CaMKIIa-Cre* mice; most of this reduction is due to diminution of layers I&II and VI, while layers III and V were significantly thicker than that of age-matched controls. Layer IV did not appear to show any differences from control mice. Cortical thinning was more significant at 6 weeks-old coincident with previously reported neurodegeneration and behavioural changes, including spatial memory deficits (Bedford et al., 2008). At 6 weeks of age we found that neocortical thickness was decreased approximately 20% in both cortical areas in *Psmc1*$^{fl/fl}$*;CaMKIIa-*

Cre mice and this was due to diminution of all cortical layers. Previous histopathological studies reported that AD and FTD pathologies were associated with damage to specific cortical layers; layer II of the entorhinal cortex and layer III of the neocortex in AD, and layer III and V of frontal and temporal lobes in FTD (Kersaitis et al., 2004, Gomez-Isla et al., 1996).

Our observation that cortical layers III and V are thicker or hypertrophic at 4 weeks-old in *Psmc1*$^{fl/fl}$*;CaMKIIa-Cre* mice is unexpected, but has precedent. It is possible that increased Ub accumulation following 26S proteasomal dysfunction in cortical neurons increases volume in the absence of brain tissue loss at this age. A previous study using high-resolution post-mortem MRI and deformation-based morphometry showed a transitory thickening preceding thinning associated with disease progression in pre-symptomatic familial AD mutation carriers (Fortea et al., 2010, Badhwar et al., 2013). An alternative explanation is that the increased thickness of these cortical layers is a compensatory neuronal hypertrophy; an early cellular attempt to offset increasing neuronal injury caused by 26S proteasome dysfunction and Ub-accumulation in these layers. Cortical and hippocampal neuronal hypertrophy has been demonstrated in asymptomatic AD cohorts from the Baltimore Longitudinal Study of Aging (Driscoll and Troncoso, 2011, Fortea et al., 2010, Iacono et al., 2009, Riudavets et al., 2007). Further investigations of neuronal size in layers III and V of the AU and SS cortices of mice with 26S proteasome dysfunction would be interesting in the future.

5.4.2 Hypertrophy of neurons with 26S proteasome dysfunction in mouse cortical neurons

Morphometric analysis of brain tissue is widely used to study morphological changes associated with neurodegenerative disease, including neuronal number and nuclear size (Bundgaard et al., 2001, Andrade-Moraes et al., 2013, Gagyi et al., 2012). Morphometric analysis of post mortem brains from AD and control patients showed the neuronal nuclear volume was significantly

higher in AD patients than controls, and demonstrated that this nuclear hypertrophy was more obvious in the large neocortical neurons (Bundgaard et al., 2001). The authors found that there were no significant differences in the perikaryal volume of neocortical neurons (Bundgaard et al., 2001). Increased neuronal nucleus volume, referred as nuclear hypertrophy, was observed in the anterior cingulate gyrus and hippocampal CA1 region in asymptomatic AD patients compared to patients with mild cognitive impairment and controls (Riudavets et al., 2007). The hypertrophy of cortical neurons and their nuclei in hippocampal CA1 and anterior cingulate gyrus neurons in asymptomatic AD may represent an early compensatory mechanism that prevents the progression of disease into dementia (Iacono et al., 2008, Iacono et al., 2009).

Here we show that the median nuclear size of neurons in layers III and V of the AU cortex is significantly increased in *Psmc1*$^{fl/fl}$*;CaMKIIα-Cre* mice compared to age-matched controls. This observation was more significant at 4 than 6 weeks-old. The increased nuclear size in *Psmc1*$^{fl/fl}$*;CaMKIIα-Cre* cortical neurons could be an early response to neuronal defects and/or cellular Ub-accumulation following 26S proteasomal dysfunction. In addition to the nuclear hypertrophy and as expected we found the number of Ub-positive neurons significantly increased in the *Psmc1*$^{fl/fl}$*;CaMKIIα-Cre* AU cortex with increased age compared to controls. However, the total number of neurons in layers III and V of the AU cortex in *Psmc1*$^{fl/fl}$*;CaMKIIα-Cre* mice at 4 weeks-old was not significantly different from control mice. In contrast, the total number of neurons in these layers at 6 weeks-old was significantly decreased in *Psmc1*$^{fl/fl}$*;CaMKIIα-Cre* compared to control mice.

Increased nuclear size of neurons has been described previously as a compensatory mechanism to allow the brain to function normally despite the presence of AD lesions (Riudavets et al., 2007). An increase in cytoskeleton proteins is accompanied by

increasing nucleolar, nuclear and cell body size in spinal motor neurons following axotomy (McIlwain and Hoke, 2005). It is possible that the increased nuclear volume is related to abnormalities in transport between the nucleus and cytoplasm (Sheffield et al., 2006). Our observations are consistent with a previous stereological study that found cortical and hippocampal neurons undergo significant nuclear hypertrophy in asymptomatic AD, probably as a reaction to Aβ, long before the onset of cognitive decline or dementia (Iacono et al., 2009, Iacono et al., 2008).

5.4.3 Neurofilament changes caused by 26S proteasome dysfunction in mouse cortical neurons

Abnormal accumulation of neurofilaments in the cell body and proximal axons of neurons is a consistent observation in many neurodegenerative disorders, such as amyotrophic lateral sclerosis (ALS), PD, AD and dementia with Lewy bodies (DLB) (Xu et al., 1993, Tu et al., 1997). We have shown changes in NF expression and in cortical neurons following 26S proteasome dysfunction, providing a novel perspective on the underlying processes involved in neurodegeneration diseases. In this study, we observed significantly increased NFH, NFL and NFM protein levels with progressive 26S proteasome dysfunction. Interestingly, this was associated with significantly decreased mRNA expression for these proteins. We also found increased arborisation and length of apical dendrites in layers III and V pyramidal neurons in *Psmc1*$^{fl/fl}$*;CaMKIIa-Cre* mice, suggesting a complex interplay between the UPS and neurofilament levels and distribution.

5.4.4 Increased neurofilament proteins following disruption of the 26S proteasome in mouse cortical neurons

Our results show significantly increased levels of all three neurofilament proteins with increasing age and progressive neurodegeneration in *Psmc1*$^{fl/fl}$*;CaMKIIa-Cre* mice. The levels of NFH and NFL were significantly increased at both 4 and 6 weeks-

old; NFM was only significantly increased at the later time point. Previous studies have suggested a potential mechanism for regulating NF content within the axon may be degradation of NFs by the UPS (Gou and Leterrier, 1995, Balastik et al., 2008, Dale and Garcia, 2012). Therefore, it is possible that the increased levels of NF proteins in our model are a consequence of 26S proteasome dysfunction. TRIM2 is a ubiquitin ligase that binds to and ubiquitinates NFL for NFL degeneration. TRIM2 deficiency has been shown to lead to neurodegeneration in mice by altering NFL metabolism with consequent NFL accumulation in axons and impairment of axonal transport (Balastik et al., 2008). In addition, NFM has been identified as a target of the E3 enzyme carboxyl-terminus of Hsc70 interacting protein CHIP, which enhanced NFM ubiquitination and degradation (Wang et al., 2011, Dale and Garcia, 2012).

Increased NF protein expression is a major hallmark of neurodegenerative disease, but it is not clear whether the accumulation of NFs has a harmful or beneficial role. A previous study showed that overexpressing the neurofilament subunits NFL, NFM or NFH in transgenic mice led to prominent motor neuropathy and abnormal NF accumulation resembling changes found in ALS (Xu et al., 1993). A major pathological hallmark of ALS is intraneuronal accumulation of phosphorylated neurofilament proteins in degenerating motor neurons (Murayama et al., 1992). More recent studies have shown that plasma NFH levels increase significantly with disease progression in the mouse model of ALS and this increase in plasma NFH correlates with later stages of motor neurodegeneration in this disease (Lu et al., 2015, Lu et al., 2012). Proteomic analysis of the post mortem AD brain showed presence of NF proteins in the fibrillary plaque core, suggest these proteins may have important role in the formation of plaques (Liao et al., 2004).

Beneficial roles of NF proteins have also been described in ALS (Kong and Xu, 2000, Couillard-Després et al., 2000). Studies

showed that overexpression of NFL and NFH proteins had a protective effect on ALS progression in SOD1 mutant G93A mice and this effect was greater with NFH (Kong and Xu, 2000). Absence of the NFL subunit in NFL knockout mice led to accumulation of NFM and NFH proteins in the cell body of motor neurons and slowed progression of SOD1 G85R-mediated toxicity in motor neurons (Williamson et al., 1998). It is possible that increased expression of NF proteins following 26S proteasome dysfunction in neurons may be a protective response that requires further investigation.

5.4.5 Decreased neurofilament mRNA following disruption of the 26S proteasome in mouse cortical neurons

NF gene expression plays an important role in nervous system development (Moore, 2005). Previous studies have shown that transcriptional regulation of NF genes was important for NF protein levels in neurodegenerative disease and neural regeneration (Thyagarajan et al., 2007, Wang et al., 2012). NF gene expression is altered in spinal cord sections from sporadic ALS patients; NFL mRNA was selectively decreased in degenerating motor neurons, while NFM and NFH mRNA levels were unchanged (Wang et al., 2012, Wong et al., 2000). Decreased NFL mRNA was also observed in AD neocortical tissue (McLachlan et al., 1988). An earlier study found that decreased NFH and NFL mRNA levels contributed to the degeneration of substantia nigra neurons in PD and correlating with the severity of this disease (Hill et al., 1993). However, it was unclear whether the decreased gene expression reflected the degeneration of neurons, or was an active process of the disease.

Transcriptional levels of NFH, NFM and NFL were investigated in 4 and 6 week-old control and *Psmc1*$^{fl/fl}$*;CaMKIIa-Cre* mice. We show that the levels of NFH and NFL mRNA were not significantly different, but that NFM was significantly increased, in *Psmc1*$^{fl/fl}$*;CaMKIIa-Cre* mice compared to controls at 4 weeks-old. At 6 weeks-old, the mRNA level of all NF subunits was significantly decreased compared to control mice.

In normal neurons NFL and NFM are expressed earlier than NFH during initial neurite outgrowth (Giasson and Mushynski, 1997). In rodents, NFs are synthesized according to a 4:2:1 ratio of NFL:NFM:NFH and this ratio is continuously altered during neuronal formation (Carter et al., 1998). In vivo, a study showed that NFM plays an important role in regulating of the levels of NFL protein, the stoichiometry of NF subunits and the phosphorylation state of NFH (Tu et al., 1995). The amount of NFM in optic axon NFs decreased as the ratio of NFH to NFL increased, suggesting that NFH may compete with NFM in binding to NFL. Comparing the subunit stoichiometry at different postnatal ages of in Shiverer mutant mice confirms a net reduction in NFM content on NFs when NFH appears (Sánchez et al., 2000). Increased NFM mRNA levels in *Psmc1*$^{fl/fl}$*;CaMKIIa-Cre* mice at 4 weeks-old may be involved in regulating the NF ratio under conditions of stress in an attempt to maintain the NF network. It is clear that increased levels of NF proteins following 26S proteasome dysfunction is not due to transcriptional upregulation of the NF genes. It is possible that the accumulation of NF proteins induces a feedback mechanism that regulates NF production by downregulating NF gene expression.

5.4.6 NF immunoreactivity and increase apical dendrite length following 26S proteasome dysfunction in mouse cortical neurons

In this study NF immunostaining in layers III and V pyramidal neurons of the AU and SS cortices was compared between control and *Psmc1*$^{fl/fl}$*;CaMKIIa-Cre* mice. NF immunostaining was clear in layers III and V pyramidal neurons as previously reported in human, mouse and cat cortical neurons (Hof et al., 1992, Kirkcaldie et al., 2002, Van der Gucht et al., 2007, Mellott et al., 2010, Paulussen et al., 2011).

Overall, the intensity of NF staining appeared to be increased in *Psmc1*$^{fl/fl}$*;CaMKIIa-Cre* mice compared to controls, supporting the accumulation of NF proteins in *Psmc1*$^{fl/fl}$*;CaMKIIa-Cre* mouse pyramidal neurons. In control and *Psmc1*$^{fl/fl}$*;CaMKIIa-Cre* mice NFH

and NFL immunostaining was evident in the perykaria, and apical and basal dendritic processes of pyramidal neurons. NFM immunostaining was mainly evident in the perykaria, with slight staining in the apical dendritic processes of *Psmc1*$^{fl/fl}$*;CaMKIIα-Cre* mice.

Neurofilaments are synthesized and assembled in cell bodies then transported along the axon by a process called axonal transport (Liu et al., 2011). The phosphorylated form of NF subunits are found in the axoplasm, while the non-phosphorylated form located in the neuronal perikarya and dendrites (Nixon et al., 1994). Non-phosphorylated NFs have been shown to be rapidly degraded by the UPS, where increased NF phosphorylation prevented NF turnover by this mechanism (Dale and Garcia, 2012). An in vitro study using PC12 cells showed that the proteasome inhibitor lactacystin can induce the neuropathological features associated with a perikaryal accumulation of phosphorylated NFs (Masaki et al., 2000). Accumulation of phosphorylated NF proteins in the neuronal soma indicated neuronal dysfunction and degeneration in MS patients (Gray et al., 2012).

The NF antibodies used here detect endogenous levels of total NF proteins, including their phosphorylated and non-phosphorylated form. Several factors may contribute to the accumulation of NFs in the perikarya of the *Psmc1*$^{fl/fl}$*;CaMKIIα-Cre* mouse pyramidal neurons observed in the present study, such as (1) increased MT instability, which can affect the ability of the axon to transport NF proteins; (2) decreased degradation of NF proteins by the UPS in affected neurons as previously discussed.

NF immunostaining of pyramidal neurons in cortical layers III and V of *Psmc1*$^{fl/fl}$*;CaMKIIα-Cre* mice was divided into three populations according to their cell body shape, apical dendrite length and dendritic arborisation. The first population were referred to as intact and therefore similar to neurons found in control mice. While the second and third populations were affected pyramidal neurons (26S proteasome-deleted neurons). The second population of

neurons had thick, long apical dendrites, whereas the third population had thick, short, branched apical dendrites associated with extensive fine branches extended from these dendritic processes.

The second population of pyramidal neurons in *Psmc1*$^{fl/fl}$*;CaMKIIa-Cre* mice was more obvious at 4 than 6 weeks of age, suggesting accumulation of NFs in perikarya, around inclusion bodies and in apical dendrites is an early change following 26S proteasome dysfunction. Transgenic mice overexpressing NFL, NFM or NFH show substantial NF accumulation in the perikarya, dendrites and axons of spinal motor neurons, indicating that altered NF metabolism may result in the formation of NF-rich inclusions (Bussiere et al., 2003, Julien and Kriz, 2006, Mendonca et al., 2005). These mice eventually develop ALS-like neuronal cell loss (Nakamura et al., 1999, Hashiguchi et al., 2014). Furthermore, the degenerating motor neurons in NFH transgenic mice had large cytoplasmic accumulations of neurofilaments surrounding mitochondria aggregates near the nucleus. This study suggests NF accumulation may lead to axonal degeneration by impeding the transport of mitochondria required for axonal maintenance (Collard et al., 1995). Importantly, protein inclusions in the affected neurons of *Psmc1*$^{fl/fl}$*;CaMKIIa-Cre* mice also show aggregation of mitochondria (Ugun-Klusek et al., 2017).

The third population of pyramidal neurons was most evident at 6 week-old, with short thick apical dendrites. Correlating with these changes, the dendritic arborisation of pyramidal neurons appeared to be more evident at 6 compared to 4 weeks of age in *Psmc1*$^{fl/fl}$*;CaMKIIa-Cre* mice. It is possible that the increased dendritic arborisation of these neurons is an attempt to extend NF expression into dendrites. A previous study found that increasing NFH and/or NFM inhibited dendritic arborisation, but these changes were reversed by elevating the level of NFL with either NFH or NFM (Kong et al., 1998a). A lower ratio of NFH and NFM to NFL is critical for the growth of complex dendritic trees in motor neurons.

Increased dendritic arborisation in the *Psmc1*$^{fl/fl}$*;CaMKIIα-Cre* mice pyramidal neurons is further supported by apical dendritic length measurement data. In Section 5.3.7 we showed apical dendritic length of pyramidal neurons in cortical layer III and V was significantly increased in *Psmc1*$^{fl/fl}$*;CaMKIIα-Cre* compared to control mice.

Previous study in AD mouse models, Tg2576 amyloid precursor protein (APP) mutant mouse, showed that significantly increased dendritic lengths with more complex proximal apical dendrite branching patterns in layer III pyramidal neurons from 12-month-old Tg2576 mice compared to wild-type mice (Rocher et al., 2008). Another study29 investigated morphological changes in these mouse frontal pyramidal neurons at 9 and 24 months of age, noted no difference in dendritic structure in layer III pyramidal neurons between the Tg2576 and wild-type neurons at 9 months of age, prior to substantial deposition of plaques. But a significant reduction in apical dendritic length was observed at 24 months of age, when amyloid plaques are abundant, compared with wild type mice. The data from these studies indicate that dendritic length and structure were changed with aged in Tg2576 mice cortical pyramidal neurons, which involved an initial by elongation of dendritic length at 12 months followed by regression at 24 months (Luebke et al., 2010).

This may explain the reduction the apical dendrites length in *Psmc1*$^{fl/fl}$*;CaMKIIα-Cre* mice pyramidal neurons in cortical layer III and V in 6 weeks age compared to 4 weeks age mice. Although, the underlying mechanism of increased dendritic arborisation and apical dendrites length following 26S proteasome dysfunction is not clear, a number of factors could plausibly underlie these changes. First, dendritic elongation may be related to the increased level of NFL observed in 4 weeks age of *Psmc1*$^{fl/fl}$*;CaMKIIα-Cre* mice in section 5.3.6. This may lead to many more dendrite filaments, neurons and long dendrites radiating from pyramidal neurons in cortical layer III and V of the *Psmc1*$^{fl/fl}$*;CaMKIIα-Cre* mice. Previous

studies showing increased NFL can protect against NFH-mediated pathogenesis from increased NFH alone (Meier et al., 1999). The motor neurons regulate the ratio of NFH to NFL in order to maintain a balance between plasticity and stability of neuronal processes during different stages of development (Kong and Xu, 2000)

Second, the overexpression of P-Akt in the *Psmc1*$^{fl/fl}$*;CaMKIIa-Cre* mice could lead to dendritic elongation; indeed active phosphorylated Akt promotes neurite outgrowth and enhances the dendritic branching, and dendritic complexity in cultured mature hippocampal neurons (Jaworski et al., 2005). There is also evidence that increased activity of the protein kinase Akt can increase axonal branching and soma size in primary sensory neurons via activation of mTOR (Grider et al., 2009).

These findings suggest that increased NF and P-Akt expression and/or activity may be involved in neuroprotection mechanism following 26S proteasome dysfunction. Further investigations in the *Psmc1*$^{fl/fl}$*;CaMKIIa-Cre* cortex should investigate these proteins to elucidate these role in the brain in this context.

Chapter 6

General discussion and conclusion

6.1 General discussion

The ubiquitin proteasome system (UPS) plays a key role in the maintenance of intracellular protein homeostasis by degrading unwanted proteins in cells. This system has an essential role in regulating the stability of cytoskeletal proteins, which are mostly degraded via the UPS (Vakifahmetoglu-Norberg et al., 2013).

Depletion of 26S proteasomes in mouse brain cortical neurons is associated with neurodegeneration and the formation of intraneuronal protein inclusions in surviving neurons (Bedford et al., 2008). Here we show that these neuropathological changes are associated with significant changes in cytoskeletal proteins, including NFs and MTs, and MT stability. Our study investigated cytoskeletal changes following 26S proteasome dysfunction in cortical neurons at 4 and 6 weeks of age, reflecting early- and late-stage neurodegeneration.

We show 26S proteasome dysfunction leads to increased levels of NF proteins (Figure 6.1). This is not associated with increased NF gene transcription because NF mRNA was significantly decreased at 4 and 6 weeks-old. Transcriptional downregulation could be an early event following 26S proteasome dysfunction to compensate for increasing NF proteins (Figure 6.1). This study provides the first in vivo evidence in brain that 26S proteasomal dysfunction directly causes increased NF protein, most likely as a result to defective degradation.

NF changes were accompanied by changes in MT protein expression and stability at later stages following 26S proteasome dysfunction. At 4 weeks-old, no significant differences were observed in the levels of α-tubulin, neuron-specific βIII-tubulin and MT-associated proteins, or MT stability. Our observations are supported by a study showing early changes in the axonal distribution of NF proteins preceded changes in MT distribution in response to focal axon compression in rats (Fournier et al., 2015).

It is possible that increased NF expression may be involved in decreased expression of α-tubulin and neuron-specific βIII-tubulin, and increased MT instability at 6 weeks-old in *Psmc1*$^{fl/fl}$;*CaMKIIα-Cre* mice (Figure 6.1). A previous study showed that increased levels of NFs coincided with lack of axonal growth and increased dynamic instability of axonal MTs (Collard et al., 1995). Depletion of NFL can enhance the stability of MTs by increasing the phosphorylation of Stat3 and its interaction with STMN, inhibiting STMN role in destabilizing microtubules. This increases the levels of soluble tubulin heterodimers available for the maintenance of axonal microtubules in motor neurons (Yadav et al., 2016).

In our study, STMN1 levels were dramatically decreased at 6 weeks-old and STMN1 mRNA level was decreased at both 4 and 6 weeks-old (Figure 6.1). Although STMN1 was significantly decreased, our data shows MT instability following 26S proteasome dysfunction. MT instability was evident at 6 weeks of age by increased free/polymerised tubulin ratio, leading to decreased MT polymerization. In addition, decreased expression of α–tubulin, neuron-specific βIII-tubulin and detyrosinated-tubulin, together with increased tyrosinated-tubulin was observed. MT-associated proteins tau and MAP2 were also decreased in the polymerized fraction (Figure 6.1). Taken together, these changes would be expected to be associated with increased STMN1 expression since MAPs tau and MAP2, and STMN1 play opposite, but complimentary roles, in MT stability. Therefore, decreased STMN1 expression at 6 weeks-old may be a negative feedback loop in an attempt by neurons to stabilizing their MT following 26S proteasome dysfunction. Decreased STMN1 mRNA from 4 weeks-old suggests transcriptional downregulation as an early response to increasing cytoskeletal changes in neurons caused by 26S proteasome dysfunction (Figure 6.1).

STMN1 levels and activity could be affected by the p53 and p27 proteins (Figure 6.1), and also activation of the PI3K/Akt pathway (Karst et al., 2011). It is possible that decreased STMN1 mRNA levels in *Psmc1*$^{fl/fl}$*;CaMKIIα-Cre* cortices is linked to increased expression of p53, and this may be part of a p53-regulated apoptotic signalling process following 26S proteasome dysfunction given that STMN1 is a p53-target gene (Johnsen et al., 2000, Fang et al., 2010). Increased p53 in *Psmc1*$^{fl/fl}$*;CaMKIIα-Cre* cortices correlates with decreased P-Akt expression at 4 weeks-old, which may also have an effect on STMN1 expression. Decreased Akt activity by the PI3K/Akt inhibitor has been associated with significantly decreased STMN1 expression in tumour cells (Wang et al., 2010, Schimmack et al., 2015).

Pro-apoptotic and anti-apoptotic members of the Bcl-2 family, such as Bax, Bcl-2 and p27, may be effected by changes in the expression of both p53 and P-Akt. However, these proteins were not significantly different between control and *Psmc1*$^{fl/fl}$*;CaMKIIα-Cre* mice. As proteins of the Bcl-2 family regulate the mitochondrial death pathway, multiple pathways may promote apoptosis following 26S proteasome dysfunction that do not depend on the intrinsic pathway.

Decreased P-Akt expression at 4 weeks of age was followed by dramatically increased P-Akt expression 6 weeks of age. These changes are accompanied by intraneuronal protein inclusions and extensive neurodegeneration in the cortex of *Psmc1*$^{fl/fl}$*;CaMKIIα-Cre* mice (Bedford et al., 2008). These findings suggest that increased P-Akt expression and/or activity following 26S proteasome dysfunction may be involved in neuroprotection against p53, indicated by the inverse relationship between levels of P-Akt and p53. As p53 can negatively regulates the Akt pathway by inducing the expression of p53-target genes PTEN, which led to shut down Akt pathway and decrease activation of Akt (Feng et al., 2007). Increased PTEN levels degrades PIP3 to PIP2 and diminishes the function of PIP3 in the activation of PDK-

1 and mTORC2 and inhibits the activity of Akt (Feng, 2010). On the other hand, The Akt can phosphorylate and activates MDM2 which can decrease p53 levels and activity (Zhou et al., 2001). This is the feedback loop in the p53–Akt pathway that can regulates p53 activity after stress, and higher levels of p53 to an apoptotic response.

Increased activity of the PI3K/Akt pathway in late-stage AD was significantly correlated with decreased autophagy and increased amounts of Aβ deposition (Tramutola et al., 2015). A recent study from our lab showed that short-term 26S proteasome dysfunction activates autophagy, but continued dysfunction in neurons leads to impaired autophagy and cell death (Ugun-Klusek et al., 2017).

Immunohistochemical studies of the AU and SS cortical areas were also carried out at 4 and 6 weeks of age in *Psmc1*$^{fl/fl}$*;CaMKIIa-Cre* mice. Morphometric analysis of the cortex and neurons may provide a better understanding of the pathogenesis of degenerative diseases (Ihara et al., 2010, Iacono et al., 2009, Iacono et al., 2008, Everall et al., 1997, Bussiere et al., 2003, Bundgaard et al., 2001). Neurodegeneration in our model was associated with decreased cortical thickness and neuronal number. Furthermore, we observed increased nuclear size, length of apical dendrites and dendritic arborisation in layers III and V of the *Psmc1*$^{fl/fl}$*;CaMKIIa-Cre* cortices.

Increased apical dendrite length and dendritic arborisation of pyramidal neurons were evident at both 4 and 6 weeks-old following 26S proteasomal dysfunction by NFH and NFL immunostaining. At this stage it is unclear whether the increased NFs have a beneficial or detrimental in the progression of neurodegeneration following disruption of the 26S proteasome. The ratio between the three NF subunits has been implicated in the growth of complex dendritic trees in motor neurons (Kong and Xu, 2000). Studies also suggest that increased P-Akt expression can lead to increased axonal branching and soma size in primary sensory neurons via activation of mTOR (Grider et al.,

2009). In addition, increased P-Akt can promote neurite outgrowth and enhanced dendritic branching in cultured hippocampal mature neurons (Jaworski et al., 2005). Thus, the increase in P-Akt may be involved in promoting neural cell protection and repair following 26S proteasome dysfunction. Therefore, further investigations of Akt activity are needed to elucidate its role in the brain in this context.

Increased nuclear size could be an early response to neuronal defects or Ub accumulation following 26S proteasome dysfunction in the cortical neurons. Increased nuclear size of neurons has been described as a compensatory mechanism to allow neurons to function normally despite the presence of AD lesions (Riudavets et al., 2007). It is also possible that nuclear hypertrophy may reflect cytoskeleton changes or abnormalities in the transport between the nucleus and cytoplasm (Sheffield et al., 2006).

Cortical thickness was used as a very important morphological feature in assessing disease stage, identifying dementia and cognitive impairment in PD patients (Zarei et al., 2013). The greater rate of cortical thinning evident in the late age group associated with neurodegeneration and spatial memory deficits. However, the accumulation of ubiquitinated proteins in neurones may lead to the space-occupying and effects the cortical thickness different between control and 26S proteasome depleted cortical tissue. Interestingly, neuronal number in layer III and V were dramatically decreased. Taken together, loss neuronal brain tissue could be induced by 26S proteasomal dysfunction in cortical neurons.

6.2 Conclusion

Our study has provided novel information about the role of the 26S proteasome in the mechanisms of neurodegenerative disease. Increased neurofilament expression is an early event in neurodegeneration caused by 26S proteasome dysfunction,

occurring ahead of changes in microtubules. Dysfunction of proteasomal degradation and changes in cytoskeletal proteins are both important hypotheses in neurodegenerative disease and this study has provided a potential novel insight into a connection between these processes.

Summery to cytoskeletal proteins and microtubule stability change following 26S proteasome dysfunction in mouse brain cortical neurons

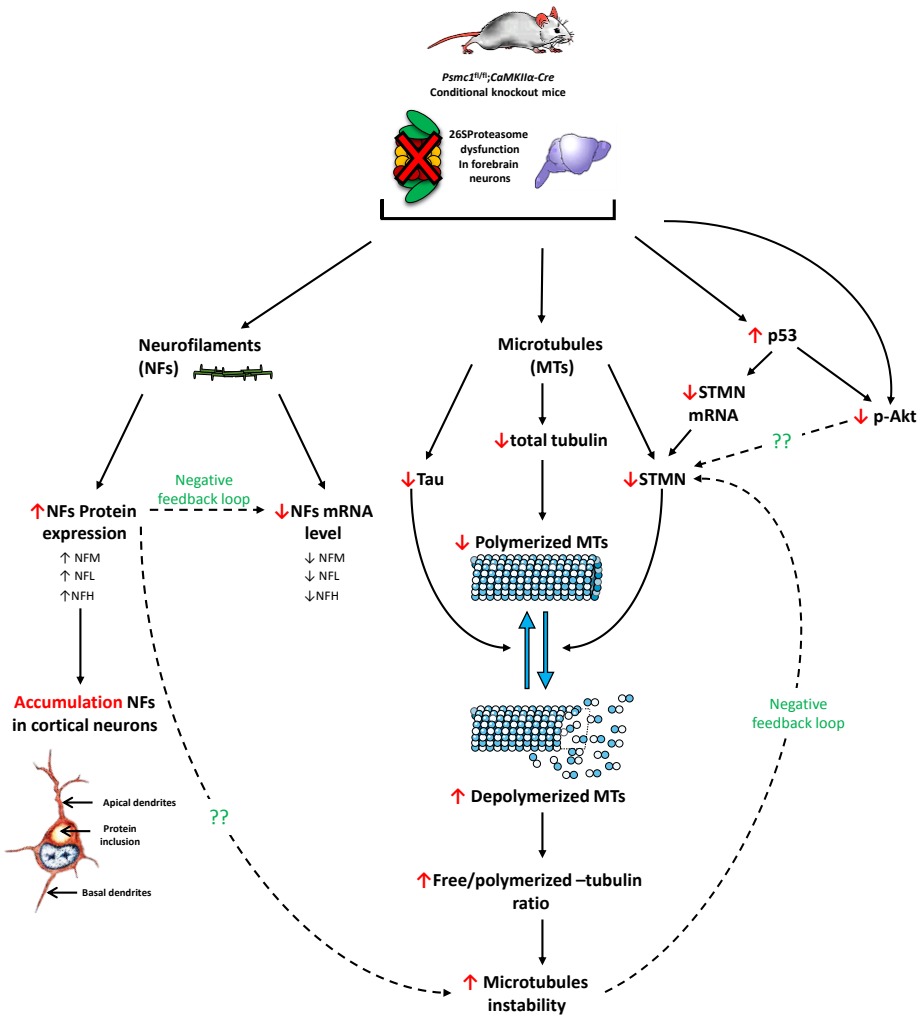


Figure 6.1 Schematic representation summering the main changes in cytoskeletal proteins and microtubule stability in *Psmc1*$^{fl/fl}$*;CaMKIIα*-Cre cortical neurons

6.3 Future work

Immunohistochemical studies in this work found several morphological changes in *Psmc1*$^{fl/fl}$*;CaMKIIα-Cre* cortical neurons compared to controls. In this work we focused on nuclear size, apical dendrite length and arborisation in the AU and SS cortical

areas. Further investigations would involve axonal morphological changes. The oval-shaped axonal swelling was noted in 50 µm brain cryosections from *Psmc1*$^{fl/fl}$*;CaMKIIα-Cre* and *Psmc1*$^{fl/fl}$*;CaMKIIα-Cre*-YFP mice, but staining method were not reliable to continue these studies (Figure 6.2).

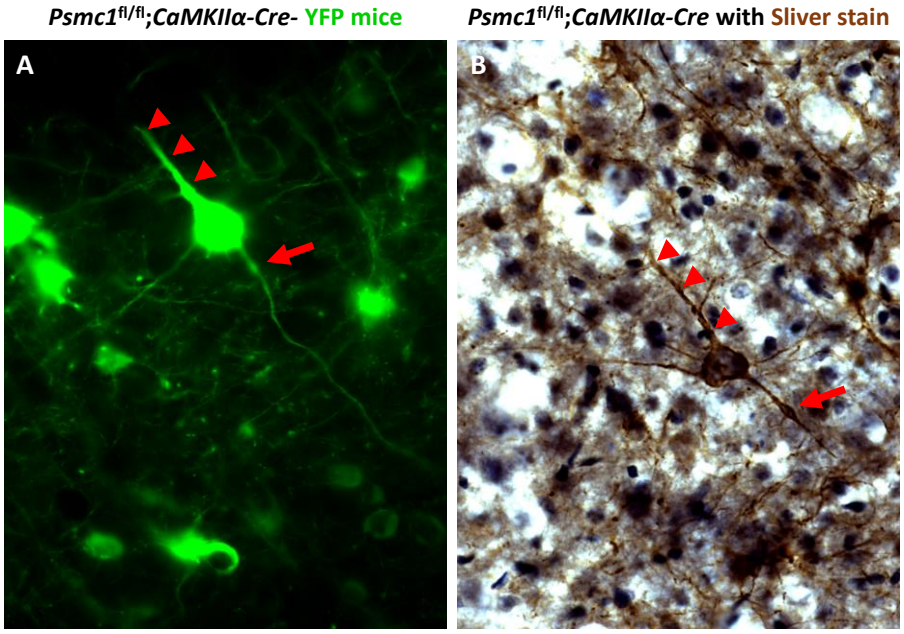


Figure 6.2 Oval-shaped axonal swelling in *Psmc1*$^{fl/fl}$*;CaMKIIα*-Cre cortical neurons.

Representative image showing SS cortical neurons with oval-shaped axonal swelling (Arrow) in 6 weeks-old 50 µm cryosections from *Psmc1*$^{fl/fl}$*;CaMKIIα-Cre*-YFP (A) and *Psmc1*$^{fl/fl}$*;CaMKIIα*-Cre (B) mice using fluorescent microscopy and silver staining respectively. Arrowheads indicate apical dendrites of targeted cortical neurons.

Golgi staining is an inexpensive method to provide reliable high-quality staining of neurons for morphometric analyses and has been used to investigate cell morphology changes in models of neurodegeneration (Bayram-Weston et al., 2016). Future work using this stain would provide a more detailed map of the morphological changes in *Psmc1*$^{fl/fl}$*;CaMKIIα-Cre* cortical neurons.

It will be important to carry out investigations of the molecular mechanisms of axonal transport and its regulation in different parts of the cortical neurons in *Psmc1*$^{fl/fl}$*;CaMKIIα-Cre* mice. This will help to understand the cell biology and biochemistry of

transport in degenerating neurons. An understanding of axonal transport is critical in identifying novel molecular targets for therapeutic development in treating these disorders (Liu et al., 2017).

Investigations into how the changes in neurofilament levels and distribution in neurons affect conduction velocity and contribute to signal integration in postsynaptic neurons and circuit function would be interesting. Electrophysiological recordings of anti-dromic and ortho-dromic latencies in response to pretectum (Pt) stimulation in *Psmc1*$^{fl/fl}$*;CaMKIIa-Cre* mice cortical neurons would further the study.

Further investigations into the consequences of increased P-Akt levels and, more so, PI3K/Akt activity in mouse brain are necessary to understand the molecular mechanisms following 26S proteasome dysfunction. As the PI3K/Akt/GSK-3β pathway has been shown to play a pivotal role in neuroprotection, enhancing cell survival by stimulating cell proliferation and inhibiting apoptosis (Kitagishi et al., 2014).

Bibliography

ABAL, M., KERYER, G. & BORNENS, M. 2005. Centrioles resist forces applied on centrosomes during G2/M transition. *Biol Cell,* 97**,** 425-34.

ABBOTT, D. W., YANG, Y., HUTTI, J. E., MADHAVARAPU, S., KELLIHER, M. A. & CANTLEY, L. C. 2007. Coordinated regulation of Toll-like receptor and NOD2 signaling by K63-linked polyubiquitin chains. *Mol Cell Biol,* 27**,** 6012-25.

ABERCROMBIE, M. 1946. Estimation of nuclear population from microtome sections. *Anat Rec,* 94**,** 239-47.

ABRAHA, A., GHOSHAL, N., GAMBLIN, T. C., CRYNS, V., BERRY, R. W., KURET, J. & BINDER, L. I. 2000. C-terminal inhibition of tau assembly in vitro and in Alzheimer's disease. *J Cell Sci,* 113 Pt 21**,** 3737-45.

ADAM, M. G., MATT, S., CHRISTIAN, S., HESS-STUMPP, H., HAEGEBARTH, A., HOFMANN, T. G. & ALGIRE, C. 2015. SIAH ubiquitin ligases regulate breast cancer cell migration and invasion independent of the oxygen status. *Cell Cycle,* 14**,** 3734-47.

ADAMS, P. D., LI, X., SELLERS, W. R., BAKER, K. B., LENG, X., HARPER, J. W., TAYA, Y. & KAELIN, W. G., JR. 1999. Retinoblastoma protein contains a C-terminal motif that targets it for phosphorylation by cyclin-cdk complexes. *Mol Cell Biol,* 19**,** 1068-80.

AKELLA, J. S., WLOGA, D., KIM, J., STAROSTINA, N. G., LYONS-ABBOTT, S., MORRISSETTE, N. S., DOUGAN, S. T., KIPREOS, E. T. & GAERTIG, J. 2010. MEC-17 is an alpha-tubulin acetyltransferase. *Nature,* 467**,** 218-22.

AKHMANOVA, A. & STEINMETZ, M. O. 2008. Tracking the ends: a dynamic protein network controls the fate of microtubule tips. *Nat Rev Mol Cell Biol,* 9**,** 309-22.

AL-BASSAM, J. & CHANG, F. 2011. Regulation of microtubule dynamics by TOG-domain proteins XMAP215/Dis1 and CLASP. *Trends Cell Biol,* 21**,** 604-14.

AL-BASSAM, J., OZER, R. S., SAFER, D., HALPAIN, S. & MILLIGAN, R. A. 2002. MAP2 and tau bind longitudinally along the outer ridges of microtubule protofilaments. *J Cell Biol,* 157**,** 1187-96.

ALEYASIN, H., ROUSSEAUX, M. W., MARCOGLIESE, P. C., HEWITT, S. J., IRRCHER, I., JOSELIN, A. P., PARSANEJAD, M., KIM, R. H., RIZZU, P., CALLAGHAN, S. M., SLACK, R. S., MAK, T. W. & PARK, D. S. 2010. DJ-1 protects the nigrostriatal axis from the neurotoxin MPTP by modulation of the AKT pathway. *Proc Natl Acad Sci U S A,* 107**,** 3186-91.

ALMOND, J. B. & COHEN, G. M. 2002. The proteasome: a novel target for cancer chemotherapy. *Leukemia,* 16**,** 433-43.

AMAT, J. A., FIELDS, K. L. & SCHUBART, U. K. 1991. Distribution of phosphoprotein p19 in rat brain during ontogeny: stage-specific expression in neurons and glia. *Brain Res Dev Brain Res,* 60**,** 205-18.

AN, W. G., HWANG, S. G., TREPEL, J. B. & BLAGOSKLONNY, M. V. 2000. Protease inhibitor-induced apoptosis: accumulation of wt p53, p21WAF1/CIP1, and induction of apoptosis are independent markers of proteasome inhibition. *Leukemia,* 14**,** 1276-83.

ANDERSEN, J. N., SATHYANARAYANAN, S., DI BACCO, A., CHI, A., ZHANG, T., CHEN, A. H., DOLINSKI, B., KRAUS, M., ROBERTS, B., ARTHUR, W., KLINGHOFFER, R. A., GARGANO, D., LI, L., FELDMAN, I., LYNCH, B., RUSH, J., HENDRICKSON, R. C., BLUME-JENSEN, P. & PAWELETZ, C. P. 2010. Pathway-based identification of biomarkers for targeted therapeutics: personalized oncology with PI3K pathway inhibitors. *Sci Transl Med,* 2**,** 43ra55.

ANDERSEN, S. S. 2000. Spindle assembly and the art of regulating microtubule dynamics by MAPs and stathmin/Op18. *Trends Cell Biol,* 10**,** 261-7.

ANDERSON, C. T., SHEETS, P. L., KIRITANI, T. & SHEPHERD, G. M. 2010. Sublayer-specific microcircuits of corticospinal and corticostriatal neurons in motor cortex. *Nat Neurosci,* 13**,** 739-44.

ANDRADE-MORAES, C. H., OLIVEIRA-PINTO, A. V., CASTRO-FONSECA, E., DA SILVA, C. G., GUIMARAES, D. M., SZCZUPAK, D., PARENTE-BRUNO, D. R., CARVALHO, L. R., POLICHISO, L., GOMES, B. V., OLIVEIRA, L. M., RODRIGUEZ, R. D., LEITE, R. E., FERRETTI-REBUSTINI, R. E., JACOB-FILHO, W., PASQUALUCCI, C. A., GRINBERG, L. T. & LENT, R. 2013. Cell number changes in Alzheimer's disease relate to dementia, not to plaques and tangles. *Brain,* 136**,** 3738-52.

AON, M. A. & CORTASSA, S. 2002. Coherent and robust modulation of a metabolic network by cytoskeletal organization and dynamics. *Biophys Chem,* 97**,** 213-31.

ARENDT, T., STIELER, J. T. & HOLZER, M. 2016. Tau and tauopathies. *Brain Research Bulletin,* 126**,** 238-292.

ARGARANA, C. E., BARRA, H. S. & CAPUTTO, R. 1978. Release of [14C]tyrosine from tubulinyl-[14C]tyrosine by brain extract. Separation of a carboxypeptidase from tubulin-tyrosine ligase. *Mol Cell Biochem,* 19**,** 17-21.

ARMSTRONG, R. 2012. Temporal lobe pathology in neurodegenerative disease. *a comparative study of eight disorders with special reference to the hippocampus.* Nova science.

ARREGUI, C., BUSCIGLIO, J., CACERES, A. & BARRA, H. S. 1991. Tyrosinated and detyrosinated microtubules in axonal processes of cerebellar macroneurons grown in culture. *J Neurosci Res,* 28**,** 171-81.

ARRIAGADA, P. V., GROWDON, J. H., HEDLEY-WHYTE, E. T. & HYMAN, B. T. 1992. Neurofibrillary tangles but not senile plaques parallel duration and severity of Alzheimer's disease. *Neurology,* 42**,** 631-9.

ASHER, G., TSVETKOV, P., KAHANA, C. & SHAUL, Y. 2005. A mechanism of ubiquitin-independent proteasomal

degradation of the tumor suppressors p53 and p73. *Genes Dev,* 19**,** 316-21.
ATTARDI, L. D. & JACKS, T. 1999. The role of p53 in tumour suppression: lessons from mouse models. *Cell Mol Life Sci,* 55**,** 48-63.
ATWEH, G. F. & IANCU-RUBIN, C. 2014. p27(Kip1) and STMN1: partners again? *Cell Cycle,* 13**,** 3163.
AUDEBERT, S., KOULAKOFF, A., BERWALD-NETTER, Y., GROS, F., DENOULET, P. & EDDE, B. 1994. Developmental regulation of polyglutamylated alpha- and beta-tubulin in mouse brain neurons. *J Cell Sci,* 107 (Pt 8)**,** 2313-22.
BAARS, B. J. & GAGE, N. M. 2010. Chapter 5 - The Brain. *Cognition, Brain, and Consciousness (Second Edition).* London: Academic Press.
BAAS, P. W., AHMAD, F. J., PIENKOWSKI, T. P., BROWN, A. & BLACK, M. M. 1993. Sites of microtubule stabilization for the axon. *J Neurosci,* 13**,** 2177-85.
BADHWAR, A., LERCH, J. P., HAMEL, E. & SLED, J. G. 2013. Impaired structural correlates of memory in Alzheimer's disease mice. *Neuroimage Clin,* 3**,** 290-300.
BAJIC, N., JENNER, P., BALLARD, C. G. & FRANCIS, P. T. 2012. Proteasome inhibition leads to early loss of synaptic proteins in neuronal culture. *Journal of Neural Transmission,* 119**,** 1467-1476.
BALASTIK, M., FERRAGUTI, F., PIRES-DA SILVA, A., LEE, T. H., ALVAREZ-BOLADO, G., LU, K. P. & GRUSS, P. 2008. Deficiency in ubiquitin ligase TRIM2 causes accumulation of neurofilament light chain and neurodegeneration. *Proc Natl Acad Sci U S A,* 105**,** 12016-21.
BALDASSARRE, G., BELLETTI, B., NICOLOSO, M. S., SCHIAPPACASSI, M., VECCHIONE, A., SPESSOTTO, P., MORRIONE, A., CANZONIERI, V. & COLOMBATTI, A. 2005. p27(Kip1)-stathmin interaction influences sarcoma cell migration and invasion. *Cancer Cell,* 7**,** 51-63.
BAMBURG, J. R. & BERNSTEIN, B. W. 2016. Actin dynamics and cofilin-actin rods in alzheimer`s disease. *Cytoskeleton (Hoboken),* 73**,** 477-97.
BAQUERO, M. T., HANNA, J. A., NEUMEISTER, V., CHENG, H., MOLINARO, A. M., HARRIS, L. N. & RIMM, D. L. 2012. Stathmin Expression and its Relationship to Microtubule Associated Protein Tau and Outcome in Breast Cancer. *Cancer,* 118**,** 4660-9.
BAR-NUN, S. & GLICKMAN, M. H. 2012. Proteasomal AAA-ATPases: structure and function. *Biochim Biophys Acta,* 1823**,** 67-82.
BATES, S. & VOUSDEN, K. H. 1996. p53 in signaling checkpoint arrest or apoptosis. *Curr Opin Genet Dev,* 6**,** 12-8.
BAUER, D. E., HAROUTUNIAN, V., MCCULLUMSMITH, R. E. & MEADOR-WOODRUFF, J. H. 2009. Expression of four housekeeping proteins in elderly patients with schizophrenia. *J Neural Transm (Vienna),* 116**,** 487-91.
BAYRAM-WESTON, Z., OLSEN, E., HARRISON, D. J., DUNNETT, S. B. & BROOKS, S. P. 2016. Optimising Golgi–Cox staining for

use with perfusion-fixed brain tissue validated in the zQ175 mouse model of Huntington's disease. *J Neurosci Methods,* 265**,** 81-8.

BEDFORD, L., HAY, D., DEVOY, A., PAINE, S., POWE, D. G., SETH, R., GRAY, T., TOPHAM, I., FONE, K., REZVANI, N., MEE, M., SOANE, T., LAYFIELD, R., SHEPPARD, P. W., EBENDAL, T., USOSKIN, D., LOWE, J. & MAYER, R. J. 2008. Depletion of 26S proteasomes in mouse brain neurons causes neurodegeneration and Lewy-like inclusions resembling human pale bodies. *J Neurosci,* 28**,** 8189-98.

BEDFORD, L., PAINE, S., REZVANI, N., MEE, M., LOWE, J. & MAYER, R. J. 2009. The UPS and autophagy in chronic neurodegenerative disease: six of one and half a dozen of the other--or not? *Autophagy,* 5**,** 224-7.

BEDFORD, L., PAINE, S., SHEPPARD, P. W., MAYER, R. J. & ROELOFS, J. 2010. Assembly, structure, and function of the 26S proteasome. *Trends Cell Biol,* 20**,** 391-401.

BELLETTI, B. & BALDASSARRE, G. 2011. Stathmin: a protein with many tasks. New biomarker and potential target in cancer. *Expert Opinion on Therapeutic Targets,* 15**,** 1249-1266.

BELLOUZE, S., BAILLAT, G., BUTTIGIEG, D., DE LA GRANGE, P., RABOUILLE, C. & HAASE, G. 2016. Stathmin 1/2-triggered microtubule loss mediates Golgi fragmentation in mutant SOD1 motor neurons. *Molecular Neurodegeneration,* 11**,** 43.

BELMONT, L. D. & MITCHISON, T. J. 1996. Identification of a protein that interacts with tubulin dimers and increases the catastrophe rate of microtubules. *Cell,* 84**,** 623-31.

BEN-NISSAN, G. & SHARON, M. 2014. Regulating the 20S proteasome ubiquitin-independent degradation pathway. *Biomolecules,* 4**,** 862-84.

BENARROCH, E. E. 2009. Brain iron homeostasis and neurodegenerative disease. *Neurology,* 72**,** 1436-40.

BERETTA, L., DOBRANSKY, T. & SOBEL, A. 1993. Multiple phosphorylation of stathmin. Identification of four sites phosphorylated in intact cells and in vitro by cyclic AMP-dependent protein kinase and p34cdc2. *J Biol Chem,* 268**,** 20076-84.

BERGERON, C., BERIC-MASKAREL, K., MUNTASSER, S., WEYER, L., SOMERVILLE, M. J. & PERCY, M. E. 1994. Neurofilament light and polyadenylated mRNA levels are decreased in amyotrophic lateral sclerosis motor neurons. *J Neuropathol Exp Neurol,* 53**,** 221-30.

BERTON, S., PELLIZZARI, I., FABRIS, L., D'ANDREA, S., SEGATTO, I., CANZONIERI, V., MARCONI, D., SCHIAPPACASSI, M., BENEVOL, S., GATTEI, V., COLOMBATTI, A., BELLETTI, B. & BALDASSARRE, G. 2014. Genetic characterization of p27(kip1) and stathmin in controlling cell proliferation in vivo. *Cell Cycle,* 13**,** 3100-11.

BESSON, A., GURIAN-WEST, M., CHEN, X., KELLY-SPRATT, K. S., KEMP, C. J. & ROBERTS, J. M. 2006. A pathway in quiescent cells that controls p27Kip1 stability, subcellular localization, and tumor suppression. *Genes Dev,* 20**,** 47-64.

BILLGER, M., WALLIN, M. & KARLSSON, J. O. 1988. Proteolysis of tubulin and microtubule-associated proteins 1 and 2 by calpain I and II. Difference in sensitivity of assembled and disassembled microtubules. *Cell Calcium,* 9**,** 33-44.

BILLINGSLEY, M. L. & KINCAID, R. L. 1997. Regulated phosphorylation and dephosphorylation of tau protein: effects on microtubule interaction, intracellular trafficking and neurodegeneration. *Biochemical Journal,* 323**,** 577-9.

BINLEY, K. E., NG, W. S., TRIBBLE, J. R., SONG, B. & MORGAN, J. E. 2014. Sholl analysis: A quantitative comparison of semi-automated methods. *Journal of Neuroscience Methods,* 225**,** 65-70.

BLOOM, J. & PAGANO, M. 2003. Deregulated degradation of the cdk inhibitor p27 and malignant transformation. *Semin Cancer Biol,* 13**,** 41-7.

BOCQUET, A., BERGES, R., FRANK, R., ROBERT, P., PETERSON, A. C. & EYER, J. 2009. Neurofilaments bind tubulin and modulate its polymerization. *J Neurosci,* 29**,** 11043-54.

BOEKHOORN, K., VAN DIS, V., GOEDKNEGT, E., SOBEL, A., LUCASSEN, P. J. & HOOGENRAAD, C. C. 2014. The microtubule destabilizing protein stathmin controls the transition from dividing neuronal precursors to postmitotic neurons during adult hippocampal neurogenesis. *Dev Neurobiol,* 74**,** 1226-42.

BOHM, M. R., MELKONYAN, H. & THANOS, S. 2015. Life-time expression of the proteins peroxiredoxin, beta-synuclein, PARK7/DJ-1, and stathmin in the primary visual and primary somatosensory cortices in rats. *Front Neuroanat,* 9**,** 16.

BOUCHER, D., LARCHER, J. C., GROS, F. & DENOULET, P. 1994. Polyglutamylation of tubulin as a progressive regulator of in vitro interactions between the microtubule-associated protein Tau and tubulin. *Biochemistry,* 33.

BOZULIC, L. & HEMMINGS, B. A. 2009. PIKKing on PKB: regulation of PKB activity by phosphorylation. *Curr Opin Cell Biol,* 21**,** 256-61.

BRATTON, S. B. & COHEN, G. M. 2001. Apoptotic death sensor: an organelle's alter ego? *Trends Pharmacol Sci,* 22**,** 306-15.

BRATTSAND, G., MARKLUND, U., NYLANDER, K., ROOS, G. & GULLBERG, M. 1994. Cell-cycle-regulated phosphorylation of oncoprotein 18 on Ser16, Ser25 and Ser38. *Eur J Biochem,* 220**,** 359-68.

BRAZIL, D. P., YANG, Z. Z. & HEMMINGS, B. A. 2004. Advances in protein kinase B signalling: AKTion on multiple fronts. *Trends Biochem Sci,* 29**,** 233-42.

BROWN, A., LI, Y., SLAUGHTER, T. & BLACK, M. M. 1993. Composite microtubules of the axon: quantitative analysis of tyrosinated and acetylated tubulin along individual axonal microtubules. *J Cell Sci,* 104 (Pt 2)**,** 339-52.

BROWN, A., SLAUGHTER, T. & BLACK, M. M. 1992. Newly assembled microtubules are concentrated in the proximal and distal regions of growing axons. *J Cell Biol,* 119**,** 867-82.

BROWN, S. P. & HESTRIN, S. 2009. Intracortical circuits of pyramidal neurons reflect their long-range axonal targets. *Nature,* 457**,** 1133-6.

BRUNDEN, K. R., ZHANG, B., CARROLL, J., YAO, Y., POTUZAK, J. S., HOGAN, A. M., IBA, M., JAMES, M. J., XIE, S. X., BALLATORE, C., SMITH, A. B., 3RD, LEE, V. M. & TROJANOWSKI, J. Q. 2010. Epothilone D improves microtubule density, axonal integrity, and cognition in a transgenic mouse model of tauopathy. *J Neurosci,* 30**,** 13861-6.

BRUNET, A., DATTA, S. R. & GREENBERG, M. E. 2001. Transcription-dependent and -independent control of neuronal survival by the PI3K-Akt signaling pathway. *Curr Opin Neurobiol,* 11**,** 297-305.

BUDHACHANDRA, K., BROJEN SINGH, R. K. & MENON, G. I. 2008. Microtubule dynamics regulated by stathmin. *Comput Biol Chem,* 32**,** 141-4.

BUNDGAARD, M. J., REGEUR, L., GUNDERSEN, H. J. & PAKKENBERG, B. 2001. Size of neocortical neurons in control subjects and in Alzheimer's disease. *J Anat,* 198**,** 481-9.

BUREAU, I., VON SAINT PAUL, F. & SVOBODA, K. 2006. Interdigitated paralemniscal and lemniscal pathways in the mouse barrel cortex. *PLoS Biol,* 4**,** e382.

BURGERING, B. M. T. & COFFER, P. J. 1995. Protein kinase B (c-Akt) in phosphatidylinositol-3-OH kinase signal transduction. *Nature,* 376**,** 599-602.

BUSSIERE, T., GIANNAKOPOULOS, P., BOURAS, C., PERL, D. P., MORRISON, J. H. & HOF, P. R. 2003. Progressive degeneration of nonphosphorylated neurofilament protein-enriched pyramidal neurons predicts cognitive impairment in Alzheimer's disease: stereologic analysis of prefrontal cortex area 9. *J Comp Neurol,* 463**,** 281-302.

BUTTS, B. D., HUDSON, H. R., LINSEMAN, D. A., LE, S. S., RYAN, K. R., BOUCHARD, R. J. & HEIDENREICH, K. A. 2005. Proteasome inhibition elicits a biphasic effect on neuronal apoptosis via differential regulation of pro-survival and pro-apoptotic transcription factors. *Molecular and Cellular Neuroscience,* 30**,** 279-289.

CAIRNS, N. J., LEE, V. M. Y. & TROJANOWSKI, J. Q. 2004. The cytoskeleton in neurodegenerative diseases. *J Pathol,* 204**,** 438-49.

CARDEN, M. J., TROJANOWSKI, J. Q., SCHLAEPFER, W. W. & LEE, V. M. 1987. Two-stage expression of neurofilament polypeptides during rat neurogenesis with early establishment of adult phosphorylation patterns. *J Neurosci,* 7**,** 3489-504.

CARDINALE, F., CHINNICI, G., BRAMERIO, M., MAI, R., SARTORI, I., COSSU, M., LO RUSSO, G., CASTANA, L., COLOMBO, N., CABORNI, C., DE MOMI, E. & FERRIGNO, G. 2014. Validation of FreeSurfer-estimated brain cortical thickness: comparison with histologic measurements. *Neuroinformatics,* 12**,** 535-42.

CARNEY, B. K., CARUSO SILVA, V. & CASSIMERIS, L. 2012. The microtubule cytoskeleton is required for a G2 cell cycle delay in cancer cells lacking stathmin and p53. *Cytoskeleton (Hoboken),* 69**,** 278-89.

CARNEY, B. K. & CASSIMERIS, L. 2010. Stathmin/oncoprotein 18, a microtubule regulatory protein, is required for survival of both normal and cancer cell lines lacking the tumor suppressor, p53. *Cancer Biol Ther,* 9**,** 699-709.

CARPENTIER, P. A., HADITSCH, U., BRAUN, A. E., CANTU, A. V., MOON, H. M., PRICE, R. O., ANDERSON, M. P., SARAVANAPANDIAN, V., ISMAIL, K., RIVERA, M., WEIMANN, J. M. & PALMER, T. D. 2013. Stereotypical alterations in cortical patterning are associated with maternal illness-induced placental dysfunction. *J Neurosci,* 33**,** 16874-88.

CARTELLI, D., CASAGRANDE, F., BUSCETI, C. L., BUCCI, D., MOLINARO, G., TRAFICANTE, A., PASSARELLA, D., GIAVINI, E., PEZZOLI, G., BATTAGLIA, G. & CAPPELLETTI, G. 2013. Microtubule alterations occur early in experimental parkinsonism and the microtubule stabilizer epothilone D is neuroprotective. *Sci Rep,* 3**,** 1837.

CARTELLI, D., RONCHI, C., MAGGIONI, M. G., RODIGHIERO, S., GIAVINI, E. & CAPPELLETTI, G. 2010. Microtubule dysfunction precedes transport impairment and mitochondria damage in MPP+ -induced neurodegeneration. *J Neurochem,* 115**,** 247-58.

CARTER, J., GRAGEROV, A., KONVICKA, K., ELDER, G., WEINSTEIN, H. & LAZZARINI, R. A. 1998. Neurofilament (NF) assembly; divergent characteristics of human and rodent NF-L subunits. *J Biol Chem,* 273**,** 5101-8.

CARVALHO, A. N., MARQUES, C., RODRIGUES, E., HENDERSON, C. J., WOLF, C. R., PEREIRA, P. & GAMA, M. J. 2013. Ubiquitin-Proteasome System Impairment and MPTP-Induced Oxidative Stress in the Brain of C57BL/6 Wild-type and GSTP Knockout Mice. *Molecular Neurobiology,* 47**,** 662-672.

CASH, A. D., ALIEV, G., SIEDLAK, S. L., NUNOMURA, A., FUJIOKA, H., ZHU, X., RAINA, A. K., VINTERS, H. V., TABATON, M., JOHNSON, A. B., PAULA-BARBOSA, M., AVILA, J., JONES, P. K., CASTELLANI, R. J., SMITH, M. A. & PERRY, G. 2003. Microtubule reduction in Alzheimer's disease and aging is independent of tau filament formation. *Am J Pathol,* 162**,** 1623-7.

CASSIMERIS, L. 2002. The oncoprotein 18/stathmin family of microtubule destabilizers. *Current Opinion in Cell Biology,* 14**,** 18-24.

CASSIMERIS, L. & SPITTLE, C. 2001. Regulation of microtubule-associated proteins. *Int Rev Cytol,* 210**,** 163-226.

CASTANO, Z. & KYPTA, R. M. 2008. Housekeeping Proteins: Limitations as References During Neuronal Differentiation. *The Open Neuroscience Journal,* 2**,** 36-40.

CATZAVELOS, C., BHATTACHARYA, N., UNG, Y. C., WILSON, J. A., RONCARI, L., SANDHU, C., SHAW, P., YEGER, H., MORAVA-PROTZNER, I., KAPUSTA, L., FRANSSEN, E., PRITCHARD, K.

I. & SLINGERLAND, J. M. 1997. Decreased levels of the cell-cycle inhibitor p27Kip1 protein: prognostic implications in primary breast cancer. *Nat Med,* 3**,** 227-30.
CAUDRON, F., DENARIER, E., THIBOUT-QUINTANA, J. C., BROCARD, J., ANDRIEUX, A. & FOUREST-LIEUVIN, A. 2010. Mutation of Ser172 in yeast beta tubulin induces defects in microtubule dynamics and cell division. *PLoS One,* 5**,** e13553.
CHAN, N. L. & HILL, C. P. 2001. Defining polyubiquitin chain topology. *Nat Struct Biol,* 8**,** 650-2.
CHANG, F., LEE, J. T., NAVOLANIC, P. M., STEELMAN, L. S., SHELTON, J. G., BLALOCK, W. L., FRANKLIN, R. A. & MCCUBREY, J. A. 2003. Involvement of PI3K//Akt pathway in cell cycle progression, apoptosis, and neoplastic transformation: a target for cancer chemotherapy. *Leukemia,* 17**,** 590-603.
CHANG, J. R., GHAFOURI, M., MUKERJEE, R., BAGASHEV, A., CHABRASHVILI, T. & SAWAYA, B. E. 2012. Role of p53 in Neurodegenerative Diseases. *Neurodegener Dis,* 9**,** 68-80.
CHAPIN, S. J. & BULINSKI, J. C. 1992. Microtubule stabilization by assembly-promoting microtubule-associated proteins: a repeat performance. *Cell Motil Cytoskeleton,* 23**,** 236-43.
CHARBAUT, E., CURMI, P. A., OZON, S., LACHKAR, S., REDEKER, V. & SOBEL, A. 2001. Stathmin family proteins display specific molecular and tubulin binding properties. *J Biol Chem,* 276**,** 16146-54.
CHAU, V., TOBIAS, J. W., BACHMAIR, A., MARRIOTT, D., ECKER, D. J., GONDA, D. K. & VARSHAVSKY, A. 1989. A multiubiquitin chain is confined to specific lysine in a targeted short-lived protein. *Science,* 243**,** 1576-83.
CHAUVIN, S. & SOBEL, A. 2015. Neuronal stathmins: A family of phosphoproteins cooperating for neuronal development, plasticity and regeneration. *Progress in Neurobiology,* 126**,** 1-18.
CHEN, S., LIU, Y., RONG, X., LI, Y., ZHOU, J. & LU, L. 2017. Neuroprotective rRole of the PI3 Kinase/Akt signaling pathway in zebrafish. *Front Endocrinol (Lausanne),* 8.
CHEN, X. & YIN, X. M. 2011. Coordination of autophagy and the proteasome in resolving endoplasmic reticulum stress. *Vet Pathol,* 48**,** 245-53.
CHEN, Y. L., UEN, Y. H., LI, C. F., HORNG, K. C., CHEN, L. R., WU, W. R., TSENG, H. Y., HUANG, H. Y., WU, L. C. & SHIUE, Y. L. 2013. The E2F transcription factor 1 transactives stathmin 1 in hepatocellular carcinoma. *Ann Surg Oncol,* 20**,** 4041-54.
CHEON, M. S., FOUNTOULAKIS, M., CAIRNS, N. J., DIERSSEN, M., HERKNER, K. & LUBEC, G. 2001. Decreased protein levels of stathmin in adult brains with Down syndrome and Alzheimer's disease. *J Neural Transm Suppl***,** 281-8.
CHESSER, A. S., PRITCHARD, S. M. & JOHNSON, G. V. W. 2013. Tau Clearance Mechanisms and Their Possible Role in the Pathogenesis of Alzheimer Disease. *Front Neurol,* 4.

CHO, J. H. & JOHNSON, G. V. 2003. Glycogen synthase kinase 3beta phosphorylates tau at both primed and unprimed sites. Differential impact on microtubule binding. *J Biol Chem,* 278**,** 187-93.

CHOI, W. H., DE POOT, S. A. H., LEE, J. H., KIM, J. H., HAN, D. H., KIM, Y. K., FINLEY, D. & LEE, M. J. 2016. Open-gate mutants of the mammalian proteasome show enhanced ubiquitin-conjugate. *Nat Commun,* 7.

CHONDROGIANNI, N., GEORGILA, K., KOURTIS, N., TAVERNARAKIS, N. & GONOS, E. S. 2015. 20S proteasome activation promotes life span extension and resistance to proteotoxicity in Caenorhabditis elegans. *FASEB J,* 29**,** 611-22.

CHONG, Z. Z., LI, F. & MAIESE, K. 2006. Attempted cell cycle induction in post-mitotic neurons occurs in early and late apoptotic programs through Rb, E2F1, and caspase 3. *Curr Neurovasc Res,* 3**,** 25-39.

CHONG, Z. Z., SHANG, Y. C., WANG, S. & MAIESE, K. 2012. A critical kinase cascade in neurological disorders: PI 3-K, Akt, and mTOR. *Future Neurol,* 7**,** 733-48.

CHOW, K. L. & LEIMAN, A. L. 1970. Aspects of the structural and functional organization of the neocortex. *Neurosci Res Program Bull,* 8**,** 157-220.

CHU, C. W., HOU, F., ZHANG, J., PHU, L., LOKTEV, A. V., KIRKPATRICK, D. S., JACKSON, P. K., ZHAO, Y. & ZOU, H. 2011. A novel acetylation of beta-tubulin by San modulates microtubule polymerization via down-regulating tubulin incorporation. *Mol Biol Cell,* 22**,** 448-56.

CHU, I. M., HENGST, L. & SLINGERLAND, J. M. 2008. The Cdk inhibitor p27 in human cancer: prognostic potential and relevance to anticancer therapy. *Nat Rev Cancer,* 8**,** 253-267.

CHU, Z., GALARRETA, M. & HESTRIN, S. 2003. Synaptic interactions of late-spiking neocortical neurons in layer 1. *J Neurosci,* 23**,** 96-102.

CICHON, J., SUN, C., CHEN, B., JIANG, M., CHEN, X. A., SUN, Y., WANG, Y. & CHEN, G. 2012. Cofilin aggregation blocks intracellular trafficking and induces synaptic loss in hippocampal neurons. *J Biol Chem,* 287**,** 3919-29.

CIECHANOVER, A. 2005. Intracellular protein degradation: from a vague idea thru the lysosome and the ubiquitin-proteasome system and onto human diseases and drug targeting. *Cell Death Differ,* 12**,** 1178-90.

CIECHANOVER, A. 2013. Intracellular protein degradation: from a vague idea through the lysosome and the ubiquitin-proteasome system and onto human diseases and drug targeting. *Bioorg Med Chem,* 21**,** 3400-10.

CIECHANOVER, A. & BRUNDIN, P. 2003. The ubiquitin proteasome system in neurodegenerative diseases: sometimes the chicken, sometimes the egg. *Neuron,* 40**,** 427-46.

CIECHANOVER, A. & KWON, Y. T. 2015. Degradation of misfolded proteins in neurodegenerative diseases: therapeutic targets and strategies. *Exp Mol Med,* 47**,** e147-.
CIECHANOVER, A. & SCHWARTZ, A. L. 1998. The ubiquitin-proteasome pathway: the complexity and myriad functions of proteins death. *Proc Natl Acad Sci U S A,* 95**,** 2727-30.
CIFUENTES-DIAZ, C., NICOLE, S., VELASCO, M. E., BORRA-CEBRIAN, C., PANOZZO, C., FRUGIER, T., MILLET, G., ROBLOT, N., JOSHI, V. & MELKI, J. 2002. Neurofilament accumulation at the motor endplate and lack of axonal sprouting in a spinal muscular atrophy mouse model. *Hum Mol Genet,* 11**,** 1439-47.
CIPELLETTI, B., AVANZINI, G., VITELLARO-ZUCCARELLO, L., FRANCESCHETTI, S., SANCINI, G., LAVAZZA, T., ACAMPORA, D., SIMEONE, A., SPREAFICO, R. & FRASSONI, C. 2002. Morphological organization of somatosensory cortex in Otx1(-/-) mice. *Neuroscience,* 115**,** 657-67.
CLEMENT, M. J., JOURDAIN, I., LACHKAR, S., SAVARIN, P., GIGANT, B., KNOSSOW, M., TOMA, F., SOBEL, A. & CURMI, P. A. 2005. N-terminal stathmin-like peptides bind tubulin and impede microtubule assembly. *Biochemistry,* 44**,** 14616-25.
CLEVELAND, D. W., LOPATA, M. A., SHERLINE, P. & KIRSCHNER, M. W. 1981. Unpolymerized tubulin modulates the level of tubulin mRNAs. *Cell,* 25**,** 537-46.
CLEVELAND, D. W., PITTENGER, M. F. & FERAMISCO, J. R. 1983. Elevation of tubulin levels by microinjection suppresses new tubulin synthesis. *Nature,* 305**,** 738-40.
COATS, S., FLANAGAN, W. M., NOURSE, J. & ROBERTS, J. M. 1996. Requirement of p27Kip1 for restriction point control of the fibroblast cell cycle. *Science,* 272**,** 877-80.
COLLARD, J. F., COTE, F. & JULIEN, J. P. 1995. Defective axonal transport in a transgenic mouse model of amyotrophic lateral sclerosis. *Nature,* 375**,** 61-4.
CONNORS, B. W. & GUTNICK, M. J. 1990. Intrinsic firing patterns of diverse neocortical neurons. *Trends Neurosci,* 13**,** 99-104.
COPP, J., MANNING, G. & HUNTER, T. 2009. TORC-specific phosphorylation of mTOR: phospho-Ser2481 is a marker for intact mTORC2. *Cancer Res,* 69**,** 1821-7.
COUILLARD-DESPRÉS, S., MEIER, J. & JULIEN, J.-P. 2000. Extra axonal neurofilaments do not exacerbate disease caused by mutant Cu,Zn superoxide dismutase. *Neurobiology of Disease,* 7**,** 462-470.
CROWDER, R. J. & FREEMAN, R. S. 1998. Phosphatidylinositol 3-kinase and Akt protein kinase are necessary and sufficient for the survival of nerve growth factor-dependent sympathetic neurons. *J Neurosci,* 18**,** 2933-43.
CUANALO-CONTRERAS, K., MUKHERJEE, A. & SOTO, C. 2013. Role of protein misfolding and proteostasis deficiency in protein misfolding diseases and aging. *Int J Cell Biol,* 2013**,** 638083.
CUBELOS, B., SEBASTIAN-SERRANO, A., BECCARI, L., CALCAGNOTTO, M. E., CISNEROS, E., KIM, S., DOPAZO, A.,

ALVAREZ-DOLADO, M., REDONDO, J. M., BOVOLENTA, P., WALSH, C. A. & NIETO, M. 2010. Cux1 and Cux2 regulate dendritic branching, spine morphology, and synapses of the upper layer neurons of the cortex. *Neuron,* 66**,** 523-35.

CUNNINGHAM, J. J., LEVINE, E. M., ZINDY, F., GOLOUBEVA, O., ROUSSEL, M. F. & SMEYNE, R. J. 2002. The cyclin-dependent kinase inhibitors p19(Ink4d) and p27(Kip1) are coexpressed in select retinal cells and act cooperatively to control cell cycle exit. *Mol Cell Neurosci,* 19**,** 359-74.

D'ANDREA, M. R., ILYIN, S. & PLATA-SALAMAN, C. R. 2001. Abnormal patterns of microtubule-associated protein-2 (MAP-2) immunolabeling in neuronal nuclei and Lewy bodies in Parkinson's disease substantia nigra brain tissues. *Neurosci Lett,* 306**,** 137-40.

DAHLMANN, B. 2005. Proteasomes. *Essays Biochem,* 41**,** 31-48.

DAI, C. & GU, W. 2010. p53 post-translational modification: deregulated in tumorigenesis. *Trends Mol Med,* 16**,** 528-36.

DALE, J. M. & GARCIA, M. L. 2012. Neurofilament phosphorylation during development and disease: which came first, the phosphorylation or the accumulation? *J Amino Acids,* 2012**,** 382107.

DATTA, S. R., DUDEK, H., TAO, X., MASTERS, S., FU, H., GOTOH, Y. & GREENBERG, M. E. 1997. Akt phosphorylation of BAD couples survival signals to the cell-intrinsic death machinery. *Cell,* 91**,** 231-41.

DAVID, D. C., LAYFIELD, R., SERPELL, L., NARAIN, Y., GOEDERT, M. & SPILLANTINI, M. G. 2002. Proteasomal degradation of tau protein. *Journal of Neurochemistry,* 83**,** 176-185.

DE BLAS, A. L., VITORICA, J. & FRIEDRICH, P. 1988. Localization of the GABAA receptor in the rat brain with a monoclonal antibody to the 57,000 Mr peptide of the GABAA receptor/benzodiazepine receptor/Cl- channel complex. *J Neurosci,* 8**,** 602-14.

DE FORGES, H., BOUISSOU, A. & PEREZ, F. 2012. Interplay between microtubule dynamics and intracellular organization. *Int J Biochem Cell Biol,* 44**,** 266-74.

DEFELIPE, J. & FARIÑAS, I. 1992. The pyramidal neuron of the cerebral cortex: Morphological and chemical characteristics of the synaptic inputs. *Progress in Neurobiology,* 39**,** 563-607.

DEHMELT, L. & HALPAIN, S. 2005. The MAP2/Tau family of microtubule-associated proteins. *Genome Biol,* 6**,** 204.

DEL PESO, L., GONZALEZ-GARCIA, M., PAGE, C., HERRERA, R. & NUNEZ, G. 1997. Interleukin-3-induced phosphorylation of BAD through the protein kinase Akt. *Science,* 278**,** 687-9.

DESAI, A. & MITCHISON, T. J. 1997. Microtubule polymerization dynamics. *Annu Rev Cell Dev Biol,* 13**,** 83-117.

DI PAOLO, G., ANTONSSON, B., KASSEL, D., RIEDERER, B. M. & GRENNINGLOH, G. 1997. Phosphorylation regulates the microtubule-destabilizing activity of stathmin and its interaction with tubulin. *FEBS Lett,* 416**,** 149-52.

DING, W. X., NI, H. M., CHEN, X., YU, J., ZHANG, L. & YIN, X. M. 2007. A coordinated action of Bax, PUMA, and p53 promotes MG132-induced mitochondria activation and apoptosis in colon cancer cells. *Mol Cancer Ther,* 6**,** 1062-9.

DITTMER, A. & DITTMER, J. 2006. Beta-actin is not a reliable loading control in Western blot analysis. *Electrophoresis,* 27**,** 2844-5.

DOMPIERRE, J. P., GODIN, J. D., CHARRIN, B. C., CORDELIERES, F. P., KING, S. J., HUMBERT, S. & SAUDOU, F. 2007. Histone deacetylase 6 inhibition compensates for the transport deficit in Huntington's disease by increasing tubulin acetylation. *J Neurosci,* 27**,** 3571-83.

DOS REMEDIOS, C. G., CHHABRA, D., KEKIC, M., DEDOVA, I. V., TSUBAKIHARA, M., BERRY, D. A. & NOSWORTHY, N. J. 2003. Actin binding proteins: regulation of cytoskeletal microfilaments. *Physiol Rev,* 83**,** 433-73.

DOUBLE, K. L., HALLIDAY, G. M., MCRITCHIE, D. A., REID, W. G., HELY, M. A. & MORRIS, J. G. 1996. Regional brain atrophy in idiopathic Parkinson's disease and diffuse Lewy body disease. *Dementia,* 7**,** 304-13.

DRECHSEL, D. N., HYMAN, A. A., COBB, M. H. & KIRSCHNER, M. W. 1992. Modulation of the dynamic instability of tubulin assembly by the microtubule-associated protein tau. *Molecular Biology of the Cell,* 3**,** 1141-1154.

DREWES, G., EBNETH, A. & MANDELKOW, E. M. 1998. MAPs, MARKs and microtubule dynamics. *Trends Biochem Sci,* 23**,** 307-11.

DREWES, G., TRINCZEK, B., ILLENBERGER, S., BIERNAT, J., SCHMITT-ULMS, G., MEYER, H. E., MANDELKOW, E. M. & MANDELKOW, E. 1995. Microtubule-associated protein/microtubule affinity-regulating kinase (p110mark). A novel protein kinase that regulates tau-microtubule interactions and dynamic instability by phosphorylation at the Alzheimer-specific site serine 262. *J Biol Chem,* 270**,** 7679-88.

DRISCOLL, I. & TRONCOSO, J. 2011. Asymptomatic Alzheimer's disease: a prodrome or a state of resilience? *Curr Alzheimer Res,* 8**,** 330-5.

DUBEY, J., RATNAKARAN, N. & KOUSHIKA, S. P. 2015. Neurodegeneration and microtubule dynamics: death by a thousand cuts. *Front Cell Neurosci,* 9**,** 343.

DUNCAN, J. E., LYTLE, N. K., ZUNIGA, A. & GOLDSTEIN, L. S. B. 2013. The microtubule regulatory protein stathmin is required to maintain the integrity of axonal microtubules in Drosophila. *Plos One,* 8**,** e68324. .

DURONIO, V. 2008. The life of a cell: apoptosis regulation by the PI3K/PKB pathway. *Biochem J,* 415**,** 333-44.

EASTON, R. M., CHO, H., ROOVERS, K., SHINEMAN, D. W., MIZRAHI, M. & FORMAN, M. S. 2005. Role for Akt3/protein kinase Bgamma in attainment of normal brain size. *Mol Cell Biol,* 25**,** 1869–1878.

EATON, S. L., HURTADO, M. L., OLDKNOW, K. J., GRAHAM, L. C., MARCHANT, T. W., GILLINGWATER, T. H., FARQUHARSON, C. & WISHART, T. M. 2014. A guide tomodern quantitative fluorescent western blotting with troubleshooting strategies. *J Vis Exp***,** 52099.

EATON, S. L., ROCHE, S. L., LLAVERO HURTADO, M., OLDKNOW, K. J., FARQUHARSON, C., GILLINGWATER, T. H. & WISHART, T. M. 2013. Total protein analysis as a reliable loading control for quantitative fluorescent western blotting. *PLoS One,* 8**,** e72457.

EDDE, B., ROSSIER, J., CAER, J. P., DESBRUYERES, E., GROS, F. & DENOULET, P. 1990. Posttranslational glutamylation of alpha-tubulin. *Science,* 247**,** 83-85.

ELDER, G. A., FRIEDRICH, V. L., JR., BOSCO, P., KANG, C., GOUROV, A., TU, P. H., LEE, V. M. & LAZZARINI, R. A. 1998. Absence of the mid-sized neurofilament subunit decreases axonal calibers, levels of light neurofilament (NF-L), and neurofilament content. *J Cell Biol,* 141**,** 727-39.

ELKHARAZ, J., UGUN-KLUSEK, A., CONSTANTIN-TEODOSIU, D., LAWLER, K., MAYER, R. J., BILLETT, E., LOWE, J. & BEDFORD, L. 2013. Implications for oxidative stress and astrocytes following 26S proteasomal depletion in mouse forebrain neurones. *Biochim Biophys Acta,* 1832**,** 1930-8.

ELLEDGE, S. J. & HARPER, J. W. 1994. Cdk inhibitors: on the threshold of checkpoints and development. *Curr Opin Cell Biol,* 6**,** 847-52.

ELMORE, S. 2007. Apoptosis: a review of programmed cell death. *Toxicol Pathol,* 35**,** 495-516.

ERCK, C., PERIS, L., ANDRIEUX, A., MEISSIREL, C., GRUBER, A. D., VERNET, M., SCHWEITZER, A., SAOUDI, Y., POINTU, H., BOSC, C., SALIN, P. A., JOB, D. & WEHLAND, J. 2005. A vital role of tubulin-tyrosine-ligase for neuronal organization. *Proc Natl Acad Sci U S A,* 102**,** 7853-8.

ERIKSSON, P. S., PERFILIEVA, E., BJORK-ERIKSSON, T., ALBORN, A. M., NORDBORG, C., PETERSON, D. A. & GAGE, F. H. 1998. Neurogenesis in the adult human hippocampus. *Nat Med,* 4**,** 1313-7.

ERSFELD, K., WEHLAND, J., PLESSMANN, U., DODEMONT, H., GERKE, V. & WEBER, K. 1993. Characterization of the tubulin-tyrosine ligase. *J Cell Biol,* 120**,** 725-32.

EVERALL, I. P., DETERESA, R., TERRY, R. & MASLIAH, E. 1997. Comparison of two quantitative methods for the evaluation of neuronal number in the frontal cortex in Alzheimer`s disease. *J Neuropathol Exp Neurol,* 56**,** 1202-6.

FANARA, P., BANERJEE, J., HUECK, R. V., HARPER, M. R., AWADA, M., TURNER, H., HUSTED, K. H., BRANDT, R. & HELLERSTEIN, M. K. 2007. Stabilization of hyperdynamic microtubules is neuroprotective in amyotrophic lateral sclerosis. *J Biol Chem,* 282**,** 23465-72.

FANG, L., MIN, L., LIN, Y., PING, G., RUI, W., YING, Z., XI, W., TING, H., LI, L., KE, D., JIHONG, R. & HUIZHONG, Z. 2010. Downregulation of stathmin expression is mediated directly

by Egr1 and associated with p53 activity in lung cancer cell line A549. *Cell Signal,* 22**,** 166-73.
FARAH, C. A. & LECLERC, N. 2008. HMWMAP2: new perspectives on a pathway to dendritic identity. *Cell Motil Cytoskeleton,* 65**,** 515-27.
FAYARD, E., XUE, G., PARCELLIER, A., BOZULIC, L. & HEMMINGS, B. A. 2010. Protein kinase B (PKB/Akt), a key mediator of the PI3K signaling pathway. *Curr Top Microbiol Immunol,* 346**,** 31-56.
FENG, Z. 2010. p53 regulation of the IGF-1/AKT/mTOR pathways and the endosomal compartment. *Cold Spring Harb Perspect Biol,* 2**,** 001057.
FENG, Z., HU, W., DE STANCHINA, E., TERESKY, A. K., JIN, S., LOWE, S. & LEVINE, A. J. 2007. The regulation of AMPK beta1, TSC2, and PTEN expression by p53: stress, cell and tissue specificity, and the role of these gene products in modulating the IGF-1-AKT-mTOR pathways. *Cancer Res,* 67**,** 3043-53.
FENG, Z., JIN, S., ZUPNICK, A., HOH, J., DE STANCHINA, E., LOWE, S., PRIVES, C. & LEVINE, A. J. 2006. p53 tumor suppressor protein regulates the levels of huntingtin gene expression. *Oncogene,* 25**,** 1-7.
FERGUSON, R. E., CARROLL, H. P., HARRIS, A., MAHER, E. R., SELBY, P. J. & BANKS, R. E. 2005. Housekeeping proteins: a preliminary study illustrating some limitations as useful references in protein expression studies. *Proteomics,* 5**,** 566-71.
FERO, M. L., RIVKIN, M., TASCH, M., PORTER, P., CAROW, C. E., FIRPO, E., POLYAK, K., TSAI, L.-H., BROUDY, V., PERLMUTTER, R. M., KAUSHANSKY, K. & ROBERTS, J. M. 1996. A syndrome of multiorgan hyperplasia with features of gigantism, tumorigenesis, and female sterility in p27-deficient Mice. *Cell,* 85**,** 733-744.
FERRALLI, J., DOLL, T. & MATUS, A. 1994. Sequence analysis of MAP2 function in living cells. *J Cell Sci,* 107 (Pt 11)**,** 3115-25.
FIFKOVA, E. & MORALES, M. 1992. Actin matrix of dendritic spines, synaptic plasticity, and long-term potentiation. *Int Rev Cytol,* 139**,** 267-307.
FIFRE, A., SPONNE, I., KOZIEL, V., KRIEM, B., YEN POTIN, F. T., BIHAIN, B. E., OLIVIER, J. L., OSTER, T. & PILLOT, T. 2006. Microtubule-associated protein MAP1A, MAP1B, and MAP2 proteolysis during soluble amyloid beta-peptide-induced neuronal apoptosis. Synergistic involvement of calpain and caspase-3. *J Biol Chem,* 281**,** 229-40.
FLETCHER, P. D., DOWNEY, L. E., GOLDEN, H. L., CLARK, C. N., SLATTERY, C. F., PATERSON, R. W., SCHOTT, J. M., ROHRER, J. D., ROSSOR, M. N. & WARREN, J. D. 2015. Auditory hedonic phenotypes in dementia: A behavioural and neuroanatomical analysis. *Cortex,* 67**,** 95-105.
FORTEA, J., SALA-LLONCH, R., BARTRES-FAZ, D., BOSCH, B., LLADO, A., BARGALLO, N., MOLINUEVO, J. L. & SANCHEZ-

VALLE, R. 2010. Increased cortical thickness and caudate volume precede atrophy in PSEN1 mutation carriers. *J Alzheimers Dis,* 22**,** 909-22.
FOUREST-LIEUVIN, A., PERIS, L., GACHE, V., GARCIA-SAEZ, I., JUILLAN-BINARD, C., LANTEZ, V. & JOB, D. 2006. Microtubule regulation in mitosis: tubulin phosphorylation by the cyclin-dependent kinase Cdk1. *Mol Biol Cell,* 17**,** 1041-50.
FOURNIER, A. J., HOGAN, J. D., RAJBHANDARI, L., SHRESTHA, S., VENKATESAN, A. & RAMESH, K. T. 2015. Changes in neurofilament and microtubule distribution following focal axon compression. *PLoS One,* 10**,** e0131617.
FRANKE, T. F., KAPLAN, D. R. & CANTLEY, L. C. 1997. PI3K: downstream AKTion blocks apoptosis. *Cell,* 88**,** 435-437.
FRANKE, T. F., YANG, S. I., CHAN, T. O., DATTA, K., KAZLAUSKAS, A., MORRISON, D. K., KAPLAN, D. R. & TSICHLIS, P. N. 1995. The protein kinase encoded by the Akt proto-oncogene is a target of the PDGF-activated phosphatidylinositol 3-kinase. *Cell,* 81**,** 727-36.
FRANKER, M. A. M. & HOOGENRAAD, C. C. 2013. Microtubule-based transport -basic mechanisms, traffic rules and role in neurological pathogenesis. *Journal of Cell Science,* 126**,** 2319-2329.
FRIDMAN, J. S. & LOWE, S. W. 2003. Control of apoptosis by p53. *Oncogene,* 22**,** 9030-9040.
FRIEDE, R. L. & SAMORAJSKI, T. 1970. Axon caliber related to neurofilaments and microtubules in sciatic nerve fibers of rats and mice. *The Anatomical Record,* 167**,** 379-387.
FRIEDMANN, D. R., AGUILAR, A., FAN, J., NACHURY, M. V. & MARMORSTEIN, R. 2012. Structure of the α-tubulin acetyltransferase, αTAT1, and implications for tubulin-specific acetylation. *Proceedings of the National Academy of Sciences,* 109**,** 19655-19660.
FRIEDRICH, P. & ASZODI, A. 1991. MAP2: a sensitive cross-linker and adjustable spacer in dendritic architecture. *FEBS Lett,* 295**,** 5-9.
FROST, D. O. & CAVINESS, V. S., JR. 1980. Radial organization of thalamic projections to the neocortex in the mouse. *J Comp Neurol,* 194**,** 369-93.
FUJITA, N., SATO, S. & TSURUO, T. 2003. Phosphorylation of p27Kip1 at threonine 198 by p90 ribosomal protein S6 kinases promotes its binding to 14-3-3 and cytoplasmic localization. *J Biol Chem,* 278**,** 49254-60.
FUKUSHIMA, N., FURUTA, D., HIDAKA, Y., MORIYAMA, R. & TSUJIUCHI, T. 2009. Post-translational modifications of tubulin in the nervous system. *J Neurochem,* 109**,** 683-93.
FULGA, T. A., ELSON-SCHWAB, I., KHURANA, V., STEINHILB, M. L., SPIRES, T. L., HYMAN, B. T. & FEANY, M. B. 2007. Abnormal bundling and accumulation of F-actin mediates tau-induced neuronal degeneration in vivo. *Nat Cell Biol,* 9**,** 139-48.

FULLER, H. R., MANDEFRO, B., SHIRRAN, S. L., GROSS, A. R., KAUS, A. S., BOTTING, C. H., MORRIS, G. E. & SAREEN, D. 2015. Spinal muscular atrophy patient iPSC-derived motor neurons have reduced expression of proteins important in neuronal development. *Front Cell Neurosci,* 9**,** 506.

GAGYI, E., KORMOS, B., CASTELLANOS, K. J., VALYI-NAGY, K., KORNEFF, D., LOPRESTI, P., WOLTJER, R. & VALYI-NAGY, T. 2012. Decreased oligodendrocyte nuclear diameter in Alzheimer's disease and Lewy body dementia. *Brain Pathol,* 22**,** 803-10.

GAO, Y. H., ZHANG, H. P., YANG, S. M., YANG, Y., MA, Y. Y., ZHANG, X. Y. & YANG, Y. M. 2014. Inactivation of Akt by arsenic trioxide induces cell death via mitochondrial-mediated apoptotic signaling in SGC-7901 human gastric cancer cells. *Oncol Rep,* 31**,** 1645-52.

GARD, D. L. & KIRSCHNER, M. W. 1985. A polymer-dependent increase in phosphorylation of beta-tubulin accompanies differentiation of a mouse neuroblastoma cell line. *The Journal of Cell Biology,* 100**,** 764.

GAREY, L. J., ONG, W. Y., PATEL, T. S., KANANI, M., DAVIS, A., MORTIMER, A. M., BARNES, T. R. & HIRSCH, S. R. 1998. Reduced dendritic spine density on cerebral cortical pyramidal neurons in schizophrenia. *J Neurol Neurosurg Psychiatry,* 65**,** 446-53.

GAVET, O., EL MESSARI, S., OZON, S. & SOBEL, A. 2002. Regulation and subcellular localization of the microtubule-destabilizing stathmin family phosphoproteins in cortical neurons. *J Neurosci Res,* 68**,** 535-50.

GE, F., XIAO, C. L., BI, L. J., TAO, S. C., XIONG, S., YIN, X. F., LI, L. P., LU, C. H., JIA, H. T. & HE, Q. Y. 2010. Quantitative phosphoproteomics of proteasome inhibition in multiple myeloma cells. *PLoS One,* 5**,** e13095.

GEBHARDT, F. M., SCOTT, H. A. & DODD, P. R. 2010. Housekeepers for accurate transcript expression analysis in Alzheimer's disease autopsy brain tissue. *Alzheimers Dement,* 6**,** 465-74.

GHOSH, R., GILDA, J. E. & GOMES, A. V. 2014. The necessity of and strategies for improving confidence in the accuracy of western blots. *Expert Rev Proteomics,* 11**,** 549-60.

GIANNAKAKOU, P., NAKANO, M., NICOLAOU, K. C., O'BRATE, A., YU, J., BLAGOSKLONNY, M. V., GREBER, U. F. & FOJO, T. 2002. Enhanced microtubule-dependent trafficking and p53 nuclear accumulation by suppression of microtubule dynamics. *Proc Natl Acad Sci U S A,* 99**,** 10855-60.

GIANNAKAKOU, P., SACKETT, D. L., WARD, Y., WEBSTER, K. R., BLAGOSKLONNY, M. V. & FOJO, T. 2000. p53 is associated with cellular microtubules and is transported to the nucleus by dynein. *Nat Cell Biol,* 2**,** 709-17.

GIASSON, B. I. & MUSHYNSKI, W. E. 1997. Developmentally regulated stabilization of neuronal intermediate filaments in rat cerebral cortex. *Neurosci Lett,* 229**,** 77-80.

GILDA, J. E., GHOSH, R., CHEAH, J. X., WEST, T. M., BODINE, S. C. & GOMES, A. V. 2015. Western blotting inaccuracies with unverified antibodies: need for a western blotting minimal reporting standard (WBMRS). *PLoS One,* 10**,** e0135392.

GIUSTINIANI, J., DAIRE, V., CANTALOUBE, I., DURAND, G., POUS, C. & PERDIZ, D. 2009. Tubulin acetylation favors Hsp90 recruitment to microtubules and stimulates the signaling function of the Hsp90 clients Akt/PKB and p53. *Cell Signal,* 21**,** 529-39.

GLICKMAN, M. H. 2000. Getting in and out of the proteasome. *Semin Cell Dev Biol,* 11**,** 149-58.

GLICKMAN, M. H. & CIECHANOVER, A. 2002. The ubiquitin-proteasome proteolytic pathway: destruction for the sake of construction. *Physiol Rev,* 82**,** 373-428.

GLOSTER, A., WU, W., SPEELMAN, A., WEISS, S., CAUSING, C., POZNIAK, C., REYNOLDS, B., CHANG, E., TOMA, J. G. & MILLER, F. D. 1994. The T alpha 1 alpha-tubulin promoter specifies gene expression as a function of neuronal growth and regeneration in transgenic mice. *J Neurosci,* 14**,** 7319-30.

GOEDERT, M., SPILLANTINI, M. G., CAIRNS, N. J. & CROWTHER, R. A. 1992. Tau proteins of Alzheimer paired helical filaments: abnormal phosphorylation of all six brain isoforms. *Neuron,* 8**,** 159-68.

GOLL, J. C., KIM, L. G., HAILSTONE, J. C., LEHMANN, M., BUCKLEY, A., CRUTCH, S. J. & WARREN, J. D. 2011. Auditory object cognition in dementia. *Neuropsychologia,* 49**,** 2755-65.

GOMEZ-ISLA, T., PRICE, J. L., MCKEEL, D. W., JR., MORRIS, J. C., GROWDON, J. H. & HYMAN, B. T. 1996. Profound loss of layer II entorhinal cortex neurons occurs in very mild Alzheimer's disease. *J Neurosci,* 16**,** 4491-500.

GONG, C. X., WANG, J. Z., IQBAL, K. & GRUNDKE-IQBAL, I. 2003. Inhibition of protein phosphatase 2A induces phosphorylation and accumulation of neurofilaments in metabolically active rat brain slices. *Neurosci Lett,* 340**,** 107-10.

GOODWIN, S. S. & VALE, R. D. 2010. Patronin Regulates the Microtubule Network by Protecting Microtubule Minus Ends. *Cell,* 143**,** 263-274.

GOU, J. P. & LETERRIER, J. F. 1995. Possible involvement of ubiquitination in neurofilament degradation. *Biochem Biophys Res Commun,* 217**,** 529-38.

GOZES, I. & SWEADNER, K. J. 1981. Multiple tubulin forms are expressed by a single neurone. *Nature,* 294**,** 477-480.

GRAND'MAISON, M., ZEHNTNER, S. P., HO, M.-K., HÉBERT, F., WOOD, A., CARBONELL, F., ZIJDENBOS, A. P., HAMEL, E. & BEDELL, B. J. 2013. Early cortical thickness changes predict β-amyloid deposition in a mouse model of Alzheimer's disease. *Neurobiology of Disease,* 54**,** 59-67.

GRAY, E., RICE, C., NIGHTINGALE, H., GINTY, M., HARES, K., KEMP, K., COHEN, N., LOVE, S., SCOLDING, N. & WILKINS, A. 2012. Accumulation of cortical hyperphosphorylated

neurofilaments as a marker of neurodegeneration in multiple sclerosis. *Multiple Sclerosis Journal,* 19**,** 153-161.
GREENE, L. A., LEVY, O. & MALAGELADA, C. 2011. Akt as a victim, villain and potential hero in Parkinson's disease pathophysiology and treatment. *Cell Mol Neurobiol,* 31**,** 969-78.
GRIDER, M. H., PARK, D., SPENCER, D. M. & SHINE, H. D. 2009. Lipid raft-targeted Akt promotes axonal branching and growth cone expansion via mTOR and Rac1, respectively. *J Neurosci Res,* 87**,** 3033-42.
GRIFFIN, J. W., HOFFMAN, P. N., CLARK, A. W., CARROLL, P. T. & PRICE, D. L. 1978. Slow axonal transport of neurofilament proteins: impairment of beta,beta'-iminodipropionitrile administration. *Science,* 202**,** 633-5.
GRIFFIN, P., FURUKAWA, R., PIGGOTT, C., MASELLI, A. & FECHHEIMER, M. 2014. Requirements for Hirano body formation. *Eukaryot Cell,* 13**,** 625-34.
GRIFFIN, R. J., MOLONEY, A., KELLIHER, M., JOHNSTON, J. A., RAVID, R., DOCKERY, P., O'CONNOR, R. & O'NEILL, C. 2005. Activation of Akt/PKB, increased phosphorylation of Akt substrates and loss and altered distribution of Akt and PTEN are features of Alzheimer's disease pathology. *J Neurochem,* 93**,** 105-17.
GRIMMLER, M., WANG, Y., MUND, T., CILENSEK, Z., KEIDEL, E. M., WADDELL, M. B., JAKEL, H., KULLMANN, M., KRIWACKI, R. W. & HENGST, L. 2007. Cdk-inhibitory activity and stability of p27Kip1 are directly regulated by oncogenic tyrosine kinases. *Cell,* 128**,** 269-80.
GROSS, A., MCDONNELL, J. M. & KORSMEYER, S. J. 1999. BCL-2 family members and the mitochondria in apoptosis. *Genes Dev,* 13**,** 1899-911.
GRUNE, T., BOTZEN, D., ENGELS, M., VOSS, P., KAISER, B., JUNG, T., GRIMM, S., ERMAK, G. & DAVIES, K. J. A. 2010. Tau protein degradation is catalyzed by the ATP/ubiquitin-independent 20S proteasome under normal cell conditions. *Arch Biochem Biophys,* 500**,** 181-8.
GUMY, L. F., TAN, C. L. & FAWCETT, J. W. 2010. The role of local protein synthesis and degradation in axon regeneration. *Experimental Neurology,* 223**,** 28-37.
GUO, J., QIANG, M. & LUDUEÑA, R. F. 2011. The distribution of β-tubulin isotypes in cultured neurons from embryonic, newborn, and adult mouse brains. *Brain Research,* 1420**,** 8-18.
GUO, J., WALSS-BASS, C. & LUDUEÑA, R. F. 2010. The β isotypes of tubulin in neuronal differentiation. *Cytoskeleton (Hoboken),* 67**,** 431-41.
GUZIK, B. W. & GOLDSTEIN, L. S. 2004. Microtubule-dependent transport in neurons: steps towards an understanding of regulation, function and dysfunction. *Curr Opin Cell Biol,* 16**,** 443-50.
HALLAK, M. E., RODRIGUEZ, J. A., BARRA, H. S. & CAPUTTO, R. 1977. Release of tyrosine from tyrosinated tubulin. Some

common factors that affect this process and the assembly of tubulin. *FEBS Lett,* 73**,** 147-50.
HAMAZAKI, J., SASAKI, K., KAWAHARA, H., HISANAGA, S., TANAKA, K. & MURATA, S. 2007. Rpn10-mediated degradation of ubiquitinated proteins is essential for mouse development. *Mol Cell Biol,* 27**,** 6629-38.
HAMILTON, A. M. & ZITO, K. 2013. Breaking it down: the ubiquitin proteasome system in neuronal morphogenesis. *Neural Plasticity,* 2013**,** 10.
HAMMOND, J. W., HUANG, C. F., KAECH, S., JACOBSON, C., BANKER, G. & VERHEY, K. J. 2010. Posttranslational modifications of tubulin and the polarized transport of kinesin-1 in neurons. *Mol Biol Cell,* 21**,** 572-83.
HAN, Q., WANG, X., YANG, M., ZHANG, Z., LI, P., CHEN, A., HU, C. & LI, S. 2013. IBP-mediated suppression of autophagy promotes growth and metastasis of breast cancer cells via activating mTORC2/Akt/FOXO3a signaling pathway. *Cell Death Dis,* 4**,** e842.
HARADA, A., TENG, J., TAKEI, Y., OGUCHI, K. & HIROKAWA, N. 2002. MAP2 is required for dendrite elongation, PKA anchoring in dendrites, and proper PKA signal transduction. *J Cell Biol,* 158**,** 541-9.
HARBOUR, J. W. & DEAN, D. C. 2000. The Rb/E2F pathway: expanding roles and emerging paradigms. *Genes Dev,* 14**,** 2393-409.
HARDY, J. & SELKOE, D. J. 2002. The amyloid hypothesis of Alzheimer's disease: progress and problems on the road to therapeutics. *Science,* 297**,** 353-6.
HASHIGUCHI, A., HIGUCHI, Y., NOMURA, M., NAKAMURA, T., ARATA, H., YUAN, J., YOSHIMURA, A., OKAMOTO, Y., MATSUURA, E. & TAKASHIMA, H. 2014. Neurofilament light mutation causes hereditary motor and sensory neuropathy with pyramidal signs. *J Peripher Nerv Syst,* 19**,** 311-6.
HAUPT, Y., MAYA, R., KAZAZ, A. & OREN, M. 1997. Mdm2 promotes the rapid degradation of p53. *Nature,* 387**,** 296-299.
HAYASHI, K., PAN, Y., SHU, H., OHSHIMA, T., KANSY, J. W., WHITE, C. L., 3RD, TAMMINGA, C. A., SOBEL, A., CURMI, P. A., MIKOSHIBA, K. & BIBB, J. A. 2006. Phosphorylation of the tubulin-binding protein, stathmin, by Cdk5 and MAP kinases in the brain. *J Neurochem,* 99**,** 237-50.
HE, W., WANG, X., CHEN, L. & GUAN, X. 2012. A crosstalk imbalance between p27(Kip1) and its interacting molecules enhances breast carcinogenesis. *Cancer Biother Radiopharm,* 27**,** 399-402.
HEGDE, A. N. & UPADHYA, S. C. 2011. Role of ubiquitin-proteasome-mediated proteolysis in nervous system disease. *Biochim Biophys Acta,* 1809**,** 128-40.
HEIMANN, R., SHELANSKI, M. L. & LIEM, R. K. 1985. Microtubule-associated proteins bind specifically to the 70-kDa neurofilament protein. *Journal of Biological Chemistry,* 260**,** 12160-12166.

HELLAL, F., HURTADO, A., RUSCHEL, J., FLYNN, K. C., LASKOWSKI, C. J., UMLAUF, M., KAPITEIN, L. C., STRIKIS, D., LEMMON, V., BIXBY, J., HOOGENRAAD, C. C. & BRADKE, F. 2011. Microtubule stabilization reduces scarring and causes axon regeneration after spinal cord injury. *Science,* 331**,** 928-31.

HENGST, L., DULIC, V., SLINGERLAND, J. M., LEES, E. & REED, S. I. 1994. A cell cycle-regulated inhibitor of cyclin-dependent kinases. *Proc Natl Acad Sci U S A,* 91**,** 5291-5.

HENKE, W., FERRELL, K., BECH-OTSCHIR, D., SEEGER, M., SCHADE, R., JUNGBLUT, P., NAUMANN, M. & DUBIEL, W. 1999. Comparison of human COP9 signalsome and 26S proteasome lid'. *Mol Biol Rep,* 26**,** 29-34.

HERCULANO-HOUZEL, S., MOTA, B. & LENT, R. 2006. Cellular scaling rules for rodent brains. *Proc Natl Acad Sci U S A,* 103**,** 12138-43.

HERNANDEZ, M. A., WANDOSELL, F. & AVILA, J. 1987. Localization of the phosphorylation sites for different kinases in the microtubule-associated protein MAP2. *J Neurochem,* 48**,** 84-93.

HIEBERT, S. W., CHELLAPPAN, S. P., HOROWITZ, J. M. & NEVINS, J. R. 1992. The interaction of RB with E2F coincides with an inhibition of the transcriptional activity of E2F. *Genes Dev,* 6**,** 177-85.

HILL, W. D., ARAI, M., COHEN, J. A. & TROJANOWSKI, J. Q. 1993. Neurofilament mRNA is reduced in Parkinson's disease substantia nigra pars compacta neurons. *J Comp Neurol,* 329**,** 328-36.

HIRANO, A. 1994. Hirano bodies and related neuronal inclusions. *Neuropathol Appl Neurobiol,* 20**,** 3-11.

HIRANO, Y., HENDIL, K. B., YASHIRODA, H., IEMURA, S., NAGANE, R., HIOKI, Y., NATSUME, T., TANAKA, K. & MURATA, S. 2005. A heterodimeric complex that promotes the assembly of mammalian 20S proteasomes. *Nature,* 437**,** 1381-5.

HIROKAWA, N. 1982. Cross-linker system between neurofilaments, microtubules, and membranous organelles in frog axons revealed by the quick-freeze, deep-etching method. *J Cell Biol,* 94**,** 129-42.

HIROKAWA, N., FUNAKOSHI, T., SATO-HARADA, R. & KANAI, Y. 1996. Selective stabilization of tau in axons and microtubule-associated protein 2C in cell bodies and dendrites contributes to polarized localization of cytoskeletal proteins in mature neurons. *J Cell Biol,* 132**,** 667-79.

HISANAGA, S. & HIROKAWA, N. 1990. Dephosphorylation-induced interactions of neurofilaments with microtubules. *J Biol Chem,* 265**,** 21852-8.

HOF, P. R., GLEZER, II, ARCHIN, N., JANSSEN, W. G., MORGANE, P. J. & MORRISON, J. H. 1992. The primary auditory cortex in cetacean and human brain: a comparative analysis of neurofilament protein-containing pyramidal neurons. *Neurosci Lett,* 146**,** 91-5.

HOFFMAN, P. N. & LASEK, R. J. 1975. The slow component of axonal transport. Identification of major structural polypeptides of the axon and their generality among mammalian neurons. *J Cell Biol,* 66**,** 351-66.
HONNAPPA, S., JAHNKE, W., SEELIG, J. & STEINMETZ, M. O. 2006. Control of intrinsically disordered stathmin by multisite phosphorylation. *Journal of Biological Chemistry,* 281**,** 16078-16083.
HOOPER, C., MEIMARIDOU, E., TAVASSOLI, M., MELINO, G., LOVESTONE, S. & KILLICK, R. 2007. p53 is upregulated in Alzheimer's disease and induces tau phosphorylation in HEK293a cells. *Neurosci Lett,* 418**,** 34-7.
HOWARD, J. & HYMAN, A. A. 2003. Dynamics and mechanics of the microtubule plus end. *Nature,* 422**,** 753-8.
HOWARD, J. & HYMAN, A. A. 2009. Growth, fluctuation and switching at microtubule plus ends. *Nat Rev Mol Cell Biol,* 10**,** 569-74.
HOWES, S. C., ALUSHIN, G. M., SHIDA, T., NACHURY, M. V. & NOGALES, E. 2014. Effects of tubulin acetylation and tubulin acetyltransferase binding on microtubule structure. *Mol Biol Cell,* 25**,** 257-66.
HUANG, Q. & FIGUEIREDO-PEREIRA, M. E. 2010. Ubiquitin/proteasome pathway impairment in neurodegeneration: therapeutic implications. *Apoptosis,* 15**,** 1292-311.
HUANG, Z. J., DI CRISTO, G. & ANGO, F. 2007. Development of GABA innervation in the cerebral and cerebellar cortices. *Nat Rev Neurosci,* 8**,** 673-86.
HUBBERT, C., GUARDIOLA, A., SHAO, R., KAWAGUCHI, Y., ITO, A., NIXON, A., YOSHIDA, M., WANG, X. F. & YAO, T. P. 2002. HDAC6 is a microtubule-associated deacetylase. *Nature,* 417**,** 455-8.
HUFF, L. M., SACKETT, D. L., PORUCHYNSKY, M. S. & FOJO, T. 2010. Microtubule disrupting chemotherapeutics result in enhanced proteasome-mediated degradation and disappearance of tubulin in neural cells. *Cancer Res,* 70**,** 5870-9.
HUGHES, J. R. 1984. Cerebral cortex. Vol. 1. Cellular components of the cerebral cortex. *Electroencephalography and Clinical Neurophysiology,* 58**,** 385.
HUSNJAK, K., ELSASSER, S., ZHANG, N., CHEN, X., RANDLES, L., SHI, Y., HOFMANN, K., WALTERS, K. J., FINLEY, D. & DIKIC, I. 2008. Proteasome subunit Rpn13 is a novel ubiquitin receptor. *Nature,* 453**,** 481-8.
HUTSLER, J. J., LEE, D. G. & PORTER, K. K. 2005. Comparative analysis of cortical layering and supragranular layer enlargement in rodent carnivore and primate species. *Brain Res,* 1052**,** 71-81.
HUTTON, M., LENDON, C. L., RIZZU, P., BAKER, M., FROELICH, S., HOULDEN, H., PICKERING-BROWN, S., CHAKRAVERTY, S., ISAACS, A., GROVER, A., HACKETT, J., ADAMSON, J., LINCOLN, S., DICKSON, D., DAVIES, P., PETERSEN, R. C.,

STEVENS, M., DE GRAAFF, E., WAUTERS, E., VAN BAREN, J., HILLEBRAND, M., JOOSSE, M., KWON, J. M., NOWOTNY, P., CHE, L. K., NORTON, J., MORRIS, J. C., REED, L. A., TROJANOWSKI, J., BASUN, H., LANNFELT, L., NEYSTAT, M., FAHN, S., DARK, F., TANNENBERG, T., DODD, P. R., HAYWARD, N., KWOK, J. B., SCHOFIELD, P. R., ANDREADIS, A., SNOWDEN, J., CRAUFURD, D., NEARY, D., OWEN, F., OOSTRA, B. A., HARDY, J., GOATE, A., VAN SWIETEN, J., MANN, D., LYNCH, T. & HEUTINK, P. 1998. Association of missense and 5'-splice-site mutations in tau with the inherited dementia FTDP-17. *Nature,* 393**,** 702-5.

IACONO, D., MARKESBERY, W. R., GROSS, M., PLETNIKOVA, O., RUDOW, G., ZANDI, P. & TRONCOSO, J. C. 2009. The Nun Study: Clinically silent AD, neuronal hypertrophy, and linguistic skills in early life. *Neurology,* 73**,** 665-73.

IACONO, D., O'BRIEN, R., RESNICK, S. M., ZONDERMAN, A. B., PLETNIKOVA, O., RUDOW, G., AN, Y., WEST, M. J., CRAIN, B. & TRONCOSO, J. C. 2008. Neuronal hypertrophy in asymptomatic Alzheimer`s disease. *J Neuropathol Exp Neurol,* 67**,** 578-89.

IHARA, M., POLVIKOSKI, T. M., HALL, R., SLADE, J. Y., PERRY, R. H., OAKLEY, A. E., ENGLUND, E., O'BRIEN, J. T., INCE, P. G. & KALARIA, R. N. 2010. Quantification of myelin loss in frontal lobe white matter in vascular dementia, Alzheimer's disease, and dementia with Lewy bodies. *Acta Neuropathol,* 119**,** 579-89.

IKEGAMI, K., HEIER, R. L., TARUISHI, M., TAKAGI, H., MUKAI, M. & SHIMMA, S. 2007. Loss of alpha-tubulin polyglutamylation in ROSA22 mice is associated with abnormal targeting of KIF1A and modulated synaptic function. *Proc Natl Acad Sci U S A,* 104**,** 3213–3218.

IKEGAMI, K. & SETOU, M. 2010. Unique post-translational modifications in specialized microtubule architecture. *Cell Struct Funct,* 35**,** 15-22.

IQBAL, K., LIU, F., GONG, C. X., ALONSO, A. C. & GRUNDKE-IQBAL, I. 2009. Mechanisms of tau-induced neurodegeneration. *Acta Neuropathol,* 118**,** 53-69.

ITO, M. 1992. Simultaneous visualization of cortical barrels and horseradish peroxidase-injected layer 5b vibrissa neurones in the rat. *J Physiol,* 454**,** 247-65.

JANKE, C. 2014. The tubulin code: Molecular components, readout mechanisms, and functions. *The Journal of Cell Biology,* 206**,** 461–472.

JANKE, C. & BULINSKI, J. C. 2011. Post-translational regulation of the microtubule cytoskeleton: mechanisms and functions. *Nat Rev Mol Cell Biol,* 12**,** 773-86.

JANKE, C. & KNEUSSEL, M. 2010. Tubulin post-translational modifications: encoding functions on the neuronal microtubule cytoskeleton. *Trends Neurosci,* 33**,** 362-72.

JANKE, C., ROGOWSKI, K. & DIJK, J. 2008. Polyglutamylation: a fine-regulator of protein function? 'Protein Modifications:

beyond the usual suspects' review series. *EMBO Rep,* 9**,** 636–641.
JANKE, C., ROGOWSKI, K., WLOGA, D., REGNARD, C., KAJAVA, A. V., STRUB, J. M., TEMURAK, N., VAN DIJK, J., BOUCHER, D., VAN DORSSELAER, A., SURYAVANSHI, S., GAERTIG, J. & EDDE, B. 2005. Tubulin polyglutamylase enzymes are members of the TTL domain protein family. *Science,* 308**,** 1758-62.
JAWORSKI, J., KAPITEIN, L. C., GOUVEIA, S. M., DORTLAND, B. R., WULF, P. S., GRIGORIEV, I., CAMERA, P., SPANGLER, S. A., DI STEFANO, P., DEMMERS, J., KRUGERS, H., DEFILIPPI, P., AKHMANOVA, A. & HOOGENRAAD, C. C. 2009. Dynamic microtubules regulate dendritic spine morphology and synaptic plasticity. *Neuron,* 61**,** 85-100.
JAWORSKI, J., SPANGLER, S., SEEBURG, D. P., HOOGENRAAD, C. C. & SHENG, M. 2005. Control of dendritic arborization by the phosphoinositide-3'-kinase-Akt-mammalian target of rapamycin pathway. *J Neurosci,* 25**,** 11300-12.
JIANG, Q., YAN, Z. & FENG, J. 2006. Neurotrophic factors stabilize microtubules and protect against rotenone toxicity on dopaminergic neurons. *J Biol Chem,* 281**,** 29391-400.
JIN, L. W., MASLIAH, E., IIMOTO, D., DETERESA, R., MALLORY, M., SUNDSMO, M., MORI, N., SOBEL, A. & SAITOH, T. 1996. Neurofibrillary tangle-associated alteration of stathmin in Alzheimer's disease. *Neurobiol Aging,* 17**,** 331-41.
JOHNSEN, J. I., AURELIO, O. N., KWAJA, Z., JORGENSEN, G. E., PELLEGATA, N. S., PLATTNER, R., STANBRIDGE, E. J. & CAJOT, J. F. 2000. p53-mediated negative regulation of stathmin/Op18 expression is associated with G(2)/M cell-cycle arrest. *Int J Cancer,* 88**,** 685-91.
JOSHI, H. C. & CLEVELAND, D. W. 1989. Differential utilization of beta-tubulin isotypes in differentiating neurites. *J Cell Biol,* 109**,** 663-73.
JULIEN, J.-P. & KRIZ, J. 2006. Transgenic mouse models of amyotrophic lateral sclerosis. *Biochimica et Biophysica Acta (BBA) - Molecular Basis of Disease,* 1762**,** 1013-1024.
KALEBIC, N., SORRENTINO, S., PERLAS, E., BOLASCO, G., MARTINEZ, C. & HEPPENSTALL, P. A. 2013. alphaTAT1 is the major alpha-tubulin acetyltransferase in mice. *Nat Commun,* 4**,** 1962.
KAPITEIN, LUKAS C. & HOOGENRAAD, CASPER C. 2015. Building the neuronal microtubule cytoskeleton. *Neuron,* 87**,** 492-506.
KARST, A. M., LEVANON, K., DURAISAMY, S., LIU, J. F., HIRSCH, M. S., HECHT, J. L. & DRAPKIN, R. 2011. Stathmin 1, a marker of PI3K pathway activation and regulator of microtubule dynamics, is expressed in early pelvic serous carcinomas. *Gynecologic Oncology,* 123**,** 5-12.
KATSETOS, C. D., DRABEROVA, E., LEGIDO, A., DUMONTET, C. & DRABER, P. 2009. Tubulin targets in the pathobiology and therapy of glioblastoma multiforme. I. Class III beta-tubulin. *J Cell Physiol,* 221**,** 505-13.

KAUFMANN, W. E., MACDONALD, S. M. & ALTAMURA, C. R. 2000. Dendritic cytoskeletal protein expression in mental retardation: an immunohistochemical study of the neocortex in Rett syndrome. *Cereb Cortex,* 10**,** 992-1004.

KAWAGUCHI, Y. 1995. Physiological subgroups of nonpyramidal cells with specific morphological characteristics in layer II/III of rat frontal cortex. *J Neurosci,* 15**,** 2638-55.

KEAYS, D. A., TIAN, G., POIRIER, K., HUANG, G. J., SIEBOLD, C., CLEAK, J., OLIVER, P. L., FRAY, M., HARVEY, R. J., MOLNAR, Z., PINON, M. C., DEAR, N., VALDAR, W., BROWN, S. D., DAVIES, K. E., RAWLINS, J. N., COWAN, N. J., NOLAN, P., CHELLY, J. & FLINT, J. 2007. Mutations in alpha-tubulin cause abnormal neuronal migration in mice and lissencephaly in humans. *Cell,* 128**,** 45-57.

KENNEDY, S. G., WAGNER, A. J., CONZEN, S. D., JORDAN, J., BELLACOSA, A., TSICHLIS, P. N. & HAY, N. 1997. The PI 3-kinase/Akt signaling pathway delivers an anti-apoptotic signal. *Genes Dev,* 11**,** 701-13.

KERSAITIS, C., HALLIDAY, G. M. & KRIL, J. J. 2004. Regional and cellular pathology in frontotemporal dementia: relationship to stage of disease in cases with and without Pick bodies. *Acta Neuropathol,* 108**,** 515-23.

KERSSEMAKERS, J. W., MUNTEANU, E. L., LAAN, L., NOETZEL, T. L., JANSON, M. E. & DOGTEROM, M. 2006. Assembly dynamics of microtubules at molecular resolution. *Nature,* 442**,** 709-12.

KHATOON, S., GRUNDKE-IQBAL, I. & IQBAL, K. 1994. Levels of normal and abnormally phosphorylated tau in different cellular and regional compartments of Alzheimer disease and control brains. *FEBS Lett,* 351**,** 80-4.

KIERNAN, J. A. 2012. Anatomy of the temporal lobe. *Epilepsy Res Treat,* 2012**,** 176157.

KIM, T. H., ZHANG, Y., LECOQ, J., JUNG, J. C., LI, J., ZENG, H., NIELL, C. M. & SCHNITZER, M. J. 2016. Long-term optical access to an estimated one million neurons in the live mouse cortex. *Cell Rep,* 17**,** 3385-3394.

KIRKCALDIE, M. T., DICKSON, T. C., KING, C. E., GRASBY, D., RIEDERER, B. M. & VICKERS, J. C. 2002. Neurofilament triplet proteins are restricted to a subset of neurons in the rat neocortex. *J Chem Neuroanat,* 24**,** 163-71.

KIRKCALDIE, M. T. K. 2012. Chapter 4 - Neocortex A2 - Watson, Charles. *In:* PAXINOS, G. & PUELLES, L. (eds.) *The Mouse Nervous System.* San Diego: Academic Press.

KIRKPATRICK, L., BRADY, S., SIEGEL, G., AGRANOFF, B. & ALBERS, R. 1999. Molecular components of the neuronal cytoskeleton. *Neuron* 87**,** 492 - 506.

KITADA, T., ASAKAWA, S., HATTORI, N., MATSUMINE, H., YAMAMURA, Y., MINOSHIMA, S., YOKOCHI, M., MIZUNO, Y. & SHIMIZU, N. 1998. Mutations in the parkin gene cause autosomal recessive juvenile parkinsonism. *Nature,* 392**,** 605-8.

KITAGAWA, H., TANI, E., IKEMOTO, H., OZAKI, I., NAKANO, A. & OMURA, S. 1999. Proteasome inhibitors induce mitochondria-independent apoptosis in human glioma cells. *FEBS Letters,* 443**,** 181-186.

KITAGISHI, Y., NAKANISHI, A., OGURA, Y. & MATSUDA, S. 2014. Dietary regulation of PI3K/AKT/GSK-3β pathway in Alzheimer's disease. *Alzheimers Res Ther,* 6**,** 35.

KITTUR, S., HOH, J., ENDO, H., TOURTELLOTTE, W., WEEKS, B. S., MARKESBERY, W. & ADLER, W. 1994. Cytoskeletal Neurofilament Gene Expression in Brain Tissue from Alzheimer's Disease Patients. I. Decrease in NF-L and NF-M Message. *Journal of Geriatric Psychiatry and Neurology,* 7**,** 153-158.

KLEELE, T., MARINKOVIC, P., WILLIAMS, P. R., STERN, S., WEIGAND, E. E., ENGERER, P., NAUMANN, R., HARTMANN, J., KARL, R. M., BRADKE, F., BISHOP, D., HERMS, J., KONNERTH, A., KERSCHENSTEINER, M., GODINHO, L. & MISGELD, T. 2014. An assay to image neuronal microtubule dynamics in mice. *Nat Commun,* 5**,** 4827.

KNECHT, E., AGUADO, C., CARCEL, J., ESTEBAN, I., ESTEVE, J. M., GHISLAT, G., MORUNO, J. F., VIDAL, J. M. & SAEZ, R. 2009. Intracellular protein degradation in mammalian cells: recent developments. *Cell Mol Life Sci,* 66**,** 2427-43.

KOLLINS, K. & DAVENPORT, R. 2000. Branching morphogenesis in vertebrate neurons. in: madame curie bioscience database. *Landes Bioscience***,** 2000-2013.

KONG, J., TUNG, V., AGHAJANIAN, J. & XU, Z. 1998. Antagonistic roles of neurofilament subunits NF-H and NF-M against NF-L in shaping dendritic arborization in spinal motor neurons. *J Cell Biol,* 140**,** 1167-76.

KONG, J. & XU, Z. 2000. Overexpression of neurofilament subunit NF-L and NF-H extends survival of a mouse model for amyotrophic lateral sclerosis. *Neuroscience Letters,* 281**,** 72-74.

KONISHI, Y. & SETOU, M. 2009. Tubulin tyrosination navigates the kinesin-1 motor domain to axons. *Nat Neurosci,* 12**,** 559-67.

KOWALSKI, R. J. & WILLIAMS, R. C., JR. 1993. Microtubule-associated protein 2 alters the dynamic properties of microtubule assembly and disassembly. *J Biol Chem,* 268**,** 9847-55.

KRAVTSOVA-IVANTSIV, Y. & CIECHANOVER, A. 2012. Non-canonical ubiquitin-based signals for proteasomal degradation. *J Cell Sci,* 125**,** 539-48.

KREITZER, G., LIAO, G. & GUNDERSEN, G. G. 1999. Detyrosination of tubulin regulates the interaction of intermediate filaments with microtubules in vivo via a kinesin-dependent mechanism. *Mol Biol Cell,* 10**,** 1105-18.

KRUISWIJK, F., LABUSCHAGNE, C. F. & VOUSDEN, K. H. 2015. p53 in survival, death and metabolic health: a lifeguard with a licence to kill. *Nat Rev Mol Cell Biol,* 16**,** 393-405.

KUNZ, S., NIEDERBERGER, E., EHNERT, C., COSTE, O., PFENNINGER, A., KRUIP, J., WENDRICH, T. M., SCHMIDTKO,

A., TEGEDER, I. & GEISSLINGER, G. 2004. The calpain inhibitor MDL 28170 prevents inflammation-induced neurofilament light chain breakdown in the spinal cord and reduces thermal hyperalgesia. *Pain,* 110**,** 409-18.

KUREPA, J., WANG, S. & SMALLE, J. 2012. The role of 26S proteasome-dependent proteolysis in the formation and restructuring of microtubule networks. *Plant Signal Behav,* 7**,** 1289-95.

KWAN, K. Y., ŠESTAN, N. & ANTON, E. S. 2012. Transcriptional co-regulation of neuronal migration and laminar identity in the neocortex. *Development,* 139**,** 1535.

KWEI, S. L., CLEMENT, A., FAISSNER, A. & BRANDT, R. 1998. Differential interactions of MAP2, tau and MAP5 during axogenesis in culture. *Neuroreport,* 9**,** 1035-40.

KWON, C. H., LUIKART, B. W., POWELL, C. M., ZHOU, J., MATHENY, S. A., ZHANG, W., LI, Y., BAKER, S. J. & PARADA, L. F. 2006. Pten regulates neuronal arborization and social interaction in mice. *Neuron,* 50**,** 377-88.

L'HERNAULT, S. W. & ROSENBAUM, J. L. 1985. Chlamydomonas alpha-tubulin is posttranslationally modified by acetylation on the epsilon-amino group of a lysine. *Biochemistry,* 24.

LAM, Y. W. & SHERMAN, S. M. 2010. Functional organization of the somatosensory cortical layer 6 feedback to the thalamus. *Cereb Cortex,* 20**,** 13-24.

LANDER, G. C., ESTRIN, E., MATYSKIELA, M. E., BASHORE, C., NOGALES, E. & MARTIN, A. 2012. Complete subunit architecture of the proteasome regulatory particle. *Nature,* 482**,** 186-91.

LANG-ROLLIN, I., VEKRELLIS, K., WANG, Q., RIDEOUT, H. J. & STEFANIS, L. 2004. Application of proteasomal inhibitors to mouse sympathetic neurons activates the intrinsic apoptotic pathway. *J Neurochem,* 90**,** 1511-20.

LARIVIERE, R. C. & JULIEN, J. P. 2004. Functions of intermediate filaments in neuronal development and disease. *J Neurobiol,* 58**,** 131-48.

LARKMAN, A. U. 1991. Dendritic morphology of pyramidal neurones of the visual cortex of the rat: I. Branching patterns. *J Comp Neurol,* 306**,** 307-19.

LARKMAN, A. U., MAJOR, G., STRATFORD, K. J. & JACK, J. J. 1992. Dendritic morphology of pyramidal neurones of the visual cortex of the rat. IV: Electrical geometry. *J Comp Neurol,* 323**,** 137-52.

LARSSON, N., MARKLUND, U., GRADIN, H. M., BRATTSAND, G. & GULLBERG, M. 1997. Control of microtubule dynamics by oncoprotein 18: dissection of the regulatory role of multisite phosphorylation during mitosis. *Molecular and Cellular Biology,* 17**,** 5530-5539.

LASER-AZOGUI, A., KORNREICH, M., MALKA-GIBOR, E. & BECK, R. 2015. Neurofilament assembly and function during neuronal development. *Curr Opin Cell Biol,* 32**,** 92-101.

LAYFIELD, R., LOWE, J. & BEDFORD, L. 2005. The ubiquitin-proteasome system and neurodegenerative disorders. *Essays Biochem,* 41**,** 157-71.

LE GOUVELLO, S., MANCEAU, V. & SOBEL, A. 1998. Serine 16 of stathmin as a cytosolic target for Ca2+/calmodulin-dependent kinase II after CD2 triggering of human T lymphocytes. *J Immunol,* 161**,** 1113-22.

LE TALLEC, B., BARRAULT, M. B., COURBEYRETTE, R., GUEROIS, R., MARSOLIER-KERGOAT, M. C. & PEYROCHE, A. 2007. 20S proteasome assembly is orchestrated by two distinct pairs of chaperones in yeast and in mammals. *Mol Cell,* 27**,** 660-74.

LEDERGERBER, D. & LARKUM, M. E. 2010. Properties of layer 6 pyramidal neuron apical dendrites. *J Neurosci,* 30**,** 13031-44.

LEE, M. J., LEE, J. H. & RUBINSZTEIN, D. C. 2013. Tau degradation: The ubiquitin–proteasome system versus the autophagy-lysosome system. *Progress in Neurobiology,* 105**,** 49-59.

LEE, M. K., TUTTLE, J. B., REBHUN, L. I., CLEVELAND, D. W. & FRANKFURTER, A. 1990. The expression and posttranslational modification of a neuron-specific beta-tubulin isotype during chick embryogenesis. *Cell Motil Cytoskeleton,* 17**,** 118-32.

LEE, M. K., XU, Z., WONG, P. C. & CLEVELAND, D. W. 1993. Neurofilaments are obligate heteropolymers in vivo. *J Cell Biol,* 122**,** 1337-50.

LEFORT, S., TOMM, C., FLOYD SARRIA, J. C. & PETERSEN, C. C. 2009. The excitatory neuronal network of the C2 barrel column in mouse primary somatosensory cortex. *Neuron,* 61**,** 301-16.

LENKA, A., NADUTHOTA, R. M., JHA, M., PANDA, R., PRAJAPATI, A., JHUNJHUNWALA, K., SAINI, J., YADAV, R., BHARATH, R. D. & PAL, P. K. 2016. Freezing of gait in Parkinson's disease is associated with altered functional brain connectivity. *Parkinsonism Relat Disord,* 24**,** 100-6.

LERCH, J. P., CARROLL, J. B., DORR, A., SPRING, S., EVANS, A. C., HAYDEN, M. R., SLED, J. G. & HENKELMAN, R. M. 2008. Cortical thickness measured from MRI in the YAC128 mouse model of Huntington's disease. *NeuroImage,* 41**,** 243-251.

LERCH, J. P., PRUESSNER, J. C., ZIJDENBOS, A., HAMPEL, H., TEIPEL, S. J. & EVANS, A. C. 2005. Focal decline of cortical thickness in Alzheimer's disease identified by computational neuroanatomy. *Cereb Cortex,* 15**,** 995-1001.

LEWIS, S. A., WANG, D. H. & COWAN, N. J. 1988. Microtubule-associated protein MAP2 shares a microtubule binding motif with tau protein. *Science,* 242**,** 936-9.

LI, J., HU, G., KONG, F., WU, K., SONG, K., HE, J. & SUN, W. 2015. Elevated STMN1 expression correlates with poor prognosis in patients with pancreatic ductal adenocarcinoma. *Pathology & Oncology Research,* 21**,** 1013-1020.

LIAO, L., CHENG, D., WANG, J., DUONG, D. M., LOSIK, T. G., GEARING, M., REES, H. D., LAH, J. J., LEVEY, A. I. & PENG, J. 2004. Proteomic characterization of postmortem amyloid

plaques isolated by laser capture microdissection. *J Biol Chem,* 279**,** 37061-8.
LIEDTKE, W., LEMAN, E. E., FYFFE, R. E., RAINE, C. S. & SCHUBART, U. K. 2002. Stathmin-deficient mice develop an age-dependent axonopathy of the central and peripheral nervous systems. *Am J Pathol,* 160**,** 469-80.
LIN, C. H., YEH, S. H., LIN, C. H., LU, K. T., LEU, T. H., CHANG, W. C. & GEAN, P. W. 2001. A role for the PI-3 kinase signaling pathway in fear conditioning and synaptic plasticity in the amygdala. *Neuron,* 31**,** 841-51.
LIN, Y. C., CHEN, K. C., CHEN, C. C., CHENG, A. L. & CHEN, K. F. 2012. CIP2A-mediated Akt activation plays a role in bortezomib-induced apoptosis in head and neck squamous cell carcinoma cells. *Oral Oncol,* 48**,** 585-93.
LINCK, R., FU, X., LIN, J., OUCH, C., SCHEFTER, A., STEFFEN, W., WARREN, P. & NICASTRO, D. 2014. Insights into the structure and function of ciliary and flagellar doublet microtubules: tektins, calicum-binding proteins, and stable protofilaments. *Journal of Biological Chemistry,* 289**,** 17427-17444.
LIU, C. W. & JACOBSON, A. D. 2013. Functions of the 19S complex in proteasomal degradation. *Trends Biochem Sci,* 38**,** 103-10.
LIU, Q., XIE, F., ALVARADO-DIAZ, A., SMITH, M. A., MOREIRA, P. I., ZHU, X. & PERRY, G. 2011. Neurofilamentopathy in neurodegenerative diseases. *Open Neurol J,* 5**,** 58-62.
LIU, Q., XIE, F., SIEDLAK, S. L., NUNOMURA, A., HONDA, K., MOREIRA, P. I., ZHUA, X., SMITH, M. A. & PERRY, G. 2004. Neurofilament proteins in neurodegenerative diseases. *Cell Mol Life Sci,* 61**,** 3057-75.
LIU, S. Y., CHAN, P. & STOESSL, A. J. 2017. The underlying mechanism of prodromal PD: insights from the parasympathetic nervous system and the olfactory system. *Translational Neurodegeneration* 6**,** 2017.
LIU, Y.-H., WEI, W., YIN, J., LIU, G.-P., WANG, Q., CAO, F.-Y. & WANG, J.-Z. 2009. Proteasome inhibition increases tau accumulation independent of phosphorylation. *Neurobiology of Aging,* 30**,** 1949-1961.
LIU, Y., STAAL, J. A., CANTY, A. J., KIRKCALDIE, M. T., KING, A. E., BIBARI, O., MITEW, S. T., DICKSON, T. C. & VICKERS, J. C. 2013. Cytoskeletal changes during development and aging in the cortex of neurofilament light protein knockout mice. *J Comp Neurol,* 521**,** 1817-27.
LIVAK, K. J. & SCHMITTGEN, T. D. 2001. Analysis of relative gene expression data using real-time quantitative PCR and the 2(-Delta Delta C(T)) Method. *Methods,* 25**,** 402-8.
LLOYD, T. E., MACHAMER, J., O'HARA, K., KIM, J. H., COLLINS, S. E., WONG, M. Y., SAHIN, B., IMLACH, W., YANG, Y., LEVITAN, E. S., MCCABE, B. D. & KOLODKIN, A. L. 2012. The p150(Glued) CAP-Gly domain regulates initiation of retrograde transport at synaptic termini. *Neuron,* 74**,** 344-60.

LODA, M., CUKOR, B., TAM, S. W., LAVIN, P., FIORENTINO, M., DRAETTA, G. F., JESSUP, J. M. & PAGANO, M. 1997. Increased proteasome-dependent degradation of the cyclin-dependent kinase inhibitor p27 in aggressive colorectal carcinomas. *Nat Med,* 3**,** 231-4.

LOHR, K., MORITZ, C., CONTENTE, A. & DOBBELSTEIN, M. 2003. p21/CDKN1A mediates negative regulation of transcription by p53. *J Biol Chem,* 278**,** 32507-16.

LOPES, S., TEPLYTSKA, L., VAZ-SILVA, J., DIOLI, C., TRINDADE, R., MORAIS, M., WEBHOFER, C., MACCARRONE, G., ALMEIDA, O. F. X., TURCK, C. W., SOUSA, N., SOTIROPOULOS, I. & FILIOU, M. D. 2016. Tau deletion prevents stress-induced dendritic atrophy in prefrontal cortex: role of synaptic mitochondria. *Cerebral Cortex,* 27**,** 2580-2591.

LOPES, U. G., ERHARDT, P., YAO, R. & COOPER, G. M. 1997. p53-dependent induction of apoptosis by proteasome inhibitors. *Journal of Biological Chemistry,* 272**,** 12893-12896.

LOPEZ-PICON, F. R., KUKKO-LUKJANOV, T. K. & HOLOPAINEN, I. E. 2006. The calpain inhibitor MDL-28170 and the AMPA/KA receptor antagonist CNQX inhibit neurofilament degradation and enhance neuronal survival in kainic acid-treated hippocampal slice cultures. *Eur J Neurosci,* 23**,** 2686-94.

LU, C. H., PETZOLD, A., KALMAR, B., DICK, J., MALASPINA, A. & GREENSMITH, L. 2012. Plasma neurofilament heavy chain levels correlate to markers of late stage disease progression and treatment response in SOD1(G93A) mice that model ALS. *PLoS One,* 7**,** e40998.

LU, C. H., PETZOLD, A., TOPPING, J., ALLEN, K., MACDONALD-WALLIS, C., CLARKE, J., PEARCE, N., KUHLE, J., GIOVANNONI, G., FRATTA, P., SIDLE, K., FISH, M., ORRELL, R., HOWARD, R., GREENSMITH, L. & MALASPINA, A. 2015. Plasma neurofilament heavy chain levels and disease progression in amyotrophic lateral sclerosis: insights from a longitudinal study. *J Neurol Neurosurg Psychiatry,* 86**,** 565-73.

LUDIN, B., ASHBRIDGE, K., FUNFSCHILLING, U. & MATUS, A. 1996. Functional analysis of the MAP2 repeat domain. *J Cell Sci,* 109 (Pt 1)**,** 91-9.

LUDUEÑA, R. F. 1993. Are tubulin isotypes functionally significant. *Mol Biol Cell,* 4**,** 445-57.

LUEBKE, J. I., WEAVER, C. M., ROCHER, A. B., RODRIGUEZ, A., CRIMINS, J. L., DICKSTEIN, D. L., WEARNE, S. L. & HOF, P. R. 2010. Dendritic vulnerability in neurodegenerative disease: insights from analyses of cortical pyramidal neurons in transgenic mouse models. *Brain Struct Funct,* 214**,** 181-99.

LUKASZEWICZ, A., SAVATIER, P., CORTAY, V., GIROUD, P., HUISSOUD, C., BERLAND, M., KENNEDY, H. & DEHAY, C. 2005. G1 phase regulation, area-specific cell cycle control, and cytoarchitectonics in the primate cortex. *Neuron,* 47**,** 353-64.

LUND, J. S. 1988. Anatomical organization of macaque monkey striate visual cortex. *Annu Rev Neurosci,* 11**,** 253-88.
LUO, T., LIU, G., MA, H., LU, B., XU, H., WANG, Y., WU, J., GE, P. & LIANG, J. 2014. Inhibition of autophagy via activation of PI3K/Akt pathway contributes to the protection of ginsenoside Rb1 against neuronal death caused by ischemic insults. *Int J Mol Sci,* 15**,** 15426-42.
LYOO, C. H., RYU, Y. H. & LEE, M. S. 2010. Topographical distribution of cerebral cortical thinning in patients with mild Parkinson's disease without dementia. *Mov Disord,* 25**,** 496-9.
MA, Q. L., ZUO, X., YANG, F., UBEDA, O. J., GANT, D. J., ALAVERDYAN, M., KIOSEA, N. C., NAZARI, S., CHEN, P. P., NOTHIAS, F., CHAN, P., TENG, E., FRAUTSCHY, S. A. & COLE, G. M. 2014. Loss of MAP Function Leads to Hippocampal Synapse Loss and Deficits in the Morris Water Maze with Aging. *J Neurosci,* 34**,** 7124-36.
MAATUF, Y., STERN, E. A. & SLOVIN, H. 2016. Abnormal population responses in the somatosensory cortex of Alzheimer's disease model mice. *Scientific Reports,* 6**,** 24560.
MACCIONI, R. B. & CAMBIAZO, V. 1995. Role of microtubule-associated proteins in the control of microtubule assembly. *Physiol Rev,* 75**,** 835-64.
MACLAREN, A. P., CHAPMAN, R. S., WYLLIE, A. H. & WATSON, C. J. 2001. p53-dependent apoptosis induced by proteasome inhibition in mammary epithelial cells. *Cell Death Differ,* 8**,** 210-218.
MADAY, S., TWELVETREES, A. E., MOUGHAMIAN, A. J. & HOLZBAUR, E. L. 2014. Axonal transport: cargo-specific mechanisms of motility and regulation. *Neuron,* 84**,** 292-309.
MAGIERA, M. M. & JANKE, C. 2014. Post-translational modifications of tubulin. *Curr Biol,* 24**,** R351-4.
MAK, E., SU, L., WILLIAMS, G. B., WATSON, R., FIRBANK, M. J., BLAMIRE, A. M. & O'BRIEN, J. T. 2015. Progressive cortical thinning and subcortical atrophy in dementia with Lewy bodies and Alzheimer's disease. *Neurobiol Aging,* 36**,** 1743-50.
MAKHOV, P., GOLOVINE, K., TEPER, E., KUTIKOV, A., MEHRAZIN, R., CORCORAN, A., TULIN, A., UZZO, R. G. & KOLENKO, V. M. 2014. Piperlongumine promotes autophagy via inhibition of Akt/mTOR signalling and mediates cancer cell death. *Br J Cancer,* 110**,** 899-907.
MALAGELADA, C., JIN, Z. H. & GREENE, L. A. 2008. RTP801 is induced in Parkinson's disease and mediates neuron death by inhibiting Akt phosphorylation/activation. *J Neurosci,* 28**,** 14363-71.
MALMENDAL, A., HALPAIN, S. & CHAZIN, W. J. 2003. Nascent structure in the kinase anchoring domain of microtubule-associated protein 2. *Biochem Biophys Res Commun,* 301**,** 136-42.

MANDELKOW, E. M. & MANDELKOW, E. 2012. Biochemistry and cell biology of tau protein in neurofibrillary degeneration. *Cold Spring Harb Perspect Med,* 2**,** a006247.
MANN, D. M., YATES, P. O. & MARCYNIUK, B. 1985. Some morphometric observations on the cerebral cortex and hippocampus in presenile Alzheimer's disease, senile dementia of Alzheimer type and Down's syndrome in middle age. *J Neurol Sci,* 69**,** 139-59.
MANNING, B. D. & CANTLEY, L. C. 2007. AKT/PKB signaling: navigating downstream. *Cell,* 129**,** 1261-74.
MARCOS, S., MOREAU, J., BACKER, S., JOB, D., ANDRIEUX, A. & BLOCH-GALLEGO, E. 2009. Tubulin tyrosination is required for the proper organization and pathfinding of the growth cone. *PLoS One,* 4**,** e5405.
MARKRAM, H., TOLEDO-RODRIGUEZ, M., WANG, Y., GUPTA, A., SILBERBERG, G. & WU, C. 2004. Interneurons of the neocortical inhibitory system. *Nature Reviews Neuroscience,* 5**,** 793-807.
MARTIN, N., JAUBERT, J., GOUNON, P., SALIDO, E., HAASE, G., SZATANIK, M. & GUENET, J. L. 2002. A missense mutation in Tbce causes progressive motor neuronopathy in mice. *Nat Genet,* 32**,** 443-7.
MARTIN, N. E., GERKE, T., SINNOTT, J. A., STACK, E. C., ANDRÉN, O., ANDERSSON, S. O., JOHANSSON, J. E., FIORENTINO, M., FINN, S., FEDELE, G., STAMPFER, M., KANTOFF, P. W., MUCCI, L. A. & LODA, M. 2015. Measuring PI3K activation: clinicopathologic, immunohistochemical, and RNA expression analysis in prostate cancer. *Mol Cancer Res,* 13**,** 1431-40.
MARTIN, W. R., WIELER, M., GEE, M. & CAMICIOLI, R. 2009. Temporal lobe changes in early, untreated Parkinson's disease. *Mov Disord,* 24**,** 1949-54.
MASAKI, R., SAITO, T., YAMADA, K. & OHTANI-KANEKO, R. 2000. Accumulation of phosphorylated neurofilaments and increase in apoptosis-specific protein and phosphorylated c-Jun induced by proteasome inhibitors. *J Neurosci Res,* 62**,** 75-83.
MCILWAIN, D. L. & HOKE, V. B. 2005. The role of the cytoskeleton in cell body enlargement, increased nuclear eccentricity and chromatolysis in axotomized spinal motor neurons. *BMC Neurosci,* 6**,** 19.
MCLACHLAN, D. R., LUKIW, W. J., WONG, L., BERGERON, C. & BECH-HANSEN, N. T. 1988. Selective messenger RNA reduction in Alzheimer's disease. *Brain Res,* 427**,** 255-61.
MCVICKER, D. P., MILLETTE, M. M. & DENT, E. W. 2015. Signaling to the microtubule cytoskeleton: An unconventional role for CaMKII. *Dev Neurobiol,* 75**,** 423-34.
MEGIORNI, F., MORA, B., INDOVINA, P. & MAZZILLI, M. C. 2005. Expression of neuronal markers during NTera2/cloneD1 differentiation by cell aggregation method. *Neurosci Lett,* 373**,** 105-9.

MEIER, J., COUILLARD-DESPRÉS, S., JACOMY, H., GRAVEL, C. & JULIEN, J.-P. 1999. Extra neurofilament NF-L subunits rescue motor neuron disease caused by overexpression of the human NF-H gene in mice. *Journal of Neuropathology & Experimental Neurology,* 58**,** 1099-1110.

MELLOTT, J. G., VAN DER GUCHT, E., LEE, C. C., CARRASCO, A., WINER, J. A. & LOMBER, S. G. 2010. Areas of cat auditory cortex as defined by neurofilament proteins expressing SMI-32. *Hearing Research,* 267**,** 119-136.

MENDONCA, D. M., CHIMELLI, L. & MARTINEZ, A. M. 2005. Quantitative evidence for neurofilament heavy subunit aggregation in motor neurons of spinal cords of patients with amyotrophic lateral sclerosis. *Braz J Med Biol Res,* 38**,** 925-33.

MEREGALLI, C., CHIORAZZI, A., CAROZZI, V. A., CANTA, A., SALA, B., COLOMBO, M., OGGIONI, N., CERESA, C., FOUDAH, D., LA RUSSA, F., MILOSO, M., NICOLINI, G., MARMIROLI, P., BENNETT, D. L. & CAVALETTI, G. 2014. Evaluation of tubulin polymerization and chronic inhibition of proteasome as citotoxicity mechanisms in bortezomib-induced peripheral neuropathy. *Cell Cycle,* 13**,** 612-21.

MIHARA, M., ERSTER, S., ZAIKA, A., PETRENKO, O., CHITTENDEN, T., PANCOSKA, P. & MOLL, U. M. 2003. p53 has a direct apoptogenic role at the mitochondria. *Mol Cell,* 11**,** 577-90.

MILLECAMPS, S. & JULIEN, J. P. 2013. Axonal transport deficits and neurodegenerative diseases. *Nat Rev Neurosci,* 14**,** 161-76.

MILLER, F. D., NAUS, C. C., DURAND, M., BLOOM, F. E. & MILNER, R. J. 1987. Isotypes of alpha-tubulin are differentially regulated during neuronal maturation. *J Cell Biol,* 105**,** 3065-73.

MILLER, F. D., POZNIAK, C. D. & WALSH, G. S. 2000. Neuronal life and death: an essential role for the p53 family. *Cell Death Differ,* 7**,** 880-8.

MINAMIDE, L. S., STRIEGL, A. M., BOYLE, J. A., MEBERG, P. J. & BAMBURG, J. R. 2000. Neurodegenerative stimuli induce persistent ADF/cofilin-actin rods that disrupt distal neurite function. *Nat Cell Biol,* 2**,** 628-36.

MITCHISON, T. & KIRSCHNER, M. 1984a. Dynamic instability of microtubule growth. *Nature,* 312**,** 237-42.

MITCHISON, T. & KIRSCHNER, M. 1984b. Dynamic instability of microtubule growth. *Nature,* 312**,** 237-242.

MIYASAKA, H., OKABE, S., ISHIGURO, K., UCHIDA, T. & HIROKAWA, N. 1993. Interaction of the tail domain of high molecular weight subunits of neurofilaments with the COOH-terminal region of tubulin and its regulation by tau protein kinase II. *J Biol Chem,* 268**,** 22695-702.

MIYASAKA, T., SATO, S., TATEBAYASHI, Y. & TAKASHIMA, A. 2010. Microtubule destruction induces tau liberation and its subsequent phosphorylation. *FEBS Lett,* 584**,** 3227-32.

MOCANU, M. M., NISSEN, A., ECKERMANN, K., KHLISTUNOVA, I., BIERNAT, J., DREXLER, D., PETROVA, O., SCHONIG, K., BUJARD, H., MANDELKOW, E., ZHOU, L., RUNE, G. &

MANDELKOW, E. M. 2008. The potential for beta-structure in the repeat domain of tau protein determines aggregation, synaptic decay, neuronal loss, and coassembly with endogenous Tau in inducible mouse models of tauopathy. *J Neurosci,* 28**,** 737-48.

MOGI, M., KONDO, T., MIZUNO, Y. & NAGATSU, T. 2007. p53 protein, interferon-gamma, and NF-kappaB levels are elevated in the parkinsonian brain. *Neurosci Lett,* 414**,** 94-7.

MOLLINEDO, F. & GAJATE, C. 2003. Microtubules, microtubule-interfering agents and apoptosis. *Apoptosis,* 8**,** 413-50.

MOLNAR, Z. & CHEUNG, A. F. 2006. Towards the classification of subpopulations of layer V pyramidal projection neurons. *Neurosci Res,* 55**,** 105-15.

MOMAND, J., WU, H. H. & DASGUPTA, G. 2000. MDM2--master regulator of the p53 tumor suppressor protein. *Gene,* 242**,** 15-29.

MONTEIRO, M. R., KANDRATAVICIUS, L. & LEITE, J. P. 2011. O papel das proteínas do citoesqueleto na fisiologia celular normal e em condições patológicas. *Journal of Epilepsy and Clinical Neurophysiology,* 17**,** 17-23.

MOORE, M. J. 2005. From birth to death: the complex lives of eukaryotic mRNAs. *Science,* 309**,** 1514-8.

MORGAN, D. O. 1995. Principles of CDK regulation. *Nature,* 374**,** 131-4.

MORI, H., KONDO, J. & IHARA, Y. 1987. Ubiquitin is a component of paired helical filaments in Alzheimer's disease. *Science,* 235**,** 1641-4.

MORI, N. & MORII, H. 2002. SCG10-related neuronal growth-associated proteins in neural development, plasticity, degeneration, and aging. *J Neurosci Res,* 70**,** 264-73.

MOTIL, J., CHAN, W. K., DUBEY, M., CHAUDHURY, P., PIMENTA, A., CHYLINSKI, T. M., ORTIZ, D. T. & SHEA, T. B. 2006. Dynein mediates retrograde neurofilament transport within axons and anterograde delivery of NFs from perikarya into axons: regulation by multiple phosphorylation events. *Cell Motil Cytoskeleton,* 63**,** 266-86.

MUKAI, M., IKEGAMI, K., SUGIURA, Y., TAKESHITA, K., NAKAGAWA, A. & SETOU, M. 2009. Recombinant mammalian tubulin polyglutamylase TTLL7 performs both initiation and elongation of polyglutamylation on beta-tubulin through a random sequential pathway. *Biochemistry,* 48**,** 1084-93.

MUNSIE, L. N. & TRUANT, R. 2012. The role of the cofilin-actin rod stress response in neurodegenerative diseases uncovers potential new drug targets. *Bioarchitecture,* 2**,** 204-8.

MURATA, S., YASHIRODA, H. & TANAKA, K. 2009. Molecular mechanisms of proteasome assembly. *Nat Rev Mol Cell Biol,* 10**,** 104-15.

MURAYAMA, S., BOULDIN, T. W. & SUZUKI, K. 1992. Immunocytochemical and ultrastructural studies of upper

motor neurons in amyotrophic lateral sclerosis. *Acta Neuropathol,* 83**,** 518-24.
MURONETZ, V. I., WANG, Z. X., KEITH, T. J., KNULL, H. R. & SRIVASTAVA, D. K. 1994. Binding constants and stoichiometries of glyceraldehyde 3-phosphate dehydrogenase-tubulin complexes. *Arch Biochem Biophys,* 313**,** 253-60.
MURPHY, M., AHN, J., WALKER, K. K., HOFFMAN, W. H., EVANS, R. M., LEVINE, A. J. & GEORGE, D. L. 1999. Transcriptional repression by wild-type p53 utilizes histone deacetylases, mediated by interaction with mSin3a. *Genes Dev,* 13**,** 2490-501.
NAIR, V. D., MCNAUGHT, K. S., GONZALEZ-MAESO, J., SEALFON, S. C. & OLANOW, C. W. 2006. p53 mediates nontranscriptional cell death in dopaminergic cells in response to proteasome inhibition. *J Biol Chem,* 281**,** 39550-60.
NAKAMURA, M., SAATMAN, K. E., GALVIN, J. E., SCHERBEL, U., RAGHUPATHI, R., TROJANOWSKI, J. Q. & MCINTOSH, T. K. 1999. Increased vulnerability of NFH-LacZ transgenic mouse to traumatic brain injury-induced behavioral deficits and cortical damage. *J Cereb Blood Flow Metab,* 19**,** 762-70.
NANDI, D., TAHILIANI, P., KUMAR, A. & CHANDU, D. 2006. The ubiquitin-proteasome system. *J Biosci,* 31**,** 137-55.
NEGIS, Y. & KARABAY, A. 2016. Expression of cell cycle proteins in cortical neurons-Correlation with glutamate-induced neurotoxicity. *Biofactors,* 42**,** 358-67.
NIGG, E. A. 1993. Targets of cyclin-dependent protein kinases. *Current Opinion in Cell Biology,* 5**,** 187-193.
NIWA, S., TAKAHASHI, H. & HIROKAWA, N. 2013. beta-Tubulin mutations that cause severe neuropathies disrupt axonal transport. *EMBO J,* 32**,** 1352-64.
NIXON, R. A. & MAROTTA, C. A. 1984. Degradation of neurofilament proteins by purified human brain cathepsin D. *J Neurochem,* 43**,** 507-16.
NIXON, R. A., PASKEVICH, P. A., SIHAG, R. K. & THAYER, C. Y. 1994. Phosphorylation on carboxyl terminus domains of neurofilament proteins in retinal ganglion cell neurons in vivo: influences on regional neurofilament accumulation, interneurofilament spacing, and axon caliber. *J Cell Biol,* 126**,** 1031-46.
NOGALES, E., WHITTAKER, M., MILLIGAN, R. A. & DOWNING, K. H. 1999. High-resolution model of the microtubule. *Cell,* 96**,** 79-88.
NORTH, B. J., MARSHALL, B. L., BORRA, M. T., DENU, J. M. & VERDIN, E. 2003. The human Sir2 ortholog, SIRT2, is an NAD+-dependent tubulin deacetylase. *Mol Cell,* 11**,** 437-44.
OGAWA, O., LEE, H. G., ZHU, X., RAINA, A., HARRIS, P. L., CASTELLANI, R. J., PERRY, G. & SMITH, M. A. 2003. Increased p27, an essential component of cell cycle control, in Alzheimer's disease. *Aging Cell,* 2**,** 105-10.

OHKAWA, N., FUJITANI, K., TOKUNAGA, E., FURUYA, S. & INOKUCHI, K. 2007a. The microtubule destabilizer stathmin mediates the development of dendritic arbors in neuronal cells. *Journal of Cell Science,* 120**,** 1447.

OHKAWA, N., HASHIMOTO, K., HINO, T., MIGISHIMA, R., YOKOYAMA, M., KANO, M. & INOKUCHI, K. 2007b. Motor discoordination of transgenic mice overexpressing a microtubule destabilizer, stathmin, specifically in Purkinje cells. *Neurosci Res,* 59**,** 93-100.

OKAZAKI, T., WANG, H., MASLIAH, E., CAO, M., JOHNSON, S. A., SUNDSMO, M., SAITOH, T. & MORI, N. 1995. SCG10, a neuron-specific growth-associated protein in Alzheimer's disease. *Neurobiol Aging,* 16**,** 883-94.

ORIKE, N., MIDDLETON, G., BORTHWICK, E., BUCHMAN, V., COWEN, T. & DAVIES, A. M. 2001. Role of PI 3-kinase, Akt and Bcl-2-related proteins in sustaining the survival of neurotrophic factor-independent adult sympathetic neurons. *J Cell Biol,* 154**,** 995-1005.

ORR, M. E., PITSTICK, R., CANINE, B., ASHE, K. H. & CARLSON, G. A. 2012. Genotype-specific differences between mouse CNS stem cell lines expressing frontotemporal dementia mutant or wild type human tau. *PLoS One,* 7**,** e39328.

OUTEIRO, T. F., KONTOPOULOS, E., ALTMANN, S. M., KUFAREVA, I., STRATHEARN, K. E., AMORE, A. M., VOLK, C. B., MAXWELL, M. M., ROCHET, J. C., MCLEAN, P. J., YOUNG, A. B., ABAGYAN, R., FEANY, M. B., HYMAN, B. T. & KAZANTSEV, A. G. 2007. Sirtuin 2 inhibitors rescue alpha-synuclein-mediated toxicity in models of Parkinson's disease. *Science,* 317**,** 516-9.

OZER, R. S. & HALPAIN, S. 2000. Phosphorylation-dependent localization of microtubule-associated protein MAP2c to the actin cytoskeleton. *Mol Biol Cell,* 11**,** 3573-87.

OZON, S., BYK, T. & SOBEL, A. 1998. SCLIP: a novel SCG10-like protein of the stathmin family expressed in the nervous system. *J Neurochem,* 70**,** 2386-96.

OZON, S., GUICHET, A., GAVET, O., ROTH, S. & SOBEL, A. 2002. Drosophila stathmin: a microtubule-destabilizing factor involved in nervous system formation. *Mol Biol Cell,* 13**,** 698-710.

OZON, S., MAUCUER, A. & SOBEL, A. 1997. The stathmin family -- molecular and biological characterization of novel mammalian proteins expressed in the nervous system. *Eur J Biochem,* 248**,** 794-806.

PACHTER, J. S. & LIEM, R. K. 1984. The differential appearance of neurofilament triplet polypeptides in the developing rat optic nerve. *Dev Biol,* 103**,** 200-10.

PACHTER, J. S., YEN, T. J. & CLEVELAND, D. W. 1987. Autoregulation of tubulin expression is achieved through specific degradation of polysomal tubulin mRNAs. *Cell,* 51**,** 283-292.

PAGANO, M., TAM, S. W., THEODORAS, A. M., BEER-ROMERO, P., DEL SAL, G., CHAU, V., YEW, P. R., DRAETTA, G. F. & ROLFE,

M. 1995. Role of the ubiquitin-proteasome pathway in regulating abundance of the cyclin-dependent kinase inhibitor p27. *Science,* 269**,** 682-5.

PAGONABARRAGA, J., KULISEVSKY, J., LLEBARIA, G., GARCIA-SANCHEZ, C., PASCUAL-SEDANO, B. & GIRONELL, A. 2008. Parkinson's disease-cognitive rating scale: a new cognitive scale specific for Parkinson's disease. *Mov Disord,* 23**,** 998-1005.

PAINE, S., LOWE, J., BEDFORD, L. & MAYER, R. J. 2011. Can neurodegeneration be separated from neuropathological hallmarks of chronic idiopathic human neurodegenerative disease? A perspective from modelling! *Biochem Soc Trans,* 39**,** 917-9.

PAINE, S. M., ANDERSON, G., BEDFORD, K., LAWLER, K., MAYER, R. J., LOWE, J. & BEDFORD, L. 2013. Pale body-like inclusion formation and neurodegeneration following depletion of 26S proteasomes in mouse brain neurones are independent of alpha-synuclein. *PLoS One,* 8**,** e54711.

PANDIT, B. & GARTEL, A. L. 2011. Proteasome Inhibitors Induce p53-Independent Apoptosis in Human Cancer Cells. *Am J Pathol,* 178**,** 355-60.

PANT, H. C. 1988. Dephosphorylation of neurofilament proteins enhances their susceptibility to degradation by calpain. *Biochem J,* 256**,** 665-8.

PARISIADOU, L. & CAI, H. 2010. LRRK2 function on actin and microtubule dynamics in Parkinson disease. *Commun Integr Biol,* 3**,** 396-400.

PARK, J. Y., JANG, S. Y., SHIN, Y. K., SUH, D. J. & PARK, H. T. 2013. Calcium-dependent proteasome activation is required for axonal neurofilament degradation. *Neural Regen Res,* 8**,** 3401-9.

PARKER, A. L., KAVALLARIS, M. & MCCARROLL, J. A. 2014. Microtubules and their role in cellular stress in cancer. *Front Oncol,* 4**,** 153.

PAULUSSEN, M., JACOBS, S., VAN DER GUCHT, E., HOF, P. R. & ARCKENS, L. 2011. Cytoarchitecture of the mouse neocortex revealed by the low-molecular-weight neurofilament protein subunit. *Brain Structure and Function,* 216**,** 183-199.

PELLICANO, C., ASSOGNA, F., PIRAS, F., CALTAGIRONE, C., PONTIERI, F. E. & SPALLETTA, G. 2012. Regional cortical thickness and cognitive functions in non-demented Parkinson's disease patients: a pilot study. *Eur J Neurol,* 19**,** 172-5.

PENG, J., SCHWARTZ, D., ELIAS, J. E., THOREEN, C. C., CHENG, D., MARSISCHKY, G., ROELOFS, J., FINLEY, D. & GYGI, S. P. 2003. A proteomics approach to understanding protein ubiquitination. *Nat Biotechnol,* 21**,** 921-6.

PERDIZ, D., MACKEH, R., POUS, C. & BAILLET, A. 2011. The ins and outs of tubulin acetylation: more than just a post-translational modification? *Cell Signal,* 23**,** 763-71.

PEREZ-GALAN, P., ROUE, G., VILLAMOR, N., MONTSERRAT, E., CAMPO, E. & COLOMER, D. 2006. The proteasome inhibitor

bortezomib induces apoptosis in mantle-cell lymphoma through generation of ROS and Noxa activation independent of p53 status. *Blood,* 107**,** 257-64.
PÉREZ-TENORIO, G. & STÅL, O. 2002. Activation of AKT/PKB in breast cancer predicts a worse outcome among endocrine treated patients. *Br J Cancer,* 86**,** 540-5.
PERIS, L., WAGENBACH, M., LAFANECHERE, L., BROCARD, J., MOORE, A. T., KOZIELSKI, F., JOB, D., WORDEMAN, L. & ANDRIEUX, A. 2009. Motor-dependent microtubule disassembly driven by tubulin tyrosination. *J Cell Biol,* 185**,** 1159-66.
PERROT, R., BERGES, R., BOCQUET, A. & EYER, J. 2008. Review of the multiple aspects of neurofilament functions, and their possible contribution to neurodegeneration. *Mol Neurobiol,* 38**,** 27-65.
PERROT, R. & EYER, J. 2009. Neuronal intermediate filaments and neurodegenerative disorders. *Brain Res Bull,* 80**,** 282-95.
PERROT, R. & JULIEN, J. P. 2009. Real-time imaging reveals defects of fast axonal transport induced by disorganization of intermediate filaments. *FASEB J,* 23**,** 3213-25.
PESTRONK, A. 1997. Histology of the Nervous System of Man and Vertebrates. *Neurology,* 48**,** 299-300.
PETROSKI, M. D. & DESHAIES, R. J. 2005. Mechanism of lysine 48-linked ubiquitin-chain synthesis by the cullin-RING ubiquitin-ligase complex SCF-Cdc34. *Cell,* 123**,** 1107-20.
PETRUCELLI, L., DICKSON, D., KEHOE, K., TAYLOR, J., SNYDER, H., GROVER, A., DE LUCIA, M., MCGOWAN, E., LEWIS, J., PRIHAR, G., KIM, J., DILLMANN, W. H., BROWNE, S. E., HALL, A., VOELLMY, R., TSUBOI, Y., DAWSON, T. M., WOLOZIN, B., HARDY, J. & HUTTON, M. 2004. CHIP and Hsp70 regulate tau ubiquitination, degradation and aggregation. *Hum Mol Genet,* 13**,** 703-14.
PICKART, C. M. & EDDINS, M. J. 2004. Ubiquitin: structures, functions, mechanisms. *Biochim Biophys Acta,* 1695**,** 55-72.
PICKERING, A. M. & DAVIES, K. J. 2012. Degradation of damaged proteins: the main function of the 20S proteasome. *Prog Mol Biol Transl Sci,* 109**,** 227-48.
PORUCHYNSKY, M. S., SACKETT, D. L., ROBEY, R. W., WARD, Y., ANNUNZIATA, C. & FOJO, T. 2008. Proteasome inhibitors increase tubulin polymerization and stabilization in tissue culture cells: a possible mechanism contributing to peripheral neuropathy and cellular toxicity following proteasome inhibition. *Cell Cycle,* 7**,** 940-9.
POULAIN, F. E. & SOBEL, A. 2010. The microtubule network and neuronal morphogenesis: Dynamic and coordinated orchestration through multiple players. *Mol Cell Neurosci,* 43**,** 15-32.
PRASAD, S. B., YADAV, S. S., DAS, M., MODI, A., KUMARI, S., PANDEY, L. K., SINGH, S., PRADHAN, S. & NARAYAN, G. 2015. PI3K/AKT pathway-mediated regulation of p27(Kip1) is associated with cell cycle arrest and apoptosis in cervical cancer. *Cell Oncol (Dordr),* 38**,** 215-25.

PRICE, J. L. & STERN, R. 1983. Individual cells in the nucleus basalis--diagonal band complex have restricted axonal projections to the cerebral cortex in the rat. *Brain Res,* 269**,** 352-6.
PROTA, A. E., MAGIERA, M. M., KUIJPERS, M., BARGSTEN, K., FREY, D., WIESER, M., JAUSSI, R., HOOGENRAAD, C. C., KAMMERER, R. A., JANKE, C. & STEINMETZ, M. O. 2013. Structural basis of tubulin tyrosination by tubulin tyrosine ligase. *J Cell Biol,* 200**,** 259-70.
PRZYBORSKI, S. A. & CAMBRAY-DEAKIN, M. A. 1996. Developmental regulation of alpha-tubulin mRNAs during the differentiation of cultured cerebellar granule cells. *Brain Res Mol Brain Res,* 36**,** 179-83.
QI, X., DAVIS, B., CHIANG, Y.-H., FILICHIA, E., BARNETT, A., GREIG, N. H., HOFFER, B. & LUO, Y. 2016. Dopaminergic neuron-specific deletion of p53 gene is neuroprotective in an experimental Parkinson's disease model. *Journal of Neurochemistry,* 138**,** 746-757.
QUINIOU, E., GUICHARD, P., PERAHIA, D., MARCO, S. & MOUAWAD, L. 2013. An atomistic view of microtubule stabilization by GTP. *Structure,* 21**,** 833-43.
QUINLAN, E. M. & HALPAIN, S. 1996. Postsynaptic Mechanisms for Bidirectional Control of MAP2 Phosphorylation by Glutamate Receptors. *Neuron,* 16**,** 357-368.
RAMOS, R. L., TAM, D. M. & BRUMBERG, J. C. 2008. Physiology and morphology of callosal projection neurons in mouse. *Neuroscience,* 153**,** 654-63.
RAPOPORT, M., DAWSON, H. N., BINDER, L. I., VITEK, M. P. & FERREIRA, A. 2002. Tau is essential to beta -amyloid-induced neurotoxicity. *Proc Natl Acad Sci U S A,* 99**,** 6364-9.
RASHIDIAN, J., IYIRHIARO, G., ALEYASIN, H., RIOS, M., VINCENT, I., CALLAGHAN, S., BLAND, R. J., SLACK, R. S., DURING, M. J. & PARK, D. S. 2005. Multiple cyclin-dependent kinases signals are critical mediators of ischemia/hypoxic neuronal death in vitro and in vivo. *Proc Natl Acad Sci U S A,* 102**,** 14080-5.
RASPAGLIO, G., PETRILLO, M., MARTINELLI, E., LI PUMA, D. D., MARIANI, M., DE DONATO, M., FILIPPETTI, F., MOZZETTI, S., PRISLEI, S., ZANNONI, G. F., SCAMBIA, G. & FERLINI, C. 2014. Sox9 and Hif-2α regulate TUBB3 gene expression and affect ovarian cancer aggressiveness. *Gene,* 542**,** 173-181.
RAYBIN, D. & FLAVIN, M. 1975. An enzyme tyrosylating alpha-tubulin and its role in microtubule assembly. *Biochem Biophys Res Commun,* 65**,** 1088-95.
READ, D. E. & GORMAN, A. M. 2009. Involvement of Akt in neurite outgrowth. *Cell Mol Life Sci,* 66**,** 2975-84.
REED, N. A., CAI, D., BLASIUS, T. L., JIH, G. T., MEYHOFER, E., GAERTIG, J. & VERHEY, K. J. 2006. Microtubule acetylation promotes kinesin-1 binding and transport. *Curr Biol,* 16**,** 2166-72.

REGEUR, L. 2000. Increasing loss of brain tissue with increasing dementia: a stereological study of post-mortem brains from elderly females. *Eur J Neurol,* 7**,** 47-54.
REGGIORI, F. & PELHAM, H. R. 2001. Sorting of proteins into multivesicular bodies: ubiquitin-dependent and -independent targeting. *EMBO J,* 20**,** 5176-86.
REN, Q.-G., LIAO, X.-M., CHEN, X.-Q., LIU, G.-P. & WANG, J.-Z. 2007. Effects of tau phosphorylation on proteasome activity. *FEBS Letters,* 581**,** 1521-1528.
REN, R. J., DAMMER, E. B., WANG, G., SEYFRIED, N. T. & LEVEY, A. I. 2014. Proteomics of protein post-translational modifications implicated in neurodegeneration. *Transl Neurodegener,* 3.
REN, Y., LIU, W., JIANG, H., JIANG, Q. & FENG, J. 2005. Selective vulnerability of dopaminergic neurons to microtubule depolymerization. *J Biol Chem,* 280**,** 34105-12.
REN, Y., ZHAO, J. & FENG, J. 2003. Parkin binds to alpha/beta tubulin and increases their ubiquitination and degradation. *J Neurosci,* 23**,** 3316-24.
REZVANI, N., ELKHARAZ, J., LAWLER, K., MEE, M., MAYER, R. J. & BEDFORD, L. 2012. Heterozygosity for the proteasomal Psmc1 ATPase is insufficient to cause neuropathology in mouse brain, but causes cell cycle defects in mouse embryonic fibroblasts. *Neurosci Lett,* 521**,** 130-5.
RICE, L. M., MONTABANA, E. A. & AGARD, D. A. 2008. The lattice as allosteric effector: structural studies of alphabeta- and gamma-tubulin clarify the role of GTP in microtubule assembly. *Proc Natl Acad Sci U S A,* 105**,** 5378-83.
RICKLE, A., BOGDANOVIC, N., VOLKMAN, I., WINBLAD, B., RAVID, R. & COWBURN, R. F. 2004. Akt activity in Alzheimer's disease and other neurodegenerative disorders. *Neuroreport,* 15**,** 955-9.
RINGHOFF, D. N. & CASSIMERIS, L. 2009. Stathmin regulates centrosomal nucleation of microtubules and tubulin dimer/polymer partitioning. *Mol Biol Cell,* 20**,** 3451-8.
RINNE, J. O., PALJARVI, L. & RINNE, U. K. 1987. Neuronal size and density in the nucleus basalis of Meynert in Alzheimer's disease. *J Neurol Sci,* 79**,** 67-76.
RIUDAVETS, M. A., IACONO, D., RESNICK, S. M., O'BRIEN, R., ZONDERMAN, A. B., MARTIN, L. J., RUDOW, G., PLETNIKOVA, O. & TRONCOSO, J. C. 2007. Resistance to Alzheimer's pathology is associated with nuclear hypertrophy in neurons. *Neurobiol Aging,* 28**,** 1484-92.
ROBSON, S. J. & BURGOYNE, R. D. 1989. Differential localisation of tyrosinated, detyrosinated, and acetylated alpha-tubulins in neurites and growth cones of dorsal root ganglion neurons. *Cell Motil Cytoskeleton,* 12**,** 273-82.
ROCHER, A. B., KINSON, M. S. & LUEBKE, J. I. 2008. Significant structural but not physiological changes in cortical neurons of 12-month-old Tg2576 mice. *Neurobiol Dis,* 32**,** 309-18.
RODIER, G., MONTAGNOLI, A., DI MARCOTULLIO, L., COULOMBE, P., DRAETTA, G. F., PAGANO, M. & MELOCHE, S. 2001. p27

cytoplasmic localization is regulated by phosphorylation on Ser10 and is not a prerequisite for its proteolysis. *EMBO J,* 20**,** 6672-82.

ROGOWSKI, K., JUGE, F., VAN DIJK, J., WLOGA, D., STRUB, J. M., LEVILLIERS, N., THOMAS, D., BRE, M. H., VAN DORSSELAER, A., GAERTIG, J. & JANKE, C. 2009. Evolutionary divergence of enzymatic mechanisms for posttranslational polyglycylation. *Cell,* 137**,** 1076-87.

ROMAND, S., WANG, Y., TOLEDO-RODRIGUEZ, M. & MARKRAM, H. 2011. Morphological Development of Thick-Tufted Layer V Pyramidal Cells in the Rat Somatosensory Cortex. *Front Neuroanat,* 5.

ROY, S., COFFEE, P., SMITH, G., LIEM, R. K., BRADY, S. T. & BLACK, M. M. 2000. Neurofilaments are transported rapidly but intermittently in axons: implications for slow axonal transport. *J Neurosci,* 20**,** 6849-61.

RUBIN, C. I. & ATWEH, G. F. 2004. The role of stathmin in the regulation of the cell cycle. *J Cell Biochem,* 93**,** 242-50.

RUDRABHATLA, P., GRANT, P., JAFFE, H., STRONG, M. J. & PANT, H. C. 2010. Quantitative phosphoproteomic analysis of neuronal intermediate filament proteins (NF-M/H) in Alzheimer's disease by iTRAQ. *FASEB J,* 24**,** 4396-407.

RYU, E. J., ANGELASTRO, J. M. & GREENE, L. A. 2005. Analysis of gene expression changes in a cellular model of Parkinson disease. *Neurobiol Dis,* 18**,** 54-74.

SAAL, L. H., JOHANSSON, P., HOLM, K., GRUVBERGER-SAAL, S. K., SHE, Q. B., MAURER, M., KOUJAK, S., FERRANDO, A. A., MALMSTROM, P., MEMEO, L., ISOLA, J., BENDAHL, P. O., ROSEN, N., HIBSHOOSH, H., RINGNER, M., BORG, A. & PARSONS, R. 2007. Poor prognosis in carcinoma is associated with a gene expression signature of aberrant PTEN tumor suppressor pathway activity. *Proc Natl Acad Sci U S A,* 104**,** 7564-9.

SADOWSKI, M., SURYADINATA, R., TAN, A. R., ROESLEY, S. N. & SARCEVIC, B. 2012. Protein monoubiquitination and polyubiquitination generate structural diversity to control distinct biological processes. *IUBMB Life,* 64**,** 136-42.

SAEKI, Y. & TANAKA, K. 2012. Assembly and function of the proteasome. *Methods Mol Biol,* 832**,** 315-37.

SAETRE, P., JAZIN, E. & EMILSSON, L. 2011. Age-related changes in gene expression are accelerated in Alzheimer's disease. *Synapse,* 65**,** 971-4.

SALINAS, M., MARTIN, D., ALVAREZ, A. & CUADRADO, A. 2001. Akt1/PKBalpha protects PC12 cells against the parkinsonism-inducing neurotoxin 1-methyl-4-phenylpyridinium and reduces the levels of oxygen-free radicals. *Mol Cell Neurosci,* 17**,** 67-77.

SALINAS, S., CARAZO-SALAS, R. E., PROUKAKIS, C., COOPER, J. M., WESTON, A. E., SCHIAVO, G. & WARNER, T. T. 2005. Human spastin has multiple microtubule-related functions. *J Neurochem,* 95**,** 1411-20.

SANCHEZ, C., DIAZ-NIDO, J. & AVILA, J. 2000. Phosphorylation of microtubule-associated protein 2 (MAP2) and its relevance for the regulation of the neuronal cytoskeleton function. *Prog Neurobiol,* 61**,** 133-68.

SÁNCHEZ, I., HASSINGER, L., SIHAG, R. K., CLEVELAND, D. W., MOHAN, P. & NIXON, R. A. 2000. Local Control of Neurofilament Accumulation during Radial Growth of Myelinating Axons in Vivo. *The Journal of Cell Biology,* 151**,** 1013.

SASAKI, S. & IWATA, M. 2007. Mitochondrial alterations in the spinal cord of patients with sporadic amyotrophic lateral sclerosis. *J Neuropathol Exp Neurol,* 66**,** 10-6.

SCHEFFNER, M., NUBER, U. & HUIBREGTSE, J. M. 1995. Protein ubiquitination involving an E1-E2-E3 enzyme ubiquitin thioester cascade. *Nature,* 373**,** 81-3.

SCHEVZOV, G., CURTHOYS, N. M., GUNNING, P. W. & FATH, T. 2012. Functional diversity of actin cytoskeleton in neurons and its regulation by tropomyosin. *Int Rev Cell Mol Biol,* 298**,** 33-94.

SCHIMMACK, S., TAYLOR, A., LAWRENCE, B., SCHMITZ-WINNENTHAL, H., FISCHER, L., BUCHLER, M. W., MODLIN, I. M., KIDD, M. & TANG, L. H. 2015. Stathmin in pancreatic neuroendocrine neoplasms: a marker of proliferation and PI3K signaling. *Tumour Biol,* 36**,** 399-408.

SCHRAEN-MASCHKE, S., SERGEANT, N., DHAENENS, C. M., BOMBOIS, S., DERAMECOURT, V., CAILLET-BOUDIN, M. L., PASQUIER, F., MAURAGE, C. A., SABLONNIERE, B., VANMECHELEN, E. & BUEE, L. 2008. Tau as a biomarker of neurodegenerative diseases. *Biomark Med,* 2**,** 363-84.

SELVARAJ, B. T., FRANK, N., BENDER, F. L. P., ASAN, E. & SENDTNER, M. 2012. Local axonal function of STAT3 rescues axon degeneration in the pmn model of motoneuron disease. *J Cell Biol,* 199**,** 437-51.

SHAFEY, D., MACKENZIE, A. E. & KOTHARY, R. 2008. Neurodevelopmental abnormalities in neurosphere-derived neural stem cells from SMN-depleted mice. *J Neurosci Res,* 86**,** 2839-47.

SHAFIT-ZAGARDO, B. & KALCHEVA, N. 1998. Making sense of the multiple MAP-2 transcripts and their role in the neuron. *Molecular Neurobiology,* 16**,** 149-162.

SHAW, G. & WEBER, K. 1982. Differential expression of neurofilament triplet proteins in brain development. *Nature,* 298**,** 277-9.

SHEA, T. B. & FLANAGAN, L. A. 2001. Kinesin, dynein and neurofilament transport. *Trends Neurosci,* 24**,** 644-8.

SHEA, T. B., PASKEVICH, P. A. & BEERMANN, M. L. 1993. The protein phosphatase inhibitor okadaic acid increases axonal neurofilaments and neurite caliber, and decreases axonal microtubules in NB2a/d1 cells. *J Neurosci Res,* 35**,** 507-21.

SHEA, T. B., ZHENG, Y. L., ORTIZ, D. & PANT, H. C. 2004. Cyclin-dependent kinase 5 increases perikaryal neurofilament

phosphorylation and inhibits neurofilament axonal transport in response to oxidative stress. *J Neurosci Res,* 76**,** 795-800.
SHEFFIELD, L. G., MISKIEWICZ, H. B., TANNENBAUM, L. B. & MIRRA, S. S. 2006. Nuclear pore complex proteins in Alzheimer disease. *J Neuropathol Exp Neurol,* 65**,** 45-54.
SHELTON, M. A., NEWMAN, J. T., GU, H., SAMPSON, A. R., FISH, K. N., MACDONALD, M. L., MOYER, C. E., DIBITETTO, J. V., DORPH-PETERSEN, K. A., PENZES, P., LEWIS, D. A. & SWEET, R. A. 2015. Loss of microtubule-associated protein 2 immunoreactivity linked to dendritic spine loss in Schizophrenia. *Biol Psychiatry,* 78**,** 374-85.
SHEN, Y. & YU, L. C. 2008. Potential protection of curcumin against hypoxia-induced decreases in beta-III tubulin content in rat prefrontal cortical neurons. *Neurochem Res,* 33**,** 2112-7.
SHIMURA, H., SCHWARTZ, D., GYGI, S. P. & KOSIK, K. S. 2004. CHIP-Hsc70 complex ubiquitinates phosphorylated tau and enhances cell survival. *Journal of Biological Chemistry,* 279**,** 4869-4876.
SHIN, I., YAKES, F. M., ROJO, F., SHIN, N. Y., BAKIN, A. V., BASELGA, J. & ARTEAGA, C. L. 2002. PKB/Akt mediates cell-cycle progression by phosphorylation of p27(Kip1) at threonine 157 and modulation of its cellular localization. *Nat Med,* 8**,** 1145-52.
SHIRANE, M., HARUMIYA, Y., ISHIDA, N., HIRAI, A., MIYAMOTO, C., HATAKEYAMA, S., NAKAYAMA, K. & KITAGAWA, M. 1999. Down-regulation of p27(Kip1) by two mechanisms, ubiquitin-mediated degradation and proteolytic processing. *J Biol Chem,* 274**,** 13886-93.
SHUMYATSKY, G. P., MALLERET, G., SHIN, R. M., TAKIZAWA, S., TULLY, K., TSVETKOV, E., ZAKHARENKO, S. S., JOSEPH, J., VRONSKAYA, S., YIN, D., SCHUBART, U. K., KANDEL, E. R. & BOLSHAKOV, V. Y. 2005. Stathmin, a gene enriched in the amygdala, controls both learned and innate fear. *Cell,* 123**,** 697-709.
SIGISMUND, S., WOELK, T., PURI, C., MASPERO, E., TACCHETTI, C., TRANSIDICO, P., DI FIORE, P. P. & POLO, S. 2005. Clathrin-independent endocytosis of ubiquitinated cargos. *Proc Natl Acad Sci U S A,* 102**,** 2760-5.
SILLIMAN, C. C. & STURGILL, T. W. 1989. Phosphorylation of microtubule-associated protein 2 by MAP kinase primarily involves the projection domain. *Biochem Biophys Res Commun,* 160**,** 993-8.
SILVEIRA, W. A., GONCALVES, D. A., GRACA, F. A., ANDRADE-LOPES, A. L., BERGANTIN, L. B., ZANON, N. M., GODINHO, R. O., KETTELHUT, I. C. & NAVEGANTES, L. C. 2014. Activating cAMP/PKA signaling in skeletal muscle suppresses the ubiquitin-proteasome-dependent proteolysis: implications for sympathetic regulation. *J Appl Physiol (1985),* 117**,** 11-9.
SIONOV, R. V. & HAUPT, Y. 1999. The cellular response to p53: the decision between life and death. *Oncogene,* 18**,** 6145-57.

SIRAJUDDIN, M., RICE, L. M. & VALE, R. D. 2014. Regulation of microtubule motors by tubulin isotypes and post-translational modifications. *Nat Cell Biol,* 16**,** 335-44.

SIRI, S., BENAGLIO, I., FRIGERIO, A., BINETTI, G. & CAPPA, S. F. 2001. A brief neuropsychological assessment for the differential diagnosis between frontotemporal dementia and Alzheimer's disease. *Eur J Neurol,* 8**,** 125-32.

SLOBODA, R. D. 2009. Posttranslational protein modifications in cilia and flagella. *Methods Cell Biol,* 94**,** 347-63.

SLOSS, C. M., WANG, F., LIU, R., XIA, L., HOUSTON, M., LJUNGMAN, D., PALLADINO, M. A. & CUSACK, J. C. 2008. Proteasome inhibition activates EGFR and EGFR-independent mitogenic kinase signaling pathways in pancreatic cancer cells: Implications for combination therapy. *Clin Cancer Res,* 14**,** 5116-23.

SOBEL, A., BOUTTERIN, M. C., BERETTA, L., CHNEIWEISS, H., DOYE, V. & PEYRO-SAINT-PAUL, H. 1989. Intracellular substrates for extracellular signaling. Characterization of a ubiquitous, neuron-enriched phosphoprotein (stathmin). *J Biol Chem,* 264**,** 3765-72.

SONEGO, M., SCHIAPPACASSI, M., LOVISA, S., DALL'ACQUA, A., BAGNOLI, M., LOVAT, F., LIBRA, M., D'ANDREA, S., CANZONIERI, V., MILITELLO, L., NAPOLI, M., GIORDA, G., PIVETTA, B., MEZZANZANICA, D., BARBARESCHI, M., VALERI, B., CANEVARI, S., COLOMBATTI, A., BELLETTI, B., DEL SAL, G. & BALDASSARRE, G. 2013. Stathmin regulates mutant p53 stability and transcriptional activity in ovarian cancer. *EMBO Mol Med,* 5**,** 707-22.

SONG, W., CHO, Y., WATT, D. & CAVALLI, V. 2015. Tubulin-tyrosine ligase (TTL)-mediated increase in tyrosinated alpha-tubulin in injured axons is required for retrograde injury signaling and axon regeneration. *J Biol Chem,* 290**,** 14765-75.

SOPPINA, V., HERBSTMAN, J. F., SKINIOTIS, G. & VERHEY, K. J. 2012. Luminal localization of alpha-tubulin K40 acetylation by cryo-EM analysis of fab-labeled microtubules. *PLoS One,* 7**,** e48204.

SOROKIN, A. V., KIM, E. R. & OVCHINNIKOV, L. P. 2009. Proteasome system of protein degradation and processing. *Biochemistry (Mosc),* 74**,** 1411-42.

SOUSA, V. L., BELLANI, S., GIANNANDREA, M., YOUSUF, M., VALTORTA, F., MELDOLESI, J. & CHIEREGATTI, E. 2009. {alpha}-synuclein and its A30P mutant affect actin cytoskeletal structure and dynamics. *Mol Biol Cell,* 20**,** 3725-39.

SPRINGER, J. E., AZBILL, R. D., KENNEDY, S. E., GEORGE, J. & GEDDES, J. W. 1997. Rapid calpain I activation and cytoskeletal protein degradation following traumatic spinal cord injury: attenuation with riluzole pretreatment. *J Neurochem,* 69**,** 1592-600.

SPRUSTON, N. 2008. Pyramidal neurons: dendritic structure and synaptic integration. *Nat Rev Neurosci,* 9**,** 206-21.

STAIGER, J. F., FLAGMEYER, I., SCHUBERT, D., ZILLES, K., KÖTTER, R. & LUHMANN, H. J. 2004. Functional diversity of Layer IV spiny neurons in rat somatosensory cortex: quantitative morphology of electrophysiologically characterized and biocytin labeled cells. *Cerebral Cortex,* 14**,** 690-701.

STEHBENS, S. & WITTMANN, T. 2012. Targeting and transport: How microtubules control focal adhesion dynamics. *The Journal of Cell Biology,* 198**,** 481-489.

STEINMETZ, M. O. 2007. Structure and thermodynamics of the tubulin-stathmin interaction. *J Struct Biol,* 158**,** 137-47.

STEINMETZ, M. O., JAHNKE, W., TOWBIN, H., GARCIA-ECHEVERRIA, C., VOSHOL, H., MULLER, D. & VAN OOSTRUM, J. 2001. Phosphorylation disrupts the central helix in Op18/stathmin and suppresses binding to tubulin. *EMBO Rep,* 2**,** 505-10.

STEPHEN, J. M., MONTAÑO, R., DONAHUE, C. H., ADAIR, J. C., KNOEFEL, J., QUALLS, C., HART, B., RANKEN, D. & AINE, C. J. 2010. Somatosensory responses in normal aging, mild cognitive impairment, and Alzheimer's disease. *J Neural Transm,* 117**,** 217-25.

STOOTHOFF, W. H. & JOHNSON, G. V. W. 2005. Tau phosphorylation: physiological and pathological consequences. *Biochimica et Biophysica Acta (BBA) - Molecular Basis of Disease,* 1739**,** 280-297.

STRONG, M. J. 2010. The evidence for altered RNA metabolism in amyotrophic lateral sclerosis (ALS). *J Neurol Sci,* 288**,** 1-12.

STYS, P. K. & JIANG, Q. 2002. Calpain-dependent neurofilament breakdown in anoxic and ischemic rat central axons. *Neuroscience Letters,* 328**,** 150-154.

SULLIVAN, K. F. & CLEVELAND, D. W. 1986. Identification of conserved isotype-defining variable region sequences for four vertebrate beta tubulin polypeptide classes. *Proc Natl Acad Sci U S A,* 83**,** 4327-31.

SUN, C., ZHAO, J., JIN, Y., HOU, C., ZONG, W., LU, T., LI, H. & GAO, J. 2014. PTEN regulation of the proliferation and differentiation of auditory progenitors through the PTEN/PI3K/Akt-signaling pathway in mice. *Neuroreport,* 25**,** 177-83.

SYDOW, A., VAN DER JEUGD, A., ZHENG, F., AHMED, T., BALSCHUN, D., PETROVA, O., DREXLER, D., ZHOU, L., RUNE, G., MANDELKOW, E., D'HOOGE, R., ALZHEIMER, C. & MANDELKOW, E. M. 2011a. Reversibility of Tau-related cognitive defects in a regulatable FTD mouse model. *J Mol Neurosci,* 45**,** 432-7.

SYDOW, A., VAN DER JEUGD, A., ZHENG, F., AHMED, T., BALSCHUN, D., PETROVA, O., DREXLER, D., ZHOU, L., RUNE, G., MANDELKOW, E., D'HOOGE, R., ALZHEIMER, C. & MANDELKOW, E. M. 2011b. Tau-induced defects in synaptic plasticity, learning, and memory are reversible in transgenic mice after switching off the toxic Tau mutant. *J Neurosci,* 31**,** 2511-25.

SZARO, B. G. & STRONG, M. J. 2010. Post-transcriptional control of neurofilaments: New roles in development, regeneration and neurodegenerative disease. *Trends Neurosci,* 33**,** 27-37.
SZYK, A., DEACONESCU, A. M., PISZCZEK, G. & ROLL-MECAK, A. 2011. Tubulin tyrosine ligase structure reveals adaptation of an ancient fold to bind and modify tubulin. *Nat Struct Mol Biol,* 18**,** 1250-8.
SZYK, A., PISZCZEK, G. & ROLL-MECAK, A. 2013. Tubulin tyrosine ligase and stathmin compete for tubulin binding in vitro. *J Mol Biol,* 425**,** 2412-4.
TAM, C. W., BURTON, E. J., MCKEITH, I. G., BURN, D. J. & O'BRIEN, J. T. 2005. Temporal lobe atrophy on MRI in Parkinson disease with dementia: a comparison with Alzheimer disease and dementia with Lewy bodies. *Neurology,* 64**,** 861-5.
TANG, B., CAI, J., SUN, L., LI, Y., QU, J., SNIDER, B. J. & WU, S. 2014. Proteasome inhibitors activate autophagy involving inhibition of PI3K-Akt-mTOR pathway as an anti-oxidation defense in human RPE cells. *PLoS One,* 9**,** e103364.
TANNER, J. J., MARECI, T. H., OKUN, M. S., BOWERS, D., LIBON, D. J. & PRICE, C. C. 2015. Temporal lobe and frontal-subcortical dissociations in non-demented Parkinson's disease with verbal memory impairment. *PLOS ONE,* 10**,** e0133792.
TAYLOR, S. C., BERKELMAN, T., YADAV, G. & HAMMOND, M. 2013. A defined methodology for reliable quantification of Western blot data. *Mol Biotechnol,* 55**,** 217-26.
TENG, J., TAKEI, Y., HARADA, A., NAKATA, T., CHEN, J. & HIROKAWA, N. 2001. Synergistic effects of MAP2 and MAP1B knockout in neuronal migration, dendritic outgrowth, and microtubule organization. *J Cell Biol,* 155**,** 65-76.
THEISS, C., NAPIREI, M. & MELLER, K. 2005. Impairment of anterograde and retrograde neurofilament transport after anti-kinesin and anti-dynein antibody microinjection in chicken dorsal root ganglia. *Eur J Cell Biol,* 84**,** 29-43.
THYAGARAJAN, A., STRONG, M. J. & SZARO, B. G. 2007. Post-transcriptional control of neurofilaments in development and disease. *Exp Cell Res,* 313**,** 2088-97.
TIMMONS, S., COAKLEY, M. F., MOLONEY, A. M. & C, O. N. 2009. Akt signal transduction dysfunction in Parkinson's disease. *Neurosci Lett,* 467**,** 30-5.
TISCHFIELD, M. A. & ENGLE, E. C. 2010. Distinct alpha- and beta-tubulin isotypes are required for the positioning, differentiation and survival of neurons: new support for the 'multi-tubulin' hypothesis. *Biosci Rep,* 30**,** 319-30.
TRAMUTOLA, A., TRIPLETT, J. C., DI DOMENICO, F., NIEDOWICZ, D. M., MURPHY, M. P., COCCIA, R., PERLUIGI, M. & BUTTERFIELD, D. A. 2015. Alteration of mTOR signaling occurs early in the progression of Alzheimer disease (AD): analysis of brain from subjects with pre-clinical AD, amnestic mild cognitive impairment and late-stage AD. *J Neurochem,* 133**,** 739-49.

TU, P. H., ELDER, G., LAZZARINI, R. A., NELSON, D., TROJANOWSKI, J. Q. & LEE, V. M. 1995. Overexpression of the human NFM subunit in transgenic mice modifies the level of endogenous NFL and the phosphorylation state of NFH subunits. *J Cell Biol,* 129**,** 1629-40.

TU, P. H., ROBINSON, K. A., DE SNOO, F., EYER, J., PETERSON, A., LEE, V. M. & TROJANOWSKI, J. Q. 1997. Selective degeneration fo Purkinje cells with Lewy body-like inclusions in aged NFHLACZ transgenic mice. *J Neurosci,* 17**,** 1064-74.

TUTAR, Y., ÖZGUR, A. & TUTAR, L. T. 2013. Role of Protein Aggregation in Neurodegenerative Diseases. *In:* KISHORE, U. (ed.) *Neurodegenerative Diseases.* Rijeka: InTech.

UCHIDA, S. & SHUMYATSKY, G. P. 2015. Deceivingly dynamic: Learning-dependent changes in stathmin and microtubules. *Neurobiol Learn Mem,* 124**,** 52-61.

UGUN-KLUSEK, A., TATHAM, M. H., ELKHARAZ, J., CONSTANTIN-TEODOSIU, D., LAWLER, K., MOHAMED, H., PAINE, S. M., ANDERSON, G., JOHN MAYER, R., LOWE, J., ELLEN BILLETT, E. & BEDFORD, L. 2017. Continued 26S proteasome dysfunction in mouse brain cortical neurons impairs autophagy and the Keap1-Nrf2 oxidative defence pathway. *Cell Death Dis,* 8**,** e2531.

UNDAMATLA, J. & SZARO, B. G. 2001. Differential expression and localization of neuronal intermediate filament proteins within newly developing neurites in dissociated cultures of Xenopus laevis embryonic spinal cord. *Cell Motil Cytoskeleton,* 49**,** 16-32.

VAKIFAHMETOGLU-NORBERG, H., NORBERG, E., PERDOMO, A. B., OLSSON, M., CICCOSANTI, F., ORRENIUS, S., FIMIA, G. M., PIACENTINI, M. & ZHIVOTOVSKY, B. 2013. Caspase-2 promotes cytoskeleton protein degradation during apoptotic cell death. *Cell Death Dis,* 4**,** e940.

VAN DER GUCHT, E., HOF, P. R., VAN BRUSSEL, L., BURNAT, K. & ARCKENS, L. 2007. Neurofilament protein and neuronal activity markers define regional architectonic parcellation in the mouse visual cortex. *Cereb Cortex,* 17**,** 2805-19.

VAN DER VAART, B., AKHMANOVA, A. & STRAUBE, A. 2009. Regulation of microtubule dynamic instability. *Biochem Soc Trans,* 37**,** 1007-13.

VAZIRI, S. A., GRABOWSKI, D. R., HILL, J., RYBICKI, L. R., BURK, R., BUKOWSKI, R. M., GANAPATHI, M. K. & GANAPATHI, R. 2009. Inhibition of proteasome activity by bortezomib in renal cancer cells is p53 dependent and VHL independent. *Anticancer Res,* 29**,** 2961-9.

VIDAL, A. & KOFF, A. 2000. Cell-cycle inhibitors: three families united by a common cause. *Gene,* 247**,** 1-15.

VOGES, D., ZWICKL, P. & BAUMEISTER, W. 1999. The 26S proteasome: a molecular machine designed for controlled proteolysis. *Annu Rev Biochem,* 68**,** 1015-68.

WANG, H., WU, M., ZHAN, C., MA, E., YANG, M., YANG, X. & LI, Y. 2012. Neurofilament proteins in axonal regeneration and neurodegenerative diseases. *Neural Regen Res,* 7**,** 620-6.

WANG, H. W. & NOGALES, E. 2005. Nucleotide-dependent bending flexibility of tubulin regulates microtubule assembly. *Nature,* 435**,** 911-5.
WANG, J.-Z., TUNG, Y. C., WANG, Y., LI, X. T., IQBAL, K. & GRUNDKE-IQBAL, I. 2001. Hyperphosphorylation and accumulation of neurofilament proteins in Alzheimer disease brain and in okadaic acid-treated SY5Y cells. *FEBS Letters,* 507**,** 81-87.
WANG, L., CHENG, S., YIN, Z., XU, C., LU, S., HOU, J., YU, T., ZHU, X., ZOU, X., PENG, Y., XU, Y., YANG, Z. & CHEN, G. 2015. Conditional inactivation of Akt three isoforms causes tau hyperphosphorylation in the brain. *Molecular Neurodegeneration,* 10**,** 33.
WANG, Q., SONG, F., ZHANG, C., ZHAO, X., ZHU, Z., YU, S. & XIE, K. 2011. Carboxyl-terminus of Hsc70 interacting protein mediates 2,5-hexanedione-induced neurofilament medium chain degradation. *Biochem Pharmacol,* 81**,** 793-9.
WANG, T. & MORGAN, J. I. 2007. The Purkinje cell degeneration (pcd) mouse: An unexpected molecular link between neuronal degeneration and regeneration. *Brain Research,* 1140**,** 26-40.
WANG, W., BU, B., XIE, M., ZHANG, M., YU, Z. & TAO, D. 2009. Neural cell cycle dysregulation and central nervous system diseases. *Progress in Neurobiology,* 89**,** 1-17.
WANG, X., REN, J. H., LIN, F., WEI, J. X., LONG, M., YAN, L. & ZHANG, H. Z. 2010. Stathmin is involved in arsenic trioxide-induced apoptosis in human cervical cancer cell lines via PI3K linked signal pathway. *Cancer Biol Ther,* 10**,** 632-43.
WANG, Y., GAO, Z., ZHANG, D., BO, X., WANG, Y., WANG, J., SHEN, S., LIU, H., SUO, T., PAN, H., AI, Z. & LIU, H. 2017. Stathmin decreases cholangiocarcinoma cell line sensitivity to staurosporine-triggered apoptosis via the induction of ERK and Akt signaling. *Oncotarget,* 8**,** 15775-88.
WANG, Y. & MANDELKOW, E. 2012. Degradation of tau protein by autophagy and proteasomal pathways. *Biochemical Society Transactions,* 40**,** 644.
WANG, Y. H. & SCADDEN, D. T. 2015. Harnessing the apoptotic programs in cancer stem-like cells. *EMBO Rep,* 16**,** 1084-98.
WATANABE, A., SUZUKI, H., YOKOBORI, T., TSUKAGOSHI, M., ALTAN, B., KUBO, N., SUZUKI, S., ARAKI, K., WADA, S., KASHIWABARA, K., HOSOUCHI, Y. & KUWANO, H. 2014. Stathmin1 regulates p27 expression, proliferation and drug resistance, resulting in poor clinical prognosis in cholangiocarcinoma. *Cancer Sci,* 105**,** 690-6.
WEN, H.-L., TING, C.-H., LIU, H.-C., LI, H. & LIN-CHAO, S. 2013. Decreased stathmin expression ameliorates neuromuscular defects but fails to prolong survival in a mouse model of spinal muscular atrophy. *Neurobiology of Disease,* 52**,** 94-103.
WEN, H. L., LIN, Y. T., TING, C. H., LIN-CHAO, S., LI, H. & HSIEH-LI, H. M. 2010. Stathmin, a microtubule-destabilizing

protein, is dysregulated in spinal muscular atrophy. *Hum Mol Genet,* 19**,** 1766-78.
WILLIAMS-GRAY, C. H., FOLTYNIE, T., BRAYNE, C. E., ROBBINS, T. W. & BARKER, R. A. 2007. Evolution of cognitive dysfunction in an incident Parkinson's disease cohort. *Brain,* 130**,** 1787-98.
WILLIAMSON, T. L., BRUIJN, L. I., ZHU, Q., ANDERSON, K. L., ANDERSON, S. D., JULIEN, J. P. & CLEVELAND, D. W. 1998. Absence of neurofilaments reduces the selective vulnerability of motor neurons and slows disease caused by a familial amyotrophic lateral sclerosis-linked superoxide dismutase 1 mutant. *Proc Natl Acad Sci U S A,* 95**,** 9631-6.
WITTE, H., NEUKIRCHEN, D. & BRADKE, F. 2008. Microtubule stabilization specifies initial neuronal polarization. *J Cell Biol,* 180**,** 619-32.
WOLFE, M. S. 2012. The Role of Tau in Neurodegenerative Diseases and Its Potential as a Therapeutic Target. *Scientifica,* 2012**,** 20.
WONG, N. K., HE, B. P. & STRONG, M. J. 2000. Characterization of neuronal intermediate filament protein expression in cervical spinal motor neurons in sporadic amyotrophic lateral sclerosis (ALS). *J Neuropathol Exp Neurol,* 59**,** 972-82.
WONG, P. C., MARSZALEK, J., CRAWFORD, T. O., XU, Z., HSIEH, S. T., GRIFFIN, J. W. & CLEVELAND, D. W. 1995. Increasing neurofilament subunit NF-M expression reduces axonal NF-H, inhibits radial growth, and results in neurofilamentous accumulation in motor neurons. *J Cell Biol,* 130**,** 1413-22.
WU, Y. T., OUYANG, W., LAZORCHAK, A. S., LIU, D., SHEN, H. M. & SU, B. 2011. mTOR complex 2 targets Akt for proteasomal degradation via phosphorylation at the hydrophobic motif. *J Biol Chem,* 286**,** 14190-8.
XIE, C. & MIYASAKA, T. 2016. *The Role of the Carboxyl-Terminal Sequence of Tau and MAP2 in the Pathogenesis of Dementia*, Front Mol Neurosci. 2016;9:158. doi:10.3389/fnmol.2016.00158.
XIE, C., MIYASAKA, T., YOSHIMURA, S., HATSUTA, H., YOSHINA, S., KAGE-NAKADAI, E., MITANI, S., MURAYAMA, S. & IHARA, Y. 2014. The Homologous Carboxyl-Terminal Domains of Microtubule-Associated Protein 2 and TAU Induce Neuronal Dysfunction and Have Differential Fates in the Evolution of Neurofibrillary Tangles. *PLoS One,* 9.
XIE, C., SOEDA, Y., SHINZAKI, Y., IN, Y., TOMOO, K., IHARA, Y. & MIYASAKA, T. 2015. Identification of key amino acids responsible for the distinct aggregation properties of microtubule-associated protein 2 and tau. *J Neurochem,* 135**,** 19-26.
XU, Z., CORK, L. C., GRIFFIN, J. W. & CLEVELAND, D. W. 1993. Increased expression of neurofilament subunit NF-L produces morphological alterations that resemble the pathology of human motor neuron disease. *Cell,* 73**,** 23-33.
XUE, B., HUANG, W., YUAN, X., XU, B., LOU, Y., ZHOU, Q., RAN, F., GE, Z., LI, R. & CUI, J. 2015. YSY01A, a novel proteasome

inhibitor, induces cell cycle arrest on G2 phase in MCF-7 cells via ERα and PI3K/Akt pathways. *J Cancer,* 6**,** 319-26.
YABE, J. T., JUNG, C., CHAN, W. K. & SHEA, T. B. 2000. Phospho-dependent association of neurofilament proteins with kinesin in situ. *Cell Motil Cytoskeleton,* 45**,** 249-62.
YADAV, P., SELVARAJ, B. T., BENDER, F. L., BEHRINGER, M., MORADI, M., SIVADASAN, R., DOMBERT, B., BLUM, R., ASAN, E., SAUER, M., JULIEN, J. P. & SENDTNER, M. 2016. Neurofilament depletion improves microtubule dynamics via modulation of Stat3/stathmin signaling. *Acta Neuropathol*.
YAMAGUCHI, A., TAMATANI, M., MATSUZAKI, H., NAMIKAWA, K., KIYAMA, H., VITEK, M. P., MITSUDA, N. & TOHYAMA, M. 2001. Akt activation protects hippocampal neurons from apoptosis by inhibiting transcriptional activity of p53. *J Biol Chem,* 276**,** 5256-64.
YAMAMOTO, H., SAITOH, Y., FUKUNAGA, K., NISHIMURA, H. & MIYAMOTO, E. 1988. Dephosphorylation of microtubule proteins by brain protein phosphatases 1 and 2A, and its effect on microtubule assembly. *J Neurochem,* 50**,** 1614-23.
YAN, D., GUO, L. & WANG, Y. 2006. Requirement of dendritic Akt degradation by the ubiquitin–proteasome system for neuronal polarity. *J Cell Biol,* 174**,** 415-24.
YANG, Y. & HERRUP, K. 2007. Cell division in the CNS: protective response or lethal event in post-mitotic neurons? *Biochim Biophys Acta,* 1772**,** 457-66.
YANG, Y., LI, C.-C. H. & WEISSMAN, A. M. 2004. Regulating the p53 system through ubiquitination. *Oncogene,* 23**,** 2096-2106.
YANG, Z.-Z., TSCHOPP, O., HEMMINGS-MIESZCZAK, M., FENG, J., BRODBECK, D., PERENTES, E. & HEMMINGS, B. A. 2003a. Protein kinase Bα/Akt1 regulates placental development and fetal growth. *Journal of Biological Chemistry,* 278**,** 32124-32131.
YANG, Z. Z., TSCHOPP, O., HEMMINGS-MIESZCZAK, M., FENG, J., BRODBECK, D. & PERENTES, E. 2003b. Protein kinase B alpha/Akt1 regulates placental development and fetal growth. *J Biol Chem,* 278.
YAO, J., HENNESSEY, T., FLYNT, A., LAI, E., BEAL, M. F. & LIN, M. T. 2010. MicroRNA-related cofilin abnormality in Alzheimer's disease. *PLoS One,* 5**,** e15546.
YING, L., SU, D., ZHU, J., MA, S., KATSAROS, D. & YU, H. 2013. Genotyping of stathmin and its association with clinical factors and survival in patients with ovarian cancer. *Oncol Lett,* 5**,** 1315-20.
YIP, Y. Y., YEAP, Y. Y. C., BOGOYEVITCH, M. A. & NG, D. C. H. 2014. cAMP-dependent protein kinase and c-Jun N-terminal kinase mediate stathmin phosphorylation for the maintenance of interphase microtubules during osmotic stress. *J Biol Chem,* 289**,** 2157-69.
YLIKALLIO, E., POYHONEN, R., ZIMON, M., DE VRIENDT, E., HILANDER, T., PAETAU, A., JORDANOVA, A., LONNQVIST, T. & TYYNISMAA, H. 2013. Deficiency of the E3 ubiquitin ligase

TRIM2 in early-onset axonal neuropathy. *Hum Mol Genet,* 22**,** 2975-83.
YOUNG, J. E., MARTINEZ, R. A. & LA SPADA, A. R. 2009. Nutrient deprivation induces neuronal autophagy and implicates reduced. *J Biol Chem,* 284**,** 2363-73.
YU, D., CARROLL, M. & THOMAS-TIKHONENKO, A. 2007. p53 status dictates responses of B lymphomas to monotherapy with proteasome inhibitors. *Blood,* 109**,** 4936-43.
YU, J., ANDERSON, C. T., KIRITANI, T., SHEETS, P. L., WOKOSIN, D. L., WOOD, L. & SHEPHERD, G. M. 2008. Local-circuit phenotypes of Layer 5 neurons in motor-frontal cortex of YFP-H mice. *Front Neural Circuits,* 2**,** 3389.
YUAN, A., RAO, M. V., KUMAR, A., JULIEN, J. P. & NIXON, R. A. 2003. Neurofilament transport in vivo minimally requires hetero-oligomer formation. *J Neurosci,* 23**,** 9452-8.
YUAN, A., RAO, M. V., SASAKI, T., CHEN, Y., KUMAR, A., VEERANNA, LIEM, R. K., EYER, J., PETERSON, A. C., JULIEN, J. P. & NIXON, R. A. 2006. Alpha-internexin is structurally and functionally associated with the neurofilament triplet proteins in the mature CNS. *J Neurosci,* 26**,** 10006-19.
YUAN, A., RAO, M. V., VEERANNA & NIXON, R. A. 2012. Neurofilaments at a glance. *J Cell Sci,* 125**,** 3257-63.
YUAN, B. Z., CHAPMAN, J., DING, M., WANG, J., JIANG, B., ROJANASAKUL, Y. & REYNOLDS, S. H. 2013. TRAIL and proteasome inhibitors combination induces a robust apoptosis in human malignant pleural mesothelioma cells through Mcl-1 and Akt protein cleavages. *BMC Cancer,* 13**,** 140.
YUSTE, R. & TANK, D. W. 1996. Dendritic integration in mammalian neurons, a century after Cajal. *Neuron,* 16**,** 701-16.
ZAREI, M., IBARRETXE-BILBAO, N., COMPTA, Y., HOUGH, M., JUNQUE, C., BARGALLO, N., TOLOSA, E. & MARTI, M. J. 2013. Cortical thinning is associated with disease stages and dementia in Parkinson's disease. *J Neurol Neurosurg Psychiatry,* 84**,** 875-81.
ZHANG, B., CARROLL, J., TROJANOWSKI, J. Q., YAO, Y., IBA, M., POTUZAK, J. S., HOGAN, A. M., XIE, S. X., BALLATORE, C., SMITH, A. B., 3RD, LEE, V. M. & BRUNDEN, K. R. 2012. The microtubule-stabilizing agent, epothilone D, reduces axonal dysfunction, neurotoxicity, cognitive deficits, and Alzheimer-like pathology in an interventional study with aged tau transgenic mice. *J Neurosci,* 32**,** 3601-11.
ZHANG, F., SU, B., WANG, C., SIEDLAK, S. L., MONDRAGON-RODRIGUEZ, S., LEE, H.-G., WANG, X., PERRY, G. & ZHU, X. 2015a. Posttranslational modifications of α-tubulin in alzheimer disease. *Translational Neurodegeneration,* 4**,** 9.
ZHANG, H.-Z., WANG, Y., GAO, P., LIN, F., LIU, L., YU, B., REN, J.-H., ZHAO, H. & WANG, R. 2006. Silencing stathmin gene expression by survivin promoter-driven siRNA vector to reverse malignant phenotype of tumor cells. *Cancer Biology & Therapy,* 5**,** 1457-1461.

ZHANG, J. & DONG, X. P. 2012. Dysfunction of microtubule-associated proteins of MAP2/tau family in Prion disease. *Prion,* 6**,** 334-8.
ZHANG, J. Y., LIU, S. J., LI, H. L. & WANG, J. Z. 2005. Microtubule-associated protein tau is a substrate of ATP/Mg(2+)-dependent proteasome protease system. *J Neural Transm (Vienna),* 112**,** 547-55.
ZHANG, M., YUAN, X., XU, B., GUO, W., RAN, F. X., LI, R. T. & CUI, J. R. 2015b. Anticancer Effect of a Novel Proteasome Inhibitor, YSY01A, via G2/M Arrest in PC-3M Cells in vitro and in vivo. *J Cancer,* 6**,** 701-8.
ZHANG, X., TANG, N., HADDEN, T. J. & RISHI, A. K. 2011. Akt, FoxO and regulation of apoptosis. *Biochimica et Biophysica Acta (BBA) - Molecular Cell Research,* 1813**,** 1978-1986.
ZHANG, Z., CASEY, D. M., JULIEN, J. P. & XU, Z. 2002. Normal dendritic arborization in spinal motoneurons requires neurofilament subunit L. *J Comp Neurol,* 450**,** 144-52.
ZHANG, Z. W. & DESCHENES, M. 1997. Intracortical axonal projections of lamina VI cells of the primary somatosensory cortex in the rat: a single-cell labeling study. *J Neurosci,* 17**,** 6365-79.
ZHOU, B. P., LIAO, Y., XIA, W., ZOU, Y., SPOHN, B. & HUNG, M. C. 2001. HER-2/neu induces p53 ubiquitination via Akt-mediated MDM2 phosphorylation. *Nat Cell Biol,* 3**,** 973-82.
ZHU, H., ZHANG, L., DONG, F., GUO, W., WU, S., TERAISHI, F., DAVIS, J. J., CHIAO, P. J. & FANG, B. 2005. Bik/NBK accumulation correlates with apoptosis-induction by bortezomib (PS-341, Velcade) and other proteasome inhibitors. *Oncogene,* 24**,** 4993-9.
ZHU, Q., COUILLARD-DESPRÉS, S. & JULIEN, J.-P. 1997. Delayed Maturation of Regenerating Myelinated Axons in Mice Lacking Neurofilaments. *Experimental Neurology,* 148**,** 299-316.
ZHU, Y. & ZHU, J. J. 2004. Rapid arrival and integration of ascending sensory information in layer 1 nonpyramidal neurons and tuft dendrites of layer 5 pyramidal neurons of the neocortex. *J Neurosci,* 24**,** 1272-9.
ZHUANG, Y., BERENS-NORMAN, H. M., LESER, J. S., CLARKE, P. & TYLER, K. L. 2016. Mitochondrial p53 Contributes to Reovirus-Induced Neuronal Apoptosis and Central Nervous System Injury in a Mouse Model of Viral Encephalitis. *J Virol,* 90**,** 7684-91.

Appendix

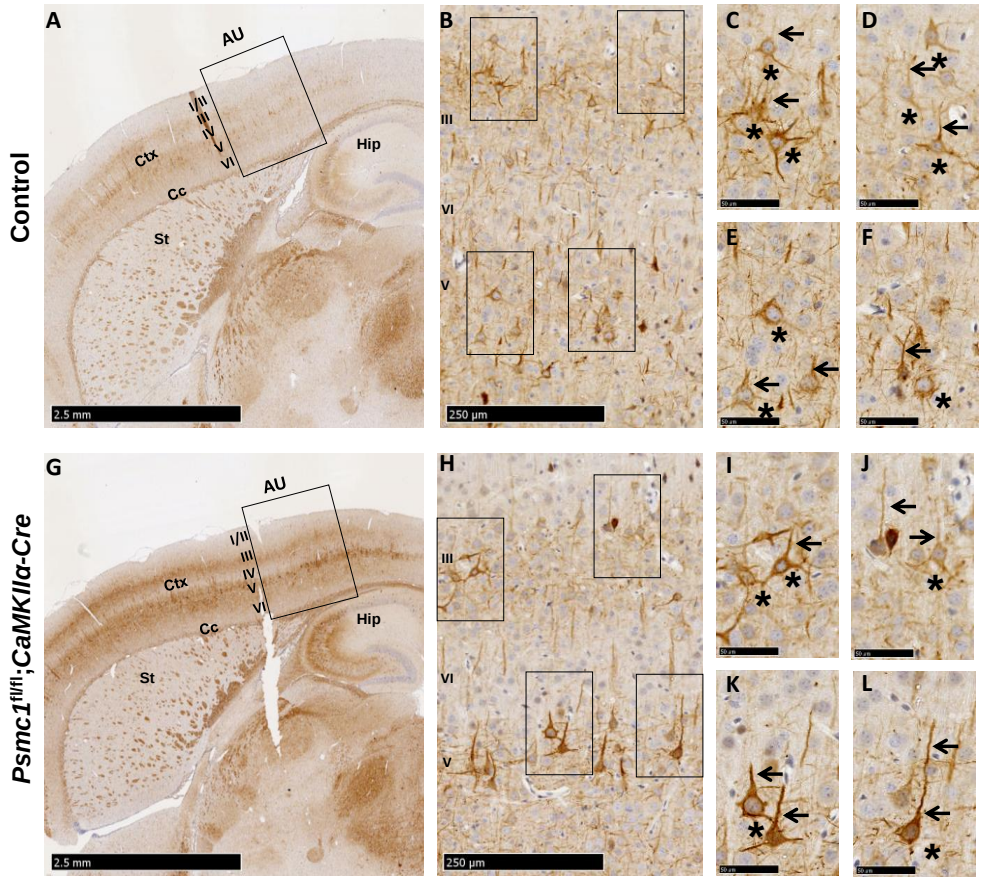


Figure 1 NFH immunoreactivity in 4 week-old *Psmc1*$^{fl/fl}$*;CaMKIIα-Cre* mouse cortical neurons

(A and G) Low magnification images of NFH immunostaining of 7 µm horizontal brain sections from 4 week-old control (A-F) and *Psmc1*$^{fl/fl}$*;CaMKIIα-Cre* mice (G-L) showing obvious staining of cortical layers III and V, and more intense staining in *Psmc1*$^{fl/fl}$*;CaMKIIα-Cre* mice compared to controls. Higher magnification images of the boxed AU areas in A and G are shown in B and H respectively. Enlarged views of individual neurons in the boxed areas in layers III and V (B and H) are shown in C-F and I-L respectively. Immunostaining is evident in the cell body, apical and basal dendrites in both control and *Psmc1*$^{fl/fl}$*;CaMKIIα-Cre* neurons. Arrows, Asterisks and Arrowheads indicate apical dendrites, basal dendritic processes and targeted neurons containing protein inclusions respectively. AU, auditory cortex; Ctx, cortex; Hip, hippocampus; Cc, corpus callosum; St, striatum.

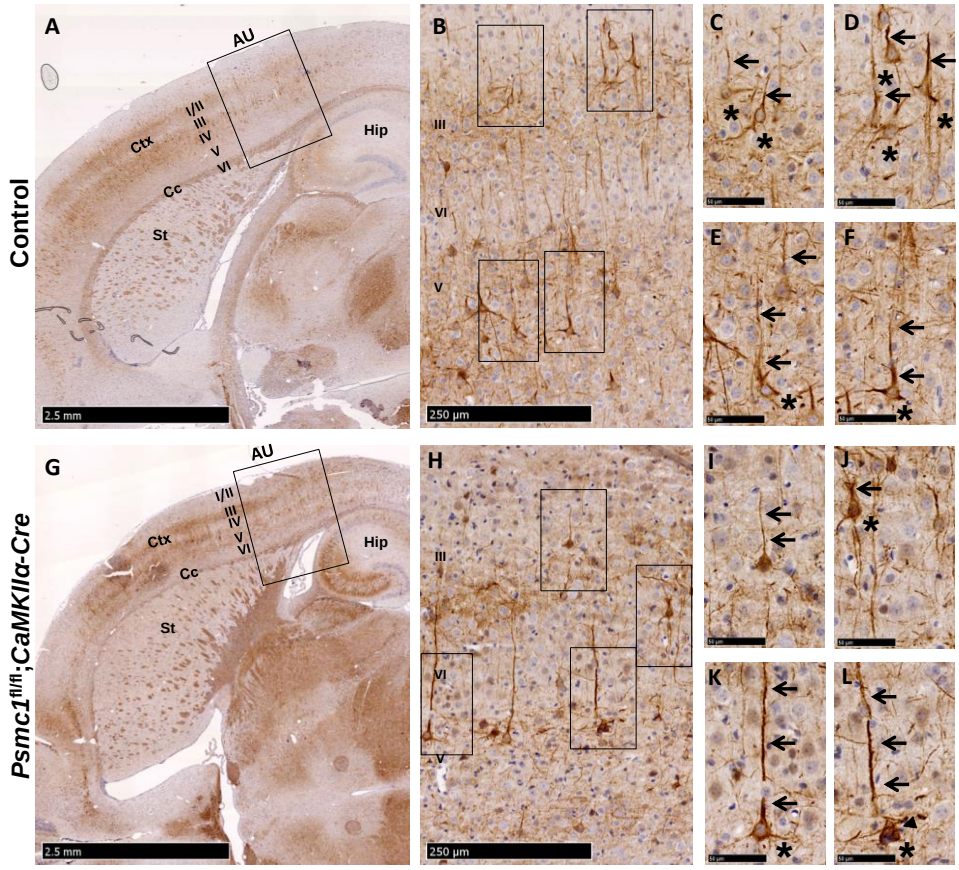


Figure 2 NFH immunoreactivity in 6 week-old *Psmc1*$^{fl/fl}$*;CaMKIIα-Cre* mouse cortical neurons

(A and G) Low magnification images of NFH immunostaining of 7 µm horizontal brain sections from 6 week-old control (A-F) and *Psmc1*$^{fl/fl}$*;CaMKIIα-Cre* mice (G-L) showing obvious staining of cortical layers III and V, and more intense staining in *Psmc1*$^{fl/fl}$*;CaMKIIα-Cre* mice compared to controls. Higher magnification images of the boxed AU areas in A and G are shown in B and H respectively. Enlarged views of individual neurons in the boxed areas in layers III and V (B and H) are shown in C-F and I-L respectively. Immunostaining is evident in the cell body, apical and basal dendrites in both control and *Psmc1*$^{fl/fl}$*;CaMKIIα-Cre* neurons. Arrows, Asterisks and Arrowheads indicate apical dendrites, basal dendritic processes and targeted neurons containing protein inclusions respectively. AU, auditory cortex; Ctx, cortex; Hip, hippocampus; Cc, corpus callosum; St, striatum.

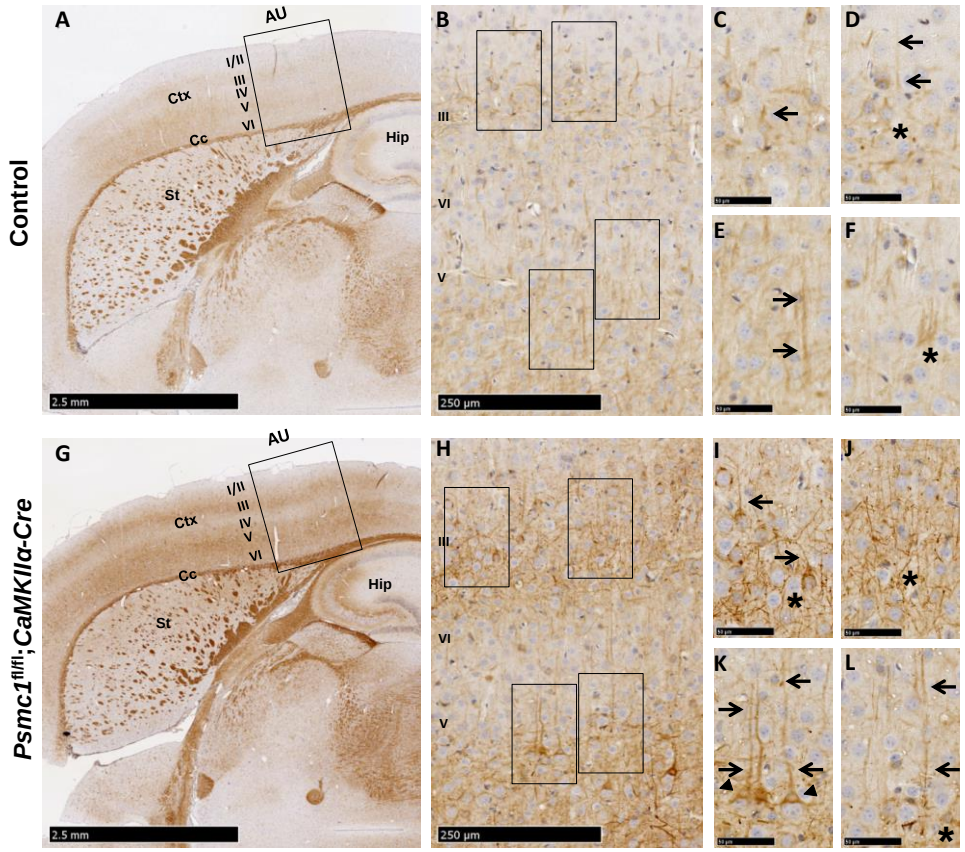


Figure 3 NFL immunoreactivity in 4 week-old *Psmc1*$^{fl/fl}$*;CaMKIIa-Cre* mouse cortical neurons

(A and G) Low magnification images of NFL immunostaining of 7 µm horizontal brain sections from 4 week-old control (A-F) and *Psmc1*$^{fl/fl}$*;CaMKIIa-Cre* mice (G-L) showing obvious staining of cortical layers III and V, and more intense staining in *Psmc1*$^{fl/fl}$*;CaMKIIa-Cre* mice compared to controls. Higher magnification images of the boxed AU areas in A and G are shown in B and H respectively. Enlarged views of individual neurons in the boxed areas in layers III and V (B and H) are shown in C-F and I-L respectively. Immunostaining is evident in the cell body, apical and basal dendrites in both control and *Psmc1*$^{fl/fl}$*;CaMKIIa-Cre* neurons. Arrows, Asterisks and Arrowheads indicate apical dendrites, basal dendritic processes and targeted neurons containing protein inclusions respectively. AU, auditory cortex; Ctx, cortex; Hip, hippocampus; Cc, corpus callosum; St, striatum.

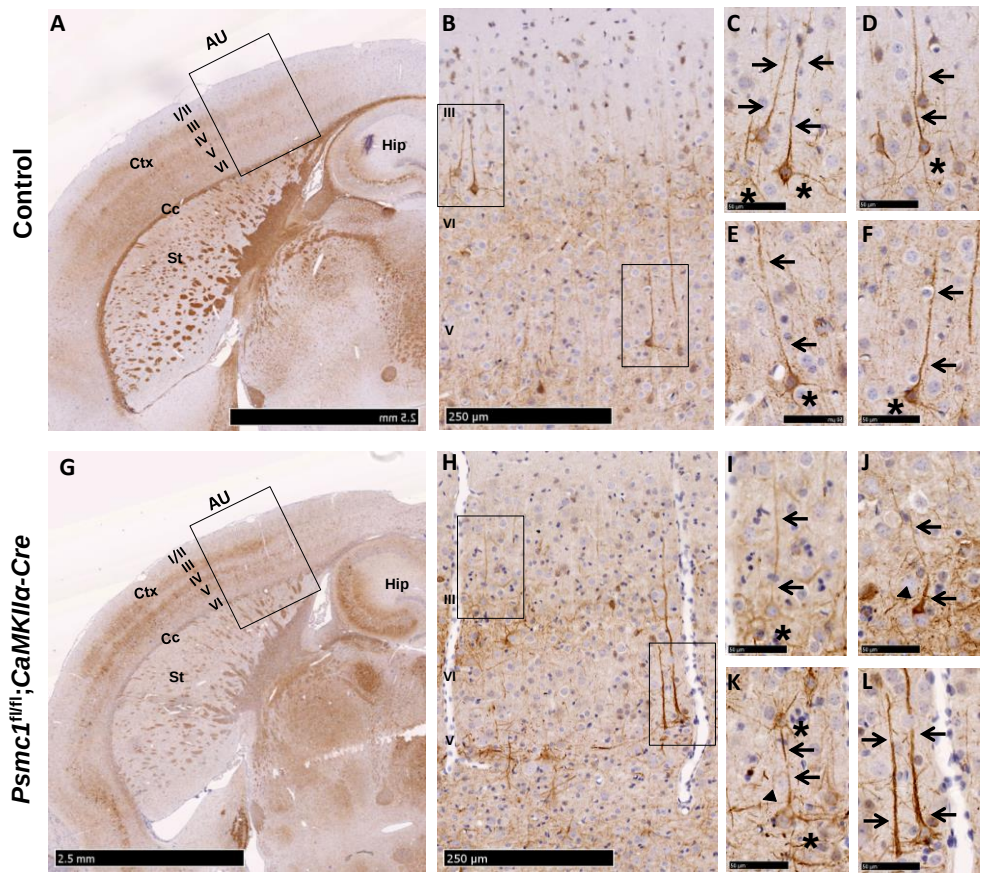


Figure 4 NFL immunoreactivity in 6 week-old *Psmc1*$^{fl/fl}$*;CaMKIIα-Cre* mouse cortical neurons

(A and G) Low magnification images of NFL immunostaining of 7 µm horizontal brain sections from 6 week-old control (A-F) and *Psmc1*$^{fl/fl}$*;CaMKIIα-Cre* mice (G-L) showing obvious staining of cortical layers III and V, and more intense staining in *Psmc1*$^{fl/fl}$*;CaMKIIα-Cre* mice compared to controls. Higher magnification images of the boxed AU areas in A and G are shown in B and H respectively. Enlarged views of individual neurons in the boxed areas in layers III and V (B and H) are shown in C-F and I-L respectively. Immunostaining is evident in the cell body, apical and basal dendrites in both control and *Psmc1*$^{fl/fl}$*;CaMKIIα-Cre* neurons. Arrows, Asterisks and Arrowheads indicate apical dendrites, basal dendritic processes and targeted neurons containing protein inclusions respectively. AU, auditory cortex; Ctx, cortex; Hip, hippocampus; Cc, corpus callosum; St, striatum.

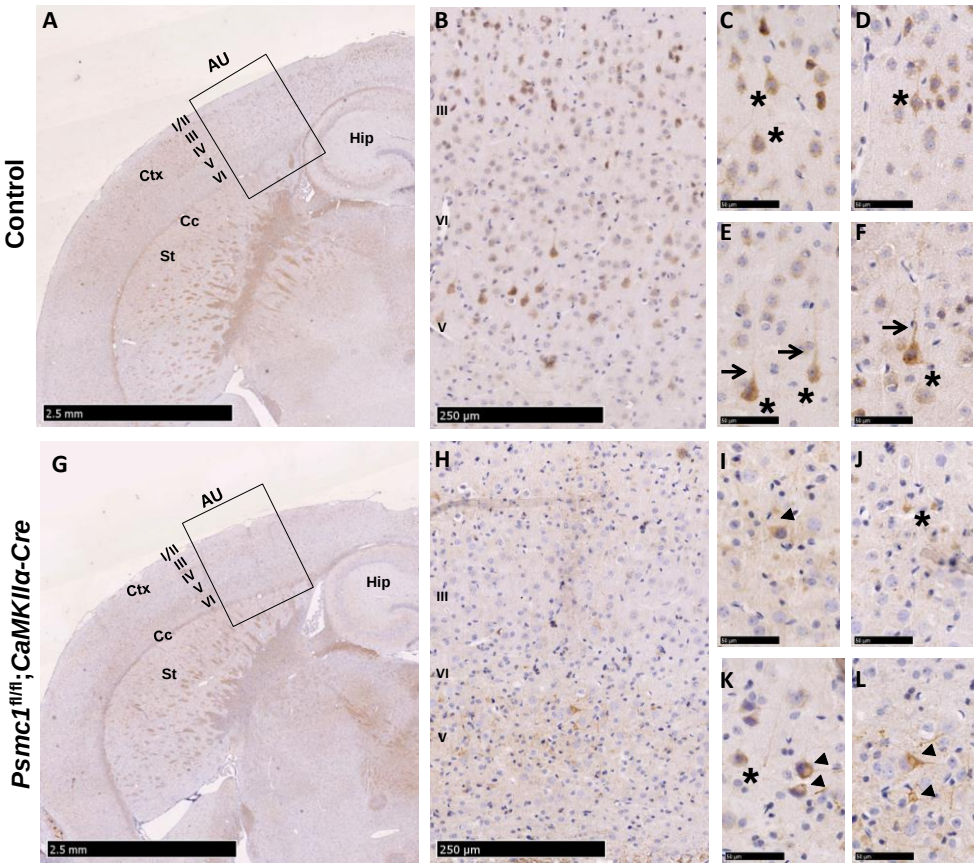


Figure 5 NFM immunostaining in 6 week-old mouse cortical pyramidal neurons.

(A and G) Low magnification images of NFM immunostaining of 7 µm horizontal brain sections from 6 week-old control (A-F) and *Psmc1*$^{fl/fl}$*;CaMKIIα-Cre* (G-L) mice. Higher magnification images of the boxed AU areas in A and G are shown in B and H respectively. Enlarged views of individual neurons in the boxed areas of cortical layers III and V (B and H) are shown in C-F and I-L respectively. Asterisks indicate NFM immunostaining in the cell body. Arrows indicate part-labelling of apical dendrites with absent basal dendritic processes. Arrowheads indicate targeted neurons containing protein inclusions in *Psmc1*$^{fl/fl}$*;CaMKIIα-Cre* mice. AU, auditory cortex; Ctx, cortex; Hip, hippocampus; Cc, corpus callosum; St, striatum. Ctx, cortex; Hip, hippocampus; Cc, corpus callosum; St, striatum.